frontiers | Research Topics

Innovative microbial technologies for future and sustainable food science

Edited by
Yu Xia, Ana Lopez Contreras and Chun Cui

Published in
Frontiers in Microbiology

ISSN 1664-8714
ISBN 978-2-8325-2813-6
DOI 10.3389/978-2-8325-2813-6

About Frontiers

Frontiers is more than just an open access publisher of scholarly articles: it is a pioneering approach to the world of academia, radically improving the way scholarly research is managed. The grand vision of Frontiers is a world where all people have an equal opportunity to seek, share and generate knowledge. Frontiers provides immediate and permanent online open access to all its publications, but this alone is not enough to realize our grand goals.

Frontiers journal series

The Frontiers journal series is a multi-tier and interdisciplinary set of open-access, online journals, promising a paradigm shift from the current review, selection and dissemination processes in academic publishing. All Frontiers journals are driven by researchers for researchers; therefore, they constitute a service to the scholarly community. At the same time, the *Frontiers journal series* operates on a revolutionary invention, the tiered publishing system, initially addressing specific communities of scholars, and gradually climbing up to broader public understanding, thus serving the interests of the lay society, too.

Dedication to quality

Each Frontiers article is a landmark of the highest quality, thanks to genuinely collaborative interactions between authors and review editors, who include some of the world's best academicians. Research must be certified by peers before entering a stream of knowledge that may eventually reach the public - and shape society; therefore, Frontiers only applies the most rigorous and unbiased reviews. Frontiers revolutionizes research publishing by freely delivering the most outstanding research, evaluated with no bias from both the academic and social point of view. By applying the most advanced information technologies, Frontiers is catapulting scholarly publishing into a new generation.

What are Frontiers Research Topics?

Frontiers Research Topics are very popular trademarks of the *Frontiers journals series*: they are collections of at least ten articles, all centered on a particular subject. With their unique mix of varied contributions from Original Research to Review Articles, Frontiers Research Topics unify the most influential researchers, the latest key findings and historical advances in a hot research area.

Find out more on how to host your own Frontiers Research Topic or contribute to one as an author by contacting the Frontiers editorial office: frontiersin.org/about/contact

Innovative microbial technologies for future and sustainable food science

Topic editors

Yu Xia — Jiangnan University, China

Ana Lopez Contreras — Wageningen University and Research, Netherlands

Chun Cui — South China University of Technology, China

Topic Coordinator

Zhe Zeng — Wageningen University and Research, Netherlands

Citation

Xia, Y., Contreras, A. L., Cui, C., eds. (2023). *Innovative microbial technologies for future and sustainable food science*. Lausanne: Frontiers Media SA.

doi: 10.3389/978-2-8325-2813-6

Table of contents

frontiers | Frontiers in Microbiology

TYPE Editorial
PUBLISHED 12 June 2023
DOI 10.3389/fmicb.2023.1215775

OPEN ACCESS

EDITED AND REVIEWED BY
Giovanna Suzzi,
University of Teramo, Italy

*CORRESPONDENCE
Yu Xia
✉ yuxia@jiangnan.edu.cn

†These authors have contributed equally to this work

RECEIVED 02 May 2023
ACCEPTED 30 May 2023
PUBLISHED 12 June 2023

CITATION
Xia Y, Zeng Z, López Contreras A and Cui C (2023) Editorial: Innovative microbial technologies for future and sustainable food science. *Front. Microbiol.* 14:1215775. doi: 10.3389/fmicb.2023.1215775

Editorial: Innovative microbial technologies for future and sustainable food science

Yu Xia[1*†], Zhe Zeng[2†], Ana López Contreras[2] and Chun Cui[3]

[1]State Key Laboratory of Food Science and Technology, School of Food Science and Technology, Jiangnan University, Wuxi, China, [2]Wageningen University and Research, Wageningen, Netherlands, [3]School of Food Science and Engineering, South China University of Technology, Guangzhou, China

KEYWORDS

food microbiology, microbial technology, future foods, sustainability, food safety and control, food processing and brewing

Editorial on the Research Topic
Innovative microbial technologies for future and sustainable food science

Introduction

Microbial technology has revolutionized the field of food sciences, allowing for the development of new food products and food ingredients, improving food safety and even better understanding on the interactions in the gut microbiome. Microorganisms play a crucial role in production of many foods, including cheese, yogurt, fermented meats, and alcoholic beverages. Advances in microbial technology have made it possible to better understand and manipulate these microorganisms, leading to current and future innovations. The current Research Topic collects both original research articles and reviews on traditional food fermentation, i.e. Chinese liquor fermentation (Hou et al.; Shi et al.) and yogurt production (El-Sayed et al.; Xiao et al.), sustainable production of food ingredients, e.g., isomaltulose (Hu et al.), D-allulose (Chen et al.) and ε-poly-L-lysine (Liu et al.), food safety (Wu et al.) and explorative innovation on gut microbiome (Chen et al.; Gao et al.; Yue et al.).

Beyond traditional food fermentation

Traditional food fermentation is a process that has been used for centuries to preserve and transform foods through the activity of microorganisms. Among the most widely known traditional fermentation practices are Chinese liquor fermentation and yogurt production. One of the most significant advances in microbial technology has been the development of starter cultures. In this topic, Shi et al. presented a study on the yeast *Wickerhamomyces anomalus* Y-1, which is commonly found in Chinese liquor fermentation starters, and the researchers used genomic and transcriptomic analysis to identify genes involved in flavor metabolism in this yeast and found that it produces a range of volatile compounds that contribute to the aroma and flavor of Chinese liquor. Hou et al. sheds light on the dynamic changes of Daqu, a type of fermentation starter used in Chinese liquor production, and provides insight into the factors that influence microbial communities and physicochemical properties during fermentation. Xiao et al. unveiled properties and nutritional composition

of kefir yogurt, which is a fermented dairy product resulting from adding kefir grains to milk, while El-Sayed et al. showed that stirred yogurt as a matrix for freeze-dried microcapsules could be an effective and tasty way to deliver synbiotic compounds to consumers. In short, microbial technology has significant implications for traditional food fermentation, contributing to controlling the fermentation process and the production of safe, tasty, and nutritious foods.

Sustainable production of food ingredient

Microbial synthesis of food using synthetic biology is now recognized as a sustainable and efficient approach for scaling up food production (Lv et al., 2021; Arun et al., 2023). Synthetic biology enables the design and construction of novel biomolecular components, pathways, and networks that can reprogram organisms to serve as engineered cell factories (Khalil and Collins, 2010; Lv et al., 2021). In this Research Topic, Hu et al. described a sustainable approach to produce isomaltulose, a non-cariogenic, slow-release carbohydrate, using an engineered food-grade strain of *Corynebacterium glutamicum*. By improving thermostability of sucrose isomerase and using one-step simplified cell immobilization, the production of isomaltulose was significantly increased up to 453.0 g/L when 500.0 g/L sucrose solution was used as substrate with reduced environmental impact. Liu et al. applied genome shuffling on strains obtained by ribosome engineering to generate a better ε-PL producing strain from parental strain *Streptomyces albulus* M-Z1Z8. Chen et al. systematically reviewed recent advances in the physiological functions and biosynthesis of D-allulose, a rare sugar with potential health benefits, emphasizing on the enzymes and metabolic pathways involved in D-allulose biosynthesis, highlighting the potential of microbial engineering to improve production efficiency. Application of synthetic biology in sustainable production of food ingredients will expand the range of available feedstocks and potentially lead to more sustainable and high-quality food production.

Innovation on gut microbiome

Today, more and more evidence has proved that gut microbiome plays a crucial role in our bodies, influencing our immune systems, metabolisms, and even our moods and behaviors (Gilbert et al., 2018). Innovative microbiome-related applications have created a gigantic market ranging from functional foods (e.g., foods enriched in prebiotic fibers and/or probiotic bacteria) to dietary supplements (e.g., probiotic capsules or powders) and therapeutic applications (e.g., gut microbiota transplant) (D'Hondt et al., 2021). Gao et al. investigated the effects of gut microbiota transplantation (GMT) from high-fat-diet-tolerant cynomolgus monkeys on hyperlipidemia and hepatic steatosis in rats. The results showed that the GMT led to a significant reduction in serum lipid levels and hepatic lipid accumulation in the recipient rat, suggesting that GMT may be a potential therapeutic strategy for treating metabolic disorders, such as hyperlipidemia and hepatic steatosis. Chen et al. investigated the differences in the gastric juice microbiota of pediatric patients with chronic gastritis who tested positive or negative for *Helicobacter pylori*. This study suggested that the gastric juice microbiota may play a role in the pathogenesis of chronic gastritis and could be a potential target for future therapies. On-going research of the microbiome has created an opportunity for the bioeconomy approach, providing practical solutions with potential for commercial application and enhancing social wellbeing.

Author contributions

ZZ and YX prepared the manuscript. YX revised the contexts. AL and CC provided comments to the manuscript. All authors approved the submission of this manuscript.

Conflict of interest

The authors declare that the research was conducted in the absence of any commercial or financial relationships that could be construed as a potential conflict of interest.

Publisher's note

All claims expressed in this article are solely those of the authors and do not necessarily represent those of their affiliated organizations, or those of the publisher, the editors and the reviewers. Any product that may be evaluated in this article, or claim that may be made by its manufacturer, is not guaranteed or endorsed by the publisher.

References

Arun, K. B., Anoopkumar, A. N., Sindhu, R., Binod, P., Aneesh, E. M., Madhavan, A., et al. (2023). Synthetic biology for sustainable food ingredients production: recent trends. *Syst. Microbiol. Biomanuf.* 3, 137–149. doi: 10.1007/s43393-022-00 1500-3

D'Hondt, K., Kostic, T., McDowell, R., Eudes, F., Singh, B. K., Sarkar, S., et al. (2021). Microbiome innovations for a sustainable future. *Nat. Microbiol.* 6, 138–142. doi: 10.1038/s41564-020-00 857-w

Gilbert, J. A., Blaser, M. J., Caporaso, J. G., Jansson, J. K., Lynch, S. V., Knight, R., et al. (2018). Current understanding of the human microbiome. *Nat. Med.* 24, 392–400. doi: 10.1038/nm.4517

Khalil, A. S., and Collins, J. J. (2010). Synthetic biology: applications come of age. *Nat. Rev. Genet.* 11, 367–379. doi: 10.1038/nrg2775

Lv, X., Wu, Y., Gong, M., Deng, J., Gu, Y., Liu, Y., et al. (2021). Synthetic biology for future food: research progress and future directions. *Future. Foods.* 3, 100025. doi: 10.1016/j.fufo.2021.100025

frontiers in Microbiology

ORIGINAL RESEARCH
published: 25 March 2022
doi: 10.3389/fmicb.2022.876043

Transplantation of Gut Microbiota From High-Fat-Diet-Tolerant Cynomolgus Monkeys Alleviates Hyperlipidemia and Hepatic Steatosis in Rats

Jiang-Mei Gao[1,2†], Jun-Hua Rao[1,2†], Zhi-Yuan Wei[2,3†], Shou-Yue Xia[2,3], Li Huang[1,2], Ming-Tian Tang[1,2], Geoff Hide[4], Ting-Ting Zheng[2,3], Jia-Huan Li[2,3], Guo-An Zhao[2,3], Yun-Xiao Sun[1,2] and Jian-Huan Chen[2,3*]*

[1]Guangdong Key Laboratory of Animal Conservation and Resource Utilization, Guangdong Public Laboratory of Wild Animal Conservation and Utilization, Institute of Zoology, Guangdong Academy of Sciences, Guangzhou, China, [2]Joint Primate Research Center for Chronic Diseases, Jiangnan University and Institute of Zoology, Guangdong Academy of Sciences, Guangzhou, China, [3]Laboratory of Genomic and Precision Medicine, Wuxi School of Medicine, Jiangnan University, Wuxi, China, [4]Biomedical Research Centre and Ecosystems and Environment Research Centre, School of Science, Engineering and Environment, University of Salford, Salford, United Kingdom

Emerging evidence has been reported to support the involvement of the gut microbiota in the host's blood lipid and hyperlipidemia (HLP). However, there remains unexplained variation in the host's blood lipid phenotype. Herein a nonhuman primate HLP model was established in cynomolgus monkeys fed a high-fat diet (HFD) for 19 months. At month 19%, 60% (3/5) of the HFD monkeys developed HLP, but surprisingly 40% of them (2/5) exhibited strong tolerance to the HFD (HFD-T) with their blood lipid profiles returning to normal levels. Metagenomic analysis was used to investigate the compositional changes in the gut microbiota in these monkeys. Furthermore, the relative abundance of *Megasphaera* remarkably increased and became the dominant gut microbe in HFD-T monkeys. A validation experiment showed that transplantation of fecal microbiota from HFD-T monkeys reduced the blood lipid levels and hepatic steatosis in HLP rats. Furthermore, the relative abundance of *Megasphaera* significantly increased in rats receiving transplantation, confirming the successful colonization of the microbe in the host and its correlation with the change of the host's blood lipid profiles. Our results thus suggested a potentially pivotal lipid-lowering role of *Megasphaera* in the gut microbiota, which could contribute to the variation in the host's blood lipid phenotype.

Keywords: cynomolgus monkey, hyperlipidemia, high-fat diet, fecal microbiota transplantation, *Megasphaera*

OPEN ACCESS

Edited by:
Chun Cui,
South China University of Technology, China

Reviewed by:
Yinhua Lu,
Shanghai Normal University, China
De-Hai Gou,
Sun Yat-sen University, China

****Correspondence:***
Jian-Huan Chen
cjh_bio@hotmail.com
Jun-Hua Rao
junhuar919@163.com

[†]These authors have contributed equally to this work

Specialty section:
This article was submitted to Food Microbiology, a section of the journal Frontiers in Microbiology

Received: *15 February 2022*
Accepted: *07 March 2022*
Published: *25 March 2022*

Citation:
Gao J-M, Rao J-H, Wei Z-Y, Xia S-Y, Huang L, Tang M-T, Hide G, Zheng T-T, Li J-H, Zhao G-A, Sun Y-X and Chen J-H (2022) Transplantation of Gut Microbiota From High-Fat-Diet-Tolerant Cynomolgus Monkeys Alleviates Hyperlipidemia and Hepatic Steatosis in Rats. Front. Microbiol. 13:876043. doi: 10.3389/fmicb.2022.876043

INTRODUCTION

Hyperlipidemia (HLP) is considered one of the main contributing factors in developing metabolic syndromes and increasing the risk of atherosclerosis, stroke, coronary heart disease, and myocardial infarction (Karr, 2017; Panahi et al., 2018; Libby et al., 2019). In addition, high blood cholesterol (total cholesterol, TC) is a strong risk factor for hypertension, fatty liver, and diabetes (Elkins and Friedrich, 2018).

Recently, emerging evidence suggests the role of gut microbiota in human health and disease (Nicholson et al., 2012; Qin et al., 2012; Guo et al., 2016; Tong et al., 2018). Gut dysbiosis, defined as an imbalance in gut microbial communities, has been linked to a variety of diseases, including malnutrition, inflammatory bowel disease, neurological disorders, and cancer, as well as diabetes and obesity (Blanton et al., 2016; DeGruttola et al., 2016). For example, in genetically obese (ob/ob) mice, compared with wild-type and heterozygous lean counterparts, the abundance of Firmicutes was significantly increased and Bacteroidetes were decreased (Turnbaugh et al., 2006, 2009).

Probiotics could confer health benefits on the host by protecting them from gut dysbiosis. *Akkermansia muciniphila* is currently recommended as a new potential complementary therapy for obesity, diabetes, and liver diseases in clinics (Cani and de Vos, 2017; Plovier et al., 2017). It has been demonstrated that there are metabolic benefits of *Parabacteroides distasonis* (*P. distasonis*) on decreasing weight gain, hyperglycemia, and hepatic steatosis in ob/ob and high-fat diet (HFD)-fed mice. Administration of *P. distasonis* into obese mice dramatically changed the profile of secondary bile acids (Wang et al., 2019). In addition, *Faecalibacterium prausnitzii* and the peptides secreted by it showed anti-inflammatory effects on chemically induced colitis in mice (Breyner et al., 2017). *Lactobacillus* was reported to have a lipid-lowing effect on hypercholesterolemia and hyperlipidemic rat or mice (Zhou et al., 2013; Singh et al., 2015; Jiang et al., 2019; Qian et al., 2019). Therefore, it is promising to improve such diseases and gut dysbiosis by targeting the gut microbiota using probiotics.

As a typical chronic disease, HLP is closely related to gut microbiota dysbiosis and could also be potentially alleviated and cured through gut microbiota regulation. Given the high similarity to humans in terms of genetics, anatomy, reproduction, development, and metabolism, non-human primates (NHPs) are used as distinctive and indispensable model organisms in various areas of biomedical research and disease studies (Manara et al., 2019). Furthermore, it has been found that NHPs in captivity have a similar gut microbiota composition to that in humans (Clayton et al., 2016).

To understand the role of the gut microbiota in HLP, we used NHPs (cynomolgus monkeys) fed a high-fat diet (HFD) to establish an HLP model in the current study. HFD monkeys exhibited HLP by Month 7. After 12 months of HFD feeding, some individuals of the monkeys developed tolerance to HFD with their blood lipid profiles returning to normal levels. To explore the dynamics of the gut microbiota associated with such changes in lipid profiles, we conducted metagenomic sequencing in the HFD monkeys. Furthermore, transplantation of fecal microbiota from HFD-tolerant cynomolgus monkeys alleviated HLP and hepatocyte lesion in HFD rats.

MATERIALS AND METHODS

Animals

Ten male cynomolgus monkeys were purchased from Guangdong Landau Biotechnology Co. Ltd. (Guangzhou, China) which is accredited by the Association for the Assessment and Accreditation of Laboratory Animal Care International (AAALAC). All the animals were confirmed to be in healthy condition by records and veterinary examination before the experiment.

All monkeys were kept in a well-controlled and comfortable environment with temperature (16°C–28°C) and relative humidity of 40%–70%, as well as a 12/12-h light–dark cycle. All the animals were free to access food and drinking water. The protocol for this study was approved by the Institutional Animal Care and Use Committee of Guangdong Landau Biotechnology Co., Ltd. (Code: LD20150518).

All monkeys were randomly divided into two groups, including an HFD group ($n = 5$) and a normal chow diet group (NCD, $n = 5$). The NCD group was fed normal chow, while the HFD group was fed normal chow daily plus emulsion containing 10% sucrose, 10% lard, 1% cholesterol, and 0.5% cholate (5 ml/kg body weight) *via* nasogastric gavage 6 days a week. All the monkeys in the HFD group were fed HFD for 19 months.

Twenty seven male Sprague–Dawley (SD) rats used for validation experiments were purchased from Guangzhou University of Chinese Medicine. All rats were kept in a specific pathogen-free environment with free access to food and water. The protocol for this study was approved by Institute of Zoology, Guangdong Academy of Sciences (GIABR20200908).

The rats were randomly divided into three groups ($n = 9$ for each group): an NCD group (NCD), an HFD group, and a fecal microbiota transplantation group (HFD + M). All rats were fed with an NCD. The HFD and HFD + M groups were fed normal chow daily plus the same emulsion used in the monkeys (5 ml/kg body weight) by gavage (six days a week for 12 weeks.

Fecal Microbiota Transplantation

Fresh stool samples from monkeys that showed tolerance to the HFD were pooled, suspended in sterile phosphate buffer saline (PBS, pH = 7.0), and centrifuged at 500 *g* for 5 min. 200 μl of the prepared supernatant (10^8 CFU) was given to the HFD + M group of rats *via* oral gavage 6 days per week at week 7–12 of HFD feeding.

Biochemical Analysis

Blood samples of rats and monkeys were periodically collected from the ocular vein and the upper limb saphenous vein, respectively. Serum total cholesterol (TC), triacylglycerol (TG), low-density lipoprotein cholesterol (LDL-C), and high-density lipoprotein cholesterol (HDL-C) were measured using commercially available kits from Guangdong Lewwin Pharmaceutical Research Institute Co., Ltd. (Guangzhou, China).

Histological Analysis

Liver tissues of rats were collected, fixed in 4% paraformaldehyde, paraffin-embedded, and sectioned at 5 μm. Hematoxylin and eosin (H&E) and Oil Red O staining of paraffin sections were conducted following a standard method.

Metagenomic Sequencing and Analysis

DNA of macaque fecal samples was collected at month 19 of HFD feeding and sequenced on the HiSeq-X10 platform (Illumina) using a paired-end 150 bp configuration. Cleaning data were obtained by filtering raw data using KneadData (v0.7.4).[1] Karaken2 (v2.0.8) was used for taxonomic analysis (Wood and Lu, 2019), and vegan 2.5–7 was used for diversity indices analysis.

16S rRNA Gene Sequencing and Analysis

SD rat fecal samples were collected at Week 12 for gut microbial analysis. Bacterial genomic DNA was extracted from frozen fecal samples stored at −80°C using TIANamp Stool DNA kit (Cat.#DP328, Tiangen, China) according to the manufacturer's instructions.

The hypervariable V4 regions of bacterial 16 s rRNA genes were amplified using the polymerase chain reaction and V4-specific primers as described previously (Wei et al., 2021). After quality control, PCR products were purified and sequenced on an Ion S5XL sequencer (Thermo Fisher Scientific, Waltham, Massachusetts) with a single-end 400-bp read length configuration.

Bioinformatic analysis of the 16S rRNA gene sequencing data was conducted using the QIIME2 (version 2018.6.0) analysis pipeline (Bolyen et al., 2019). Briefly, the dada2 program was used to filter and remove low-quality and chimeric sequences, and generate unique feature tables equivalent to operational taxonomic unit (OTU) tables at exact match or 100% sequence similarity. Taxonomic identifications were then assigned to these features using the q2-feature-classifier and the full-length SILVA database (release r138) at a 99% similarity cutoff (Parks et al., 2014). PICRUSt (version 1.1.4) was used to predict microbial functions from the 16S rRNA gene sequencing data, which were further categorized using the BRITE hierarchy of the KEGG database (Langille et al., 2013). Differences in the microbial functions were then analyzed by the Linear discriminant analysis (LDA) Effect Size (LEfSe) algorithm with a log (LDA) score cutoff of 2 and default settings (Segata et al., 2011).

[1]https://huttenhower.sph.harvard.edu/kneaddata/

Statistical Analysis

Statistical analysis was performed using GraphPad Prism V.7.0a (GraphPad Software, United States) and the R statistical language (version 3.6.0). The levels of serum lipid, the relative abundance of OTUs, and alpha diversity indices among groups were compared using the *Student's t*-test and evaluated for pair-wise inter-group differences with Tukey's *post-hoc* test if overall significance was found.

RESULTS

Tolerance to HFD in Monkeys After Long-Term Dietary Induction

To explore the characteristics of HLP, the levels of TC and LDL-C were significantly higher in monkeys fed HFD than NCD controls ($n = 5$) by 3 months (TC, HFD *vs* NCD, $p = 0.001$; LDL-C, HFD vs. NCD, $p = 0.003$) (**Figures 1A,B**). After 7 months, all HFD monkeys showed HLP (TC > 6.20 mmol/L and LDL-C > 3.64 mmol/L) with higher levels of TC and LDL-C compared to the NCD controls (TC, HFD vs. NCD, $p = 0.006$; LDL-C, HFD vs. NCD, $p = 0.007$). Intriguingly, after 17 months of diet induction, 2 monkeys (HFD-2 and HFD-5) exhibited obvious tolerance to HFD with their blood lipid profiles returning to normal levels (TC, HFD-2/5 vs. NCD control, $p > 0.05$; HFD-2/5 vs. HFD-1/3/4, $p = 0.004$. LDL-C, HFD-2/5 vs. NCD control, $p > 0.05$; HFD-2/5 vs. HFD-1/3/4, $p < 0.0001$). In the subsequent analysis, we refer to HFD-2 and HFD-5 as HFD-tolerant (HFD-T), and HFD-1, HFD-3, and HFD-4 as

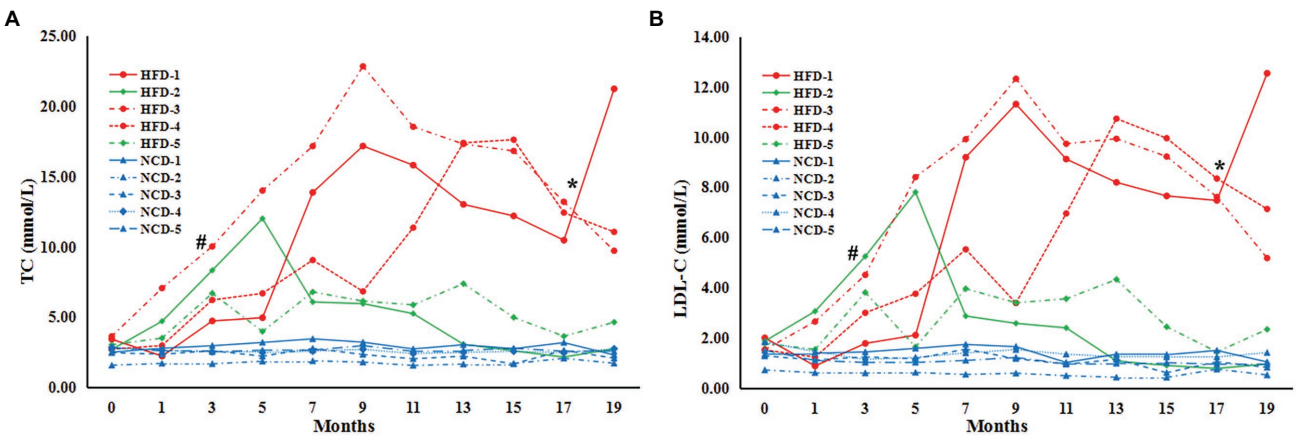

FIGURE 1 | Serum lipids in cynomolgus monkeys during HFD feeding. Serum levels (mmol/L) are shown for **(A)** total cholesterol (TC), **(B)** low-density lipoprotein cholesterol (LDL-C). HFD: high-fat diet monkeys; NCD: normal chow diet. Significant differences are indicated as #, at month 3, HFD monkeys *vs* NCD monkeys, $p < 0.05$; *, at Month 17, HFD-1/HFD-3/HFD-4 (HFD-intolerant) monkeys *vs* HFD-2/HFD-5 (HFD-tolerant) monkeys, $p < 0.05$.

HFD-intolerant (HFD-I). However, long-term HFD did not cause significant body weight changes in HFD monkeys compared to NCD monkeys by month 19 (data not shown).

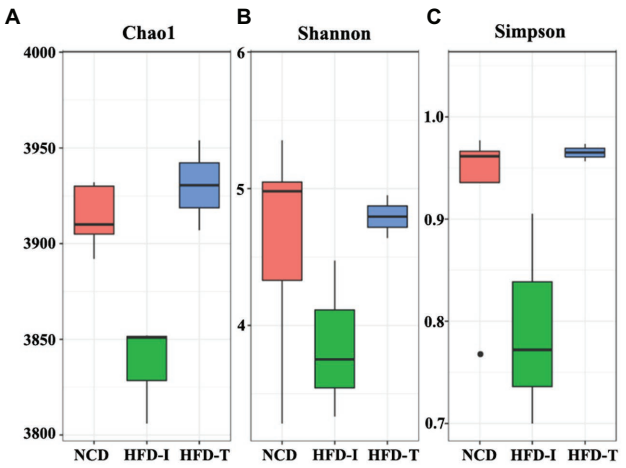

FIGURE 2 | Boxplots showing changes in alpha diversity of the gut microbiota in NCD, HFD-I, and HFD-T monkeys. Alpha diversity indices including Chao1 **(A)**, Shannon's **(B)** index, and Simpson's index **(C)** are shown.

Gut Microbiota Profiles Associated With HFD Tolerance in Monkeys

To explore the dynamics of gut microbiota associated with such changes in lipid profiles, we conducted metagenomic sequencing using fecal DNA from both HFD-T and HFD-I monkeys after HFD-induction for 19 months. Our results showed that long-term HFD induction changes the composition of the gut microbiota and slightly reduced alpha diversity indices (Chao1, *Shanno's* index, and *Simpson*'s index) in HFD-I monkeys, while HFD-T monkeys had similar alpha diversity compared to NCD controls (**Figure 2**).

Analysis at the phylum level showed that HFD markedly decreased the relative abundance of Firmicutes, and increased the relative abundance of Bacteroidetes. In addition, Spirochaetes was increased in HFD-I monkeys. However, the relative abundance of Firmicutes was found to be partially increased in HFD-T monkeys, and Bacteroidetes also increased in HFD-I monkeys (**Supplementary Figure S1**).

A detailed analysis of the bacterial genera detected in each group is shown in **Figure 3A**. The relative abundance of *Lactobacillus* was the highest in NCD monkeys but was markedly reduced in HFD monkeys (HFD-I and HFD-T groups). Intriguingly, the relative abundance of *Prevotella*, *Bacteroides, Lactobacillus,* and especially *Megasphaera* were increased in HFD-T monkeys (**Figures 3A,B**).

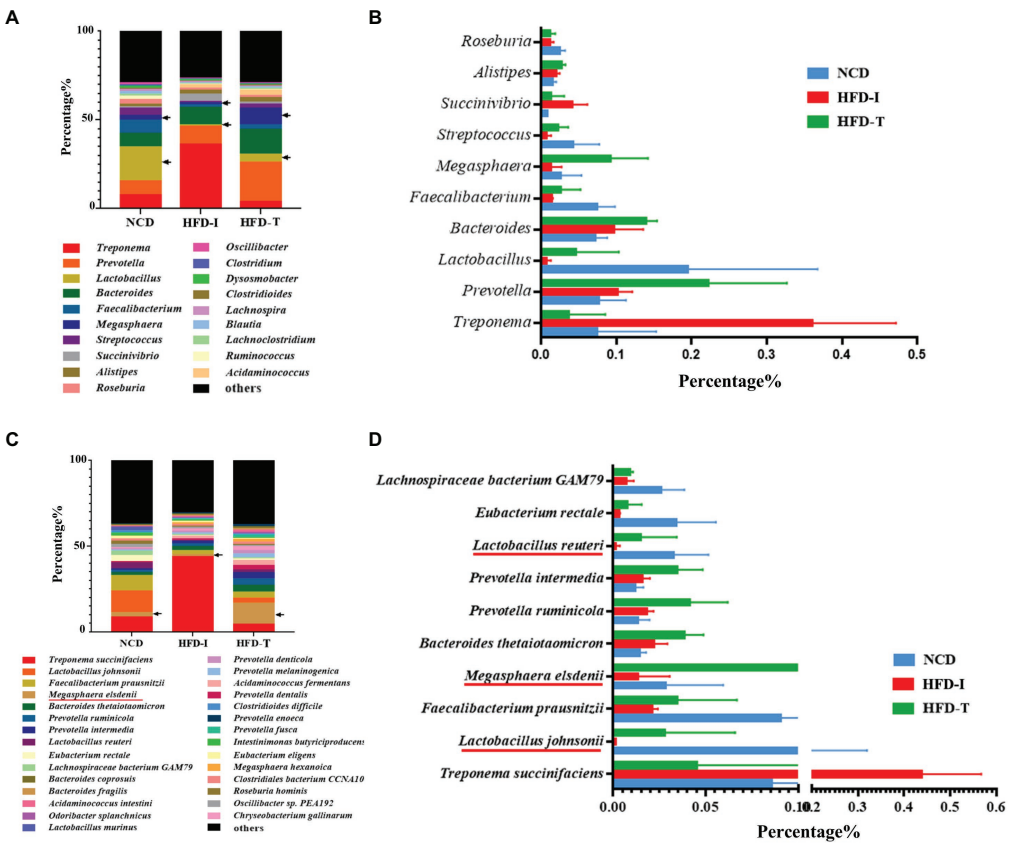

FIGURE 3 | The most abundant genera and species in the gut microbiota of NCD, HFD-I, and HFD-T monkeys. Relative abundances of the gut microbiota at the genus level **(A)**, top 10 abundant genera **(B)**, relative abundances of the gut microbiota at the species level **(C)**, and top 10 abundant species **(D)** are shown.

Further analysis at the species level showed similar results to those observed at the genus level. As shown in **Figure 3C**, the relative abundance of *Lactobacillus johnsonii*, *Lactobacillus reuteri* and *Megasphaera elsdenii* were highest in NCD monkeys. However, the relative abundance of these bacteria was markedly reduced after long-term HFD feeding (**Figure 3D**). However, the relative abundance of *L. johnsonii* and *L. reuteri* were found to be partially increased in HFD-T monkeys (**Figures 3D, 4A,B**). However, *M. elsdenii* was dramatically increased and became predominant in HFD-T monkeys (**Figures 3C,D, 4C**). In addition, another two species of *Megasphaera* (including *Megasphaera hexanoica* and *Megasphaera stantonii*) were also increased in HFD-T monkeys (**Figures 4D,E**).

Transplantation of Fecal Microbiota From HFD-T Monkeys to HFD Rats Alleviated HLP and Hepatic Steatosis

To validate the possible lipid-lowering effects of the gut microbiota in HFD-T monkeys, fecal microbiota from HFD-T monkeys was transplanted to HLP rats fed with an HFD. All rats showed significantly higher levels of TC and LDL-C compared to NCD rats after 3 weeks of HFD feeding. Transplantation of fecal microbiota from HFD-T monkeys alleviate HLP in the recipient HFD rats with significantly lower levels of TC (NCD *vs* HFD, $p < 0.0001$; NCD *vs* HFD + M, $p < 0.0001$; HFD *vs* HFD + M, $p = 0.0227$) and LDL-C (NCD *vs* HFD, $p < 0.0001$; NCD *vs* HFD + M, $p < 0.0001$; $p = 0.0094$; **Figures 5A,B**). Furthermore, HFD-fed rats showed enhanced lipid accumulation, which was markedly inhibited with improved hepatic steatosis by the fecal microbiota transplantation in the HFD + M mice (**Figure 6**).

Fecal Microbiota Transplantation Changed Gut Microbiota of HFD Rats.

To further investigate the lipid-lowering mechanism of the gut microbiota from the HFD-T monkeys, we also analyzed the gut microbiota composition of rats in the NCD, HFD, and HFD + M groups using 16S rRNA gene high-throughput sequencing. Principal component analysis (PCA), the NCD, HFD, and HFD + M groups of rats each presented

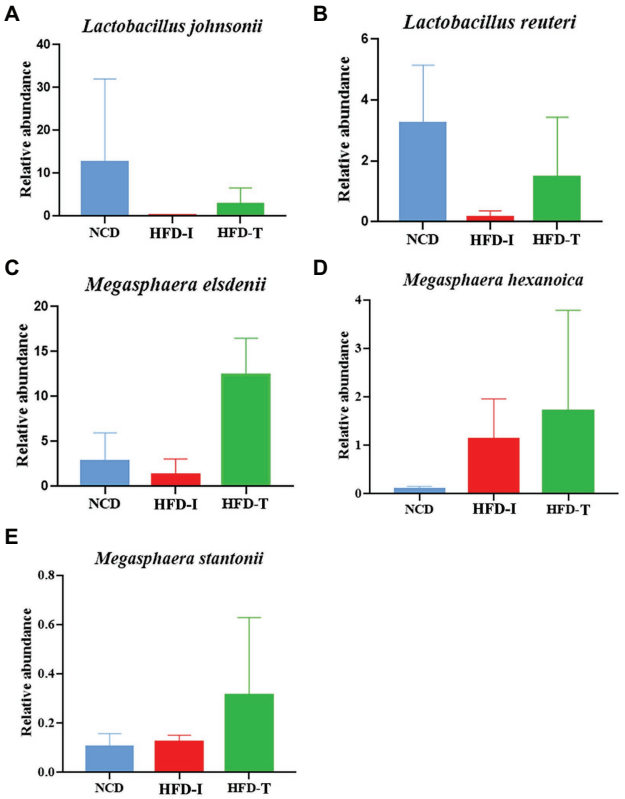

FIGURE 4 | The relative abundance of selected species in the gut microbiota in NCD, HFD-I, and HFD-T monkeys. *Lactobacillus johnsonii* **(A)**, *Lactobacillus reuteri* **(B)**, *Megasphaera elsdenii* **(C)**, *Megasphaera hexanoica* **(D)**, and *Megasphaera stantonii* **(E)**.

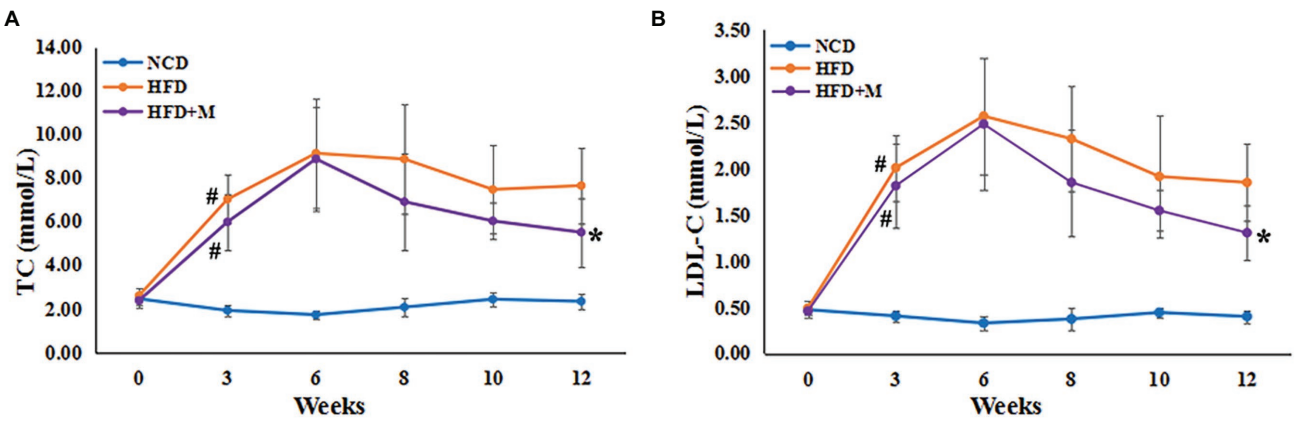

FIGURE 5 | Serum lipids in SD rats following fecal microbiota transplantation from HFD-T monkeys. Serum levels (mmol/L) are shown for **(A)** total cholesterol (TC), **(B)** low-density lipoprotein cholesterol (LDL-C). NCD, Normal Chow Diet rats; HFD, HFD rats; HFD + M, HFD rats with transplantation from the fecal microbiota from HFD-T monkeys. #, at Week 3 of HFD feeding, HFD and HFD + M rats *vs* NCD rats, $p < 0.05$; *, at Week 12, HFD rats *vs* HFD + M rats, $p < 0.05$.

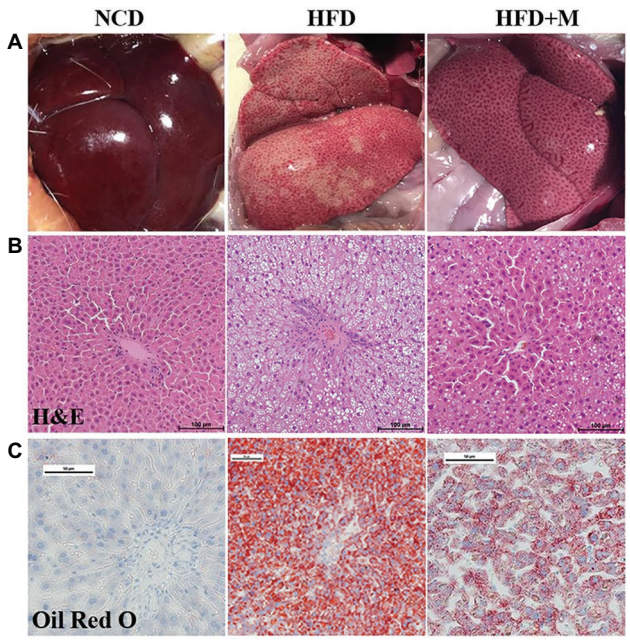

FIGURE 6 | Changes in hepatic steatosis after fecal microbiota transplantation. **(A)** Photos showing liver morphology. **(B)** H and E staining of liver section. Scale bars, 100 μm. **(C)** Liver Oil Red O staining. NCD, Normal Chow Diet rats; HFD, HFD rats; HFD + M, HFD rats received fecal microbiota transplant from HFD-T monkeys. Scale bars, 50 μm.

a separated clustering of microbiota composition (**Figure 7A**). Such results demonstrate that transplantation of fecal microbiota significantly changed the gut microbiota profiles in rats ($p = 0.001$).

In addition, it has been demonstrated that HFD could significantly reduce the richness and diversity of the gut microbiota in HFD fed rats (including both the HFD and HFD + M groups) by using a range of alpha diversity indices (Shannon, Chao1, Faith-pd, and Observed-features; **Figures 7B–E**). However, there was no significant difference in the richness and alpha diversity of the gut microbiota between the HFD and HFD + M groups (**Figures 7B–E**).

As shown in **Supplementary Figure S2**, at the phylum level analysis HFD significantly decreased the relative abundance of Firmicutes and increased the relative abundance of Bacteroidetes. These changes are consistent with findings in monkeys. However, the relative abundance of Firmicutes and Bacteroidetes in HFD + M rats showed no significant changes compared to HFD rats.

Furthermore, we analyzed the differences in the gut microbiota at the genus level. Genera *Prevotella*, *Bacteroides,* and *Lactobacillus* were predominant in the rat gut microbiota and *Bacteroides* was significantly increased in HFD and HFD + M rats (NCD *vs* HFD, $p < 0.001$; NCD *vs* HFD + M, $p < 0.0001$; **Figure 8A**). However, *Fusobacterium* (NCD *vs* HFD, $p < 0.001$; HFD *vs*

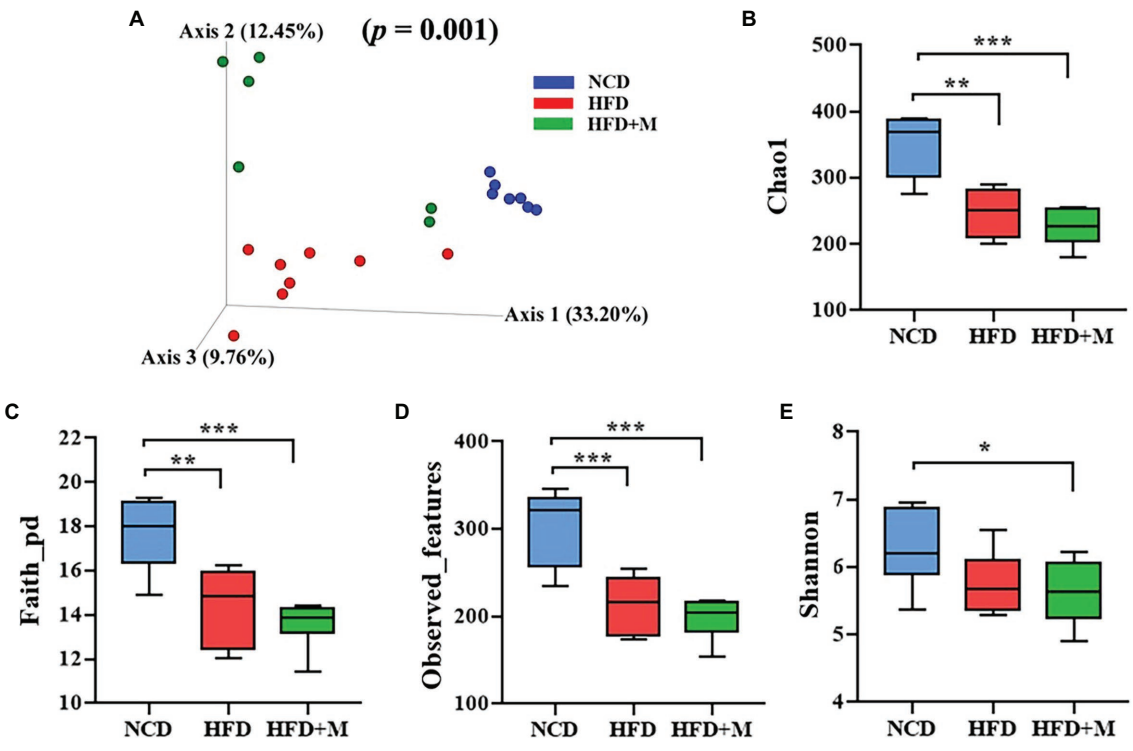

FIGURE 7 | The beta diversity, structure, and richness of the gut microbiota in three groups of rats. **(A)** Nonmetric multidimensional scaling (NMDS) score plot based on principal component analysis (PCA) score plot based on microbiota composition. **(B–E)** The gut microbiota diversity as calculated using Shannon's index **(B)**, Chao1 **(C)**, Faith-pd **(D)**, and observed-features **(E)** index of each rat group: NCD, Normal Chow Diet (control) rats; HFD, HFD rats; HFD + M, HFD rats received fecal microbiota transplant from HFD-T monkeys. Values are presented as mean ± SE. ($n = 7$). *, $p < 0.05$; **, $p < 0.01$; ***, $p < 0.001$, compared with NCD rats.

HFD + M, $p < 0.01$) and *Parabacteroides* (NCD *vs* HFD, $p < 0.01$; HFD vs. HFD + M, $p < 0.01$) were increased in HFD rats but were significantly decreased after fecal microbiota transplantation (**Figure 8B**). The abundance of *Lactobacillus* showed no significant difference among the three groups of rats ($p > 0.05$; **Figure 8B**). Interestingly, *Megasphaera* was significantly increased in HFD + M rats ($p < 0.05$), in line with its changes observed in HFD-T monkeys, implicating its role in the reduction of the host's blood lipids.

In addition, as shown in LEfSe analysis shown in **Figure 9**, PICRUSt prediction results indicated that transplantation of fecal microbiota from HFD-T monkeys changed various functions of gut microbiota in rats, particularly biosynthesis of amino acids, including L-lysine and L-isoleucine.

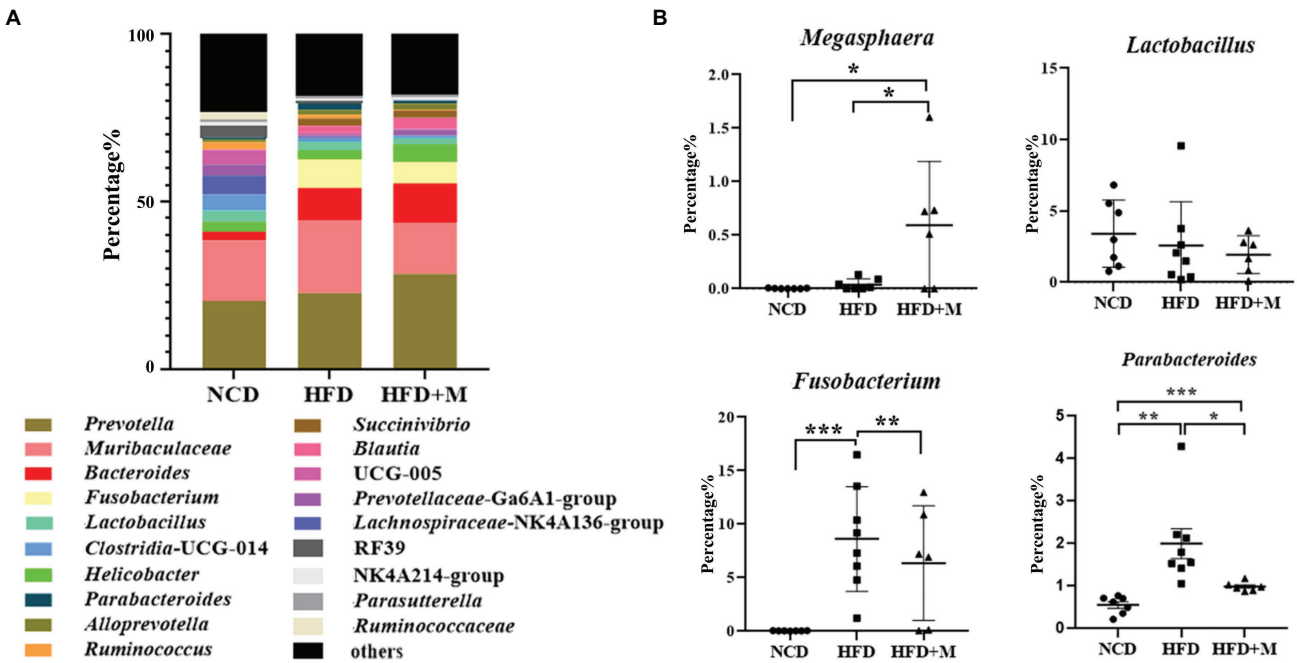

FIGURE 8 | Relative abundances of gut microbiota at genus level in different rat groups. **(A)** The most abundant genera (top 20) of the gut microbiota in SD rats of different groups. **(B)** The relative abundance of *Megasphaera*, *Lactobacillus*, *Parabacteroides,* and *Fusobacterium* in fecal microbiota. NCD, Normal Chow Diet rats; HFD, HFD rats; HFD + M, HFD rats received fecal microbiota transplant from HFD-T monkeys. *, $p < 0.05$; **, $p < 0.01$; ***, $p < 0.001$.

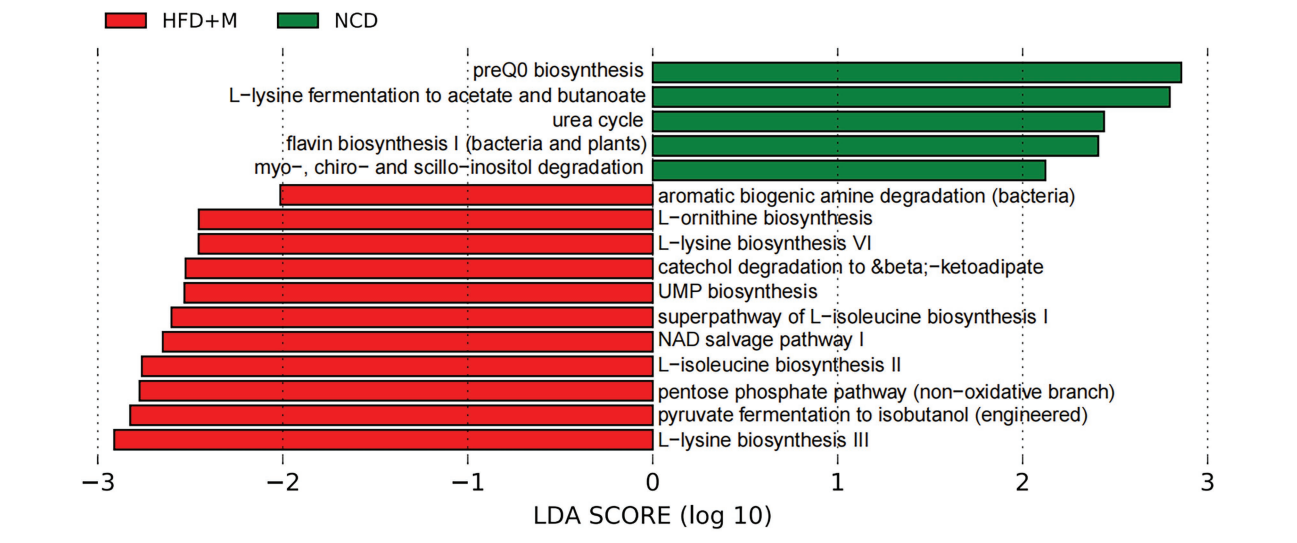

FIGURE 9 | LEfSe analysis of microbial functions predicted by PICRUSt in different rat groups. NCD, Normal Chow Diet rats; HFD, HFD rats; HFD + M, HFD rats received fecal microbiota transplant from HFD-T monkeys; LDA, linear discriminant analysis (LDA); LEfSe, linear discriminant analysis effect size.

DISCUSSION

HLP is considered an important risk factor for cardiovascular diseases (CVDs). More than 17.9 million people died from CVDs in 2019, representing 32% of all deaths worldwide (Roth et al., 2020). However, emerging evidence shows that gut microbiota plays an important role the host's energy metabolism and blood lipid level modulation (Velagapudi et al., 2010; Mestdagh et al., 2012). Therefore, we developed an NHP HLP model with high similarity to humans in genetics, physiology, and gut microbial composition, for analysis of the effect of gut microbiota on the host's blood lipids. A unique and interesting feature of such an NHP model was that 40% of the monkeys in our study developed tolerance to HFD with normal lipid profiles after prolonged exposure. Such an NHP model provided a unique tool to investigate changes in the gut microbiota related to the development of HFD tolerance.

Previous studies have demonstrated that multiple species of *Lactobacillus* can reduce serum cholesterol, TG, and LDL-C, and have been used in clinical practice as potential probiotics (Zhou et al., 2013; Singh et al., 2015; Jiang et al., 2019; Qian et al., 2019). In the current study, we found that *Lactobacillus* (such as *Lactobacillus johnsoni* and *L. reuteri*) was significantly increased in HFD-T monkeys with TC and LDL-C returning to the normal level. However, after transplantation of fecal microbiota from HFD-T monkeys to HFD rats, *Lactobacillus* showed no significant change in HFD + M rats. Therefore, *Lactobacillus* might not be the major microbial microbe responsible for the reduction of serum lipids in the HFD + M rats.

In previous studies, *Parabacteroides* showed a beneficial effect against weight gain, hyperglycemia, hepatic steatosis, and HLP (Wang et al., 2019). However, the relative abundance of *Parabacteroides* was also significantly decreased in HFD + M rats. HFD rats showed the highest relative abundance of *Parabacteroides*, suggesting that *Parabacteroides* might not play a lipid-lowering effect role in HFD + M rats.

In our previous study, *Megasphaera* was found to be a dominant genus in the primate gut microbiota throughout different life stages and a key driver that contributes to long-term gut microbiota development (Wei et al., 2021). The genus belongs to the family *Veillonellaceae* under the order Veillonellales, class Negativicutes, and phylum Firmicutes (Maki and Looft, 2018). Previous studies have demonstrated that *M. elsdenii* could metabolize lactate and buffer fat and produce acetate, propionate, and butyrate (Chen and Wang, 2016; Chen et al., 2019). These short-chain fatty acids may act through down-regulating cholesterol biosynthesis and increasing the bile acid excretion to regulate the lipid levels (Illman et al., 1988; Marcil et al., 2003; Falcinelli et al., 2015, 2018). Our results found that *Megasphaera*, especially *M. elsdenii*, was a predominant component of the microbiota, and showed a dramatic increase in abundance in HFD-T monkeys. Surprisingly, the relative abundance of *Megasphaera* was also dramatically increased in HFD + M rats and this increasing trend was consistent with changes in the abundance of *Megasphaera* species in monkeys. In contrast, *Megasphaera* is almost undetectable in NCD and HFD rats without fecal microbiota transplantation. Therefore, it is reasonable to speculate that the *Megasphaera* (more likely *M. elsdenii*) successfully colonized in HFD + M rats after fecal microbiota transplantation, and *Megasphaera* might play a critical role in lowering blood lipids in these HLP animals.

Our results also indicated the functional impact of fecal microbiota transplantation from HFD-T monkeys on the gut microbiota in HFD rats, pointing to a potential role of amino acid biosynthesis. Effects of lysine and isoleucine on lipid metabolism have been implicated in previous studies. Dietary lysine restriction in rats was reported to cause lipid accumulation in skeletal muscle (Goda et al., 2021). Branched-chain amino acids leucine and isoleucine were found to reduce lipid accumulation in HFD-induced obese mice (Ma et al., 2020). It reminds a possible mechanism *via* altered biosynthesis of such amino acids in the gut microbiota in improving the host's lipid metabolism.

Our current study demonstrates that changes in the gut microbiota are associated with variation of blood lipid phenotype in both monkeys and rats under HFD feeding. Transplantation of the gut microbiota from HFD-T monkeys alleviated HLP and hepatic steatosis in rats. Further studies are thus warranted to confirm the lipid-lowering and liver-protecting effects of *Megasphaera*, which could be potentially used as a probiotic to lower blood lipids, and improve hepatic steatosis in the treatment of HLP.

DATA AVAILABILITY STATEMENT

The datasets presented in this study can be found in online repositories. The names of the repository/repositories and accession number(s) can be found in the article/ **Supplementary Material**.

ETHICS STATEMENT

The animal study was reviewed and approved by the Institutional Animal Care and Use Committee of Guangdong Landau Biotechnology and Institute of Zoology, Guangdong Academy of Sciences.

AUTHOR CONTRIBUTIONS

J-MG, J-HR, Z-YW, and J-HC designed the study. J-MG, LH, M-TT, T-TZ, J-HL, G-AZ, and Y-XS conducted the experiments. J-MG, Z-YW, and S-YX conducted the data analysis data or performed the statistical analysis. J-MG, GH, J-HC, and J-HR drafted the manuscript. All authors contributed to the article and approved the submitted version.

FUNDING

This study was supported in part by grants from the National Natural Science Foundation of China (no. 31671311), the Guangdong Key Laboratory of Non-human Primate Research (2020B121201006), GDAS' Project of Science and Technology Development (2022GDASZH-2022010110), Guangdong Basic and Applied Basic Research Foundation (2019A1515012062 and 2020A1515010480), Natural Science Foundation of Guangdong Province (2018A030313307), the Program for High-Level Entrepreneurial and Innovative Talents Introduction of Jiangsu Province, the Taihu Lake Talent Plan, and Wuxi Institute of Translational Medicine.

SUPPLEMENTARY MATERIAL

The Supplementary Material for this article can be found online at: https://www.frontiersin.org/articles/10.3389/fmicb.2022.876043/full#supplementary-material

REFERENCES

Blanton, L. V., Charbonneau, M. R., Salih, T., Barratt, M. J., Venkatesh, S., Ilkaveya, O., et al. (2016). Gut bacteria that prevent growth impairments transmitted by microbiota from malnourished children. *Science* 351:10.1126. doi: 10.1126/science.aad3311

Bolyen, E., Rideout, J. R., Dillon, M. R., Bokulich, N. A., Abnet, C. C., Al-Ghalith, G. A., et al. (2019). Reproducible, interactive, scalable and extensible microbiome data science using QIIME 2. *Nat. Biotechnol.* 37, 852–857. doi: 10.1038/s41587-019-0209-9

Breyner, N. M., Michon, C., de SoUnited States, C. S., Vilas Boas, P. B., Chain, F., Azevedo, V. A., et al. (2017). Microbial anti-inflammatory molecule (MAM) from *Faecalibacterium prausnitzii* shows a protective effect on DNBS and DSS-induced colitis model in mice through inhibition of NF-κB pathway. *Front. Microbiol.* 8:114. doi: 10.3389/fmicb.2017.00114

Cani, P. D., and de Vos, W. M. (2017). Next-generation beneficial microbes: The case of *Akkermansia muciniphila*. *Front. Microbiol.* 8:1765. doi: 10.3389/fmicb.2017.01765

Chen, L., Shen, Y., Wang, C., Ding, L., Zhao, F., Wang, M., et al. (2019). *Megasphaera elsdenii* lactate degradation pattern shifts in rumen acidosis models. *Front. Microbiol.* 10:162. doi: 10.3389/fmicb.2019.00162

Chen, L., and Wang, H. (2016). Advances in the metabolism and regulation of lactic acids in the rumen. *Pratacultural Sci.* 33, 972–980.

Clayton, J. B., Vangay, P., Huang, H., Ward, T., Hillmann, B. M., Al-Ghalith, G. A., et al. (2016). Captivity humanizes the primate microbiome. *Proc. Natl. Acad. Sci. U. S. A.* 113, 10376–10381. doi: 10.1073/pnas.1521835113

DeGruttola, A. K., Low, D., Mizoguchi, A., and Mizoguchi, E. (2016). Current understanding of Dysbiosis in disease in human and animal models. *Inflamm. Bowel Dis.* 22, 1137–1150. doi: 10.1097/MIB.0000000000000750

Elkins, C., and Friedrich, D. (2018). Hypertriglyceridemia: A review of the evidence. *Nurse Pract.* 43, 22–29. doi: 10.1097/01.NPR.0000544997.22887.0b

Falcinelli, S., Picchietti, S., Rodiles, A., Cossignani, L., Merrifield, D. L., Taddei, A. R., et al. (2015). *Lactobacillus rhamnosus* lowers zebrafish lipid content by changing gut microbiota and host transcription of genes involved in lipid metabolism. *Sci. Rep.* 5:9336. doi: 10.1038/srep09336

Falcinelli, S., Rodiles, A., Hatef, A., Picchietti, S., Cossignani, L., Merrifield, D. L., et al. (2018). Influence of probiotics administration on gut microbiota core: a review on the effects on appetite control, glucose, and lipid metabolism. *J. Clin. Gastroenterol.* 52, S50–S56. doi: 10.1097/MCG.0000000000001064

Goda, Y., Yamanaka, D., Nishi, H., Masuda, M., Kamei, H., Kumano, M., et al. (2021). Dietary lysine restriction induces lipid accumulation in skeletal muscle through an increase in serum threonine levels in rats. *J. Biol. Chem.* 297:101179. doi: 10.1016/j.jbc.2021.101179

Guo, Z., Zhang, J., Wang, Z., Ang, K. Y., Huang, S., Hou, Q., et al. (2016). Intestinal microbiota distinguish gout patients from healthy humans. *Sci. Rep.* 6, 20602. doi: 10.1038/srep20602

Illman, R. J., Topping, D. L., McIntosh, G. H., Trimble, R. P., Storer, G. B., Taylor, M. N., et al. (1988). Hypocholesterolaemic effects of dietary propionate: studies in whole animals and perfused rat liver. *Ann. Nutr. Metab.* 32, 95–107. doi: 10.1159/000177414

Jiang, J., Feng, N., Zhang, C., Liu, F., Zhao, J., Zhang, H., et al. (2019). *Lactobacillus reuteri A9* and *lactobacillus mucosae A13* isolated from Chinese superlongevity people modulate lipid metabolism in a hypercholesterolemia rat model. *FEMS Microbiol. Lett.* 366:fnz254. doi: 10.1093/femsle/fnz254

Karr, S. (2017). Epidemiology and management of hyperlipidemia. *Am. J. Manag. Care* 23, S139–S148. PMID: 28978219. PMID: 28978219

Langille, M. G., Zaneveld, J., Caporaso, J. G., McDonald, D., Knights, D., Reyes, J. A., et al. (2013). Predictive functional profiling of microbial communities using 16S rRNA marker gene sequences. *Nature Biotechnology* 31, 814–821. doi: 10.1038/nbt.2676

Libby, P., Buring, J. E., Badimon, L., Hansson, G. K., Deanfield, J., Bittencourt, M. S., et al. (2019). Atherosclerosis. *Nat. Rev. Dis. Primers.* 5, 56. doi: 10.1038/s41572-019-0106-z

Ma, Q., Zhou, X., Hu, L., Chen, J., Zhu, J., and Shan, A. (2020). Leucine and isoleucine have similar effects on reducing lipid accumulation, improving insulin sensitivity and increasing the browning of WAT in high-fat diet-induced obese mice. *Food Funct.* 11, 2279–2290. doi: 10.1039/c9fo03084k

Maki, J. J., and Looft, T. (2018). *Megasphaera stantonii sp. nov.*, a butyrate-producing bacterium isolated from the cecum of a healthy chicken. *Int. J. Syst. Evol. Microbiol.* 68, 3409–3415. doi: 10.1099/ijsem.0.002991

Manara, S., Asnicar, F., Beghini, F., Bazzani, D., Cumbo, F., Zolfo, M., et al. (2019). Microbial genomes from non-human primate gut metagenomes expand the primate-associated bacterial tree of life with over 1000 novel species. *Genome Biol.* 20, 299. doi: 10.1186/s13059-019-1923-9

Marcil, V., Delvin, E., Garofalo, C., and Levy, E. (2003). Butyrate impairs lipid transport by inhibiting microsomal triglyceride transfer protein in Caco-2 cells. *J. Nutr.* 133, 2180–2183. doi: 10.1093/jn/133.7.2180

Mestdagh, R., Dumas, M. E., Rezzi, S., Kochhar, S., Holmes, E., Claus, S. P., et al. (2012). Gut microbiota modulate the metabolism of brown adipose tissue in mice. *J. Proteome Res.* 11, 620–630. doi: 10.1021/pr200938v

Nicholson, J. K., Holmes, E., Kinross, J., Burcelin, R., Gibson, G., Jia, W., et al. (2012). Host-gut microbiota metabolic interactions. *Science* 336, 1262–1267. doi: 10.1126/science.1223813

Panahi, Y., Ahmadi, Y., Teymouri, M., Johnston, T. P., and Sahebkar, A. (2018). Curcumin as a potential candidate for treating hyperlipidemia: A review of cellular and metabolic mechanisms. *J. Cell. Physiol.* 233, 141–152. doi: 10.1002/jcp.25756

Parks, D. H., Tyson, G. W., Hugenholtz, P., and Beiko, R. G. (2014). STAMP: statistical analysis of taxonomic and functional profiles. *Bioinformatics* 30, 3123–3124. doi: 10.1093/bioinformatics/btu494

Plovier, H., Everard, A., Druart, C., Depommier, C., Van Hul, M., Geurts, L., et al. (2017). A purified membrane protein from *Akkermansia muciniphila* or the pasteurized bacterium improves metabolism in obese and diabetic mice. *Nat. Med.* 23, 107–113. doi: 10.1038/nm.4236

Qian, Y., Li, M., Wang, W., Wang, H., Zhang, Y., Hu, Q., et al. (2019). Effects of *lactobacillus Casei YBJ02* on lipid metabolism in Hyperlipidemic mice. *J. Food Sci.* 84, 3793–3803. doi: 10.1111/1750-3841.14787

Qin, J., Li, Y., Cai, Z., Li, S., Zhu, J., Zhang, F., et al. (2012). A metagenome-wide association study of gut microbiota in type 2 diabetes. *Nature* 490, 55–60. doi: 10.1038/nature11450

Roth, G. A., Mensah, G. A., and Fuster, V. (2020). The global burden of cardiovascular diseases and risks: A compass for global action. *J. Am. Coll. Cardiol.* 76, 2980–2981. doi: 10.1016/j.jacc.2020.11.021

Segata, N., Izard, J., Waldron, L., Gevers, D., Miropolsky, L., Garrett, W. S., et al. (2011). Metagenomic biomarker discovery and explanation. *Genome Biol.* 12:R60. doi: 10.1186/gb-2011-12-6-r60

Singh, T. P., Malik, R. K., Katkamwar, S. G., and Kaur, G. (2015). Hypocholesterolemic effects of *lactobacillus reuteri LR6* in rats fed on high-cholesterol diet. *Int. J. Food Sci. Nutr.* 66, 71–75. doi: 10.3109/09637486.2014.953450

Tong, X., Xu, J., Lian, F., Yu, X., Zhao, Y., Xu, L., et al. (2018). Structural alteration of gut microbiota during the amelioration of human type 2 diabetes with hyperlipidemia by metformin and a traditional Chinese herbal formula: a multicenter, randomized, open label clinical trial. *mBio.* 9, e02392–e02317. doi: 10.1128/mBio.02392-17

Turnbaugh, P. J., Hamady, M., Yatsunenko, T., Cantarel, B. L., Duncan, A., Ley, R. E., et al. (2009). A core gut microbiome in obese and lean twins. *Nature* 457, 480–484. doi: 10.1038/nature07540

Turnbaugh, P. J., Ley, R. E., Mahowald, M. A., Magrini, V., Mardis, E. R., and Gordon, J. I. (2006). An obesity-associated gut microbiome with increased capacity for energy harvest. *Nature* 444, 1027–1031. doi: 10.1038/nature05414

Velagapudi, V. R., Hezaveh, R., Reigstad, C. S., Gopalacharyulu, P., Yetukuri, L., Islam, S., et al. (2010). The gut microbiota modulates host energy and lipid metabolism in mice. *J. Lipid Res.* 51, 1101–1112. doi: 10.1194/jlr.M002774

Wang, K., Liao, M., Zhou, N., Bao, L., Ma, K., Zheng, Z., et al. (2019). *Parabacteroides distasonis* alleviates obesity and metabolic dysfunctions via production of succinate and secondary bile acids. *Cell Rep.* 26, 222–235.e5. doi: 10.1016/j.celrep.2018.12.028

Wei, Z. Y., Rao, J. H., Tang, M. T., Zhao, G. A., Li, Q. C., Wu, L. M., et al. (2021). Characterization of changes and driver microbes in gut microbiota during healthy aging using a captive monkey model. *Genomics Proteomics Bioinformatics* S1672-0229:00258. doi: 10.1016/j.gpb.2021.09.009

Wood, D. E., Lu, J., and Langmead, B. (2019). Improved metagenomic analysis with kraken 2. *Genome Biol.* 20, 257. doi: 10.1186/s13059-019-1891-0

Zhou, Y., Inoue, N., Ozawa, R., Maekawa, T., Izumo, T., Kitagawa, Y., et al. (2013). Effects of heat-killed *lactobacillus pentosus S-PT84* on postprandial hypertriacylglycerolemia in rats. *Biosci. Biotechnol. Biochem.* 77, 591–594. doi: 10.1271/bbb.120830

Conflict of Interest: The authors declare that the research was conducted in the absence of any commercial or financial relationships that could be construed as a potential conflict of interest.

Publisher's Note: All claims expressed in this article are solely those of the authors and do not necessarily represent those of their affiliated organizations, or those of the publisher, the editors and the reviewers. Any product that may be evaluated in this article, or claim that may be made by its manufacturer, is not guaranteed or endorsed by the publisher.

frontiers | Frontiers in Microbiology

REVIEW
published: 14 April 2022
doi: 10.3389/fmicb.2022.881037

Recent Advances Regarding the Physiological Functions and Biosynthesis of D-Allulose

*Zhou Chen, Xiao-Dong Gao and Zijie Li**

Key Laboratory of Carbohydrate Chemistry and Biotechnology, Ministry of Education, School of Biotechnology, Jiangnan University, Wuxi, China

D-Allulose, a generally regarded as safe (GRAS) sugar, is rare in nature. It is among the most promising sweeteners for future use due to its low caloric content, sucrose-like taste, and unique functions. D-Allulose has many physiological effects, such as antiobesity, antihyperglycemia, antidiabetes, anti-inflammatory, antioxidant, and neuroprotective effects. Therefore, D-allulose has important application value in the food, pharmaceutical, and healthcare industries. However, the high cost of D-allulose production limits its large-scale application. Currently, biotransformation is very attractive for D-allulose synthesis, with the two main methods of biosynthesis being the Izumoring strategy and the DHAP-dependent aldolase strategy. This article reviews recent advances regarding the physiological functions and biosynthesis of D-allulose. In addition, future perspectives on the production of D-allulose are presented.

Keywords: rare sugars, D-allulose, D-allulose 3-epimerase, biosynthesis, aldolases, applications

OPEN ACCESS

Edited by:
Chun Cui,
South China University of Technology, China

Reviewed by:
Youqiang Xu,
Beijing Technology and Business University, China
Xinqiang Xie,
Guangdong Academy of Science, China

****Correspondence:***
Zijie Li
lizijie@jiangnan.edu.cn

Specialty section:
This article was submitted to Food Microbiology, a section of the journal Frontiers in Microbiology

Received: *22 February 2022*
Accepted: *11 March 2022*
Published: *14 April 2022*

Citation:
Chen Z, Gao X-D and Li Z (2022) Recent Advances Regarding the Physiological Functions and Biosynthesis of D-Allulose. Front. Microbiol. 13:881037. doi: 10.3389/fmicb.2022.881037

INTRODUCTION

Recently, the risks of obesity, hyperlipidemia, hypertension, and diabetes have increased rapidly throughout the world due to excessive intake of nutritious diets with high fat and sugar contents. Sucrose, a traditional food sweetener, plays an important role in the food industry due to its sweetness and palatability (Castro-Muñoz et al., 2022). However, sucrose has a few shortcomings, such as its high caloric value, ability to induce hyperglycemic reactions, and diabetes mellitus (Grassi et al., 2021). Therefore, low-calorie sweetener substitutes have aroused researchers' interest (Khan et al., 2021). More than 30 kinds of rare sugars have been reported (Granström et al., 2004). They have unique biological functions and have been used as food additives, cancer cell suppressors, and building blocks for anticancer and antiviral drugs (Zhang et al., 2016b; Li et al., 2017; Guerrero-Wyss et al., 2018; Hoshikawa et al., 2018; Xia et al., 2021). D-Allulose (also called D-psicose) is well known as the most remarkable of rare sugars. It has been more than 20 years since D-allulose was first reported by Ken Izumori (Itoh et al., 1995). It exhibits 70% of the sweetness but only 0.3% of the energy deposition of sucrose. In addition, it has almost no calories (Matsuo et al., 2002). As an industrially important bioproduct, D-allulose was listed as "generally recognized as safe" (GRAS) by the US Food and Drug Administration (FDA) in 2002 and has been approved for use in candy, fruit juices, nutritional supplements, and other dietary products. Therefore, D-allulose has important application value in the food, pharmaceutical, and healthcare industries.

D-Allulose is expected to change the sweetener market because of its low caloric content and palatability, able to compete with other sugar substitutes (sugar alcohols such as xylitol, mannitol, and sorbitol). The commercial price of D-allulose is expected to approach the prices of competing sugar-substituting sweeteners, such as xylitol (US $2–5/kg), mannitol (US $1–5/kg), and sorbitol (US $1–10/kg). D-Allulose will become competitive for large-scale production in the near future, like other sweeteners consumed in the millions of tons per year. At present, the factors restricting the output and price of D-allulose include the high price of starting materials, low yields, and difficulty of isolation. In this article, recent advances regarding the physiological functions and biosynthesis of D-allulose are summarized and discussed.

THE PHYSIOLOGICAL FUNCTIONS OF D-ALLULOSE

The Effect of D-Allulose on Lipid Metabolism

D-Allulose has been reported to have antiobesity activity in animals and humans, through reductions in food intake, fat mass, and adipose tissue weight (Kimura et al., 2017; Bilal et al., 2018). In addition, several evidences suggested that D-allulose could increase energy consumption and reduce fat accumulation in normal rats (Chung et al., 2012; Ochiai et al., 2014).

Although D-allulose can decrease the weight of adipose tissue, the mechanism remains unknown. It can decrease the fatty acid synthase (FSA) activity and increase β-oxidation and carnitine palmitoyltransferase (CPT) activity in epididymal white adipose tissue (WAT; Han et al., 2016). Furthermore, dietary D-allulose can suppress the expression of lipogenesis-related acetyl-CoA carboxylase alpha (ACCα) in epididymal WAT. In addition, dietary D-allulose can stimulate the expression of fatty-acid-oxidation-related AMP-activated protein kinase alpha 2 (AMPKα2), hormone-sensitive lipase (HSL), and peroxisome proliferator activated receptor alpha (PPARα; Chen et al., 2019). Therefore, D-allulose has potential antiobesity properties.

The Antihyperglycemic Effect of D-Allulose

Adequate nutrition has led to rapidly increasing incidences of obesity and obesity-induced type 2 diabetes mellitus (T2DM) around the world, significantly increasing the costs of treating these chronic diseases. Therefore, it is very important to identify effective therapeutic interventions for the treatment of diabetes and its complications. D-Allulose has attracted much attention because of its promising antihyperglycemic properties, being able to control plasma glucose level, body weight, and fat mass (Matsuo and Izumori, 2009; Hossain et al., 2015; Lee et al., 2020). However, the mechanism of its antidiabetes effects remains unclear. It has been speculated that D-allulose affects the levels of blood glucose and insulin secretion or the activities of glucosidase and lipolytic enzymes. D-Allulose has been shown to significantly suppress the increase in plasma glucose concentration induced by sucrose or maltose (Matsuo and Izumori, 2009). In addition, D-allulose has been found to potently inhibit the activities of intestinal sucrase and maltase. The addition of D-allulose (5 g) can significantly suppress the increase in blood glucose induced by oral maltodextrin (75 g) in normal adults. Additionally, oral D-allulose alone does not affect the blood levels of glucose and insulin (Iida et al., 2008). D-Allulose has also been found to inhibit the increase in postprandial blood glucose level, mainly in patients with borderline diabetes, with no side effects or clinical problems observed following 12 weeks of continuous D-allulose intake (Hayashi et al., 2010).

Although several investigations have revealed that D-allulose has antidiabetes activity, the mechanism has yet to be fully elucidated. D-Glucose metabolism in the liver is regulated by the nucleocytoplasmic shift of glucokinase (Hossain et al., 2015). At low glucose levels, glucokinase maintains inactive forms by binding with glucokinase regulatory protein (GKRP), which is recruited in the hepatocyte nucleus. When glucose reaches a high level, glucokinase is activated by separation from the glucokinase-GKRP complex and is translocated from the nucleus to the cytoplasm, where it participates in glycogen metabolism and blood glucose homeostasis (Liu et al., 2012). For example, activation of glucokinase can improve glucose tolerance and insulin sensitivity (Shintani et al., 2017b). Impaired functioning of hepatic glucokinase results in the pathogenesis of hyperglycemia in diabetes (Basu et al., 2001). Therefore, glucokinase is considered a candidate target for antidiabetes drugs (Lloyd et al., 2013). In addition, glucokinase is activated by a variety of fructose phosphates, such as fructose 6-phosphate (F6P) and fructose 1-phosphate (F1P; Pfefferkorn, 2013). D-Allulose 1-phosphate, similar to fructose-1-phosphate, also activates glucokinase. Therefore, D-allulose can increase the utilization of hepatic glucose (Toyoda et al., 2010). Glucose-6-phosphatase (G6Pase) contributes to hyperglycemia in diabetes mellitus and regulates the rate-limiting steps in hepatic gluconeogenic flux (Herling et al., 1998). D-Allulose can regulate blood glucose level and exert hypolipidemic effects by decreasing the activity of G6Pase (Nagata et al., 2015). It has been reported that oral administration of D-allulose can stimulate GLP-1 secretion and thus be used to prevent and treat glucose intolerance (Hayakawa et al., 2018). Recently, D-allulose was confirmed to induce GLP-1 release, activate vagal afferent signaling, reduce feeding, and restrict hyperglycemia in healthy and obese diabetic rats. Furthermore, oral D-allulose can correct arrhythmic overeating, obesity, and diabetes (Iwasaki et al., 2018).

Other Physiological Functions of D-Allulose

D-Allulose exhibits anti-inflammatory effects by suppressing serum levels of proinflammatory cytokines, such as tumor necrosis factor-alpha (TNF-α), interleukin 6 (IL-6), and monocyte chemoattractant protein 1 (MCP-1). These cytokines are derived mainly from visceral adipose tissues (Moller and Berger, 2003; Kim et al., 2017). D-Allulose also has antioxidant effects, scavenging

reactive oxygen species (ROS) to protect 6-hydroxydopamine-induced apoptosis or prevent testicular injury (Takata et al., 2005; Suna et al., 2007). D-Allulose can also extend lifespan by increasing superoxide dismutase (SOD) activity and catalase (CAT) activity (Shintani et al., 2017a). Moreover, D-allulose has been shown to alter serum cholesterol levels in hamsters, in part by reducing proprotein convertase subtilisin/kexin type 9 (Pcsk9) level (Kanasaki et al., 2019). Furthermore, D-allulose could improve systemic and muscle insulin sensitivity in conscious rats (Natsume et al., 2021). Various physiological functions of D-allulose are illustrated in **Figure 1**.

BIOLOGICAL PRODUCTION OF D-ALLULOSE

As described above, D-allulose has many useful physiological functions. However, D-allulose is rare in nature, which greatly restricts its large-scale application. Traditional chemical synthesis of D-allulose usually involves tedious reactions and many side reactions (McDonald, 1967; Doner, 1979). It is difficult to obtain a single configuration of product using chemical methods. In contrast, bioconversion approaches have many advantages, including mild reaction conditions, few byproducts, simple purification steps, and environmentally friendly properties (Zhang et al., 2021). Therefore, biotransformation has gradually become the main method of D-allulose synthesis. At present, the biological preparation of D-allulose is achieved mainly *via* two strategies: (1) the Izumoring strategy and (2) the DHAP-dependent aldolase strategy.

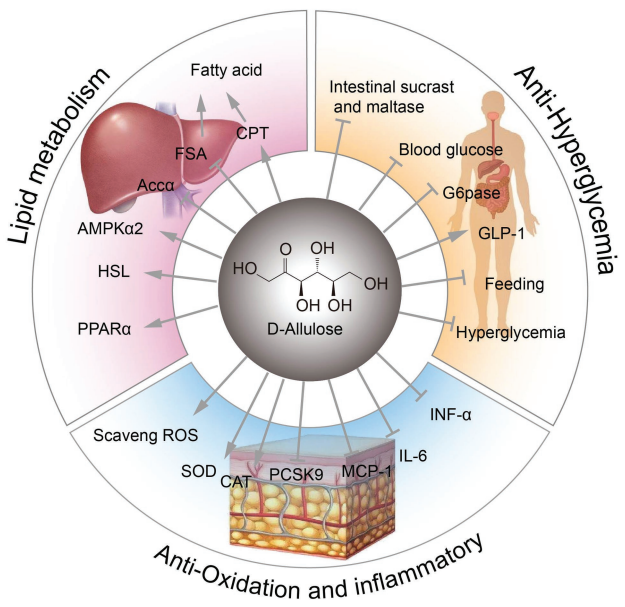

FIGURE 1 | The physiological functions of D-allulose. FSA, fatty acid synthase; CPT, carnitine palmitoyltransferase; ACCα, acetyl-CoA carboxylase alpha; AMPKα, AMP-activated protein kinase alpha; HSL, hormone-sensitive lipase; PPARα, peroxisome proliferator activated receptor alpha; ROS, reactive oxygen species; SOD, superoxide dismutase; CAT, catalase activity; Pcsk9, proprotein convertase subtilisin/kexin type 9; MCP-1, monocyte chemoattractant protein 1; G6Pase, glucose-6-phosphatase.

D-Allulose Production Using the Izumoring Strategy

D-Allulose Production From D-Fructose Using D-Tagatose 3-Epimerase Family Enzymes

The Izumoring strategy is a promising approach for the bioproduction of any kind of hexose sugar and involves D-tagatose 3-epimerases (DTEases), polyol dehydrogenases, and aldose isomerases (Izumori, 2006). In the past few decades, the Izumoring strategy has proven effective for biosynthesizing rare sugars. DTEase family enzymes are the key enzymes for the biosynthesis of D-allulose from D-fructose (**Figure 2**) and include DTEase and D-allulose 3-epimerase (DAEase). DAEase exhibits higher specificity for D-allulose than D-tagatose (Kim et al., 2006). Since the first DTEase from *Pseudomonas cichorii* ST-24 was identified in 1993, other DTEase enzymes were isolated from a variety of species, such as *Agrobacterium tumefaciens* (Kim et al., 2006), *Clostridium Bolteae* (Jia et al., 2014), *Dorea* sp. CAG317 (Zhang et al., 2015), *Ruminococcus* sp. 5_1_39BFAA (Chen et al., 2016), *Treponema primitia* ZAS-1 (Zhang et al., 2016c), *Rhodobacter sphaeroides* (Qi et al., 2017), *Ruminococcus* sp. (Li et al., 2018), *Arthrobacter globiformis* M30 (Yoshihara et al., 2017), *Clostridium cellulolyticum* H10 (Su et al., 2018), *Sinorhizobium* sp. (Zhu et al., 2019b), and *Rhodopirellula baltica* SH 1 (Zhang et al., 2020). Details of the catalytic properties of DTEase-family enzymes from different species are presented in **Table 1**. Itoh et al. (1995) first reported the immobilization of DTEase from *P. cichorii* on chitopearl beads and 90 g D-allulose from 500 g D-fructose was generated. Since then, the methods for DTEase immobilization have attracted extensive interest (Lim et al., 2009; Tseng et al., 2014; Narayan Patel et al., 2018), and the immobilized enzymes exhibited improved thermal stability and storage stability.

Biosynthesis of D-Allulose From Inexpensive Materials Based on DTEase Enzymes

Currently, agricultural byproducts, such as fruit and vegetable residue, are generating major agricultural problems (Lai et al., 2017). Agricultural residues are usually buried in landfills or incinerated (Park and Yoon, 2015). However, these residues contain large amounts of dietary fibers and sugars, including sucrose, D-glucose, and D-fructose. The conversion of dietary fiber and sugars to high value-added products represents a significant step towards alleviating agricultural problems.

Cascade catalysis is considered as a very attractive approach compared with traditional step-by-step synthesis. This strategy is often used to produce rare sugars from inexpensive materials, such as sucrose, Jerusalem artichoke, inulin, and fruit/vegetable residues (**Figure 3**; Wagner et al., 2015; Song et al., 2016, 2017; Zhang et al., 2017; Yang et al., 2019; Li et al., 2020a). D-Allulose has been efficiently synthesized from sucrose using purified recombinant invertase, D-xylose isomerase, and DTEase. Moreover, practical integration of a cascade solution with simulated moving bed (SMB) chromatography has been used

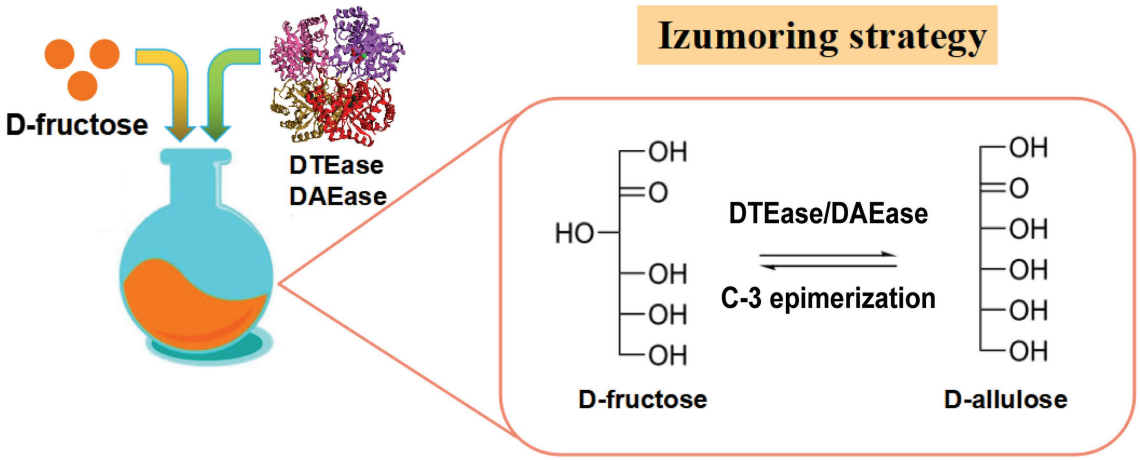

FIGURE 2 | Izumoring strategy for production of D-allulose. DTEase, D-tagatose 3-epimerase; DAEase, D-allulose 3-epimerase.

TABLE 1 | Properties of DTEase family enzymes.

Ketose 3-Epimerases	Enzyme source	pH	Temperature (°C)	Metal ion	Conversion (%)
DAEase (Jia et al., 2014)	*Clostridium Bolteae*	7.0	55	Co^{2+}	29%
DAEase (Zhang et al., 2015)	*Dorea* sp. *CAG317*	6.0	70	Co^{2+}	30%
DAEase (Chen et al., 2016)	*Ruminococcus* sp. *5_1_39BFAA*	8.0	55	Mn^{2+}	29%
DAEase (Zhang et al., 2016c)	Treponema primitiaZAS-1	8.0	70	Co^{2+}	28%
DTEase (Li et al., 2017)	*Ruminococcus* sp.	7.5–8.0	60	Mn^{2+}	26%
DAEase (Yoshihara et al., 2017)	*Arthrobacter globiformis M30*	7.0–8.0	70	Mg^{2+}	24%
DAEase (Su et al., 2018)	*Clostridium cellulolyticum H10*	6.5–8.5	65	Ca^{2+}	28%
DTEase (Zhu et al., 2019b)	*Sinorhizobium* sp.	8.0	50	Mn^{2+}	42.5%
DTEase (Zhang et al., 2020)	*Rhodopirellula baltica* SH 1	7.0	35	Mn^{2+}	25.86%

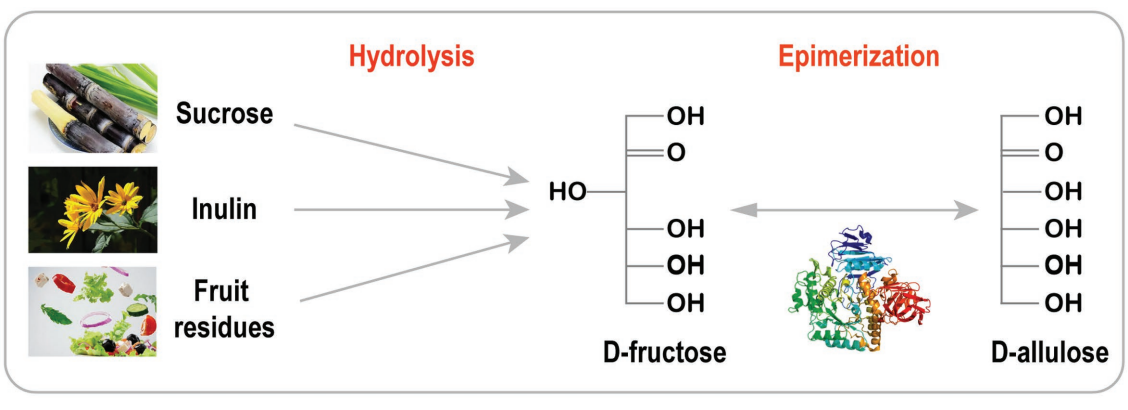

FIGURE 3 | Biosynthesis of D-allulose from inexpensive raw material.

to produce pure D-allulose (99.9%) with very high yields (89%; Wagner et al., 2015). D-Allulose can also be synthesized in a two-step cascade reaction involving Jerusalem artichoke hydrolysis (Song et al., 2017), cruciferous vegetable residue (Song et al., 2016) and inulin (Li et al., 2020a). To decrease production costs and avoid enzyme purification, Zhu et al. developed a one-pot two-enzyme reaction system with a novel exo-inulinase from *Bacillus velezensis* (BvInu) and DAEase from *Ruminococcus* sp. for the production of D-allulose from Jerusalem artichoke. BvInu and DAEase were expressed in *Bacillus subtilis* and secreted into supernatant without purification. Under the optimal ratio of BvInu/RDAE (80:40 U/g inulin) at 50°C for 2 h, 10.3 g/L of D-allulose was obtained from 50 g/L inulin (Zhu et al., 2020).

Biosynthesis of D-Allulose Using Microorganisms

Compared with one-pot cascade reactions, whole-cell biocatalyst reactions have several advantages (**Figure 4**): (1) Cells containing enzymes are easily obtained without tedious purification of enzymes; (2) the cellular context provides a suitable microenvironment and cofactor regeneration (ATP, NAD^+/NADH); (3) the cell walls and membranes protect the enzymes against harsh reaction conditions; and (4) the colocalization of multiple enzymes within the cell enhances the local concentrations of enzymes and decreases the diffusion of intermediates in cascade reactions (Wu and Li, 2018).

Engineered *Escherichia coli* is one of the most commonly used organisms for the production of D-allulose because of its clear background, fast growth rates, simple culture, and stable genetics. DAEase and D-glucose isomerase (GIase) from *Acidothermus cellulolyticus* were coexpressed to produce D-allulose from D-glucose (Zhang et al., 2017). Similarly, DAEase and xylose isomerase (XI) were coexpressed to produce D-allulose with D-glucose as the substrate (Chen et al., 2017). In the above two approaches, D-glucose was first converted to D-fructose by GIase or XI, and then, D-fructose was immediately isomerized to D-allulose by DAEase.

Although good productivity was obtained by engineering *E. coli*, which was not applicable in the food industry because of the endotoxins and their non-food grade classification. To date, DAEase has been successfully expressed in several food-safe strains, such as *B. subtilis*, *Saccharomyces cerevisiae*, and *Corynebacterium glutamicum* (Li et al., 2015b; He et al., 2016). He et al. (2016) displayed DTEase from *Clostridium scindens* ATCC 35704 on the surface of *B. subtilis* spores for the production of D-allulose from D-fructose. DAEase was fused at the C-terminus of CotZ and exhibited high thermostability. After five cycles of utilization, 60% activity was maintained (He et al., 2016). In our previous study, we innovated a spore surface display technique to produce D-allulose from D-glucose. In this approach, the key enzymes XI from *Thermus thermophilus* and DAEase from *A. tumefaciens* were immobilized on *S. cerevisiae* spores using biological and chemical methods, respectively (Li et al., 2015b). In addition, multiple DAEases and invertase (INV) were overexpressed in *C. glutamicum*, and the engineered cells immobilized with alginate were subjected to a cascade reaction in a one-pot, two-step reaction system to generate D-allulose from cane molasses. After reaction for 8 h, 61.2 g/L D-allulose was obtained, which represented 17.4% of the total monosaccharides (Yang et al., 2019). Currently, the Izumoring strategy is the main method for industrial production of D-allulose, which could be achieved by using SMB. Additionally, the separated D-fructose can be reused for D-allulose production. In brief, Izumoring strategy is the most simple and common way to biosynthesize D-allulose. However, the limitation of thermodynamic balance is a bottleneck which restricts the large-scale application of D-allulose in the food industry.

D-Allulose Production Using DHAP-Dependent Aldolases

As mentioned above, various approaches based on the Izumoring strategy have been developed for D-allulose production from inexpensive starting materials, such as Jerusalem artichoke, inulin, and agricultural residues. However, the reaction catalyzed by the key enzyme DAEase is reversible, and the conversion rate is low, which leads to a high price for the resulting D-allulose. Moreover, most strains used in the synthesis of D-allulose are not GRAS microorganisms. Therefore, it is extremely important to construct a cost-efficient and safe platform for the mass production of D-allulose.

Stereoselective aldol additions catalyzed by aldolases have become an essential tool for C-C asymmetric synthesis (Iturrate et al., 2010). Among the members of the aldolase family, DHAP-dependent aldolases are the most widely used for the synthesis of many carbohydrate compounds that are difficult

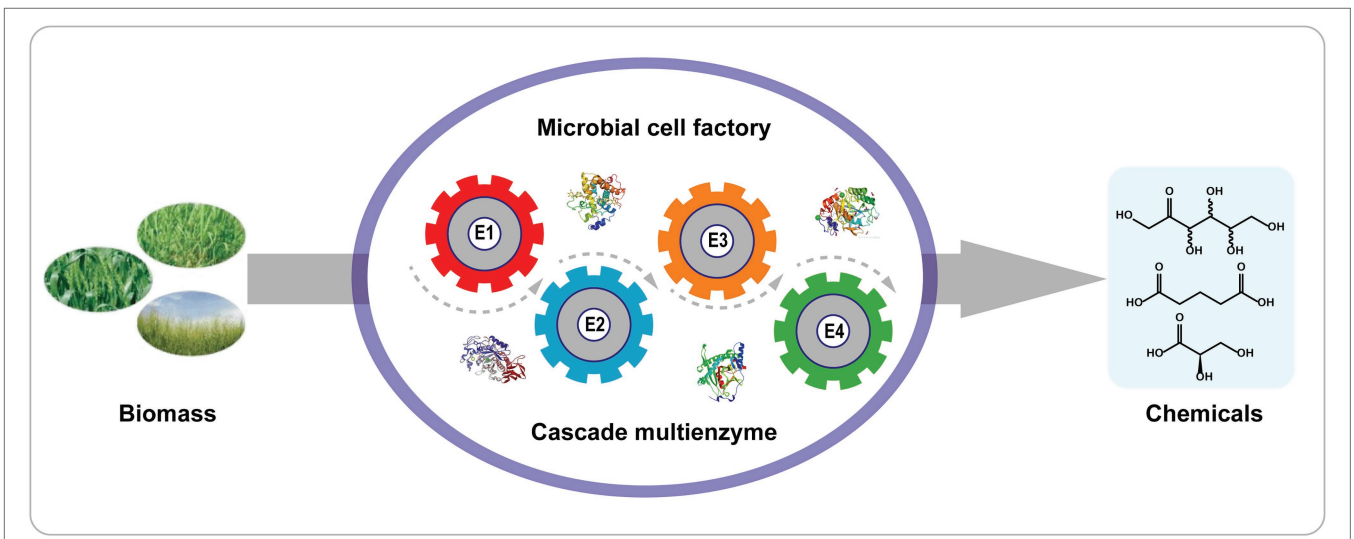

FIGURE 4 | Cascade biotransformation with a single recombinant cell. E1–E4 represent enzyme 1–4.

to synthesize by traditional chemical methods (Bosshart et al., 2013). There are four types of DHAP-dependent aldolases: L-rhamnulose-1-phosphate aldolase (RhaD), L-fuculose-1-phosphate aldolase (FucA), D-fructose-1,6-bisphosphate aldolase (FruA), and D-tagatose-1,6-bisphosphate aldolase (TagA). Stereoselective aldol reactions of these four aldolases are complementary to each other. In theory, a set of four ketoses can be obtained by using DHAP as the donor and the same aldehyde as the receptor (Gustavo, 2000). Therefore, DHAP-dependent aldolases are highly suitable for the synthesis of various rare sugars (including D-allulose, D-sorbose, D-tagatose, and L-fructose) due to their unique stereoselectivities (**Figure 5**; Brovetto et al., 2011; Dai et al., 2021).

Biosynthesis of D-Allulose Using RhaD Aldolase With D-Glyceraldehyde as the Acceptor

A main disadvantage of DHAP-dependent aldolase strategies is that the donor substrate DHAP is very expensive and unstable for large-scale synthesis (Schümperli et al., 2007). However, there are several routes for DHAP synthesis *via* enzymatic strategies. For instance, DHAP can be obtained *via* dihydroxyacetone (DHA), glycerol or glycerol 3-phosphate or through metabolic pathways from an inexpensive raw material, such as glucose or glycerol (**Figure 6**; Sánchez-Moreno et al., 2004; Li et al., 2012, 2015a; Wei et al., 2015; Yang et al., 2015, 2016). In engineered *E. coli*, catalysis of the aldol reaction by RhaD to synthesize rare sugars (D-allulose and D-sorbose) has been achieved using glucose as the carbon source and a continuous supply of D-glyceraldehyde into the medium. Following optimization of fermentative conditions, the isolated yield of D-allulose and D-sorbose was 0.21 mol/mol D-glyceraldehyde (Wei et al., 2015). D-Allulose and D-sorbose have been produced in a GRAS *C. glutamicum* strain with glucose and D-glyceraldehyde as feedstocks. The recombinant *C. glutamicum* strains harboring RhaD and fructose-1-phosphatase (YqaB) have been found to accumulate 19.5 g/L of D-sorbose and 13.4 g/L of D-allulose in a fed batch fermentation (Yang et al., 2015). In addition, D-allulose and D-sorbose have been produced in a recombinant *E. coli* strain overexpressing aldolase RhaD and YqaB from glycerol by fermentation. After 15 h of fermentation, the concentrations of D-sorbose (1.6 g/L) and D-allulose (1.23 g/L) were determined in the supernatant (Li et al., 2015a). Recently, our group constructed an efficient system for whole-cell cascade synthesis of D-sorbose and D-allulose from glycerol and D-glyceraldehyde, which yielded 15.3 g/L of D-sorbose and 6.4 g/L of D-allulose in a batch biotransformation (Chen et al., 2020a).

Biosynthesis of D-Allulose From Glycerol as the Sole Substrate

A microorganism platform for D-allulose synthesis based on aldolase RhaD would hold much promise for large-scale production. The main challenge is the high cost of the donor substrate DHAP and acceptor molecule D-glyceraldehyde. Fortunately, the problem of how to accumulate DHAP using the inexpensive industrial byproduct glycerol as a "green" carbon source has been solved. Thus, the next issue is to identify a novel enzyme to convert low-value glycerol to D-glyceraldehyde. A glycerol dehydrogenase or glycerol oxidase that can efficiently catalyze glycerol to D-glyceraldehyde is needed.

To address this issue, our group constructed a platform for the whole-cell cascade synthesis of D-sorbose and D-allulose from glycerol as the sole substrate. In this system (**Figure 7**), the donor substrate DHAP is generated by the glycerol assimilation pathway, and the endogenous DHAP is produced *via* overexpression of glycerol kinase (GK) and glycerol phosphate oxidase (GPO). The acceptor D-glyceraldehyde is directly generated from glycerol by alditol oxidase from *Streptomyces coelicolor* A3 ($AldO_{S.coe}$). Then, RhaD catalyzes the aldol reaction between DHAP and D-glyceraldehyde to form the corresponding ketose-1-phosphate. Finally, D-sorbose and D-allulose are obtained by removing the phosphate group by YqaB phosphatase. Using this system, the production yields of D-sorbose and D-allulose were enhanced approximately 1.7-fold and 1.2-fold after the overexpression of peroxidase (Prx02 or KatE) to eliminate the harmful effects of H_2O_2. A total of 7.9 g/L of D-sorbose and D-allulose was obtained from glycerol, with a total conversion rate of 17.7% (Chen et al., 2020b).

Our group also constructed a one-pot multienzyme system for the synthesis of D-sorbose and D-allulose from glycerol as the sole carbon source (**Figure 8**). Here, acid phosphatase PhoN from *Shigella flexneri* (PhoN-Sf) was introduced to the system instead of GK and YqaB, which catalyzed the phosphorylation reaction of glycerol in the first step and helped

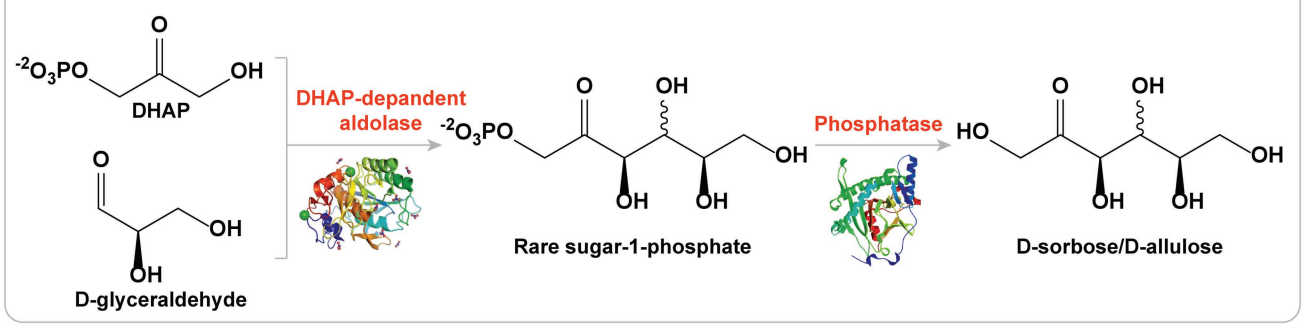

FIGURE 5 | DHAP-dependent aldolases strategy for the production of D-allulose.

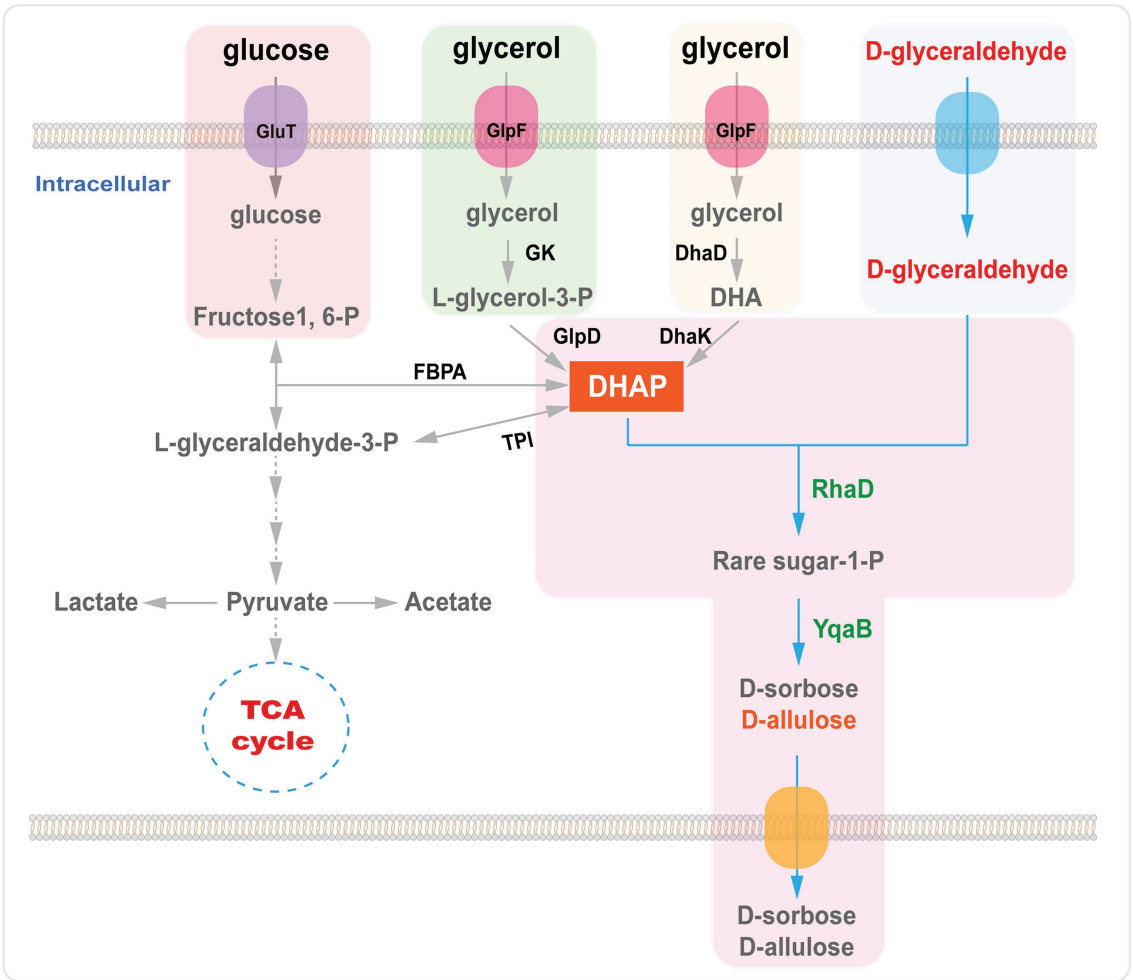

FIGURE 6 | Biosynthesis of D-allulose using RhaD aldolase from glycerol or glucose. GlpF, glycerol transporter; GK, glycerol kinase; GlpD, glycerol 3-phosphate dehydrogenase; DhaD, glycerol dehydrogenase; DhaK, dihydroxyacetone kinases; FBPA, fructose 1, 6-diphosphate aldolase; TPI, triose phosphate isomerase; RhaD, L-rhamnulose-1-phosphate aldolase; YqaB, fructose-1-phosphatase.

recycle the phosphate of ketose-1-phosphate in the last step to provide free rare-sugar molecules. $AldO_{S.coe}$ was introduced to the above multienzyme cascade to synthesize D-sorbose and D-allulose exclusively from the readily available glycerol. Finally, 14.8 g/L of D-sorbose and D-allulose was obtained from glycerol (Li et al., 2020b). The above strategy also represents a very useful and low-cost approach for producing various other rare sugars. In a word, biosynthesis of D-allulose by fermentation based on DHAP-dependent aldolases is very promising. It would be more profitable to construct a cell factory based on DHAP-dependent aldolases strategy for the synthesis of D-allulose.

Thermodynamics-Driven Production of D-Allulose Based on Phosphorylation–Dephosphorylation Strategy

In fact, the above strategies still cannot meet the food industrial demand of D-allulose. Therefore, it is interesting to develop a novel strategy for D-allulose production with highly efficient and low-cost green biomanufacturing. Recently, You et al. constructed an *in vitro* synthetic enzymatic biosystem for D-allulose from inexpensive starch based on "the thermodynamic-driven strategy" (**Figure 9**). This *in vitro* biosystem involved five core enzymes, the reactions occur as follows: (1) maltodextrin (a derivative of starch) was phosphorylated to generate glucose-1-phosphate (G1P) by α-glucan phosphorylase (αGP) with phosphate as co-substrate. (2) G1P was converted to glucose-6-phosphate (G6P) catalyzed by phosphoglucomutase (PGM). (3) G6P was converted to fructose-6-phosphate (F6P) catalyzed by phosphoglucose isomerase (PGI). (4) F6P was epimerized to generate D-allulose-6-phosphate (A6P) catalyzed by D-allulose 6-phosphate 3-epimerase (A6PE). (5) A6P was dephosphorylated to generate D-allulose and phosphate catalyzed by D-allulose-6-phosphate phosphatase (A6PP). Besides, the other four auxiliary enzymes [isoamylase (IA), 4-α-glucanotransferase (4GT), polyphosphate glucokinase (PPGK), and glucose isomerase (GI)] were added the reaction system at different timepoints to

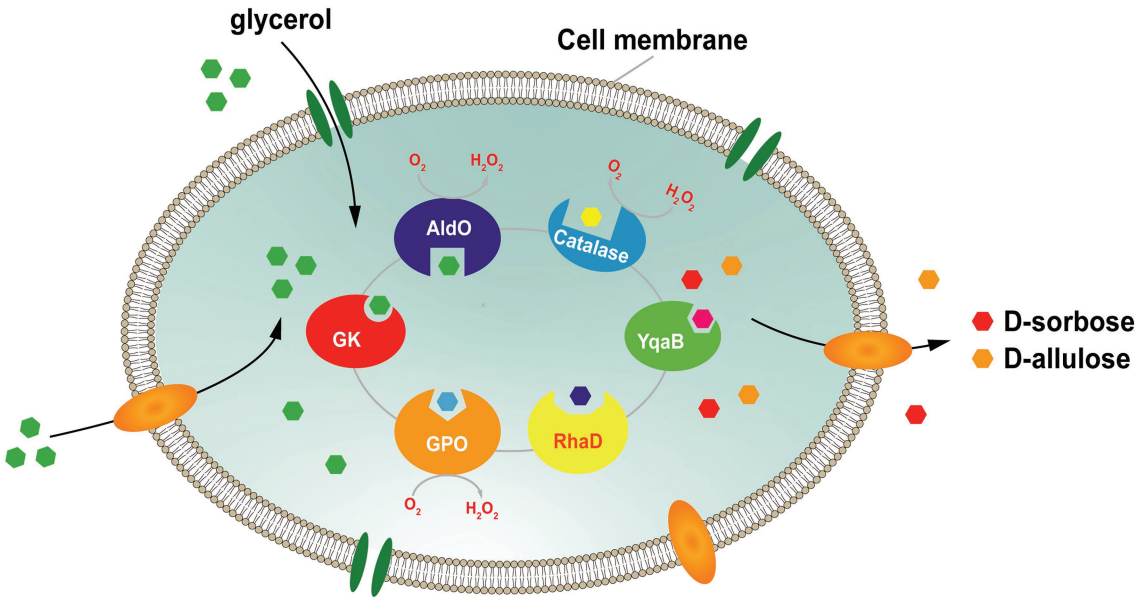

FIGURE 7 | Strategy for the whole-cell synthesis of D-sorbose and D-allulose from glycerol. GK, glycerol kinase; GPO, glycerol oxidase; AldO; alditol oxidase; RhaD, L-rhamnulose-1-phosphate aldolase; YqaB, fructose-1-phosphatase.

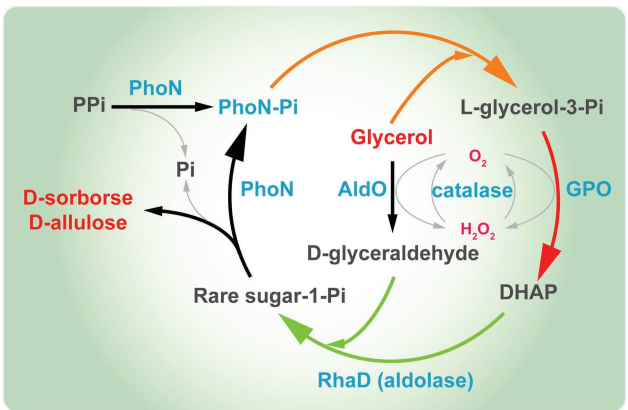

FIGURE 8 | Multienzyme synthesis of D-sorbose and D-allulose from glycerol. PhoN, acid phosphatase; GPO, glycerol oxidase; AldO; alditol oxidase; RhaD, L-rhamnulose-1-phosphate aldolase; DHAP, dihydroxyacetone phosphate.

achieve the complete utilization of maltodextrin for D-allulose production. In this biosystem, the Gibbs energy of A6P dephosphorylation to D-allulose is −15.5 kJ/mol, which is irreversible, indicating that the dephosphorylation step for D-allulose production is thermodynamically favorable and unidirectional to push the overall reaction toward completeness. After the optimization of the reaction conditions, the production yields of D-allulose from 10 and 50 g/L starch reached 88.2 and 79.2%, respectively (Li et al., 2021). All in all, this thermodynamics-driven strategy provides a promising alternative for the cost-efficient production of D-allulose. Due to the system involves multiple enzymes and the steps of enzyme purification are cumbersome, the above strategy still cannot meet the needs of industrialization.

SUMMARY AND FUTURE PERSPECTIVES

The most common method for D-allulose production is based on the Izumoring strategy, which is limited by thermodynamic equilibrium resulting in a low conversion rate and relatively high synthetic cost. Therefore, novel and robust DTEase-family enzymes need to be discovered. Moreover, the strategy of direction evolution (Zhang et al., 2016a; Zhu et al., 2019a) or enzyme immobilization (Ran et al., 2019; Wong et al., 2020) to improve the catalytic performance of DTEase will be very useful. For DHAP-dependent aldolase strategy, D-allulose and D-sorbose are generated simultaneously by RhaD with D-glyceraldehyde as the acceptor. To improve the stereoselectivity of aldolases, various advanced techniques and methods, including directed evolution (d'Oelsnitz and Ellington, 2018; Shepelin et al., 2018; Currin et al., 2021), high-throughput screening techniques (Ung et al., 2018; Rienzo et al., 2021), and rational engineering (Damborsky and Brezovsky, 2014; Windle et al., 2014; Kim et al., 2020), could be adopted. Obviously, thermodynamics-driven strategy is a promising method for D-allulose production. Construction of microbial cell factory using this approach would be a direction in the future. A variety of metabolic tools will contribute to the industrial production of D-allulose, such as CRISPR/Cas9 (Wu et al., 2019; Nishida and Kondo, 2021), self-assembly (Liu et al., 2019; Lange and Polizzi, 2021), and dynamic regulation (Hartline et al., 2021; Zhu et al., 2021). Hopefully, D-allulose will become affordable to ordinary consumers in the near future.

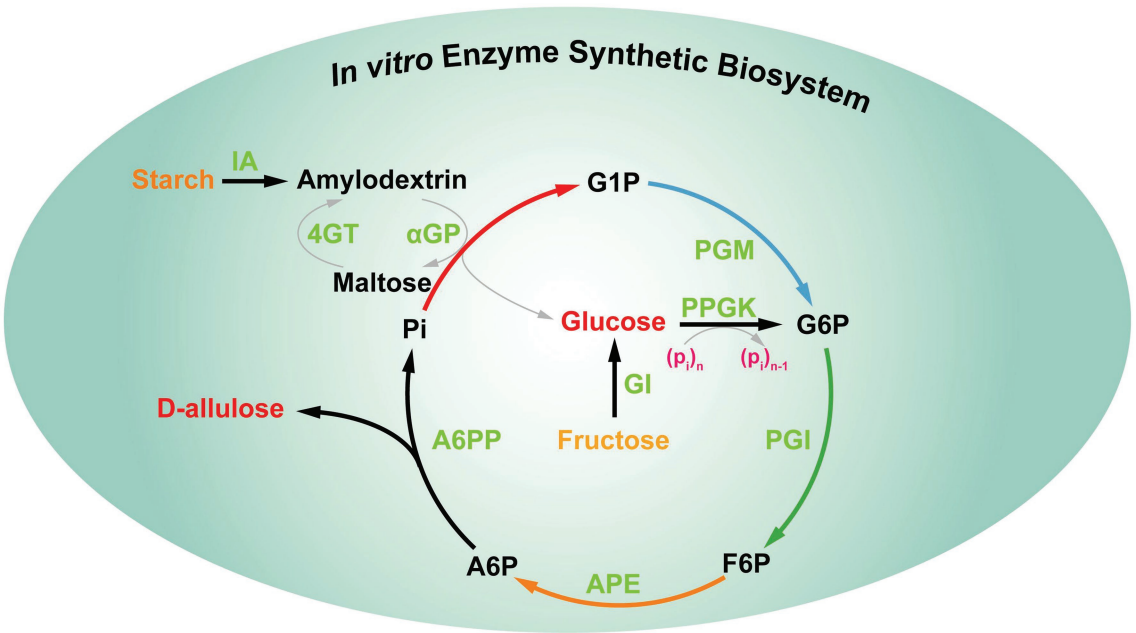

FIGURE 9 | *In vitro* multi-enzyme synthesis of D-allulose from starch. IA, isoamylase; 4GT, 4-α-glucanotransferase; αGP, α-glucan phosphorylase; PGM, phosphoglucomutase; PPGK, polyphosphate glucokinase; PGI, phosphoglucose isomerase; GI, glucose isomerase; APE, D-allulose 6-phosphate 3-epimerase; A6PP, D-allulose 6-phosphate phosphatase; G1P, glucose-1-phosphate; G6P, glucose-6-phosphate; F6P, fructose-6-phosphate; A6P, D-allulose-6-phosphate.

AUTHOR CONTRIBUTIONS

ZC performed data curation and writing—original draft preparation. X-DG was involved in visualization, investigation, and supervision. ZL performed writing—reviewing and editing. All authors contributed to the article and approved the submitted version.

FUNDING

This work was supported by the National Natural Science Foundation of China (nos. 32171475, 31971216), the China Postdoctoral Science Foundation (no. 2021M691285), Shandong Provincial Major Scientific and Technological Innovation Project (no. 2019JZZY011006), Natural Science Foundation of Jiangsu Province (no. BK20210465), and Program of Introducing Talents of Discipline to Universities (no. 111-2-06).

ACKNOWLEDGMENTS

We thank Zhou Xiaoman (Jiangnan University) for drawing.

REFERENCES

Basu, A., Basu, R., Shah, P., Vella, A., Johnson, C. M., Jensen, M., et al. (2001). Type 2 diabetes impairs splanchnic uptake of glucose but does not alter intestinal glucose absorption during enteral glucose feeding: additional evidence for a defect in hepatic glucokinase activity. *Diabetes* 50, 1351–1362. doi: 10.2337/diabetes.50.6.1351

Bilal, M., Iqbal, H. M. N., Hu, H., Wang, W., and Zhang, X. (2018). Metabolic engineering pathways for rare sugars biosynthesis, physiological functionalities, and applications-a review. *Crit. Rev. Food Sci. Nutr.* 58, 2768–2778. doi: 10.1080/10408398.2017.1341385

Bosshart, A., Panke, S., and Bechtold, M. (2013). Systematic optimization of interface interactions increases the thermostability of a multimeric enzyme. *Angew. Chem. Int. Ed. Engl.* 52, 9673–9676. doi: 10.1002/anie.201304141

Brovetto, M., Gamenara, D., Méndez, P. S., and Seoane, G. A. (2011). C-C bond-forming lyases in organic synthesis. *Chem. Rev.* 111, 4346–4403. doi: 10.1021/cr100299p

Castro-Muñoz, R., Correa-Delgado, M., Córdova-Almeida, R., Lara-Nava, D., Chávez-Muñoz, M., Velásquez-Chávez, V. F., et al. (2022). Natural sweeteners: sources, extraction and current uses in foods and food industries. *Food Chem.* 370:130991. doi: 10.1016/j.foodchem.2021.130991

Chen, J., Huang, W., Zhang, T., Lu, M., and Jiang, B. (2019). Anti-obesity potential of rare sugar D-psicose by regulating lipid metabolism in rats. *Food Funct.* 10, 2417–2425. doi: 10.1039/c8fo01089g

Chen, Z., Li, Z., Li, F., Wang, N., and Gao, X.-D. (2020b). Characterization of alditol oxidase from *Streptomyces coelicolor* and its application in the production of rare sugars. *Bioorg. Med. Chem.* 28:115464. doi: 10.1016/j.bmc.2020.115464

Chen, Z., Li, Z., Li, F., Wang, M., Wang, N., and Gao, X.-D. (2020a). Cascade synthesis of rare ketoses by whole cells based on L-rhamnulose-1-phosphate aldolase. *Enzym. Microb. Technol.* 133:109456. doi: 10.1016/j.enzmictec.2019.109456

Chen, X., Wang, W., Xu, J., Yuan, Z., Yuan, T., Zhang, Y., et al. (2017). Production of D-psicose from D-glucose by co-expression of D-psicose 3-epimerase and xylose isomerase. *Enzym. Microb. Technol.* 105, 18–23. doi: 10.1016/j.enzmictec.2017.06.003

Chen, J., Zhu, Y., Fu, G., Song, Y., Jin, Z., Sun, Y., et al. (2016). High-level intra- and extra-cellular production of D-psicose 3-epimerase via a modified xylose-inducible expression system in *Bacillus subtilis*. *J. Ind. Microbiol. Biotechnol.* 43, 1577–1591. doi: 10.1007/s10295-016-1819-6

Chung, Y. M., Hyun Lee, J., Youl Kim, D., Hwang, S. H., Hong, Y. H., Kim, S. B., et al. (2012). Dietary D-psicose reduced visceral fat mass in high-fat diet-induced obese rats. *J. Food Sci.* 77, H53–H58. doi: 10.1111/j.1750-3841.2011.02571.x

Currin, A., Parker, S., Robinson, C. J., Takano, E., Scrutton, N. S., and Breitling, R. (2021). The evolving art of creating genetic diversity: From directed evolution to synthetic biology. *Biotechnol. Adv.* 50:107762. doi: 10.1016/j.biotechadv.2021.107762

Dai, Y., Zhang, J., Jiang, B., Zhang, T., and Chen, J. (2021). New strategy for rare sugars biosynthesis: Aldol reactions using dihydroxyacetone phosphate (DHAP)-dependent aldolases. *Food Biosci.* 44:101377. doi: 10.1016/j.fbio.2021.101377

Damborsky, J., and Brezovsky, J. (2014). Computational tools for designing and engineering enzymes. *Curr. Opin. Chem. Biol.* 19, 8–16. doi: 10.1016/j.cbpa.2013.12.003

d'Oelsnitz, S., and Ellington, A. (2018). Continuous directed evolution for strain and protein engineering. *Curr. Opin. Biotechnol.* 53, 158–163. doi: 10.1016/j.copbio.2017.12.020

Doner, L. W. (1979). Isomerization of D-fructose by base: liquid-chromatographic evaluation and the isolation of D-psicose. *Carbohydr. Res.* 70, 209–216. doi: 10.1016/S0008-6215(00)87101-3

Granström, T. B., Takata, G., Tokuda, M., and Izumori, K. (2004). Izumoring: A novel and complete strategy for bioproduction of rare sugars. *J. Biosci. Bioeng.* 97, 89–94. doi: 10.1016/S1389-1723(04)70173-5

Grassi, B., Onetto, M. T., Zapata, Y., Jofré, P., and Echeverría, G. (2021). Lower versus standard sucrose dose for treating hypoglycemia in patients with type 1 diabetes mellitus in therapy with predictive low glucose suspend (PLGS) augmented insulin pumps: a randomized crossover trial in Santiago, Chile. *Diabetes Metab. Syndr. Clin. Res. Rev.* 15, 695–701. doi: 10.1016/j.dsx.2021.03.017

Guerrero-Wyss, M., Durán Agüero, S., and Angarita Dávila, L. (2018). D-Tagatose is a promising sweetener to control glycaemia: A new functional food. *Biomed. Res. Int.* 2018:8718053. doi: 10.1155/2018/8718053

Gustavo, S. (2000). Enzymatic C-C bond-forming reactions in organic synthesis. *Curr. Org. Chem.* 4, 283–304. doi: 10.2174/1385272003376283

Han, Y., Han, H. J., Kim, A. H., Choi, J. Y., Cho, S. J., Park, Y. B., et al. (2016). D-Allulose supplementation normalized the body weight and fat-pad mass in diet-induced obese mice via the regulation of lipid metabolism under isocaloric fed condition. *Mol. Nutr. Food Res.* 60, 1695–1706. doi: 10.1002/mnfr.201500771

Hartline, C. J., Schmitz, A. C., Han, Y., and Zhang, F. (2021). Dynamic control in metabolic engineering: theories, tools, and applications. *Metab. Eng.* 63, 126–140. doi: 10.1016/j.ymben.2020.08.015

Hayakawa, M., Hira, T., Nakamura, M., Iida, T., Kishimoto, Y., and Hara, H. (2018). Secretion of GLP-1 but not GIP is potently stimulated by luminal D-Allulose (D-Psicose) in rats. *Biochem. Biophys. Res. Commun.* 496, 898–903. doi: 10.1016/j.bbrc.2018.01.128

Hayashi, N., Iida, T., Yamada, T., Okuma, K., Takehara, I., Yamamoto, T., et al. (2010). Study on the postprandial blood glucose suppression effect of D-psicose in borderline diabetes and the safety of long-term ingestion by normal human subjects. *Biosci. Biotechnol. Biochem.* 74, 510–519. doi: 10.1271/bbb.90707

He, W., Jiang, B., Mu, W., and Zhang, T. (2016). Production of D-Allulose with D-psicose 3-epimerase expressed and displayed on the surface of *Bacillus subtilis* spores. *J. Agric. Food Chem.* 64, 7201–7207. doi: 10.1021/acs.jafc.6b03347

Herling, A. W., Burger, H.-J., Schwab, D., Hemmerle, H., Below, P., and Schubert, G. (1998). Pharmacodynamic profile of a novel inhibitor of the hepatic glucose-6-phosphatase system. *Am. J. Phys.* 274, G1087–G1093. doi: 10.2337/diabetes.47.5.85

Hoshikawa, H., Kamitori, K., Indo, K., Mori, T., Kamata, M., Takahashi, T., et al. (2018). Combined treatment with D-allose, docetaxel and radiation inhibits the tumor growth in an in vivo model of head and neck cancer. *Oncol. Lett.* 15, 3422–3428. doi: 10.3892/ol.2018.7787

Hossain, A., Yamaguchi, F., Matsuo, T., Tsukamoto, I., Toyoda, Y., Ogawa, M., et al. (2015). Rare sugar D-allulose: potential role and therapeutic monitoring in maintaining obesity and type 2 diabetes mellitus. *Pharmacol. Therapeut.* 155, 49–59. doi: 10.1016/j.pharmthera.2015.08.004

Iida, T., Kishimoto, Y., Yoshikawa, Y., Hayashi, N., Okuma, K., Tohi, M., et al. (2008). Acute D-psicose administration decreases the glycemic responses to an oral maltodextrin tolerance test in normal adults. *J. Nutr. Sci. Vitaminol.* 54, 511–514. doi: 10.3177/jnsv.54.511

Itoh, H., Sato, T., and Izumori, K. (1995). Preparation of D-psicose from D-fructose by immobilized D-tagatose 3-epimerase. *J. Ferment. Bioeng.* 79, 184–185. doi: 10.1016/0922-338X(95)94091-5

Iturrate, L., Sánchez-Moreno, I., Oroz-Guinea, I., Pérez-Gil, J., and García-Junceda, E. (2010). Preparation and characterization of a bifunctional aldolase/kinase enzyme: a more efficient biocatalyst for C-C bond formation. *Chemistry* 16, 4018–4030. doi: 10.1002/chem.200903096

Iwasaki, Y., Sendo, M., Dezaki, K., Hira, T., Sato, T., Nakata, M., et al. (2018). GLP-1 release and vagal afferent activation mediate the beneficial metabolic and chronotherapeutic effects of D-allulose. *Nat. Commun.* 9:113. doi: 10.1038/s41467-017-02488-y

Izumori, K. (2006). Izumoring: a strategy for bioproduction of all hexoses. *J. Biotechnol.* 124, 717–722. doi: 10.1016/j.jbiotec.2006.04.016

Jia, M., Mu, W., Chu, F., Zhang, X., Jiang, B., Zhou, L. L., et al. (2014). A D-psicose 3-epimerase with neutral pH optimum from *Clostridium bolteae* for D-psicose production: cloning, expression, purification, and characterization. *Appl. Microbiol. Biotechnol.* 98, 717–725. doi: 10.1007/s00253-013-4924-8

Kanasaki, A., Jiang, Z., Mizokami, T., Shirouchi, B., Iida, T., Nagata, Y., et al. (2019). D-allulose alters serum cholesterol levels partly via reducing serum pcsk9 levels in hamsters. *Atherosclerosis* 287:e201. doi: 10.1016/j.atherosclerosis.2019.06.611

Khan, S. A., Verma, P., Ur Rahman, L., and Parasharami, V. A. (2021). "Chapter 13 – Exploration of biotechnological studies in low-calorie sweetener *Stevia rebaudiana*: present and future prospects," in *Medicinal and Aromatic Plants: Expanding Their Horizons Through Omics*. eds. T. Aftab and K. R. Hakeem (Academic Press), 289–324.

Kim, H.-J., Hyun, E.-K., Kim, Y.-S., Lee, Y.-J., and Oh, D.-K. (2006). Characterization of an *agrobacterium tumefaciens* D-psicose 3-epimerase that converts D-fructose to D-psicose. *Appl. Environ. Microbiol.* 72, 981–985. doi: 10.1128/AEM.72.2.981-985.2006

Kim, S.-E., Kim, S. J., Kim, H.-J., and Sung, M.-K. (2017). D-Psicose, a sugar substitute, suppresses body fat deposition by altering networks of inflammatory response and lipid metabolism in C57BL/6J-ob/ob mice. *J. Funct. Foods* 28, 265–274. doi: 10.1016/j.jff.2016.11.029

Kim, T., Stogios, P. J., Khusnutdinova, A. N., Nemr, K., Skarina, T., Flick, R., et al. (2020). Rational engineering of 2-deoxyribose-5-phosphate aldolases for the biosynthesis of (R)-1,3-butanediol. *J. Biol. Chem.* 295, 597–609. doi: 10.1074/jbc.RA119.011363

Kimura, T., Kanasaki, A., Hayashi, N., Yamada, T., Iida, T., Nagata, Y., et al. (2017). D-Allulose enhances postprandial fat oxidation in healthy humans. *Nutrition* 43–44, 16–20. doi: 10.1016/j.nut.2017.06.007

Lai, W. T., Khong, N. M. H., Lim, S. S., Hee, Y. Y., Sim, B. I., Lau, K. Y., et al. (2017). A review: modified agricultural by-products for the development and fortification of food products and nutraceuticals. *Trends Food Sci. Technol.* 59, 148–160. doi: 10.1016/j.tifs.2016.11.014

Lange, O. J., and Polizzi, K. M. (2021). Click it or stick it: covalent and non-covalent methods for protein-self assembly. *Curr. Opin. Syst. Biol.* 28:100374. doi: 10.1016/j.coisb.2021.100374

Lee, D., Han, Y., Kwon, E. Y., and Choi, M. S. (2020). D-allulose ameliorates metabolic dysfunction in C57BL/KsJ-db/db mice. *Molecules* 25:3656. doi: 10.3390/molecules25163656

Li, A., Cai, L., Chen, Z., Wang, M., Wang, N., Nakanishi, H., et al. (2017). Recent advances in the synthesis of rare sugars using DHAP-dependent aldolases. *Carbohydr. Res.* 452, 108–115. doi: 10.1016/j.carres.2017.10.009

Li, Z., Cai, L., Wei, M., and Wang, P. G. (2012). One-pot four-enzyme synthesis of ketoses with fructose 1,6-bisphosphate aldolases from *Staphylococcus carnosus* and rabbit muscle. *Carbohydr. Res.* 357, 143–146. doi: 10.1016/j.carres.2012.05.007

Li, Z., He, B., Gao, Y., and Cai, L. (2015a). Synthesis of D-sorbose and D-psicose by recombinant *Escherichia coli*. *J. Carbohydr. Chem.* 34, 349–357. doi: 10.1080/07328303.2015.1068794

Li, Z., Li, F., Cai, L., Chen, Z., Qin, L., and Gao, X.-D. (2020b). One-pot multienzyme synthesis of rare ketoses from glycerol. *J. Agric. Food Chem.* 68, 1347–1353. doi: 10.1021/acs.jafc.9b06748

Li, Z., Li, Y., Duan, S., Liu, J., Yuan, P., Nakanishi, H., et al. (2015b). Bioconversion of D-glucose to D-psicose with immobilized D-xylose isomerase and D-psicose

3-epimerase on *Saccharomyces cerevisiae* spores. *J. Ind. Microbiol.* 42, 1117–1128. doi: 10.1007/s10295-015-1631-8

Li, C., Lin, J., Guo, Q., Zhang, C., Du, K., Lin, H., et al. (2018). D-Psicose 3-epimerase secretory overexpression, immobilization, and D-psicose biotransformation, separation and crystallization. *J. Chem. Technol. Biotechnol.* 93, 350–357. doi: 10.1002/jctb.5360

Li, Y., Shi, T., Han, P., and You, C. (2021). Thermodynamics-driven production of value-added D-allulose from inexpensive starch by an in vitro enzymatic synthetic biosystem. *ACS Catal.* 11, 5088–5099. doi: 10.1021/acscatal.0c05718

Li, W., Zhu, Y., Jiang, X., Zhang, W., Guang, C., and Mu, W. (2020a). One-pot production of D-allulose from inulin by a novel identified thermostable exoinulinase from *Aspergillus piperis* and *Dorea* sp. D-allulose 3-epimerase. *Process Biochem.* 99, 87–95. doi: 10.1016/j.procbio.2020.08.021

Lim, B. C., Kim, H. J., and Oh, D. K. (2009). A stable immobilized D-psicose 3-epimerase for the production of D-psicose in the presence of borate. *Process Biochem.* 44, 822–828. doi: 10.1016/j.procbio.2009.03.017

Liu, S., Ammirati, M. J., Song, X., Knafels, J. D., Zhang, J., Greasley, S. E., et al. (2012). Insights into mechanism of glucokinase activation: observation of multiple distinct protein conformations. *J. Biol. Chem.* 287, 13598–13610. doi: 10.1074/jbc.M111.274126

Liu, Z., Cao, S., Liu, M., Kang, W., and Xia, J. (2019). Self-assembled multienzyme nanostructures on synthetic protein scaffolds. *ACS Nano* 13, 11343–11352. doi: 10.1021/acsnano.9b04554

Lloyd, D. J., St Jean, D. J., Kurzeja, R. J., Wahl, R. C., Michelsen, K., Cupples, R., et al. (2013). Antidiabetic effects of glucokinase regulatory protein small-molecule disruptors. *Nature* 504, 437–440. doi: 10.1038/nature12724

Matsuo, T., and Izumori, K. (2009). D-Psicose inhibits intestinal alpha-glucosidase and suppresses the glycemic response after ingestion of carbohydrates in rats. *J. Clin. Biochem. Nutr.* 45, 202–206. doi: 10.3164/jcbn.09-36

Matsuo, T., Suzuki, H., Hashiguchi, M., and Izumori, K. (2002). D-psicose is a rare sugar that provides no energy to growing rats. *J. Nutr. Sci. Vitaminol.* 48, 77–80. doi: 10.3177/jnsv.48.77

McDonald, E. J. (1967). A new synthesis of D-psicose (D-ribo-hexulose). *Carbohydr. Res.* 5, 106–108. doi: 10.1016/0008-6215(67)85014-6

Moller, D., and Berger, J. (2003). Role of PPARs in the regulation of obesity-related insulin sensitivity and inflammation. *Int. J. Obes.* 27, S17–S21. doi: 10.1038/sj.ijo.0802494

Nagata, Y., Kanasaki, A., Tamaru, S., and Tanaka, K. (2015). D-psicose, an epimer of D-fructose, favorably alters lipid metabolism in Sprague–Dawley rats. *J. Agric. Food Chem.* 63, 3168–3176. doi: 10.1021/jf502535p

Narayan Patel, S., Singh, V., Sharma, M., Sangwan, R. S., Singhal, N. K., and Singh, S. P. (2018). Development of a thermo-stable and recyclable magnetic nanobiocatalyst for bioprocessing of fruit processing residues and D-allulose synthesis. *Bioresour. Technol.* 247, 633–639. doi: 10.1016/j.biortech.2017.09.112

Natsume, Y., Yamada, T., Iida, T., Ozaki, N., Gou, Y., Oshida, Y., et al. (2021). Investigation of D-allulose effects on high-sucrose diet-induced insulin resistance via hyperinsulinemic-euglycemic clamps in rats. *Heliyon* 7:e08013. doi: 10.1016/j.heliyon.2021.e08013

Nishida, K., and Kondo, A. (2021). CRISPR-derived genome editing technologies for metabolic engineering. *Metab. Eng.* 63, 141–147. doi: 10.1016/j.ymben.2020.12.002

Ochiai, M., Onishi, K., Yamada, T., Iida, T., and Matsuo, T. (2014). D-psicose increases energy expenditure and decreases body fat accumulation in rats fed a high-sucrose diet. *Int. J. Food Sci. Nutr.* 65, 245–250. doi: 10.3109/09637486.2013.845653

Park, S. Y., and Yoon, K. Y. (2015). Enzymatic production of soluble dietary fiber from the cellulose fraction of Chinese cabbage waste and potential use as a functional food source. *Food Sci. Biotechnol.* 24, 529–535. doi: 10.1007/s10068-015-0069-0

Pfefferkorn, J. A. (2013). Strategies for the design of hepatoselective glucokinase activators to treat type 2 diabetes. *Expert. Opin. Drug. Discov.* 8, 319–330. doi: 10.1517/17460441.2013.748744

Qi, Z., Zhu, Z., Wang, J.-W., Li, S., Guo, Q., Xu, P., et al. (2017). Biochemical analysis and the preliminary crystallographic characterization of D-tagatose 3-epimerase from *Rhodobacter sphaeroides*. *Microb. Cell Factories* 16:193. doi: 10.1186/s12934-017-0808-4

Ran, G., Tan, D., Zhao, J., Fan, F., Zhang, Q., Wu, X., et al. (2019). Functionalized polyhydroxyalkanoate nano-beads as a stable biocatalyst for cost-effective production of the rare sugar D-allulose. *Bioresour. Technol.* 289:121673. doi: 10.1016/j.biortech.2019.121673

Rienzo, M., Jackson, S. J., Chao, L. K., Leaf, T., Schmidt, T. J., Navidi, A. H., et al. (2021). High-throughput screening for high-efficiency small-molecule biosynthesis. *Metab. Eng.* 63, 102–125. doi: 10.1016/j.ymben.2020.09.004

Sánchez-Moreno, I., Francisco García-García, J., Bastida, A., and García-Junceda, E. (2004). Multienzyme system for dihydroxyacetone phosphate-dependent aldolase catalyzed C–C bond formation from dihydroxyacetone. *Chem. Commun.* 35, 1634–1635. doi: 10.1002/chin.200447149

Schümperli, M., Pellaux, R., and Panke, S. (2007). Chemical and enzymatic routes to dihydroxyacetone phosphate. *Appl. Microbiol. Biotechnol.* 75, 33–45. doi: 10.1007/s00253-007-0882-3

Shepelin, D., Hansen, A. S. L., Lennen, R., Luo, H., and Herrgård, M. J. (2018). Selecting the best: evolutionary engineering of chemical production in microbes. *Genes* 9:249. doi: 10.3390/genes9050249

Shintani, T., Sakoguchi, H., Yoshihara, A., Izumori, K., and Sato, M. (2017a). D-Allulose, a stereoisomer of D-fructose, extends Caenorhabditis elegans lifespan through a dietary restriction mechanism: a new candidate dietary restriction mimetic. *Biochem. Biophys. Res. Commun.* 493, 1528–1533. doi: 10.1016/j.bbrc.2017.09.147

Shintani, T., Yamada, T., Hayashi, N., Iida, T., Nagata, Y., Ozaki, N., et al. (2017b). Rare sugar syrup containing D-allulose but not high-fructose corn syrup maintains glucose tolerance and insulin sensitivity partly via hepatic glucokinase translocation in Wistar rats. *J. Agric. Food Chem.* 65, 2888–2894. doi: 10.1021/acs.jafc.6b05627

Song, Y., Nguyen, Q. A., Wi, S. G., Yang, J., and Bae, H. J. (2016). Strategy for dual production of bioethanol and D-psicose as value-added products from cruciferous vegetable residue. *Bioresour. Technol.* 223, 34–39. doi: 10.1016/j.biortech.2016.10.021

Song, Y., Oh, C., and Bae, H.-J. (2017). Simultaneous production of bioethanol and value-added D-psicose from Jerusalem artichoke (Helianthus tuberosus L.) tubers. *Bioresour. Technol.* 244, 1068–1072. doi: 10.1016/j.biortech.2017.08.079

Su, L., Sun, F., Liu, Z., Zhang, K., and Wu, J. (2018). Highly efficient production of *clostridium cellulolyticum* H10 D-psicose 3-epimerase in *Bacillus subtilis* and use of these cells to produce D-psicose. *Microb. Cell Factories* 17:188. doi: 10.1186/s12934-018-1037-1

Suna, S., Yamaguchi, F., Kimura, S., Tokuda, M., and Jitsunari, F. (2007). Preventive effect of D-psicose, one of rare ketohexoses, on di-(2-ethylhexyl) phthalate (DEHP)-induced testicular injury in rat. *Toxicol. Lett.* 173, 107–117. doi: 10.1016/j.toxlet.2007.06.015

Takata, M. K., Yamaguchi, F., Nakanose, K., Watanabe, Y., Hatano, N., Tsukamoto, I., et al. (2005). Neuroprotective effect of D-psicose on 6-hydroxydopamine-induced apoptosis in rat pheochromocytoma (PC12) cells. *J. Biosci. Bioeng.* 100, 511–516. doi: 10.1263/jbb.100.511

Toyoda, Y., Mori, S., Umemura, N., Futamura, N., Inoue, H., Hata, T., et al. (2010). Suppression of blood glucose levels by D-psicose in glucose tolerance test in diabetic rats. *Jpn. Pharmacol. Ther.* 65, 2888–2894. doi: 10.1021/acs.jafc.6b05627

Tseng, C.-W., Liao, C.-Y., Sun, Y., Peng, C.-C., Tzen, J. T. C., Guo, R.-T., et al. (2014). Immobilization of *clostridium cellulolyticum* D-psicose 3-epimerase on artificial oil bodies. *J. Agric. Food Chem.* 62, 6771–6776. doi: 10.1021/jf502022w

Ung, Y. T., Ong, C. E., and Pan, Y. (2018). Current high-throughput approaches of screening modulatory effects of xenobiotics on cytochrome P450 (CYP) enzymes. *High Throughput.* 7:29. doi: 10.3390/ht7040029

Wagner, N., Bosshart, A., Failmezger, J., Bechtold, M., and Panke, S. (2015). A separation-integrated cascade reaction to overcome thermodynamic limitations in rare-sugar synthesis. *Angew. Chem. Int. Ed. Engl.* 54, 4182–4186. doi: 10.1002/anie.201411279

Wei, M., Li, Z., Li, T., Wu, B., Liu, Y., Qu, J., et al. (2015). Transforming flask reaction into cell-based synthesis: production of polyhydroxylated molecules via engineered *Escherichia coli*. *ACS Catal.* 5, 4060–4065. doi: 10.1021/acscatal.5b00953

Windle, C. L., Müller, M., Nelson, A., and Berry, A. (2014). Engineering aldolases as biocatalysts. *Curr. Opin. Chem. Biol.* 19, 25–33. doi: 10.1016/j.cbpa.2013.12.010

Wong, J. X., Ogura, K., Chen, S., and Rehm, B. H. A. (2020). Bioengineered polyhydroxyalkanoates as immobilized enzyme scaffolds for industrial applications. *Front. Bioeng. Biotechnol.* 8:156. doi: 10.3389/fbioe.2020.00156

Wu, Y., Chen, T., Liu, Y., Tian, R., Lv, X., Li, J., et al. (2019). Design of a programmable biosensor-CRISPRi genetic circuits for dynamic and autonomous dual-control of metabolic flux in *Bacillus subtilis*. *Nucleic Acids Res.* 48, 996–1009. doi: 10.1093/nar/gkz1123

Wu, S., and Li, Z. (2018). Whole-cell cascade biotransformations for one-pot multistep organic synthesis. *ChemCatChem* 10, 2164–2178. doi: 10.1002/cctc.201701669

Xia, Y., Cheng, Q., Mu, W., Hu, X., Sun, Z., Qiu, Y., et al. (2021). Research advances of D-allulose: An overview of physiological functions, enzymatic biotransformation technologies, and production processes. *Foods* 10:2186. doi: 10.3390/foods10092186

Yang, J., Tian, C., Zhang, T., Ren, C., Zhu, Y., Zeng, Y., et al. (2019). Development of food-grade expression system for D-allulose 3-epimerase preparation with tandem isoenzyme genes in *Corynebacterium glutamicum* and its application in conversion of cane molasses to D-allulose. *Biotechnol. Bioeng.* 116, 745–756. doi: 10.1002/bit.26909

Yang, J., Zhu, Y., Li, J., Men, Y., Sun, Y., and Ma, Y. (2015). Biosynthesis of rare ketoses through constructing a recombination pathway in an engineered *Corynebacterium glutamicum*. *Biotechnol. Bioeng.* 112, 168–180. doi: 10.1002/bit.25345

Yang, J., Zhu, Y., Men, Y., Sun, S., Zeng, Y., Zhang, Y., et al. (2016). Pathway construction in *Corynebacterium glutamicum* and strain engineering to produce rare sugars from glycerol. *J. Agric. Food Chem.* 64, 9497–9505. doi: 10.1021/acs.jafc.6b03423

Yoshihara, A., Kozakai, T., Shintani, T., Matsutani, R., Ohtani, K., Iida, T., et al. (2017). Purification and characterization of D-allulose 3-epimerase derived from *Arthrobacter globiformis* M30, a GRAS microorganism. *J. Biosci. Bioeng.* 123, 170–176. doi: 10.1016/j.jbiosc.2016.09.004

Zhang, W., Chen, D., Chen, J., Xu, W., Chen, Q., Wu, H., et al. (2021). D-allulose, a versatile rare sugar: recent biotechnological advances and challenges. *Crit. Rev. Food Sci. Nutr.* doi: 10.1080/10408398.2021.2023091

Zhang, W., Jia, M., Yu, S., Zhang, T., Zhou, L., Jiang, B., et al. (2016a). Improving the thermostability and catalytic efficiency of the D-psicose 3-epimerase from *Clostridium bolteae* ATCC BAA-613 using site-directed mutagenesis. *J. Agric. Food Chem.* 64, 3386–3393. doi: 10.1021/acs.jafc.6b01058

Zhang, W., Li, H., Jiang, B., Zhang, T., and Mu, W. (2017). Production of D-allulose from D-glucose by *Escherichia coli* transformant cells co-expressing D-glucose isomerase and D-psicose 3-epimerase genes. *J. Sci. Food Agric.* 97, 3420–3426. doi: 10.1002/jsfa.8193

Zhang, W., Li, H., Zhang, T., Jiang, B., Zhou, L., and Mu, W. (2015). Characterization of a D-psicose 3-epimerase from *Dorea* sp. CAG317 with an acidic pH optimum and a high specific activity. *J. Mol. Catal. B Enzym.* 120, 68–74. doi: 10.1016/j.molcatb.2015.05.018

Zhang, J., Xu, C., Chen, X., Ruan, X., Zhang, Y., Xu, H., et al. (2020). Engineered *Bacillus subtilis* harbouring gene of D-tagatose 3-epimerase for the bioconversion of D-fructose into D-psicose through fermentation. *Enzym. Microb. Technol.* 136:109531. doi: 10.1016/j.enzmictec.2020.109531

Zhang, W., Yu, S., Zhang, T., Jiang, B., and Mu, W. (2016b). Recent advances in D-allulose: physiological functionalities, applications, and biological production. *Trends Food Sci. Technol.* 54, 127–137. doi: 10.1016/j.tifs.2016.06.004

Zhang, W., Zhang, T., Jiang, B., and Mu, W. (2016c). Biochemical characterization of a D-psicose 3-epimerase from Treponema primitia ZAS-1 and its application on enzymatic production of D-psicose. *J. Sci. Food Agric.* 96, 49–56. doi: 10.1002/jsfa.7187

Zhu, Z., Gao, D., Li, C., Chen, Y., Zhu, M., Liu, X., et al. (2019a). Redesign of a novel D-allulose 3-epimerase from *Staphylococcus aureus* for thermostability and efficient biocatalytic production of D-allulose. *Microb. Cell Factories* 18:59. doi: 10.1186/s12934-019-1107-z

Zhu, Z., Li, C., Liu, X., Gao, D., Wang, X., Tanokura, M., et al. (2019b). Biochemical characterization and biocatalytic application of a novel D-tagatose 3-epimerase from *Sinorhizobium* sp. *RSC Adv.* 9, 2919–2927. doi: 10.1039/C8RA10029B

Zhu, Y., Li, Y., Xu, Y., Zhang, J., Ma, L., Qi, Q., et al. (2021). Development of bifunctional biosensors for sensing and dynamic control of glycolysis flux in metabolic engineering. *Metab. Eng.* 68, 142–151. doi: 10.1016/j.ymben.2021.09.011

Zhu, P., Zeng, Y., Chen, P., Men, Y., Yang, J., Yue, X., et al. (2020). A one-pot two-enzyme system on the production of high value-added D-allulose from Jerusalem artichoke tubers. *Process Biochem.* 88, 90–96. doi: 10.1016/j.procbio.2019.10.006

Conflict of Interest: The authors declare that the research was conducted in the absence of any commercial or financial relationships that could be construed as a potential conflict of interest.

Publisher's Note: All claims expressed in this article are solely those of the authors and do not necessarily represent those of their affiliated organizations, or those of the publisher, the editors and the reviewers. Any product that may be evaluated in this article, or claim that may be made by its manufacturer, is not guaranteed or endorsed by the publisher.

frontiers | Frontiers in Microbiology

ORIGINAL RESEARCH
published: 02 May 2022
doi: 10.3389/fmicb.2022.891387

Gene Mining and Flavour Metabolism Analyses of *Wickerhamomyces anomalus* Y-1 Isolated From a Chinese Liquor Fermentation Starter

Xin Shi[1†], *Xin Wang*[1,2†], *Xiaoge Hou*[1,3], *Qing Tian*[1] and *Ming Hui*[1,2*]

[1]College of Biological Engineering, Henan University of Technology, Zhengzhou, China, [2]Industrial Microorganism Preservation and Breeding Henan Engineering Laboratory, Zhengzhou, China, [3]School of Food and Bioengineering, Henan College of Animal Husbandry Economics, Zhengzhou, China

Luzhou-flavoured liquor is one of Chinese most popular distilled liquors. Hundreds of flavoured components have been detected from this liquor, with esters as its primary flavouring substance. Among these esters, ethyl hexanoate was the main component. As an essential functional microbe that produces ethyl hexanoate, yeast is an important functional microorganism that produces ethyl hexanoate. The synthesis of ethyl hexanoate in yeast mainly involves the lipase/esterase synthesis pathway, alcohol transferase pathway and alcohol dehydrogenase pathway. In this study, whole-genome sequencing of *W. anomalus* Y-1 isolated from a Chinese liquor fermentation starter, a fermented wheat starter containing brewing microorganisms, was carried out using the Illumina HiSeq X Ten platform. The sequence had a length of 15,127,803 bp with 34.56% GC content, encoding 7,024 CDS sequences, 69 tRNAs and 1 rRNA. Then, genome annotation was performed using three high-quality databases, namely, COG, KEGG and GO databases. The annotation results showed that the ko7019 pathway of gene 6,340 contained the Eht1p enzyme, which was considered a putative acyltransferase similar to Eeb1p and had 51.57% homology with two known medium-chain fatty acid ethyl ester synthases, namely, Eht1 and Eeb1. Ethyl hexanoate in *W. anomalus* was found to be synthesised through the alcohol acyltransferase pathway, while acyl-coenzyme A and alcohol were synthesised under the catalytic action of Eht1p. The results of this study are beneficial to the exploration of key genes of ester synthesis and provide reference for the improvement of liquor flavoured.

Keywords: Luzhou-flavoured liquor, *Wickerhamomyces anomalus*, ethyl hexanoate biosynthesis pathway, medium-chain fatty acid ethyl ester, whole genome sequencing

OPEN ACCESS

Edited by:
Yu Xia,
Jiangnan University, China

Reviewed by:
Alessia Cappelli,
University of Camerino, Italy
Zhe Zeng,
Wageningen University and Research, Netherlands

***Correspondence:**
Ming Hui
huiming@haut.edu.cn

[†]*These authors have contributed equally to this work*

Specialty section:
This article was submitted to Food Microbiology, a section of the journal Frontiers in Microbiology

Received: *07 March 2022*
Accepted: *04 April 2022*
Published: *02 May 2022*

Citation:
Shi X, Wang X, Hou X, Tian Q and Hui M (2022) Gene Mining and Flavour Metabolism Analyses of Wickerhamomyces anomalus Y-1 Isolated From a Chinese Liquor Fermentation Starter. Front. Microbiol. 13:891387. doi: 10.3389/fmicb.2022.891387

INTRODUCTION

Luzhou-flavoured liquor, with thousands of years of history, is a typical traditional distilled liquor in China (Zheng et al., 2015a,b; Jin et al., 2017). The fermentation of this liquor involves the use of sorghum as raw material, a mixed steaming process and medium-temperature Daqu as saccharifying and fermentation agent. This liquor has a rich cellar,

sweet, mellow and harmonious fragrance (Qiu et al., 2016). Its main flavour component is ethyl hexanoate, and the right amount of ethyl butyrate, ethyl acetate and ethyl lactate constitute the compound aroma (Wei et al., 2020). These aromas are usually inferred to be formed by the exceptional microbial environment during brewing (Zou et al., 2018). The production of Luzhou-flavoured liquor usually consists of four stages (Liu and Sun, 2018). The first stage is the cultivation of the pit mud. An excellent pit mud is an essential condition for the production of high-quality Luzhou-flavoured liquor (Lu et al., 2020). The second stage is the production of Daqu, as the liquor saccharifying and fermentation agent (Li et al., 2019). Daqu, which resembles a brick in appearance, is a spontaneous fermentation product in an open environment and is an important fermenting agent in the fermentation of liquor (Jin et al., 2017). Daqu contains a variety of microorganisms and a variety of hydrolytic enzymes (Ling et al., 2020). It is generally accepted that the fermentation of liquor is initiated by the interaction of these enzymes, and the activity of these enzymes is an important test indicator in the production process (Zhang et al., 2019). The next stage is brewing, cooking pulverised raw materials, cooling and then the addition of Daqu for saccharification leading to fermentation. Finally, the original liquor is stored and blended to reduce the pungency and irritation of the new liquor. Blending can adjust the proportion of each component in the liquor. The addition of Daqu during the fermentation of Chinese liquor and the influence of different pit mud result in liquor with different flavour substances (He et al., 2019b; Yang et al., 2020). Due to differences in the natural environment, the flavour of Baijiu varies significantly from region to region and the specific action of different microorganisms affects the composition of the enzyme system in the fermentation grains and thus the formation of esters. Daqu provides an important source of microorganisms for the fermentation process and is a key factor in the quality and style of China liquor (He et al., 2019a).

According to the characteristics of liquor fermentation, it can be divided into three stages (Cheng et al., 2017; Yin et al., 2020). The first stage is the primary fermentation stage, which is the production of ethanol. The second stage is the biogenic acid stage. In addition to the generation of alcohol and sugar, a large number of organic acids are produced during this stage. The third stage is the production of aromas, which are produced by the interaction of microorganisms in the pit mud and daqu. The flavour analysis of China liquor revealed that ethanol and water accounted for 98% of the total mass and flavour substances accounted for 2% (Liu and Sun, 2018). Flavour substances mainly include alcohols, esters, aldehydes, ketones, acids, pyrazines, etc. (Hong et al., 2020). Esters account for more than 60% of the total flavour substances, and most esters have a low odour threshold but contribute more to the odour. In addition to this, these esters can affect the taste of China liquor together with acids and alcohols. Different types and concentrations of esters therefore have a crucial influence on the flavour of baijiu. The ester-producing yeast has been identified as one of the important microbe affecting the content of esters in liquor (Xu et al., 2017; Wang et al., 2019).

Studies have shown that esters are synthesised by the lipase/esterase pathway (Wang et al., 2008), alcohol transferase pathway (Wolter et al., 1966) and alcohol dehydrogenase pathway (Kusano et al., 1998). The lipase/esterase synthesis pathway, namely, the esterification reaction pathway, is the most common pathway used to generate esters in liquor (Papamichael, 2013). This process refers to the slow reaction of organic acids and alcohols to form esters. The acyltransferase pathway is the main synthesis pathway of ethyl hexanoate in *Saccharomyces cerevisiae* (Furukawa et al., 2003). The alcohol dehydrogenase pathway is the oxidation of hemiacetals to esters. At present, *Zygosaccharomyces rouxii* (Rojo et al., 2017), *Pichia anomala* (Zhang et al., 2014), *Kluyveromyces marxianus* (Reyes-Sánchez et al., 2020), *Saccharomycopsis fibuligera* (Yang et al., 2020), *Wickerhamomyces anomalus* (Wang et al., 2020) and other yeasts have been reported to have high esterification capacity, but the esterification mechanism of some yeasts has not been revealed. Nowadays, whole-genome sequencing has been a reliable tool for gene annotation and analysis to understand microbial metabolism, and many important results have been achieved (Wang et al., 2018).

In this study, a strain of *Wickerhamomyces anomalus* (named Y-1) with a high yield of ethyl hexanoate was isolated from a Chinese liquor fermentation starter. Then, whole-genome sequencing was performed using the second-generation sequencer, Illumina HiSeq X Ten platform. The obtained genome sequence was assembled and annotated. Genome annotation was performed based on three high-quality databases, namely, the Clusters of Orthologous Groups of proteins (COG), Kyoto Encyclopaedia of Genes and Genomes (KEGG) and Gene Ontology (GO) databases. Finally, the ethyl hexanoate biosynthesis pathway of the *W. anomalus* Y-1 was analysed, facilitating the design and construction of the industrial strains.

MATERIALS AND METHODS

Raw Materials and Culture Medium

The Chinese liquor fermentation starter was provided by Songhe Liquor Co., Ltd. (Zhoukou City, Henan Province, China), the starter is a medium-temperature Daqu and the maximum temperature during the manufacture of Daqu is less than 60°C.

The yeast screening medium consisted of glucose (20 g/l), peptone (5 g/l), agar (20 g/l) and amoxicillin (1 g/l).

The yeast extract peptone dextrose (YEPD) medium contained peptone (20 g/l), yeast extract (10 g/l), glucose (20 g/l) and agar (20 g/l).

The ester production medium consisted of yeast extract (1 g/l), glucose (10 g/l), peptone (20 g/l), $(NH_4)_2SO_4$ (0.1 g/l), KH_2PO_4 (0.1 g/l), $MgSO_4$ (0.1 g/l), $CaCl_2$ (0.1 g/l) and NH_4Cl (0.2 g/l).

The identification medium for esterase production contained yeast extract (3 g/l), peptone (5 g/l), agar (20 g/l) and 0.1% tributyrin.

Screening of Ester-Producing Yeast

Firstly, yeast was isolated from the Chinese liquor fermentation starter. Add daqu (10 g) to 90 ml sterile water. After shaking well, transfer 1 ml mixture to 9 ml pure water, in a dilution ratio of 10^{-2}. According to this method, the solution was diluted to 10^{-3}, 10^{-4} and 10^{-5} in turn. Then, 0.2 ml of the diluted solution was absorbed and spread in the yeast screening medium for each gradient and cultured at 28°C for 2 days. Single colonies were picked and purified on the YEPD plate to screen the ester-producing yeast. The YEPD medium activated the strains preserved on the oblique plane. After activation, the seed solution was inoculated in 100 ml of the ester-producing medium at 10% inoculum size and cultured at 28°C and 120 rpm for 2 days. After yeast culture, the content of total ester in the fermentation broth was determined by the saponification reflux method (Zheng et al., 2015). The screened ester-producing yeast was prepared into the seed liquid, and 2 μl of seed liquid was absorbed and coated on the esterase identification medium with triglyceride and cultured at 28°C for 2 days. Tributyrin is commonly used to screen lipase-producing and esterase-producing strains, and lipase activity is measured by observing the hydrolytic zone on nutrient Agar containing tributyrin (Farooq et al., 2021). In this experiment, by measuring the diameter of yeast colony (d) and the diameter of surrounding transparent ring (D), and calculating their ratio (D/d), to judge the size of yeast ester production capacity.

Identification of Ester-Producing Yeast

The screened strains were streaked on a YPD medium and cultured at 28°C for 2 days. The colony and microscopic morphologies were observed. The DNA was extracted using the Omega Fungal DNA Kit D3390-02 according to the manufacturer's instructions, and high-quality genomic 18SrDNA was obtained for amplification. Electrophoresis and sequencing of the amplified products were performed. The obtained sequences were compared in the NCBI online software BLAST to determine the strain type. The phylogenetic tree was constructed using the N-J method in MEGA 7.0 software.

Strain Culture and Detection of the Flavoured Components

The strain was cultured in the ester-producing medium. For liquid fermentation, 2% seed liquor was inoculated in the medium and complexed at 28°C for 2 days. The fermentation broth was centrifuged at the end of the culture, and the supernatant was taken to detect the flavoured components.

The flavoured components were extracted using a solid-phase microextraction (SPME) method, with divinylbenzene/carboxy on polydimethylsiloxane (50/30 μm) fibre. The fibre was preconditioned in the gas chromatograph (GC) injection port at 250°C for 30 min, as indicated by the manufacturer. For headspace sampling, each sample (5 ml) was placed in a 20 ml vial and determined using solid-phase microextraction (SPME) coupled with GC-mass spectrometry (MS). The SPME fibre was exposed to the headspace at 50°C for 50 min. After sampling, the SPME fibre was introduced into the GC injector and left for 5 min for the thermal desorption of the analytes (Fan et al., 2011).

GC–MS was carried out using a Thermo Scientific Trace 1,300 Gas Chromatograph coupled to a Thermo Scientific ISO 7000 Single Quadrupole Mass Spectrometer selective detector operating in electron impact mode (ionisation voltage of 70 eV; Thermo Fisher Scientific, Waltham, MA, United States). A DB-WAX capillary column (30 m × 0.25 mm i.d., 0.25 μm film thickness, J&W Scientific, USA) was equipped. Ultra-high-purity helium was used as the carrier gas at a constant flow of 1 ml/min. The split ratio was 20:1. The oven temperature was programmed as follows: column temperature starting temperature from 30°C, constant temperature for 1 min; increased rapidly by 4°C to 120°C, constant temperature for 2 min. Then, the SPME fibre volatiles was heated to 210°C at 7°C/min for 6 min. The MS conditions were as follows: ion source temperature, 280°C; transmission line temperature, 215°C; electron ionisation mode, 70 eV; and mass-to-charge (m/z) range, 33–450 in full scan acquisition mode (Ding et al., 2015). The MS spectral database library of the National Institute for Standards and Technology was used to identify the compounds. Tentatively identified compounds also had to fit logically the retention time in the chromatograms. Quantification analysis was performed using 2% n-butyl acetate as an internal standard.

Genome Sequencing

Firstly, the Y-1 strain was cultured in a liquid ester-producing medium to $OD_{600} = 0.7$, and the cell genome was extracted by centrifugation. The DNA was extracted using the Omega Fungal DNA Kit D3390-02 according to the manufacturer's instructions, and NanoDrop was employed to determine the purity and concentration of the samples. The absorbance values at 260 nm and 280 nm were measured. The A_{260}/A_{280} ratio was more significant than 1.8, indicating that the nucleic acid was more excellent than 90%, which can be used for subsequent sequencing. Qualified samples were prepared for database construction and quality inspection. The eligible gene library was sequenced, and the final data were subjected to quality control procedures.

DNA degradation and contamination were detected using 1% agarose gel. A nanophotometer was used to determine DNA purity. DNA concentration was determined by TBS-380 fluorometer (Turner BioSystems Inc., Sunnyvale, CA), and the ultrasonic processor lysed the qualified DNA. The inserted fragment was~350 bp in length. Then, end repair, base addition, sequence adapter addition, purification and PCR amplification were performed to complete the preparation of the 350 bp library. The concentration was diluted to 1 ng/μL for the initial quantification with TBS-380 fluorometer. Then, Agilent 2,100 electrophoresis bioanalyzer was used to verify the size of the inserted fragment of the library, and qPCR was performed to measure the effective quantitative concentration of the library. For the identified libraries, sequencing was performed using Illumina HiSeq X Ten, PE150 (Illumina, San Diego, CA, United States).

Genome Assembly and Annotation

The genome sequence (scaffold) was assembled from clean data that met the requirements after quality control. The assembled sequence was predicted, and the gene information of each sample was obtained (Steinberg et al., 2017). The short sequence assembly software SOAPdenovo v2.04[1] was used to splice multiple k-mer parameters of the optimised sequence, and the optimal assembly result was obtained. After comparing reads to contig, the assembly results were locally assembled and optimised according to paired-end and overlap relationships. The sequencing reads were cut into smaller units, namely, k-mer. Heterozygosity, repeatability, size, presence of plasmids and genome contamination were assessed by calculating the k-mer depth and the ratio of each depth. The coding sequence (CDS) of the genome was predicted to obtain the nucleic acid sequence and amino acid sequence of the functional genes for subsequent functional and phylogenetic analysis (Zhao et al., 2008).

Basic functional annotations were performed on the predicted encoding genes, and functional annotations were performed with three databases (COG, GO and KEGG databases). Gene annotation was mainly based on the protein sequence alignment. The gene sequence was compared with each database to obtain the corresponding functional annotation information. COG is constructed based on the protein sequences of the completed genome sequencing species (Tatusov, 2001). COG databases can be compared for functional annotation, classification and protein evolution analysis of the predicted proteins. GO standardises the biological terms with different language descriptions and facilitates direct communication among scholars (Vesztrocy and Dessimoz, 2017). GO annotation includes the cellular component, molecular function and biological process. The rich pathway information in the KEGG database facilitates a systematic understanding of the biological functions of genes (e.g. metabolic pathways), genetic information and complex biological processes (e.g. cellular processes; Kanehisa, 2017).

RESULTS AND DISCUSSION

Separation Results of Ester-Producing Yeast

Five yeast strains were isolated and purified from the Chinese liquor fermentation starter, and the strains were denoted as Y-1, Y-2, Y-3, Y-4 and Y-5. The strains were activated to prepare the seed solution. The seed solution was inoculated in the ester-producing medium at 10% inoculation and cultured at 28°C for 2 days. Among the five yeast strains, Y-1 had the highest total ester content, which was significantly higher than the other four strains (**Figure 1A**). According to the ratio between the diameter of the transparent circle (D) and the diameter of the colony (d), the esterification capacity of yeast was analysed. The greater the ratio, the greater the esterification capacity (**Figure 1B**). Among the five strains, the Y-1 strain had the most significant ratio of the fine circle diameter to the strain diameter, indicating that the strain had the strongest esterification decomposition and synthesis ability; therefore, the Y-1 strain was selected for follow-up tests.

Morphological Observation and Molecular Identification of *Wickerhamomyces anomalus* Y-1

The colonies of *W. Anomalus* Y-1 were round, indicating a moist, smooth and typical yeast morphology (**Figure 2A**). A bud protruding from one end of the cell was observed under a 40× microscope and gradually divided into single cells (**Figure 2B**).

Scanning electron microscopy shows a bulge like a bud at one end of the cell, and some buds separated from the mother cell to form independent cells (**Figure 2C**). The obtained sequences were submitted to the Gene Bank for homology analysis. The results showed that strain Y-1 was most closely related to *W. anomalus*, so this yeast was *W. anomalus*. The phylogenetic tree was constructed using MEGA7.0 software (**Figure 2D**).

(Represents 1,000 bootstrap copied values calculated by MEGA7. The percentage of replicate trees in which the associated taxa clustered together in the bootstrap test (1,000 replicates) are shown above the branches, 0.5 represents the unit length of the value of the difference between organisms.)

Flavoured Components of *Wickerhamomyces anomalus* Y-1

GC–MS analysis showed that strain Y-1 produced more than 40 flavoured components, including esters, alcohols, acids and aldehydes, of which 86% were esters. The chromatogram of flavoured components from liquid fermentation of strain Y-1 was shown in **Figure 3**. The content of ethyl hexanoate was the highest, accounting for 49.526% of the total flavour components, and the content was 381.75 μg/l, followed by ethyl palmitic acid, ethyl valerate and ethyl caprylic acid，the total volatile substance is 100% (**Supplementary Table S1**). In previous GC–MS analysis, some yeasts also produced esters, but more strains produced ethyl acetate than those that produced ethyl hexanoate (Christian et al., 2014; Zhang et al., 2020). Therefore, Y-1 can produce ethyl hexanoate, which is of great significance to improve the quality of Luzhou-flavoured liquor. In addition to more esters, the Y-1 strain could also produce alcohols, among which phenyl ethanol had the highest relative content, followed by isoamyl alcohol. This yeast could also create a small amount of 1-propanol, isobutanol and other higher alcohols. These alcohols could enhance the distinctive aroma of liquor in the appropriate range.

Y-1 Genome Characteristics

The critical genes related to the metabolic pathway of Y-1 ethyl hexanoate were further studied by whole-genome

[1]https://github.com/topics/soapdenovo

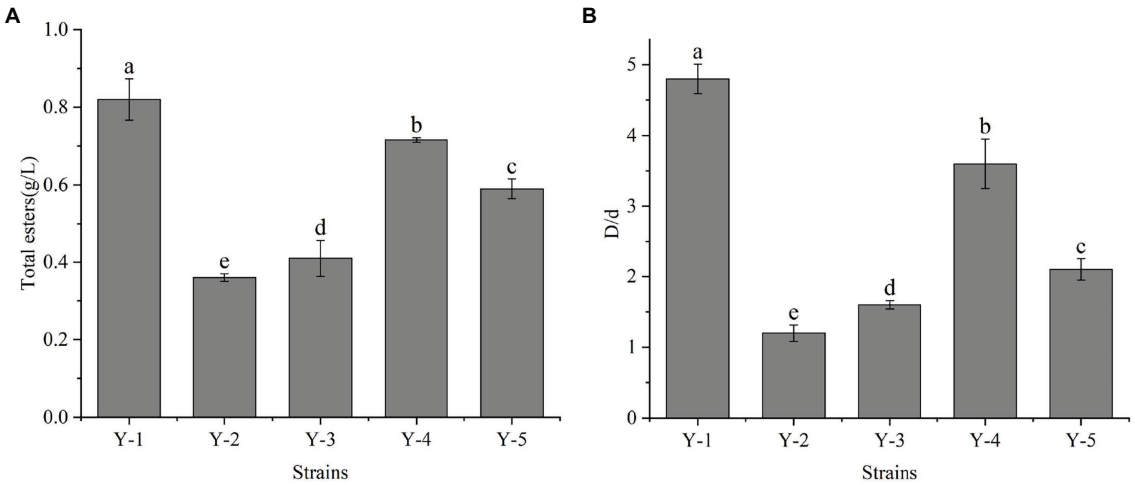

FIGURE 1 | Determination of total ester content **(A)** and esterification ability of yeast **(B)**. Different letters indicate significant differences ($p < 0.05$).

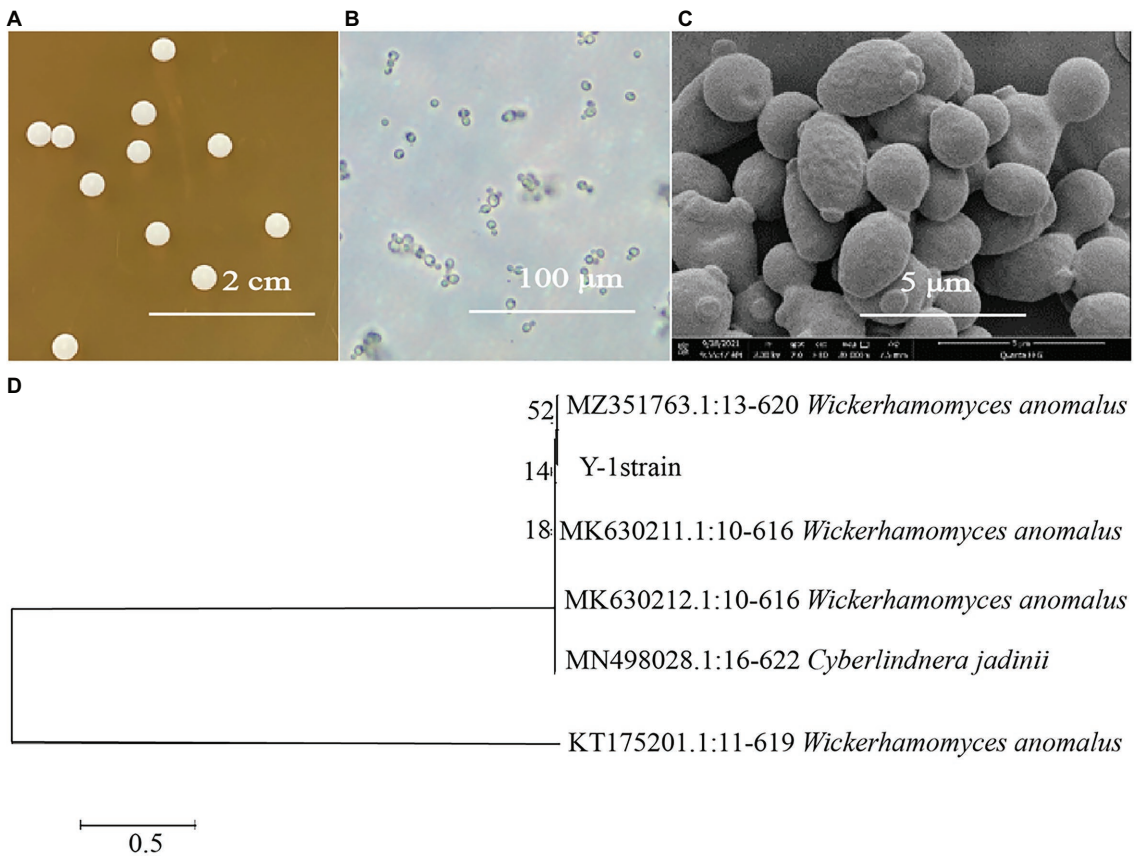

FIGURE 2 | **(A)** Y-1 colony morphology; **(B)** Y-1 morphology under the microscope; **(C)** Y-1 morphology under the scanning electron microscope; and **(D)** A neighbour phylogenetic tree of Y-1 and 5 strains with high homology was established based on the 18S rDNA fragment of Y-1.

prediction. Firstly, PE sequencing reads were used to select the intermediate high-quality sequencing region, and a certain length of K-mer base was taken to assess the genome size (Zhao et al., 2018). After quality control, the assembly results of the samples were analysed with the reads. Several genomic structure prediction software has been developed, such as

Maker2 (Holt and Yandell, 2011), Barrnap 0.4.2[2] and tRNAs can-SE V1.3.1.[3] Maker2 software was used to predict the fungal genes. According to the assembly and prediction results, the genome sequence of strain Y-1 was composed of a chromosome with a total length of 15,127,803 bp (including chromosomes and plasmids). The average GC content of the whole sequence was 34.56%. Using the eukaryotic genome annotation analysis tool (MAKER2 + V2.31.9), 7,024 CDS were annotated, including 69 tRNAs and one rRNA in the whole-genome sequence. Across the whole genome, 3,981 genes had specific pathways compared with the KEGG database, and 5,966 genes had annotated COG information compared with the EggNOG database (**Table 1**). The data of this sequence were submitted to the GeneBank database of the National Biotechnology Information Centre (NCBI) under the name *W. anomalus* Y-1, and the obtained biological project ID was PRJNA770424. These genomic features were similar to other members of the genus *Wickerhamomyces*, such as *Wickerhamomy anomalus* NRRL Y-366\u20138 (GenBank accession number: GCA_001661255.1, genome size 14.15Mbp, GC content 35%, 6,421 CDSs and 154 tRNAs).

[2]https://github.com/tseemann/barrnap
[3]http://lowelab.Ucsc.edu/tRNAsc

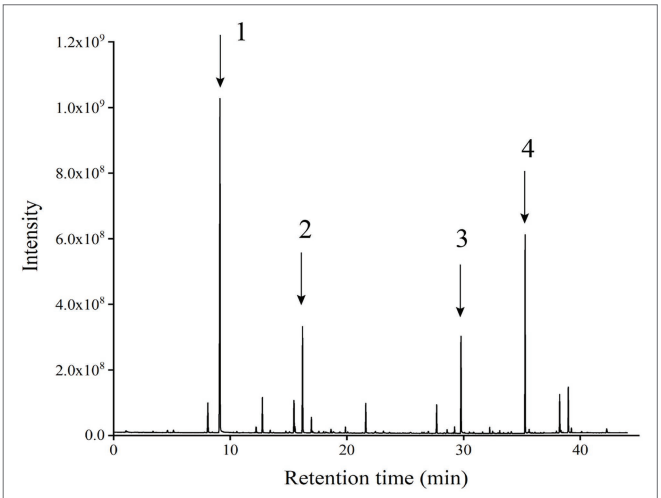

FIGURE 3 | Chromatographic patterns of flavoured components in the liquid fermentation of strain Y-1 (Numbers 1, 2, 3 and 4 represent ethyl hexanoate, ethyl caprylate, phenyl ethanol and ethyl palmitate, respectively).

TABLE 1 | Genome features of strain *Wickerhamomyces anomalus* Y-1.

Sample name	Y-1
Genome size (bp)	15,127,803
Scaffold No.	1,471
GC content (%)	34.56
CDS No.	7,024
Gene total length (bp)	11,118,812
Gene average length (bp)	1,582.97
Genes of KEGG	3,981
Genes of COG	5,966
tRNA No.	69
rRNA No.	1

Genome Annotation Analysis

The genome needed to be annotated on the database to determine the identified gene function and its descriptive information. Genome annotation can reflect the functional classification of the filtered gene set, which is of great significance for the subsequent study of cell growth and metabolism. For genome annotation comparison, three high-quality databases, namely, COG, GO and KEGG, were selected.

The function of Y-1 was studied by annotating the whole genome. Functional analysis was performed using COG (**Figure 4A; Supplementary Tables S2** and **S3**), GO (**Figure 4B; Supplementary Tables S4** and **S5**) and KEGG (**Figure 4C; Supplementary Table S6**). Based on the analysis of three annotated databases, genes with high abundance in the Y-1 genome included amino acid transport and metabolism, carbohydrate transport and metabolism. In the fermentation of Luzhou-flavoured liquor, grains rich in carbohydrates and proteins, such as sorghum and wheat, were used as raw materials. The annotation results showed that the strain could degrade starch, indicating that the strain could adapt to the particular environment of liquor fermentation. Genome annotation is of great significance for future research, especially in exploring the biosynthesis of flavoured compounds in the genome. In addition to the annotations from these three databases, the annotations were based on the Carbohydrate-Active Enzyme Database (Vincent et al., 2014).[4] This database annotates enzymes that can synthesise or decompose complex carbohydrates. According to the amino acid sequence similarity of a protein domain, carbohydrate-active enzymes are divided into different protein families. The classification and related information of the synthesis, metabolism and transport of the carbon compound and other enzymes are provided. The annotated results showed that glycosyltransferases accounted for 43.48%, glycosidases accounted for 36.41%, carbohydrate esterases accounted for 9.78% and coenzymes accounted for 10.33% (**Figure 5**; **Supplementary Table S7**). Among these compounds, carbohydrate esterases were mostly related to the synthesis of esters, such as isoamyl acetate hydrolase (EC3.1.1.-) in the CE12 family annotated by gene 1962 and carboxylesterase (EC3.1.1.1) in the CE1 family annotated by gene 4,180, which played a crucial role in the synthesis and hydrolysis of esters.

DISCUSSION

Two kinds of esters are used in liquor making, namely, acetate and medium-chain fatty acid ethyl ester (MCFA). Acetate mainly includes ethyl acetate, isoamyl acetate and phenyl ethyl acetate.

[4]http://www.cazy.org/

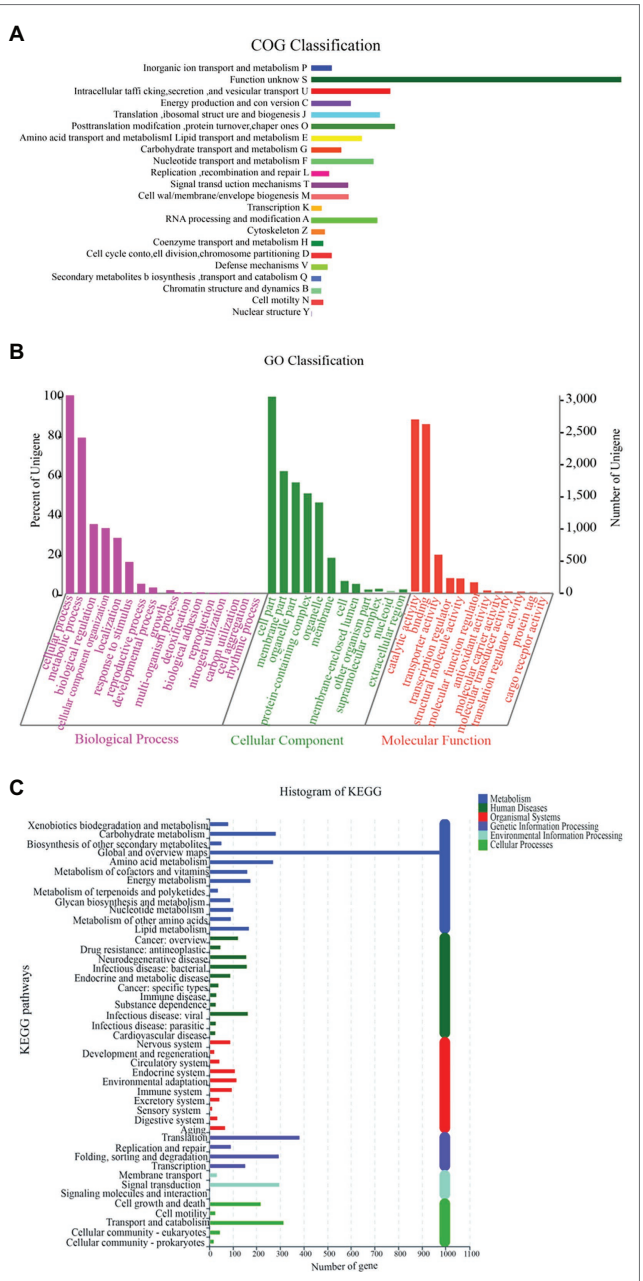

FIGURE 4 | Diagram of COG function annotation analysis **(A)**; Diagram of GO/IPR function annotation analysis **(B)**; and Diagram of KEGG function annotation analysis **(C)**.

Enzymes related to acetate synthesis have been reported, for example: using AATaseII by purifying acetate synthase led to the identification of three acyltransferases, namely, AATaseI encoded by *ATF1,* LG-AATASei encoded by *lgATF1* and AATaseII encoded by *ATF2* (Verstrepen et al., 2003; Lilly et al., 2006). Studies have shown that *ATF1* and *ATF2* exist in the *S. cerevisiae* cells, while *lgATF1* is only found in *Streptomyces*. Homology search of the *S. cerevisiae* genome did not show other homology genes with *ATF1* or *ATF2* (Yoshimoto et al., 1999; Van et al., 2008).

MCFA mainly includes ethyl hexanoate, ethyl capryate, the synthesis and regulation of MCFA are rarely studied. Malcorps and Dufour (2010) speculated that in addition to Atf1p, LG-ATF1P and Atf2p, other alcoholyltransferases should be present in the yeast group (Mason and Dufour, 2000; Malcorps and Dufour, 2010). One possible alcohol transferase was hypothesised to be alcohol acetyltransferase (Eht1p; ko7019). As a putative acyltransferase similar to Eeb1p, this enzyme is involved in synthesising MCFA esters containing ethyl hexanoate. Ethyl hexanoate is the most important ester in Luzhou-flavoured liquor, which is mainly synthesised by the alcohol acyltransferase pathway in *S. cerevisiae*, catalysing ethyl hexanoate from ethanol and hexanoyl-coenzyme A under the catalytic action of alcohol acyltransferase. The synthesis rate depended on the acyltransferase activity level and the acyl-CoA content of the substrate. Saerens (2006) reported that *EHT1* and *EEB1* of *S. cerevisiae* could encode acyltransferase, which is a key gene for the ethyl ester synthesis of MCFAs in yeast (Van et al., 2008). The acyl transferases encoded by *EHT1* and *EEB1* genes catalyse the formation of ethyl hexanoate from hexanoyl-CoA and alcohols. Sofie et al. reported that the expression of the *EHT1* gene can improve the synthesis ability of ethyl hexanoate and ethyl capryate (Saerens, 2006). In this study, according to the whole-genome study of Y-1, it was found that the pathway ko7019 of gene 6,340 contained Eht1p. Homology analysis of the amino acid sequence of Eht1p showed that Eht1p was similar to the homology sequences of different yeasts in the known database. The phylogenetic correlation between Eth1p sequences of this species was estimated by the adjacency programme (**Figure 6**).

(The percentage of replicate trees in which the associated taxa clustered together in the bootstrap test (1,000 replicates) are shown above the branches. The branch lengths are in the same units as those of the evolutionary distances used to infer the phylogenetic tree. A 0.10 represents the unit length of the difference value between sequences. The analysis involved 10 amino acid sequences.)

The amino acid sequences of Eht1p were compared with those of Eht1 and Eeb1. To find the conserved areas of homologous sequences and possible vital sequences, the same amino acid residue base was 51.75% in the multiple alignment sequence (**Figure 7**). This result confirmed the conjecture of Malcorps and Dufour (2010) that ethyl hexanoate is synthesised by catalysing ethanol and hexanoyl-CoA in the presence of alcohol hexacyltransferase. The synthesis of ethyl hexanoate of *W. anomalus* Y-1 in liquor brewing could be summarised as follows: starch and other macromolecules were converted into glucose by highly active degradation enzymes into cells. The glucose was absorbed and utilised by yeast cells to generate primary metabolites and intermediates. Ethanol and organic acids were produced through the citric acid cycle. Hexanoic acid mainly produced by hexanoic acid bacteria produced the hexanoyl coenzyme under the action of alcohol hexanoyl transferase (Yan and Dong, 2018). Then, hexanoyl coenzyme and ethanol produced ethyl hexanoate under the action of esterase. Ethyl hexanoate was the prominent aroma of Luzhou-flavoured liquor, and its content determined the quality of Luzhou-flavoured liquor.

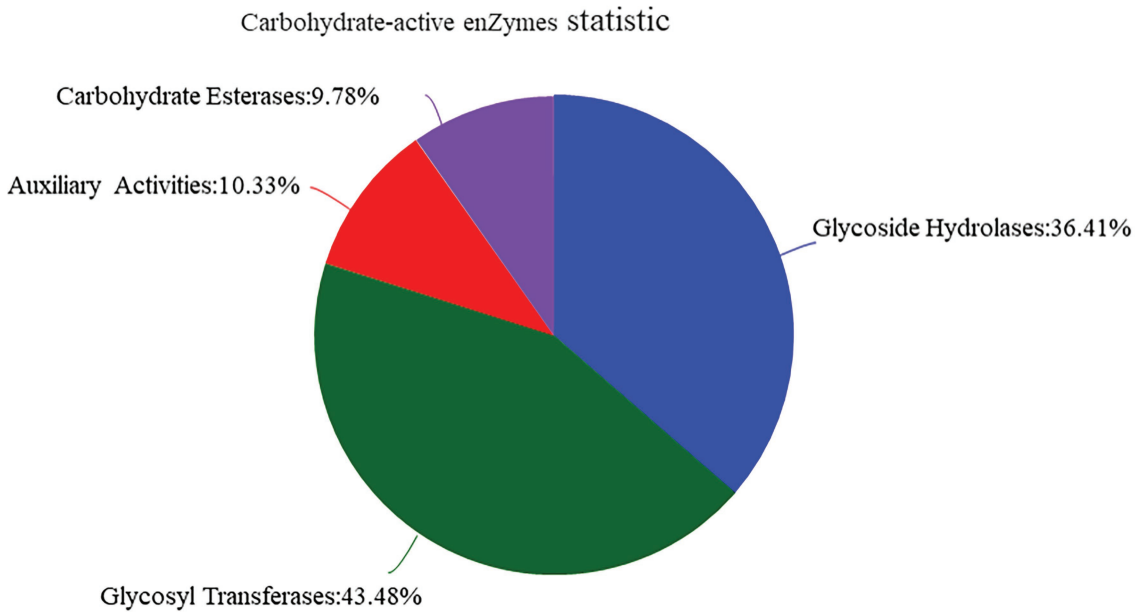

FIGURE 5 | Analysis of carbohydrate-active enzyme annotation.

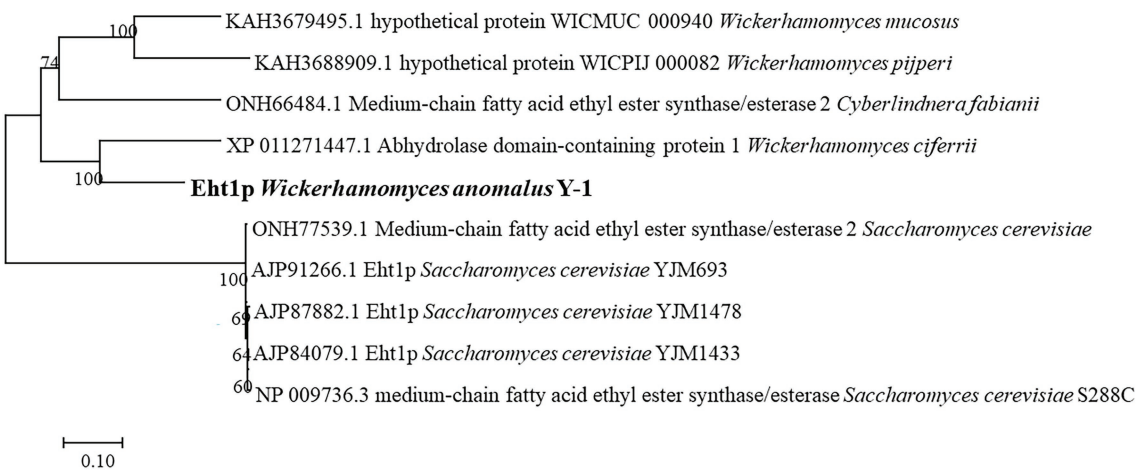

FIGURE 6 | Phylogenetic tree of Eht1p homologous fungi established by MEGA7.

In addition to the discovery of Eht1p, the full-length functional annotation of Y-1 enabled the identification of other key metabolic enzyme-encoding genes, such as genes related to carbohydrate metabolism; for example, 6-phosphate glucuronidase (EC3.1.1.31) encoding pgi (gene ID: 25796, protein sequence number: NP_036220), which acts on the ester bond belonging to carboxylesterase hydrolase and participates in the pentose phosphate and carbon metabolism pathways. The gloB-encoded hydrolase (EC3.1.2.6) also acts on the ester bond, which belongs to this hydrolase and participates in pyruvate metabolism. Inositol phosphate esterase encoding such (gene ID: 947285, protein sequence number NP_417028) belongs to phosphate monoester hydrolase, which acts on the ester bond and participates in the synthesis of secondary metabolites and carbohydrate metabolism. These enzymes are key enzymes for the synthesis of esters. Functional annotations had also identified some genes in amino acid metabolism (e.g. *argE*, *ydfG*, *metB* and *ansA*), cofactors and vitamin metabolism (e.g. *gltX*, *phoD*, *wrbA* and *phoA*), terpenes and polyketides metabolism (e.g. *mvaD*, *tktA*, *mvaK2* and *FCLY*) and lipid metabolism (e.g. *aslA*, *pgsA*, *ERG1* and *adhP*). The enzymes expressed by these genes are often involved in the degradation of macromolecular substances, such as proteins and peptides,

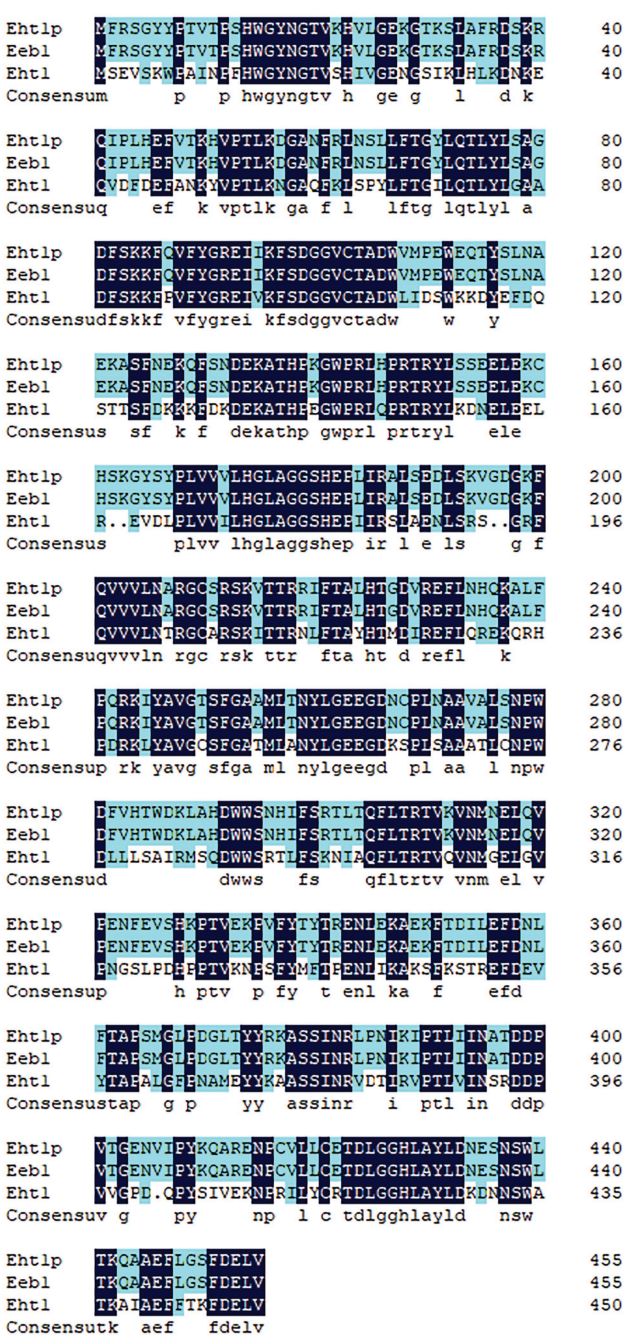

FIGURE 7 | Multiple comparisons of Eht1p, Eeb1 and Eht1 amino acid sequences of *Wickerhamomyces anomalus* Y-1. Non-conservative residues are black text on a white background. Conservative same residue as white text on dark blue background. A similar residue is a black text on a light blue background.

some of which have good acid and sugar resistance and can adapt to the unique environment of liquor brewing.

Wickerhamomyces anomalus Y-1 with strong esterification ability was selected from the Daqu. To study the synthesis of mechanism for ethyl hexanoate in the yeast, whole-genome sequencing and assembly were performed. Functional annotation was conducted using the sequencing results. Annotation results showed closely related mechanism of ethyl hexanoate to synthetic alcohol acyltransferase, and MCFA ethyl ester with known transferase was used for sequence alignment, with the same base of amino acid residues of 51.75%. In this study, the key genes for ester synthesis were identified by whole-genome sequencing of *W. anomalus* Y-1 strain. In order to prove the promoting effect of this gene on liquor flavour during liquor brewing, some validation experiments are needed.

DATA AVAILABILITY STATEMENT

The datasets presented in this study can be found in online repositories. The names of the repository/repositories and accession number(s) can be found in the article/ **Supplementary Material**.

AUTHOR CONTRIBUTIONS

XS and XW: data curation, conceptualization, writing—review and editing, supervision, and methodology. XH and QT: conceptualization and writing—review and editing. MH: writing—review and editing, funding acquisition, project administration, and supervision. All authors contributed to the article and approved the submitted version.

FUNDING

This work was financially supported by the research and application of microflora of yujiu, a sub-project of major science and technology projects of Henan province, China (181100211400–8). Henan University of Technology (no. 31401184).

SUPPLEMENTARY MATERIAL

The Supplementary Material for this article can be found online at: https://www.frontiersin.org/articles/10.3389/fmicb.2022.891387/full#supplementary-material

REFERENCES

Cheng, N., Koda, K., Tamai, Y., Yamamoto, Y., Takasuka, T. E., and Uraki, Y. (2017). Optimization of simultaneous saccharification and fermentation conditions with amphipathic lignin derivatives for concentrated bioethanol production. *Bioresour. Technol.* 232, 126–132. doi: 10.1016/j.biortech.2017.02.018

Christian, L., Thanet, U., and Thomas, B. (2014). Perspectives for the biotechnological production of ethyl acetate by yeasts. *Appl. Microbiol. Biotechnol.* 98, 5397–5415. doi: 10.1007/s00253-014-5765-9

Ding, X. F., Wu, C. D., Huang, J., and Zhou, R. Q. (2015). Changes in volatile compounds of chinese Luzhou-flavor liquor during the fermentation and distillation process. *J. Food Sci.* 80, C2373–C2381. doi: 10.1111/1750-3841.13072

Fan, W. L., Shen, H. Y., and Xu, Y. (2011). Quantification of volatile compounds in Chinese soy sauce aroma type liquor by stir bar sorptive extraction and gas chromatography-mass spectrometry. *J. Sci. Food Agric.* 91, 1187–1198. doi: 10.1002/jsfa.4294

Farooq, S., Ganai, S. A., Ganai, B. A., Mohan, S., Uqab, B., and Nazir, R. (2021). Molecular characterization of lipase from a psychrotrophic bacterium pseudomonas sp. CRBC14. *Curr. Genet.* 68, 243–251. doi: 10.1007/S00294-021-01224-W

Furukawa, K., Yamada, T., Mizoguchi, H., and Hara, S. (2003). Increased ethyl caproate production by inositol limitation in Saccharomyces cerevisiae. *J. Biosci. Bioeng.* 95, 448–454. doi: 10.1016/S1389-1723(03)80043-9

He, G. Q., Huang, J., Wu, C. D., Jin, Y., and Zhou, R. Q. (2019a). Bioturbation effect of fortified Daqu on microbial community and flavor metabolite in Chinese strong-flavor liquor brewing microecosystem. *Food Res. Int.* 129:108851. doi: 10.1016/j.foodres.2019.108851

He, G. Q., Huang, J., Zhou, R. Q., Wu, C. D., and Jin, Y. (2019b). Effect of fortified daqu on the microbial community and flavor in chinese strong-flavor liquor brewing process. *Front. Microbiol.* 10:56. doi: 10.3389/fmicb.2019.00056

Holt, C., and Yandell, M. (2011). MAKER2: An annotation pipeline and genome-database management tool for second-generation genome projects. *BMC Bioinform.* 12, 1–14. doi: 10.1186/1471-2105-12-491

Hong, J. X., Tian, W. J., and Zhao, D. R. (2020). Research progress of trace components in sesame-aroma type of baijiu. *Food Res. Int.* 137:109695. doi: 10.1016/j.foodres.2020.109695

Jin, G. Y., Zhu, Y., and Xu, Y. (2017). Mystery behind Chinese liquor fermentation. *Trends Food Sci. Tech.* 63, 18–28. doi: 10.1016/j.tifs.2017.02.016

Kanehisa, M. (2017). Enzyme annotation and metabolic reconstruction using KEGG. *Methods Mol. Biol.* 1611, 135–145. doi: 10.1007/978-1-4939-7015-5_11

Kusano, M., Sakai, Y., Kato, N., Yoshimoto, H., and Tamai, Y. (1998). Hemiacetal dehydrogenation activity of alcohol dehydrogenases in Saccharomyces cerevisiae. *Biosci. Biotech. Bioch.* 62, 1956–1961. doi: 10.1271/bbb.62.1956

Li, W. W., Fan, G. S., Fu, Z. L., Wang, W. H., and Li, X. T. (2019). Effects of fortification of daqu with various yeasts on microbial community structure and flavor metabolism. *Food Res. Int.* 129:108837. doi: 10.1016/j.foodres.2019.108837

Lilly, M., Bauer, F. F., Lambrechts, M. G., Swiegers, J. H., Cozzolino, D., and Pretorius, I. S. (2006). The effect of increased yeast alcohol acetyltransferase and esterase activity on the flavour profiles of wine and distillates. *Yeast* 23, 641–659. doi: 10.1002/yea.1382

Ling, Y. X., Li, W. Y., Tong, T., Li, Z. M., and Wang, Y. G. (2020). Assessing the microbial communities in four different daqus by using PCR-DGGE, PLFA, and biology analyses. *Pol. J. Microbiol.* 69, 1–11. doi: 10.33073/pjm-2020-004

Liu, H. L., and Sun, B. G. (2018). Effect of fermentation processing on the flavor of Baijiu. *J. Agr. Food Chem.* 66, 5425–5432. doi: 10.1021/acs.jafc.8b00692

Lu, M. M., Zhou, W. C., and Ji, F. (2020). Profiling prokaryotic community in pit mud of Chinese strong-aroma type liquor by using oligotrophic culturing. *Int. J. Food Microbiol.* 337:108951. doi: 10.1016/j.ijfoodmicro.2020.108951

Malcorps, P., and Dufour, J. P. (2010). Short-chain and medium-chain aliphatic-ester synthesis in Saccharomyces cerevisiae. *FEBS J.* 210, 1015–1022. doi: 10.1111/j.1432-1033.1992.tb17507.x

Mason, A. B., and Dufour, J. I. (2000). Alcohol acetyltransferases and the significance of ester synthesis in yeast. *Yeast* 16, 1287–1298.

Papamichael, P. S. A. A. (2013). Advances in lipase-catalyzed esterification reactions. *Biotechnol. Adv.* 31, 1846–1859. doi: 10.1016/j.biotechadv.2013.08.006

Qiu, Y., Fang, F., Zhou, X., and Zhang, L. (2016). Characterization of arginine utilization strains from fermented grains and evaluation of their contribution to citrulline accumulation in Chinese Luzhou-flavor spirits. *Acta Microbiol Sin.* 56, 1638–1646. doi: 10.13343/j.cnki.wsxb.20160007

Reyes-Sánchez, F. J., Páez-Lerma, J., Rojas-Contreras, J. A., López-Miranda, J., and Reinhart-Kirchmayr, M. (2020). Study of the enzymatic capacity of kluyveromyces marxianus for the synthesis of esters. *J. Mol. Microb. Biotech* 29, 1–9. doi: 10.1159/000507551

Rojo, M. C., Palazzolo, C. T., Cuello, R., González, M., Guevara, F., Ponsone, M. L., et al. (2017). Incidence of osmophilic yeasts and Zygosaccharomyces rouxii during the production of concentrate grape juices. *Food Microbiol.* 64, 7–14. doi: 10.1016/j.fm.2016.11.017

Saerens, S. (2006). The saccharomyces cerevisiae EHT1 and EEB1 genes encode novel enzymes with medium-chain fatty acid ethyl ester synthesis and hydrolysis capacity. *J. Biol. Chem.* 281, 4446–4456. doi: 10.1074/jbc.M512028200

Steinberg, K. M., Schneider, V. A., Alkan, C., Montague, M. J., Warren, W. C., Church, D. M., et al. (2017). Building and improving reference genome assemblies. *P. IEEE.* PP(3), 1–14. doi: 10.1109/JPROC.2016.2645402

Tatusov, R. L. (2001). The COG database: new developments in phylogenetic classification of proteins from complete genomes. *Nucleic Acids Res.* 29, 22–28. doi: 10.1093/nar/29.1.22

Van, D. M., Saerens, M. G., and Verstrepen, K. J. (2008). Flavour formation in fungi: characterisation of KlAtf, the *Kluyveromyces lactis* orthologue of the *Saccharomyces cerevisiae* alcohol acetyltransferases Atf1 and Atf2. *Appl. Microbiol. Biotechnol.* 78, 783–792. doi: 10.1007/s00253-008-1366-9

Verstrepen, K. J., Laere, S. V., Vanderhaegen, B., Derdelinckx, G., Dufour, J. P., Pretorius, I. S., et al. (2003). Expression levels of the yeast alcohol acetyltransferase genes ATF1, Lg-ATF1, and ATF2 control the formation of a broad range of volatile esters. *Appl. Environ. Microbiol.* 69, 5228–5237. doi: 10.1016/j.cej.2007.03.005

Vesztrocy, A. W., and Dessimoz, C. (2017). A gene ontology tutorial in python. *Methods Mol. Biol.* 1446, 221–229. doi: 10.1007/978-1-4939-3743-1_16

Vincent, L., Hemalatha, G. R., Elodie, D., Coutinho, P. M., and Bernard, H. (2014). The carbohydrate-active enzymes database (CAZy) in 2013. *Nucleic Acids Res.* 42, D490–D495. doi: 10.1093/nar/gkt1178

Wang, D. Q., Chen, L. Q., Yang, F., Wang, H. Y., and Wang, L. (2019). Yeasts and their importance to the flavour of traditional Chinese liquor: A review. *J. Brewing.* 125, 214–221. doi: 10.1002/jib.552

Wang, W. H., Fan, G. S., Li, X. T., Fu, Z. L., Liang, X., and Sun, B. G. (2020). Application of Wickerhamomyces anomalus in simulated solid-state fermentation for baijiu production: changes of microbial community structure and flavor metabolism. *Front. Microbiol.* 11:2994. doi: 10.3389/fmicb.2020.598758

Wang, Y. S., Li, B., Dong, H., Huang, X. D., Chen, R. Y., Chen, X. J., et al. (2018). Complete genome sequence of clostridium kluyveri JZZ applied in chinese strong-flavor liquor production. *Curr. Microbiol.* 75, 1429–1433. doi: 10.1007/s00284-018-1539-4

Wang, H. Y., Yan, X. U., Fan, L. I., and Jin, Y. G. (2008). Enzymatic characteristics of alcohol acetyltransferase from hanseniaspora valbyensis, a non-saccharomyces yeast. *J. Food Biochem.* 32, 506–520. doi: 10.1111/j.1745-4514.2008.00180.x

Wei, Y., Zou, W., Shen, C. H., and Yang, J. G. (2020). Basic flavor types and component characteristics of Chinese traditional liquors: A review. *J. Food Sci.* 85, 4096–4107. doi: 10.1111/1750-3841.15536

Wolter, H., Lietz, P., and Beubler, A. (1966). Influence of temperature and yeast strain on the formation of fermentation amyl alcohol, isobutanol and ethyl acetate in fermenting malt wort. *Folia Microbiol.* 11, 210–214. doi: 10.1007/BF02901434

Xu, Y. Q., Sun, B. G., Fan, G. S., Teng, C., and Li, X. T. (2017). The brewing process and microbial diversity of strong flavour Chinese spirits: A review. *J. Inst. Brewing.* 123, 5–12. doi: 10.1002/jib.404

Yan, S., and Dong, D. (2018). Improvement of caproic acid production in a clostridium kluyveri H068 and methanogen 166 co-culture fermentation system. *AMB Express* 8:175. doi: 10.1186/s13568-018-0705-1

Yang, Y. R., Zhong, H. Y., Yang, T., and Lan, C. H. (2020). Characterization of the key aroma compounds of a sweet rice alcoholic beverage fermented with *Saccharomycopsis fibuligera*. *J Food Sci Technol.* 58, 1–13. doi: 10.1007/s13197-020-04833-4

Yin, X., Yoshizaki, Y., Ikenaga, M., Han, X. L., Okutsu, K., Futagami, T., et al. (2020). Manufactural impact of the solid-state saccharification process in rice-flavor baijiu production – ScienceDirect. *J. Biosci. Bioeng.* 129, 315–321. doi: 10.1016/j.jbiosc.2019.09.017

Yoshimoto, H., Fujiwara, D., Momma, T., Tanaka, K., Sone, H., Nagasawa, N., et al. (1999). Isolation and characterization of the ATF2 gene encoding alcohol acetyltransferase II in the bottom fermenting yeast saccharomyces pastorianus. *Yeast* 15, 409–417. doi: 10.1002/(SICI)1097-0061(19990330)15:53.0.CO;2-Q

Zhang, S. J., Guo, F., Yan, W., Dong, W. L., and Jiang, M. (2020). Perspectives for the microbial production of ethyl acetate. *Appl. Microbiol. Biot.* 104, 7239–7245. doi: 10.1007/s00253-020-10756-z

Zhang, G. Q., Lin, Y. P., He, P., Li, L., Wang, Q. H., and Ma, Y. (2014). Characterization of the sugar alcohol-producing yeast *Pichia anomala*. *J. Ind. Microbiol. Biot.* 41, 41–48. doi: 10.1007/s10295-013-1364-5

Zhang, H. M., Meng, Y. J., Wang, Y. L., Zhou, Q. W., and Xing, X. H. (2019). Prokaryotic communities in multidimensional bottom-pit-mud from old and young pits used for the production of Chinese strong-flavor Baijiu – science direct. *Food Chem.* 312:126084. doi: 10.1016/j.foodchem.2019.126084

Zhao, X. M., Wang, Y., Chen, L., and Aihara, K. (2008). Gene function prediction using labeled and unlabeled data. *BMC Bioinform.* 9:57. doi: 10.1186/1471-2105-9-57

Zhao, L., Xie, J., Bai, L., Chen, W., Wang, M., Zhang, Z., et al. (2018). Mining statistically-solid k-mers for accurate NGS error correction. *BMC Genomics* 19:912. doi: 10.1186/s12864-018-5272-y

Zheng, J., Wu, C. D., Huang, J., Zhou, R. Q., and Liao, X. P. (2015). Spatial distribution of bacterial communities and related biochemical properties in Luzhou-flavor liquor-fermented grains. *J. Food Sci.* 79, M2491–M2498. doi: 10.1111/1750-3841.12697

Zou, W., Ye, G. B., and Zhang, K. Z. (2018). Diversity, function, and application of clostridium in Chinese strong flavor baijiu ecosystem: A review. *J. Food Sci.* 83, 1193–1199. doi: 10.1111/ 1750-3841.14134

Conflict of Interest: The authors declare that the research was conducted in the absence of any commercial or financial relationships that could be construed as a potential conflict of interest.

Publisher's Note: All claims expressed in this article are solely those of the authors and do not necessarily represent those of their affiliated organizations, or those of the publisher, the editors and the reviewers. Any product that may be evaluated in this article, or claim that may be made by its manufacturer, is not guaranteed or endorsed by the publisher.

frontiers | Frontiers in Microbiology

ORIGINAL RESEARCH
published: 19 May 2022
doi: 10.3389/fmicb.2022.893053

Stirred Yogurt as a Delivery Matrix for Freeze-Dried Microcapsules of Synbiotic EVOO Nanoemulsion and Nanocomposite

Hoda S. El-Sayed[1], *Khamis Youssef*[2,3]* *and Ayat F. Hashim*[4]

[1] Dairy Science Department, Food Industries and Nutrition Research Institute, National Research Centre, Giza, Egypt, [2] Agricultural Research Center, Plant Pathology Research Institute, Giza, Egypt, [3] Agricultural and Food Research Council, Academy of Scientific Research and Technology, Cairo, Egypt, [4] Fats and Oils Department, Food Industries and Nutrition Research Institute, National Research Centre, Giza, Egypt

Nowadays, dairy products are considered a good matrix to deliver many functional substances either vital oils or probiotic cells. Two models of microcapsules were produced from co-encapsulation of extra virgin olive oil (EVOO) nanoemulsion or nanocomposite and synbiotic bacteria (maltodextrin with *Lactobacillus acidophilus* and *Bifidobacterium bifidum*) using the freeze-drying technique. These models of microcapsules were added to stirred yogurt, and then its storage effect on microbiology, chemically, and sensory properties were evaluated for 21 days. The average droplet size and zeta potential distribution of EVOO nanoemulsion and nanocomposite were investigated. Also, oxidative stability, microencapsulation efficiency, release profile, and antioxidant activity were studied. The results showed that the average particle size of EVOO nanoemulsion and nanocomposite ranged between 416 and 475 nm, while zeta potential was −39.6 and −33.6 mV, respectively. The induction period of EVOO extracted from nanoemulsion and nanocomposite microcapsules models was 11.30 and 8 h. The microencapsulation efficiency of probiotic and EVOO was determined at 88.84 and 65.61% for the nanoemulsion microcapsules model, while the nanocomposite microcapsules model showed 98.49 and 72%. The two models of microcapsules have boosted the viability of probiotic bacteria inside stirred yogurt than free cells. Also, the presence of microcapsules did not affect the viability of stirred yogurt starter cultures, and high values for the total solid and protein were detected. Therefore, the results recommended that stirred yogurt is a good delivery carrier for highly antioxidant and healthy microcapsules of synbiotic EVOO nanoemulsion and nanocomposite.

Keywords: microencapsulation, extra virgin olive oil, nanoemulsion, nanocomposite, probiotic strains, stirred yogurt

OPEN ACCESS

Edited by:
Yu Xia,
Jiangnan University, China

Reviewed by:
Kamal A. M. Abo-Elyousr,
Assiut University, Egypt
Fang Zhong,
Jiangnan University, China
Fouad M. F. Elshaghabee,
Cairo University, Egypt

***Correspondence:**
Khamis Youssef
youssefeladawy@arc.sci.eg

Specialty section:
This article was submitted to Food Microbiology, a section of the journal Frontiers in Microbiology

Received: *09 March 2022*
Accepted: *11 April 2022*
Published: *19 May 2022*

Citation:
El-Sayed HS, Youssef K and Hashim AF (2022) Stirred Yogurt as a Delivery Matrix for Freeze-Dried Microcapsules of Synbiotic EVOO Nanoemulsion and Nanocomposite. Front. Microbiol. 13:893053. doi: 10.3389/fmicb.2022.893053

INTRODUCTION

Extra virgin olive oil (EVOO) has rapid digestion, nutritional, therapeutic, and economic properties. EVOO is a source of phenolic compounds with a powerful antioxidant activity that includes hydroxytyrosol, tyrosol, and secoiridoid derivatives (Francis et al., 2019). Despite all the proven potentiality, it has poor storage stability, especially upon exposure to oxygen, light,

moisture, and high temperature (Calvo et al., 2012). Oxidative degradation results in a loss of nutritional quality and the development of undesired flavors. Therefore, it affects the shelf stability and sensory properties of the oil (Bendini et al., 2006; Koç et al., 2015).

As well, consumer demand for functional foods with probiotics is increasing because of the health benefits (Min et al., 2019). Generally, probiotics are live microorganisms, when ordered in satisfactory amounts, give the host health benefit (Morelli and Capurso, 2012). Regular consumption of 10^7-10^8 log CFU/ml of probiotics is recommended to confirm its positive healthy functions in the human body (Terpou et al., 2019). Several types of probiotic bacteria may be affected by the condition of processing as high temperatures, pH values, low water activity, and storage time (Shah et al., 1995; Tripathi and Giri, 2014). Besides, probiotic bacteria are also exposed to enzymes, stomach acids, and bile salts during their passing through the gastrointestinal tract, which adversely affects the survivability of these bacteria (Kailasapathy and Chin, 2000; Raghuwanshiet et al., 2018).

From the previous points, microencapsulation technology is considered a promising technique to increase self-life during olive oil manufacturing (Calvo et al., 2012), prevent losing healthy properties as well as the viability of probiotic bacteria (Mahmoud et al., 2020). In addition, microencapsulation of olive oil has the opportunity to improve economic value, like healthy food, and may provide a therapeutic purpose. Microencapsulation was able to protect the core materials or sensitive cells and substances from adverse conditions by surrounding these substances or bacterial cells with coating materials (Razavi et al., 2021). So, the encapsulated ingredients can arrive in the specific target area without being undesirably affected by environmental influences.

Several encapsulating materials have been used for the microencapsulation techniques, including polysaccharides (sodium alginate, carrageenan, pectin, chitosan, xanthan, maltodextrin, and dextrin), proteins (whey protein, casein, soy protein, and gelatin). It was observed that sodium alginate was not stable in the acidic conditions, so it has poor protection to the entrapped materials in this condition. This limits its application as a coating material to enhance this disadvantage it was added or mixed with other materials like whey protein, dextrin, or chitosan (Mahmoud et al., 2020). Whey protein as coating material protected the entrapped substances, especially probiotic cells from the acidic conditions in the stomach (Doherty et al., 2011), fish oil (Aghbashlo et al., 2013), and linseed oil (Gallardo et al., 2013). Additionally, prebiotic agents like maltodextrin could be used for two purposes: capsulation material and prebiotic agents to activate entrapped probiotic cells. Also, maltodextrin is normally used as wall material in microencapsulation according to its low viscosity at high-solid concentration, good solubility, good protection, low cost, neutral aroma, and taste (Madene et al., 2006). However, it is usually used with other coating materials (such as whey protein and sodium alginate) for offering efficient and effective microencapsulation because it is poor emulsifying. Also, Bentonite is natural clay composed of montmorillonite, which is a 2:1 type aluminosilicate in the smectite group. Dong et al. (2021) prepared and tuned alginate-bentonite microcapsules by extrusion and emulsification. Hamed et al. (2020) developed nanocomposite microspheres based on alginate/chitosan to deliver vehicles of omega-3-rich oils. Nanocomposite microcapsules have a good surface structure, a higher biodegradability rate, and better protection from active chemicals than polymeric nanocomposites (Arjona et al., 2021).

Dairy products are considered the major food groups that have been supplemented with probiotic bacteria, such as cheese yogurt and ice cream (Castro et al., 2015; El-Sayed et al., 2015; El-Sayed and El-Sayed, 2020). The food matrix was considered the perfect medium to deliver microencapsulated substances either vital oils or probiotic cells to humans, especially dairy products. Stirred yogurt was considered a favorable dairy product to humans because it is a good source of proteins, vitamins, and minerals. Stirred yogurt can be used as a delivery system to transport vital substances and probiotic cells with sufficient amounts to the humans to donate vital therapeutic effects. Moghanjougi et al. (2021) produced microcapsules of probiotics (*L. acidophilus LA-5 and B. animalis BB-12*) using a freeze-drying technique based on the emulsion method in the sodium alginate and pectin. Calvo et al. (2012) used different wall materials to microencapsulate EVOO by freeze frying system.

Although several studies on microencapsulation of EVOO and probiotic bacteria have appeared in the literature, to our knowledge, this is the first study that was designated to produce two models of freeze-dried nano-in-micro microcapsules based on synbiotic EVOO nanoemulsion and nanocomposite. The main objectives of this study were (i) to apply these models in stirred yogurt as a delivery matrix for EVOO and probiotic bacteria (ii) the effect of adding these microcapsules to stirred yogurt was evaluated during 21 days of storage for microbiology, chemically, and sensory properties, and (iii) the antioxidant activity was evaluated for the two models of microcapsules and after the addition to the stirred yogurt.

MATERIALS AND METHODS

Chemicals

Maltodextrin was purchased from Loba Chemie, Mumbai, India. Extra virgin olive oil (EVOO) was gotten from the oil extraction unit, National Research Centre, Egypt. Nanoclay hydrophilic bentonite was purchased from Sigma-Aldrich (St. Louis, MO, USA). Sodium alginate from brown algae (91%) was received from Lobachemia (India). Whey protein concentrate (WPC) 80% was obtained from Agri-mark, USA. 2,2-diphenyl-1-picrylhydrazyl (DPPH, 90%) was purchased from Sigma (St. Louis, MO, USA). All other solvents and reagents were purchased from various suppliers and used without further purification.

Microbial Strains

Probiotic strains were obtained from the dairy department, National Research Center as *Bifidobacterium bifidum* NRRL B-41410 and *Lactobacillus acidophilus* CH-2.

Physicochemical Analysis of EVOO

Peroxide value (PV), iodine value (IV), acid value (AV), and saponification value (SV) were determined according to the standard methods of the [American Oil Chemists' Society (AOCS), 2005; AOCS, 2011]. Specific extinction k_{232} and k_{270} extinction coefficients were calculated from the absorbance at 232 and 270 nm, respectively, with a UV-Vis spectrophotometer (T80 UV/VIS Spectrometer, PG Instruments Ltd., UK), using a 1% solution of oil in cyclohexane and a path length of 1 cm.

Preparation of Probiotic Cell Suspensions

The probiotic strains (*Lb. acidophilus* and *B. bifidum*) were activated individually to obtain high biomasses by MRS broth (De Man-Regosa-Sharp) and incubated for 24 h at 37°C anaerobically (Fayed et al., 2018). The cell pellets were harvested by centrifugation at 6.000 rpm for 15 min at 4°C. The obtained cells pellets were washed with a sterile saline solution [0.9% (w/v) NaCl] and stored at 8°C for further use.

Microencapsulation of Synbiotic EVOO Nanoemulsion and Nanocomposite

Synbiotic EVOO nanoemulsion or nanocomposite microcapsules were prepared in three stages using: ultrasonication, blending, and freeze drying techniques as the following:

First Stage: Preparation of EVOO Nanoemulsion and Nanocomposite

EVOO nanoemulsion and nanocomposite were prepared using emulsification and the ultrasonication process. Tween 20 (2%) was mixed with distilled water as an aqueous phase using a magnetic stirrer (WiseStir MSH-20A, Korea) at 1.000 rpm. Then, this aqueous phase was added dropwise to the oil phase (10%) while magnetically stirring. The mixture was homogenized with a high-speed homogenizer (X520, CAT Ingenieurburo M. Zipperer, GmbH, Germany) for 3 min at 16.000 rpm to prepare a coarse emulsion. After that, the prepared emulsion was ultrasonicated using a bench-scale sonicator (Sonics and Materials Inc. 53 Church Hill Rd., Newtown, CT, USA) at 60% of full power amplitude (60 W) for 10 min and using a probe with a diameter of 22.5 mm. The same procedure was used for the preparation of EVOO nanocomposites. In a brief, a suspension of nano-clay hydrophilic bentonite (5 g) was stirred overnight at 30°C in distilled water (250 ml). Nano-clay suspension (50 ml) was mixed to the EVOO-dispersed phase for 2 h using a mechanical stirrer before the emulsification process. The preparation of W/O nanocomposite was ultrasonicated using a bench-scale sonicator.

Second Stage: Preparation of Synbiotic EVOO Nanoemulsion and Nanocomposite

Whey protein concentrate (WPC) solution was dispersed into deionized water overnight at room temperature for complete hydration. Sodium alginate (SA) and WPC in a ratio of 1:1 were mixed under continuous stirring. Synbiotic was prepared by blending previously prepared probiotic cell suspensions (25%) with maltodextrin biopolymer (3%). Both SA-WPC and synbiotic suspensions were blended and homogenized with EVOO nanoemulsion or nanocomposite using a high-speed homogenizer (Ingenieurbüro CAT, Germany) at 16.000 rpm for 1 min.

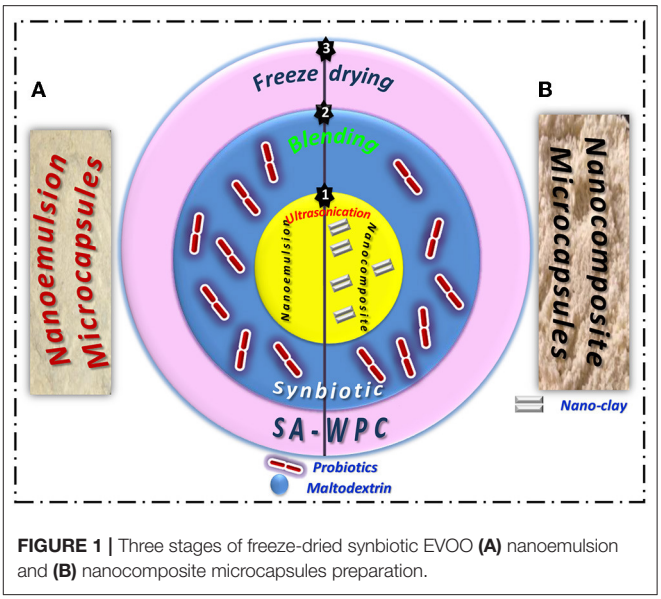

FIGURE 1 | Three stages of freeze-dried synbiotic EVOO **(A)** nanoemulsion and **(B)** nanocomposite microcapsules preparation.

Third Stage: Preparation of Two Models of Microcapsules Based on Nanoemulsion and Nanocomposite

The synbiotic EVOO nanoemulsion and nanocomposite mixture was frozen overnight at −80°C and then freeze-dried using a Christ freeze dryer (ALPHA 1-4 LSC) for 48 h. Freeze-drying has been performed under optimal conditions for receiving the highest survivability of probiotics. Dried samples were then grounded using a planetary ball mill. The resulting freeze-dried powders were packed in 250-ml sterile bottles and stored at 4°C (**Figure 1**).

Particle Sizing and Zeta Potential for EVOO Nanoemulsion and Nanocomposite

Measurement of EVOO nanoemulsion and nanocomposite size (Section. First Stage: Preparation of EVOO Nanoemulsion and Nanocomposite), distributions, and zeta potential was performed by a dynamic light scattering method (DLS) using Zetasizer Nano ZS (Malvern Instruments, UK) at room temperature. Before measurement, 30 μL of the EVOO nanoemulsion or nanocomposite was diluted with 3 ml of water at 25°C. Particle-size data were expressed as the mean of the Z-average of three independent batches of the EVOO nanoemulsion or nanocomposite.

Oxidative Stability

The oxidative stability of EVOO extracted from nanoemulsion and nanocomposite microcapsules was determined as the induction period (IP, h) using a Rancimat apparatus (Model 892 Professional Rancimat, Metrohm SA, Herisau, Switzerland) as

the reference analysis for all olive oil samples. The oxidation reactions were increased by keeping 3 g of oil at 110°C under a constant airflow of 20 L/h, and then determining the conductivity variation of water (60 ml) due to the increase in volatile oxidative compounds.

Microencapsulation Efficiency (ME)

Probiotic Strains

The microencapsulation efficiency of resulting microcapsules was evaluated according to Mahmoud et al. (2020). One gram of the different microcapsules was added to 9 ml of sterile tri-sodium citrate solution (2%, w/v) and stirred to dissolve the microcapsules, considering the first dilution (1:10). After that, prepared serial dilution using normal saline (0.9% NaCl) and added the suitable dilution to plates using the pour plate method and the MRS agar (Man-Regosa and Sharp) medium. The plates were incubated at 37°C for 48 h under anaerobic conditions. The microencapsulation efficiency percentage ($ME_{probiotic}$ %) was calculated as the following:

$$\mathbf{ME_{probiotic}\ \% = \frac{Log_{10}N}{Log_{10}N_0}\ x\ 100}$$

where N = the number of the probiotics cells inside the microcapsules; N_o = the number of the free probiotics cells was added to different formulations.

Extra Virgin Olive Oil

The surface oil content was measured to calculate the ME_{EVOO}%. Surface oil was investigated by a method described by Tonon et al. (2011). Briefly, 50-ml n-hexane was added to 3 g of microcapsules followed by shaking for 2 min at room temperature. The suspension was then filtered through Whatman No. 1 filter paper, and the residue was washed three times with 20-ml n-hexane. Then, the solvent was evaporated until constant weight at reduced pressure. The amount of surface oil was determined by the mass difference between the initial clean flask and that containing the extracted oil residue (Jafari et al., 2008). Total oil content is assumed to equal the initial oil since preliminary tests have shown that all the initial oil was retained, which was expected since the investigated oil is non-volatile. The microencapsulation efficiency percentage (ME_{EVOO} %) was calculated using the following equation:

$$\mathbf{ME_{EVOO}\ \% = \frac{Total\ oil\ content - Surface\ oil\ content}{Total\ oil\ content}\ X\ 100}$$

Morphological Features

Transmission Electron Microscope (TEM)

TEM analysis was carried out to study the structure and morphology of the prepared synbiotic EVOO nanoemulsion and nanocomposite by using a JEOL JEM-1230 transmission electron microscope. Twenty microliters of diluted samples were placed on a film-coated 200-mesh copper specimen grid for 10 min, and the fluid excess was eliminated using filter paper. The grid was then stained with one drop of 3% phosphotungstic acid (PTA) and allowed to dry for 3 min. The coated grid was dried and examined under the TEM microscope (Philips, CM12). Then, samples were observed by operating at 120 kV.

Scanning Electron Microscope (SEM)

The morphology of the developed microcapsules was determined by scanning electron microscope (SEM) (SEM, quanta Fei 250 Republic Czech).

Release Measurements

Preparation of Gastrointestinal Solutions

For stimulated gastric solution, the pH of saline solution (0.9% NaCl, w/v) was adjusted to 2 and sterilized by autoclave at 121°C for 15 min; after that, 0.3% pepsin enzyme (Group 1 pepsinogens) was added. *For stimulated intestinal solution*, the pH of the 100-ml distilled water contained 0.3% bile salts, 0.65 NaCl, 0.083 KCl, 0.022 $CaCl_2$, 0.138 $NaHCO_3$ (w/v %) and was adjusted to 7. and sterilized by autoclave at 121°C for 15 min; after that, 1% pancreatic enzyme (amylase, lipase, and protease and made from cows) was added (Chávarri et al., 2010).

In vitro Survivability and Release Evaluation of Probiotic Strains

Ten grams of each microencapsulated particle and free cells were added separately into 100-ml gastric solution for 2 h. After that time, one gram of each microencapsulated particle and free cells was obtained to calculate the viable probiotic counts after exposure to the gastric solution. The microencapsulated particles and free cells were collected by gently cooling centrifugation (1,500 rpm for 10 min at 4°C) and added to the intestinal solution for 6 h. One gram of each microencapsulated particle was collected after 2-, 4-, and 6-h intervals to calculate the viable counts of probiotics after exposure to the intestinal solution. After collecting the microencapsulated particles, 3% trisodium citrate was used as the first diluted as mentioned before (Section Microbiological Activities of Stirred Yogurt Treatments) and, after that, serially diluted in saline solution. The suitable diluted was plated using an MRS agar medium and incubated anaerobically for 48 h at 37°C (Fayed et al., 2018).

The release of probiotics from the microcapsules was determined by the method described by Lotfipour et al. (2012). Ten grams of each microcapsule and free cells were put in a dialysis bag individually and transferred into 100-ml simulated colonic solution (0.1-M KH_2PO_4, pH 7.00), mixed gently, and incubated at 37°C. At 0-, 1-, 2-, 3-, 4-, 5-, and 6-h time intervals, 1 ml of sample was taken and viable counts were enumerated with serial dilution by saline. The suitable diluted was plated using an MRS agar medium and incubated for 37°C for 48 h, anaerobically.

In vitro Release Evaluation of Extra Virgin Olive Oil

The *in vitro* release profile of the EVOO from the developed microcapsules was determined using the dialysis method for gastrointestinal conditions. In brief, the dialysis bag was soaked in distilled water to remove the preservatives and then rinsed with gastrointestinal solutions. Three milligrams of microcapsules were put into the dialysis bag and suspended in 100-ml gastric solution for 2 h. After this time, the dialysis bags containing microcapsules were picked up and suspended in intestinal solution (100 ml) for 4 h at 37°C under gentle agitation. The amount of oil

TABLE 1 | Treatments of stirred yogurt.

Treatment	Starter cultures*	Probiotics-free cells**	Nanoemulsion microcapsules	Nanocomposite microcapsules
T1	√	-	-	-
T2	√	√	-	-
T3	√	-	√	-
T4	√	-	-	√

*Starter cultures of yogurt (Lb.bulgaricus and S. thermophilus). **Probiotics-free cells (Lb. acidophilus and B. bifidum).

released was determined using a UV–Vis spectrophotometer. At specific intervals, 3 ml of the buffer was collected for analysis, and each experiment was carried out in triplicate. The time-dependent release study was performed for 6 h.

Stirred Yogurt Manufacturing Fortified With Synbiotic EVOO Nanoemulsion and Nanocomposite Microcapsules

Fresh cow's milk was heated at 80°C for 15 min and cooled to 42°C (Fayed et al., 2019). The starter cultures of yogurt (*Lb.bulgaricus* and *S.thermophilus*) were added at the concentration of 2%. The inculcated milk was divided into the following treatments (**Table 1**). All microcapsules and probiotic-free cells were added with 2% for the treatments. The treatments were then transferred into plastic cups (100 ml) and incubated at 42°C for 4 h until coagulation. After that, the resulting yogurt was stirred, and the cups were kept at 7°C for 20 days.

Microbiological Activities of Stirred Yogurt Treatments

The diluting pouring plate technique was used for enumerating microbes in the samples. In the first dilution, tri-sodium citrate (3%, w/v) was used. The followed serial dilution was prepared by saline solution. The microbial activity of samples was determined for the count of *B. bifidum* by an MRS agar medium supplemented with 2 gm/l sodium propionate and 3 gm/l lithium chloride (Fayed et al., 2019). The plates were incubated at 37°C for 72 h under anaerobic conditions. The *Lactobacillus acidophilus* counts were evaluated by the MRS agar medium supplemented with 0.02% bile salts, and the plates were incubated at 37°C for 48 h under anaerobic conditions (Gilliland and Walker, 1990). The count of *S. thermophilus* was evaluated by the M17 agar medium, and the plates were incubated under aerobic conditions at 37°C for 48 h (IDF, 1997). Also, the counts of *Lb. bulgaricus* were determined using the MRS agar medium with pH 5.5 and the plated incubated under the anaerobic condition at 37°C for 48 h (IDF, 1997). Finally, the counts of mold and yeast were detected by potato dextrose agar acidified to pH 3.5 with a sterile lactic acid solution (10%). The plates were aerobically incubated at 25°C for 4 days (APHA, 1994).

Chemical Evaluation of Stirred Yogurt Treatments

Fresh stirred yogurt treatments were analyzed for dry matter, protein, fat, and ash contents (AOAC, 2012). The titratable acidity was assessed as illustrated by Ling (1963). The pH values were measured for yogurt from the different treatments using a digital pH meter (Hanna, Germany.

Sensory Evaluation of Stirred Yogurt Treatments

Stirred yogurt treatments were sensory evaluated by Ladokun and Oni (2014). The ratings were scored on a Hedonic scale, ranging from 1 to 5, for appearance, odor, mouth, feel, and overall acceptability. Keys: 5.0 = very good, 4.9–4.0 = good, 3.9–3.0 = fair, 2.9–2.0 = poor, 1.9–1.0 = bad. The evaluation was carried out by a regular 15-member scoring panel of the Dairy Department, National Research Center.

Evaluation of the Antioxidant Activity by DPPH Assay

The DPPH free radical scavenging assay was used for the measurement of antioxidant activity of the developed microcapsules and prepared yogurt. ***In the case of microcapsules***, 3 g of dried milled microcapsules was dispersed in 100-ml methanol for 1 h and then filtered using Whatman No. 1 filter paper. The residue was re-extracted two times with additional 100-ml methanol for 15 min. Then, 5 μl of the combined filtrate was added to 2-ml methanol and 95 μl of freshly prepared 0.13-mM DPPH solution in methanol. The mixture was vigorously shaken and incubated for 30 min at room temperature in the dark. After incubation, the absorbance was measured at 517 nm against a blank (methanol) using a UV-Vis spectrophotometer (T80 UV/VIS Spectrometer, PG Instruments Ltd, UK) (A_{sample}). The control was prepared by replacing the test sample with 5-μl methanol ($A_{control}$). ***In the case of stirred yogurt***, 2.5-ml distilled water was added to 10 g of stirred yogurt (pH was set to 4 by adding 1-M HCl). The stirred yogurt was incubated at 45°C for 10 min and then centrifuged at 10.000 rpm for 10 min at 4°C. The supernatant was separated, and the pH was set to 7 by adding NaOH. Centrifugation was done again at 10.000 rpm for 10 min at 4°C, and about 250 μL of the sample was added to 2.75 ml of the methanolic solution of DPPH and stirred vigorously. Later, it was stored for 5 min at the ambient temperature, and the absorption was recorded at 517 nm (A_{sample}). In the control sample ($A_{control}$), distilled water was used instead of yogurt water (Tavakoli et al., 2018). The percentage of free radical-scavenging capacity was calculated by the following equation:

$$\textbf{Radical scavenging capacity } (\%) = \frac{\mathbf{A_{control} - A_{sample}}}{\mathbf{A_{control}}} \mathbf{X\ 100}$$

All measurements were performed in triplicate and reported as the average value.

Statistical Analysis

The data were analyzed using Statistical Analysis System Users Guide SAS (2004) (SAS Institute, Inc., USA). All data were carried out in triplicate, and mean values were calculated.

RESULTS AND DISCUSSION

Physicochemical Analysis of EVOO

The physical and chemical analysis of EVOO was evaluated according to recommended methods. Peroxide value is an indicator of initial lipid oxidation. PV is 3.8 meq.O_2/kg oil, which is lower than the legal limit of PV < 20 meq.O_2/kg oil, (EC, 1989/2003). Specific absorption coefficient K_{232} and K_{270} is indicative of the formation of conjugated dienes and trienes, respectively. The value of K_{232} and K_{270} is recorded at 1.79 and 0.16, respectively. The EU regulation established a value of K_{232} < 2.5 and K_{270} < 0.25 for extra virgin olive oil. The free acidity directly affected the flavor, color, stability, and quality of the olive oil. According to literature, free fatty acidity is a measure of the quality of the oil and reflects the care taken in production and storage processes of the oil, its stability, and its susceptibility to rancidity (Cobzaru et al., 2016). The acidity value is 0.15% that is below the maximum limit established for EVOO (≤0.8%).

The iodine value of investigated oil was found to be 90.75 g I_2/100-g oil. This value is a measure of the content of unsaturated fatty acids present in the oil. A higher value indicates a higher degree of unsaturation. The saponification value is an indication of the molecular weights of triglycerides in oil. A higher saponification value indicates a low proportion of lower fatty acids because the saponification value is inversely proportional to the average molecular weight or chain length of the fatty acids. Therefore, the shorter the average chain length, the higher is the saponification number (Atinafu and Bedemo, 2011). The saponification value of extra virgin olive oil was determined to be 189-mg KOH/g oil. All the physicochemical parameters for EVOO meet the International Olive Council (IOC) certification criteria for EVOO (IOC, 2015).

Droplet Size and Zeta Potential Analysis

EVOO nanoemulsion and nanocomposite (Section First Stage: Preparation of EVOO Nanoemulsion and Nanocomposite) were measured by Malvern Zetasizer to determine the droplet size and zeta potential distribution (**Figure 2**). EVOO nanoemulsion showed a smaller-mean droplets size of around 416 nm than EVOO nanocomposite, which has a mean droplets size of about 475 nm. In addition, the zeta potential of EVOO nanoemulsion and nanocomposite was −39.6 and −33.6 mV, respectively. In general, the two formulations have a high negative value of zeta potential charge above −30 mV, which indicates that both nanoemulsion and nanocomposite are stable (Mcclements, 2007). The zeta potential measures the electrokinetic potential of a droplet and defines the stability of the formulation system. The system is considered stable when the value is more than +25 mV and lower than −25 mV (Che Sulaiman et al., 2016). McClements (2005) confirmed that nanoemulsion having a negative zeta potential and well dispersion of droplets has good stability.

Oxidative Stability

The Rancimat method is officially recommended and is most commonly used for oxidative stability assessments of edible oils and fats (Ciemniewska-Zytkiewicz et al., 2014). The Rancimat test measures resistance to accelerated oxidation, which is a very important parameter for evaluating the quality of oils once it gives a good perception and estimation of the susceptibility to the oxidation process. The oxidative stability of EVOO extracted from prepared microcapsules in terms of measurement of induction periods (Rancimat, 20 L/ h at 110°C) was evaluated. The induction period (IP) of EVOO extracted from nanocomposite microcapsules (8 h) is lower than the IP of nanoemulsion microcapsules (11.30 h). During the extraction process of EVOO from nanocomposite microcapsules, polyphenols in EVOO (antioxidants) may be adsorbed onto nano-clay. Allaoui et al. (2020) used different solvents to recover the polyphenols after adsorption onto natural clay (ghassoul). Oxidative stability is not dependent on a single parameter but is rather affected by the fatty acid composition and a complex pool of antioxidants and prooxidants (Almoselhy, 2021).

Microencapsulation Efficiency (ME)

The microencapsulation efficiency is the main factor in evaluating the effective encapsulation method and indicating the efficiency of the chosen encapsulating materials (Bora et al., 2019). The $ME_{probiotic}$ was recorded as 88.84% for nanoemulsion microcapsules and 98.49 % for nanocomposite microcapsules. The nanocomposite microcapsules were more effective in the protection of probiotic strains inside microcapsules. This reason may be related to nano-clay material used in the preparation of nanocomposites microcapsules. Additionally, maltodextrin inside microcapsules acted as a prebiotic agent that maintained the viability of probiotic cells inside microcapsules either in the nanoemulsion or nanocomposite model (Bitaraf et al., 2013; Paim et al., 2016; Bhagwat et al., 2020; El-Sayed et al., 2021). Generally, the use of different microencapsulation techniques gave a positive impact on the viability of probiotic strains and maintained their viability for a long time as mentioned by other authors (El-Shafei et al., 2018; Chaudhary and Patel, 2019; Pourjafar et al., 2020).

Microencapsulation efficiency was evaluated by the degree of protection of the oil within the formed microcapsules. ME is the most essential factor in determining the success of oils microencapsulation, which is an indicator of a surface and coated oil content. As the wall material covered more oil droplets, the microencapsulation efficiency is higher. In the case of the nanocomposite microcapsule, ME_{EVOO} was 72%, while, in the nanoemulsion, the microcapsule was 65.61%. It can be seen that the ME value was affected by the addition of nano-clay. So, the nanocomposite microcapsule model had lower surface oil content compared to the nanoemulsion microcapsule model. According to the results, the combination of nano-clay with SA-WPC could increase the efficiency of protection of core oil. Singha and Hedenqvist (2020) reported that the barrier properties of coating composition were improved after the addition of nano-clay due to its platelet structure.

Morphological Features

The morphology of the developed synbiotic EVOO nanoemulsion and nanocomposite was observed by TEM. From the TEM micrographs, the spherical shape of the oil droplets was distributed uniformly and homogenously without any aggregation throughout the formulated nanoemulsion or

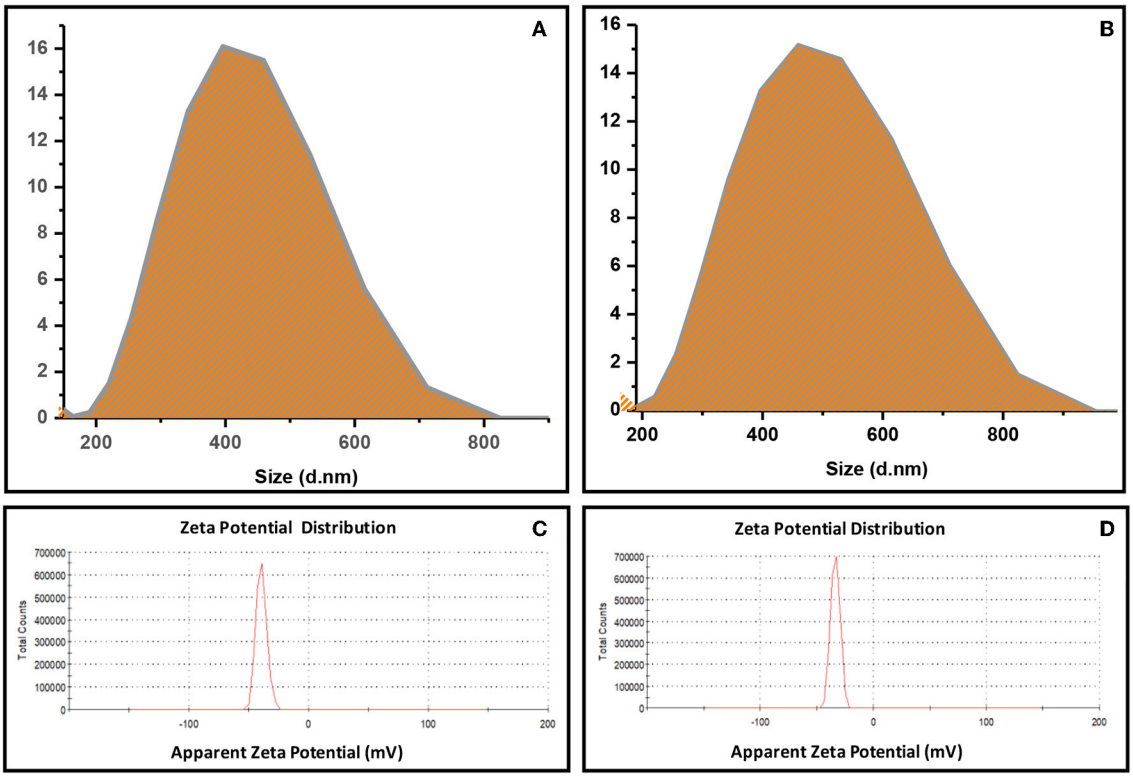

FIGURE 2 | Droplet size distribution of **(A)** EVOO nanoemulsion, **(B)** EVOO nanocomposite and Zeta potential distribution of **(C)** EVOO nanoemulsion, **(D)** EVOO nanocomposite.

nanocomposite (**Figures 31A**,**2A**). Moreover, the droplet size analyzed from TEM corresponded with the size obtained from the Zetasizer analysis. It can be also noted that probiotic bacteria were appeared and coated with the used polymers (SA-WPC) in synbiotic EVOO nanoemulsion (**Figure 31B**). In the synbiotic EVOO nanocomposite, the coated probiotic bacteria were well dispersed between clay layers (**Figure 32B**).

When examining the appearance of microcapsules models, it was seen that nanoemulsion microcapsules presented a bright white color. While the nanocomposite microcapsules were shown as beige, it may be due to the color of the nano-clay. The surface morphology of the nanoemulsion and nanocomposite microcapsules was investigated using SEM (**Figure 4**). As apparent from SEM photographs, freeze-dried microcapsules have crumpled: irregular shapes with a wide particle-size distribution and a porous structure. In the nanocomposite microcapsules, the overlapped structure of the clay was opened, and the distance between layers of the clay was observed (**Figures 4**, **3B**). In the same context, Anwar and Kunz (2011) presented evidence that microcapsules obtained by freeze-drying had an irregular, very light, and porous structure compared to those produced by spray drying. Considering the proceeding results, the existing morphology may affect the release behavior of EVOO and probiotic bacteria.

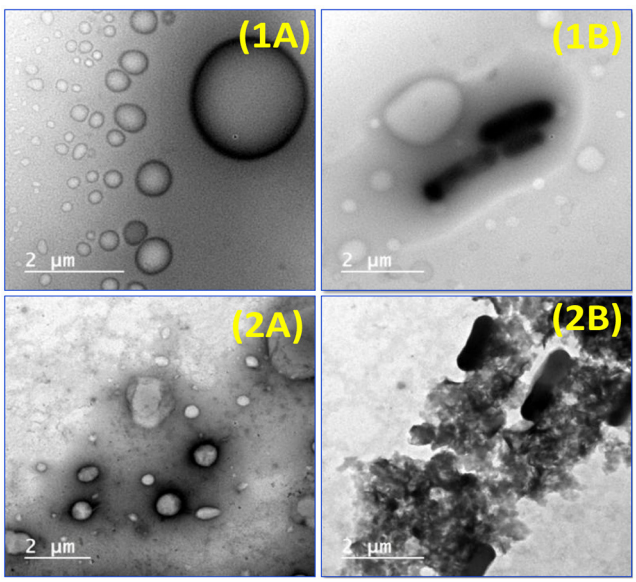

FIGURE 3 | TEM micrographs of **(1A)** EVOO nanoemulsion **(1B)** Synbiotic EVOO nanoemulsion **(2A)** EVOO nanocomposite and **(2B)** synbiotic EVOO nanocomposite.

Release Evaluation and Survivability for Microencapsulated EVOO and Probiotic Strains

In vitro Survivability of Probiotic Strains Inside Microcapsules in Simulated Gastrointestinal Conditions

The viability of probiotic strains in gastrointestinal conditions is important with the intention to get the preferred benefits of probiotics. Firstly, free and microcapsules cells were exposed to gastric juice. An instant decrease was examined in free cells in contrast to the encapsulated cells with nanoemulsion and nanocomposite microcapsules (**Table 2**). The nanocomposite microcapsules showed a 0.63 log reduction, while the nanoemulsion microcapsules showed a 1.10 log reduction as compared to free non-encapsulated cells; the reduction was around (2.28 log) after 2 h in gastric juice. The microcapsules of the probiotic cells within either nanoemulsion or nanocomposite microcapsules significantly affected ($p \leq 0.05$) the survivability of probiotic strains than free probiotic cells. Secondly, the remained free and microcapsules cells were exposed continuously to intestinal juice where the free cells and microcapsules were gently separated from gastric juice by cooling centrifugation and transferred to intestinal juice for additional 6 h. Different microcapsules models showed a protective effect on probiotic cells when exposed to intestinal conditions. From the result, a rapid log reduction was observed for free cells as compared to the encapsulated probiotics (**Table 2**).

The microencapsulated cells in either nanoemulsion or nanocomposite models had a significant outcome on cell survivability. The survivability rate after exposure to gastrointestinal juices for 6 h was recorded at 69.23, 68.84, and 37.71% for nanoemulsion microcapsules, nanocomposite microcapsules, and free cells, respectively. The results confirmed that the microencapsulated probiotic strains with prebiotic maltodextrin using biopolymers (SA-WPC) are a useful tool for the longevity of sensitive cells and other compounds. The current findings were in accordance with Pimentel-Gonza'leza et al. (2009) encapsulated *Lb. rhamnosus* by the double-emulsion technique (w/o/w), and this process increased the resistance to the culture when exposed to conditions similar to those found in gastric juice and the presence of the bile.

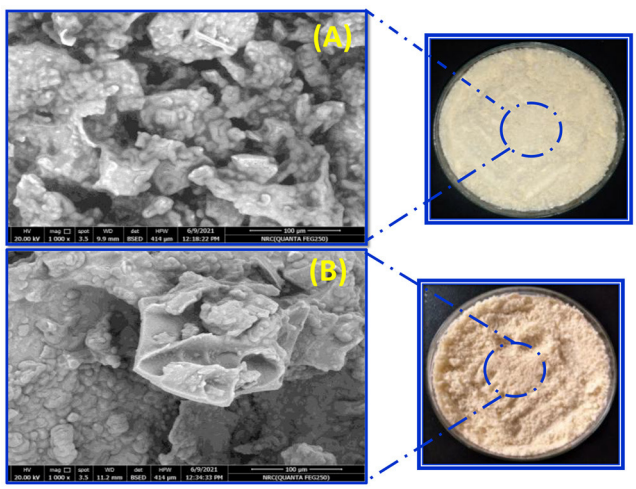

FIGURE 4 | SEM micrographs of **(A)** synbiotic EVOO nanoemulsion microcapsules and **(B)** synbiotic EVOO nanocomposite microcapsules.

EVOO and Probiotic Strains Release

The Release of Probiotic Strains

The time-dependent release of probiotic strains in microcapsules models and free cells in the simulated colonic solution is shown in **Figure 5**. In the first hour, more than 50% of the free cells were released from the dialysis bag, but about 30 and 20% of cells with nanoemulsion and nanocomposite microcapsules were released, respectively. Similarly, after 3 h, more than 50% of cells inside nanocomposite microcapsules were released. But, at the same time, more than 60% of the cells inside nanoemulsion microcapsules were released. Likewise, more than 80% of free cells were released from the dialysis bag at 3 h. The primary release for these preparations can be explained by the easy erosion of loose networks (Lotfipour et al., 2012). The release rate for cells was relatively remained stable with the same percentage for 4 h, and, after that, more released cells were observed. Also, in the case of microcomposite, the probiotic cells were aggregates and adhered to the surface of the clay, which may slow the release of the cells than nanoemulsion microcapsules (Li et al., 2014).

In vitro Release of EVOO

In vitro release profiles of EVOO from the prepared microcapsules were evaluated in gastrointestinal solutions at 37°C (**Figure 6**). The release properties of the prepared microcapsules were determined as a function of time. It

TABLE 2 | The survivability of microencapsulated probiotic strains particles in simulated gastrointestinal conditions.

Encapsulation type	Initial count	SGJ* (h)		SIJ* (h)			Survival rate (%)
		1	2	2	4	6	
Nanoemulsion microcapsules	9.10^{Aa}	8.00^{Ba}	7.50^{Cb}	7.20^{Ca}	7.00^{Da}	6.30^{Ea}	69.23^{a}
Nanocomposite microcapsules	9.50^{Aa}	8.87^{Ba}	8.49^{Ba}	7.58^{Ca}	7.00^{Da}	6.54^{Ea}	68.84^{b}
Probiotic free cells	9.18^{Aa}	6.90^{Bb}	5.85^{Cc}	5.16^{Cb}	4.60^{Db}	3.37^{Eb}	36.71^{c}

**SGJ, stimulated gastric juice; SIJ, stimulated intestinal juice. The viable count expresses as Log CFU/g beads. Rows with the same capital letter are not significant ($p \leq 0.05$). Columns with the same small letter are not significant ($p \leq 0.05$).*

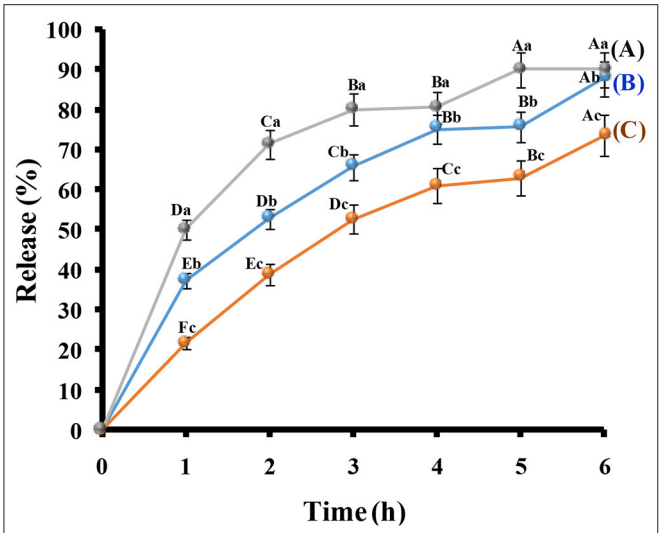

FIGURE 5 | Probiotic strains released from microcapsules (A) probiotic-free cells, (B) nanoemulsion microcapsules, and (C) nanocomposite microcapsules. The capital letters between the release time and the same capital letters are not significant ($p \leq 0.05$). The small letters between the free cells and microcapsules and the same small letters are not significant ($p \leq 0.05$).

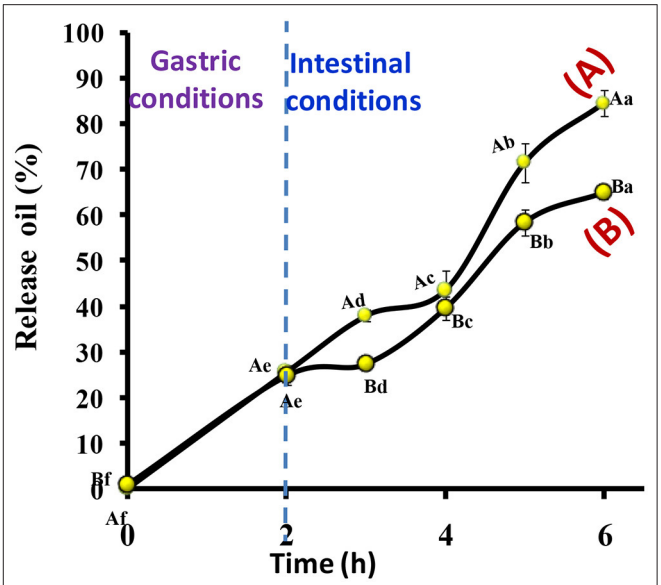

FIGURE 6 | The release profile of EVOO from (A) nanoemulsion microcapsules and (B) nanocomposite microcapsules. The capital letters between microcapsules and the same capital letter s are not significant ($p \leq 0.05$). The small letters between release time and the same small letters are not significant ($p \leq 0.05$).

was noted that nanocomposite microcapsules showed a slower release than nanoemulsion microcapsules. At gastric conditions, approximately 25% of EVOO were released from nanoemulsion and nanocomposite microcapsules in 2 h. The release at intestinal conditions was about 84 and 65% in 4 h from these microcapsules. Zhang et al. (2020) showed the release of imidacloprid and retarded by incorporating it into bentonite-alginate composites. The wall materials of microcapsules had a controlling effect on the release of EVOO as a core material. A similar trend was observed in the release behavior of the fish oil as a core of microcapsules (Pang et al., 2017). In addition, the release rate curve of the microcapsule gradually flattened with time, indicating that both EVOO and probiotic strains were successfully embedded and slowly released.

Stirred Yogurt Manufacturing Fortified With Microcapsules Models

Microbiological Activities of Stirred Yogurt Treatments

The microbiological evaluation of stirred yogurt fortified with different microcapsules models and free cells as control is shown in **Table 3**. The count of *B. bifidum* in different treatments was significantly boosted during the storage period. But the count of *B. bifidum* in the T2 that contained free cells was increased in the first 10 days, and, after that, slight decline was observed at the end of storage and reached 6.14 log CFU/ml. Additionally, the count of *B. bifidum* in the microcapsules treatments was increased during the storage period, and the maximum count was observed at 15 days where the *B. bifidum* in the T3 and T4 was enhanced in the count with about 1.00 and 1.09 log cycles, respectively. From the results, the microcapsules models were able to maintain and enhance the viability of probiotic strain inside stirred yogurt than free cells (Paredes et al., 2016; Marefati et al., 2021).

Likewise, the count of *Lb. acidophilus* in stirred yogurt was enhanced during the storage period in the treatments (T2 and T3) than in the treatment with free cells (T2). The maximum viable counts for encapsulated *Lb. acidophilus* were observed on Day 15 of storage and slightly decreased with non-significantly recorded on Day 20 of storage. Generally, the *Lb. acidophilus* counts in T3 and T4 were enhanced by about 0.94 and 0.92 log cycles at the end of storage. In contrast, in the T2 that contained free cells, the viable counts slightly declined at the end of storage (6.85 logs CFU/ml). Our results are in the same line as Chávarri et al. (2010) and El-Sayed et al. (2015), who indicated that encapsulated probiotic strains with prebiotic materials were more stable and viable than free cells during storage in dairy products.

The starter cultures used in the manufacturing of yogurt were evaluated during storage as **Table 3**. The count of *S. thermophilus* in treatments was having the same activities and counts. Where the count of *S. themophilus* in the fresh stirred yogurt was recorded in 7 log cycles, the counts were improved for 15 days to reach 8 log cycles. But the decline in the *S. thermophilus* counts was detected on Day 20 (at the end of storage time), which is related to the acidity development during storage.

Moreover, the counts of the *Lb. bulgaricus* had the same activities, which not detected significant differences in their counts for all treatments during the storage period. The counts of *Lb. bulgaricus* in treatments were ranged between 6.0 and 7.0 log cycles during fresh and Day 20 of storage. But slight enhancement at 10 days of storage was observed, where the counts in all treatments were recorded between 7.5 and 8.0 log cycles.

TABLE 3 | Microbiological evaluation of stirred yogurt treatments.

Treatments	Zero	5	10	15	20
***B. bifidum*counts (log CFU/mL)**					
T1	N.F	N.F	N.F	N.F	N.F
T2	6.96^{Bb}	7.44^{Ab}	7.84^{Ab}	6.59^{BCb}	6.14^{Cc}
T3	7.33^{Ba}	7.59^{Ba}	8.10^{Aa}	8.30^{Ab}	8.27^{Ab}
T4	7.48^{Ba}	7.76^{Ba}	8.33^{ABa}	8.58^{Aa}	8.40^{Aa}
***Lb. acidophilus* counts (log CFU/mL)**					
T1	N.F	N.F	N.F	N.F	N.F
T2	7.00^{Bb}	7.70^{Ab}	7.91^{Ac}	7.20^{Cb}	6.85^{Db}
T3	7.90^{Ba}	8.58^{Aa}	8.88^{Ab}	8.60^{Aa}	8.80^{Aa}
T4	7.87^{Ca}	8.78^{Ba}	9.00^{Aa}	8.82^{ABa}	8.85^{ABa}
***S. thermophilus* counts(log CFU/mL)**					
T1	7.29^{Ca}	7.56^{Cc}	8.28^{Ab}	7.90^{Bc}	7.55^{Ba}
T2	7.39^{Ba}	7.87^{Bb}	8.40^{Aa}	8.00^{Aa}	7.22^{Ca}
T3	7.33^{Ba}	7.57^{Bc}	8.51^{Aa}	8.17^{Ab}	7.25^{Ca}
T4	7.36^{Ba}	8.83^{Aa}	8.50^{Aa}	8.23^{Aa}	7.19^{Bb}
***Lb. bulgaricus* counts (log CFU/mL)**					
T1	6.85^{Ba}	7.30^{Aa}	7.55^{Ab}	6.40^{Cb}	6.28^{Cc}
T2	6.91^{Ca}	7.65^{Aa}	7.90^{Ab}	7.41^{Ba}	6.85^{Cb}
T3	6.96^{Da}	7.58^{Ba}	7.95^{Aa}	7.60^{Ba}	7.20^{Ca}
T4	6.87^{Ca}	7.55^{Ba}	8.00^{Aa}	6.67^{Cb}	$7.00B^{Ca}$
Mold and Yeast counts (Log CFU/mL)					
T1	N.D	1.90^{Da}	2.20^{Ca}	3.00^{Ba}	4.98^{Aa}
T2	N.D	N.D	N.D	2.10^{Bb}	3.30^{Ab}
T3	N.D	N.D	N.D	1.39^{Ac}	2.53^{Ac}
T4	N.D	N.D	N.D	2.90^{Bb}	3.00^{Ab}

Data expressed as 3 replicates. T1, plain-stirred yogurt; T2, stirred yogurt with probiotic-free cells; T3, stirred yogurt with synbiotic EVOO nanoemulsion microparticles; T4, stirred yogurt synbiotic EVOO nanocomposite microcapsules; N.F., not found; N.D., not detected. Rows with the same capital letters are not significant ($p \leq 0.05$). Columns with the same small letter are not significant ($p \leq 0.05$).

The counts of mold and yeast were detected in stirred yogurt treatments during storage (**Table 3**). The data did not detect counts for mold and yeast in the fresh samples, which were related to the hygienic rules and pasteurization that follow during manufacturing. During storage, small mold and yeast counts were detected firstly in plain treatment (T1) on Day 5 of storage. Also, in the other treatments, the count of mold and yeast was detected with the storage time on Day 15 of storage, which may be related to the antimicrobial activities of probiotic strains that are integrated into these treatments (T2, T3, and T4). At the end of storage, the mold and yeast counts were reached 4.98, 3.30, 2.53, and 3.00 log CFU/ml for T1, T2, T3, and T4, respectively. So, our data recommended that the stirred yogurt shelf life did not exceed the 15 days of storage as mentioned by authors Yoon et al. (2013) that found the shelf life of yogurt beverages at 10, 15, and 25°C was as 19, 14, and 12 days, respectively, and 17, 16, and 12 days for stirred yogurt, respectively.

Chemical Evaluation Stirred Yogurt Treatments

The chemical composition of stirred yogurt treatments was found in **Table 4**. The total solid (T.S.) was ranged between 17.08 and 17.72%, and the high total solid content was indicated in T3 and T4, which contains microcapsules. Also, the moisture content was slightly different in all treatments, and little moisture content was found in treatments integrated with microcapsules (T3 and T4). Generally, moisture content was ranged between 82.28 and 83.13. The change in the total solid and moisture content in the T3 and T4 that are integrated with microcapsules may be related to found coating materials (SA-WPC) and the prebiotic agent (maltodextrin). Additionally, the results were detected light differences but non-significantly in total protein, which ranged between 3.85 and 4.05%.

TABLE 4 | Chemical composition of stirred yogurt treatments.

Treatments	T.S	Moisture	Protein	pH	T.A
T1	16.08^{B}	83.62^{A}	3.85^{B}	4.45^{A}	0.99^{B}
T2	17.48^{A}	82.52^{A}	3.95^{B}	4.34^{B}	1.01^{A}
T3	17.53^{A}	82.47^{B}	4.03^{A}	4.35^{B}	1.02^{A}
T4	17.72^{A}	82.28^{B}	4.05^{A}	4.37^{B}	1.04^{A}

Data expressed as 3 replicates. T1, plain-stirred yogurt; T2, stirred yogurt with probiotic-free cells; T3, stirred yogurt with synbiotic EVOO nanoemulsion microparticles; T4, stirred yogurt synbiotic EVOO nanocomposite microcapsules. Columns with the same capital letter are not significant ($p \leq 0.05$).

The pH values in the treatments ranged between 4.34 and 4.45 with non-significantly differences, but a slight drop in the pH values was observed in the T1 that integrated with probiotic free cells. The development in the pH was fast in this treatment related to the metabolic activities of prebiotic free cells. Also, the titratable acidity (T.A.) was ranged between 0.99 and 1.04 and did not show significant differences between treatments. Our results are in the same line as Ribeiro et al. (2014), Fayed et al. (2019), Ismail et al. (2020) recorded that the pH values were lower in yogurt with free probiotics than in yogurt with encapsulated probiotics. Chouchouli et al. (2013) designed the study with the direct fortification of plain yogurts, producing stirred fortified yogurts.

Sensory Evaluation of Stirred Yogurt Treatments

Sensory evaluations of stirred yogurt treatments during storage are shown in **Figure 7**. Fresh treatments even with microcapsules models or free cells displayed that plain-stirred yogurt and stirred yogurt with free cells (T1 and T2) were higher white than stirred yogurt with microcapsules models (T3 and T4) due to the yellow color of microcapsules powder that added. This yellow color could be related to the EVOO and other coating materials (SA-WPC). For odor and appearance, all treatments were very good and did not detect significant differences between them. On the other hand, the highest score for the mouth feel was observed for plain-stirred yogurt and stirred yogurt with free cells (T1 and T2) followed by stirred yogurt with nanoemulsion microcapsules and nanocomposite microcapsules (T3 and T4), respectively, which could be related to the feeling with small particles during evaluation by members (Kailasapathy, 2006; Ismail et al., 2020). Overall acceptability in fresh time was recorded as 5 for T1 and T2 but slightly low as 4.9 for T3 and T4.

During the storage period, the color and appearance were decreased in all treatments; this could be related to the

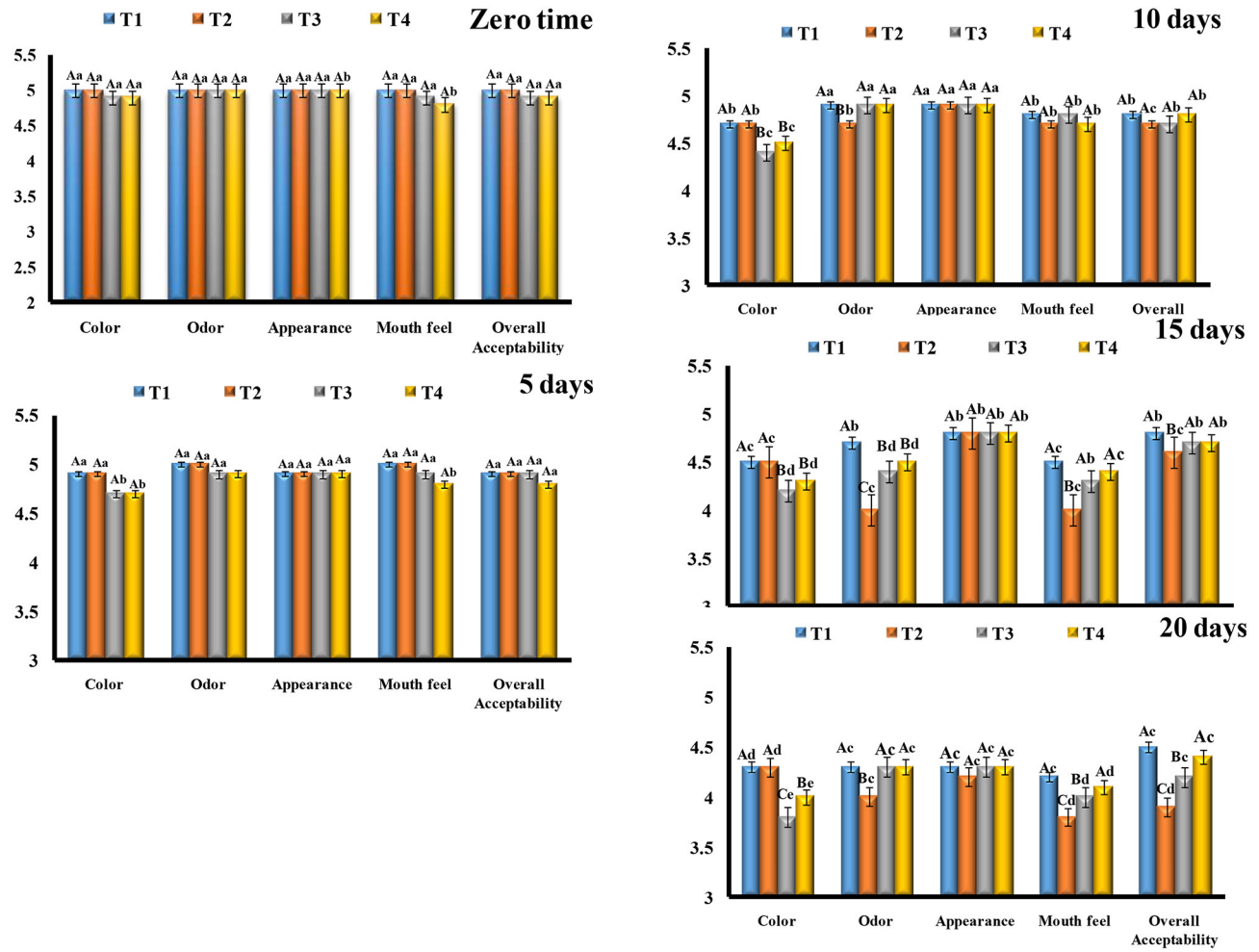

FIGURE 7 | Sensory evaluation of stirred yogurt treatments. The capital letters between treatments and the same capital letters are not significant ($p \leq 0.05$). The small letters between storage time and the same small letters are not significant ($p \leq 0.05$). Data expressed as (mean ± SD) of 3 replicates. T1, Plain-stirred yogurt; T2, stirred yogurt with probiotic-free cells; T3, stirred yogurt with synbiotic EVOO nanoemulsion microparticles; T4, stirred yogurt synbiotic EVOO nanocomposite microcapsules.

moisture lost over time, as it made the treatments more yellow, especially for treatments with microcapsules models (T3 and T4). Moreover, the mouth feel of treatments was decreased by the time of storage, and more decrease was observed for stirred yogurt with free cells (T2), followed by stirred yogurt with nanoemulsion microcapsules (T3) at the end of storage (20 days). These results could be related to the development of the acidity faster in the treatment with free cells (T2) than others that are related to the metabolic activity of free cells than encapsulated cells.

The encapsulated materials were slow down the release of the acidity that produced from the microbial strains activities during storage period (Ribeiro et al., 2014; Afzaal et al., 2019). Generally, the overall acceptability for all treatments was decreased with the storage time, but the plain-stirred yogurt (T1) was the most treatment accepted all the time, followed by stirred yogurt with nanocomposite microcapsules (T4), stirred yogurt with nanoemulsion microcapsules (T3), and stirred yogurt with free cells (T2), respectively, at the end of the storage period. During storage, the score for sensory evaluation of stirred yogurt with free cells (T2) was dropped, and then microcapsule treatments (T3 and T4) could be related to a more sour feeling and an odor that developed from metabolic activities of strains during storage. In contrast, a more drop in the score for color was observed for treatments with encapsulated particles (T3 and T4). So, our data recommended that the suitable shelf life for the stirred yogurt with microcapsules that maintained the viability of probiotic strains not exceeds 15 days to be acceptable to the consumer as plain-stirred yogurt.

Antioxidant Activity of Prepared Microcapsules and Stirred Yogurt Treatments

The antioxidant activity (AA) of prepared microcapsules and stirred yogurt was determined by the DPPH radical scavenging

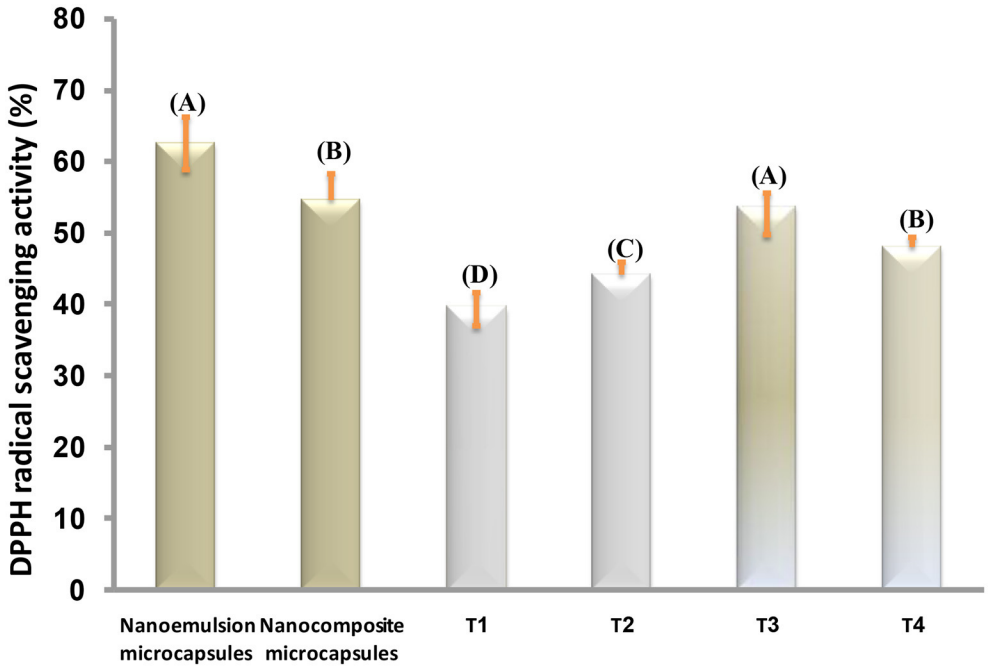

FIGURE 8 | DPPH radical scavenging activity (%) of microcapsules and stirred yogurt treatments. The same capital letters are not significant ($p \leq 0.05$). T1, plain-stirred yogurt; T2, stirred yogurt with probiotic-free cells; T3, stirred yogurt with synbiotic EVOO nanoemulsion microparticles; T4, stirred yogurt synbiotic EVOO nanocomposite microcapsules.

assay. The DPPH scavenging activity assay is widely used to evaluate the ability of compounds to scavenge free radicals or donate hydrogen and to determine the antioxidant activity in foods (Bidchol et al., 2011). EVOO is a source of phenolic compounds with a powerful antioxidant activity that includes tyrosol, hydroxytyrosol, and secoiridoid derivatives (Francisco et al., 2019). According to **Figure 8**, the antioxidant activity values of the nanoemulsion microcapsules were higher than nanocomposite microcapsules. In stirred yogurt, T1 showed AA possibly due to the presence of compounds in milk, such as low molecular weight antioxidants, free amino acids, lactose, peptides, proteins, or reducing compounds (Oliveira and Pintado, 2015). Microcapsules-fortified yogurts exhibited higher AA than plain-stirred yogurt. The addition of nanoemulsion microcapsules to stirred yogurts increased antioxidant activity more than plain yogurt (T1). It was noted that T4 has a little higher AA (48%) than T2 (44%). Ribeiro et al. (2014) showed that powder-fortified yogurts exhibited higher antioxidant activity than the control. The oxidative stability was higher for nanoemulsions than for nanocomposite microcapsules, which was consistent with the AA results.

CONCLUSION

Stirred yogurt was fortified with two models of microcapsules based on synbiotic EVOO nanoemulsion and nanocomposite. These microcapsules were prepared in three stages: nano emulsification, blending, and freeze-drying technique. EVOO nanoemulsion showed a smaller mean droplet size than EVOO nanocomposite, and both nanoemulsion and nanocomposite had good stability. The nanoemulsion microcapsules model displayed better oxidative stability than the nanocomposite model. However, the nanocomposite microcapsules were more effective in the protection of EVOO and probiotics than the nanoemulsion model. The morphology of the nanoemulsion and nanocomposite that showed the spherical shape of the oil droplets was distributed uniformly and homogenously without any aggregation. It can be also noted that probiotic bacteria appeared and coated with the used polymers (SA-WPC). From SEM photographs, the two models of microcapsules have crumpled: irregular shapes with a wide particle-size distribution and a porous structure. The nanocomposite microcapsules showed a slower release of EVOO and probiotics than nanoemulsion microcapsules. Additionally, probiotic bacteria inside developed microcapsules were enumerated with good active counts after being exposed to gastrointestinal juices. Finally, the addition of nanoemulsion microcapsules to stirred yogurts increased antioxidant activity more than plain yogurt. Moreover, the viability of probiotic strains in microcapsules form was more active in the stirred yogurt during storage. The most accepted treatment in the sensory evaluation was recorded as the plain-stirred yogurt, followed by stirred yogurt with nanocomposite

microcapsules and stirred yogurt with nanoemulsion microcapsules. Overall, stirred yogurt was an appropriate delivery carrier for microencapsulated active probiotic bacteria and EVOO.

DATA AVAILABILITY STATEMENT

The original contributions presented in the study are included in the article/supplementary material, further inquiries can be directed to the corresponding author/s.

AUTHOR CONTRIBUTIONS

HE-S and AH conceived the research idea and helped to collect the data. KY, HE-S, and AH analyzed the data and wrote the paper. All authors contributed to the article and approved the submitted version.

REFERENCES

Afzaal, M., Zahoor, T., Sadiq, F. A., Ahmad, F., Yasmeen, A., Imran, M., et al. (2019). Effect of encapsulation on the viability of probiotics in yoghurt. *Progr. Nutr.* 20, 44–52. doi: 10.1007/s12602-018-9485-9

Aghbashlo, M., Mobil, H., Madadlou, A., and Rafiee, S. (2013). Influence of wall material and inlet drying air temperature on the microencapsulation of fish oil by spray drying. *Food Bioprocess Technol.* 6, 1561–1569. doi: 10.1007/s11947-012-0796-7

Allaoui, S., Bennani, M. N., Ziyat, H., Qabaqous, O., Tijani, N., Ittobane, N., et al. (2020). Antioxidant and antimicrobial activity of polyphenols extracted after adsorption onto natural clay "Ghassoul". *J. Chem*. 2020, 8736721. doi: 10.1155/2020/8736721

Almoselhy, R. I. M. (2021). Comparative Study of Vegetable Oils Oxidative Stability using DSC and Rancimat Methods. *Egyptian J. Chem.* 64, 299–312. doi: 10.21608/ejchem.2021.51238.3051

American Oil Chemists' Society (AOCS). "*Official Methods and Recommended Practices of the American Oil Chemists' Society*", AOCS Press, Champaign, IL (2005).

Anwar, S. H., and Kunz, B. (2011). The influence of drying methods on the stabilization of fish oil microcapsules: Comparison of spray granulation, spray drying and freeze drying. *J. Food Eng.* 105, 367–378. doi: 10.1016/j.jfoodeng.2011.02.047

AOAC (2012). "*Methods of Analysis*", 19th ed. Agricultural chemicals, contaminants, drugs. Washington DC: United States. Vol. 1.

AOCS (2011). AOCS Official Method *Cd* 8b-90.

APHA (1994). *Standard Methods for Examination of Dairy Products (16thed.)*. Washington, DC: USA. American Public. Health Association.

Arjona, J. C., Silva-Valenzuela, M. G., Wang, S. H., and Valenzuela-Diaz, F. R. (2021). Biodegradable nanocomposite microcapsules for controlled release of urea. *Polymers* 13, 722. doi: 10.3390/polym13050722

Atinafu, D. G., and Bedemo, B. (2011). Estimation of total free fatty acid and cholesterol content in some commercial edible oils in Ethiopia, Bahir DAR. *Journal of Cereals and Oil seeds* 2, 71–76. doi: 10.5897/JCO11.025

Bendini, A., Cerretani, L., Vecchi, S., Carrasco-Pancorbo, A., and Lercker, G. (2006). Protective effects of extra virgin olive oil phenolics on oxidative stability in the presence or absence of copper ions. *J. Agric. Food Chem.* 54, 4880–4887. doi: 10.1021/jf060481r

Bhagwat, A., Bhushette, P., and Annapure, U. S. (2020). Spray drying studies of probiotic Enterococcus strains encapsulated with whey protein and maltodextrin. *Beni-Suef Univ J. Basic Appl. Sci.* 9, 1–8. doi: 10.1186/s43088-020-00061-z

Bidchol, A. M., Wilfred, A., Abhijna, P., and Harris, R. (2011). Free radical scavenging activity of aqueous and ethanolic extract of Brassica oleracea L. var. italica. *Food Bioproc. Technol.* 4, 1137–1143. doi: 10.1007/s11947-009-0196-9

Bitaraf, S., Abbasi, S., and Hamidi, Z. (2013). Production of low-energy prebiotic dark chocolate using inulin, polydextrose, and maltodextrin. *Iranian J. Nutr. Sci. Food Technol.* 8, 49–62. Available online at: http://nsft.sbmu.ac.ir/article-1-1128-en.html

Bora, A. F. M., Li, X., Zhu, Y., and Du, L. (2019). Improved viability of microencapsulated probiotics in a freeze-dried banana powder during storage and under simulated gastrointestinal tract. *Probiot. Antimicrob. Protein.* 11, 1330–1339. doi: 10.1007/s12602-018-9464-1

Calvo, P., Castaño, Á. L., Lozano, M., and González-Gómez, D. (2012). Influence of the microencapsulation on the quality parameters and shelf-life of extra-virgin olive oil encapsulated in the presence of BHT and different capsule wall components. *Food Res. Int.* 45, 256–261. doi: 10.1016/j.foodres.2011.10.036

Castro, J. M., Tornadijo, M. E., Fresno, J. M., and Sandoval, H. (2015). Biocheese: a food probiotic carrier. *BioMed. Res. Int.* 2015. doi: 10.1155/2015/723056

Chaudhary, H. J., and Patel, A. R. (2019). Microencapsulation technology to enhance the viability of probiotic bacteria in fermented foods: an overview. *Int. J. Ferment. Foods* 8, 63–72. doi: 10.30954/2321-712X.02.2019.1

Chávarri, M., Marañón, I., Ares, R., Ibáñez, F. C., Marzo, F., and del Carmen Villarán, M. (2010). Microencapsulation of a probiotic and prebiotic in alginate-chitosan capsules improves survival in simulated gastro-intestinal conditions. *Int. J. Food Microbiol.* 142, 185–189. doi: 10.1016/j.ijfoodmicro.2010.06.022

Che Sulaiman, I. S., Basri, M., Fard Masoumi, H. R., Ashari, S. E., and Ismail, M. (2016). Design and development of a nanoemulsion system containing extract of Clinacanthus nutans (L.) leaves for transdermal delivery system by D-optimal mixture design and evaluation of its physicochemical properties. *RSC Adv.* 6, 67378–67388. doi: 10.1039/C6RA12930G

Chouchouli, V., Kalogeropoulos, N., Konteles, S.J., Karvela, E., Makris, D. P., and Karathanos, V.T. (2013). Fortification of yoghurts with grape (Vitis vinifera) seed extracts. *LWT - Food Sci. Technol.* 53, 522–529. doi: 10.1016/j.lwt.2013.03.008

Ciemniewska-Zytkiewicz, H., Ratusz, K., Bryś, J., Reder, M., and Koczo,ń, P. (2014). Determination of the oxidative stability of hazelnut oils by PDSC and Rancimat methods. *J. Thermal Analy. Calorim.* 118, 875–881 doi: 10.1007/s10973-014-3861-9

Cobzaru, C., Bordeianu, G., Apostolescu, G. A., Marinoiu, A., and Cernatescu, C. (2016). Quality evalution of the olive oil during storage time. *Rev. Roumaine Chim.* 61, 705–710. Available online at: http://revroum.lew.ro/wp-content/uploads/2016/08/Art%2013.pdf

Doherty, S. B., Gee, V. L., Ross, R. P., Stanton, C., Fitzgerald, G. F., and Brodkorb, A. (2011). Development and characterisation of whey protein micro-beads as potential matrices for probiotic protection. *Food Hydrocoll.* 25, 1604–1617. doi: 10.1016/j.foodhyd.2010.12.012

Dong, J., He, Y., Zhang, J., and Wu, Z. (2021). Tuning alginate-bentonite microcapsule size and structure for the regulated release of P. putida Rs-198. *Chin. J. Chem. Eng.* doi: 10.1016/j.cjche.2021.03.056

EC, (1989/2003). EUCRE. Amending Regulation (EEC) (1989/2003) No 2568/91 on the characteristics of olive oil and olive-pomace oil and on the relevant methods of analysis. Official Journal of the European Union L295.

El-Sayed, H., Ismail, S., and Fayed, B. (2021). Novel assessment of synergistic stimulatory effect of prebiotic chitoologosccharide and some commercial prebiotic on the probiotic growth: a preliminary study. *J. Microbiol. Biotechnol. Food Sci.* 11, e3341–e3341. doi: 10.15414/jmbfs.3341

El-Sayed, H. S., Salama, H. H., and and, E. L.-, Sayed, S. M. (2015). Production of synbiotic ice cream. *Int. J. Chem. Tech. Res.* 7, 138–147. Available online at: https://www.semanticscholar.org/paper/Production-of-Synbiotic-Ice-Cream-El-Sayed-Salama/e9fe969a07f22e75a8b565a0d5ba0c246084e1b5

El-Sayed, S. M., and El-Sayed, H. S. (2020). Production of UF-soft cheese using probiotic bacteria and *Aloe vera* pulp as a good source of nutrients. *Ann. Agric. Sci.* 65, 13–20. doi: 10.1016/j.aoas.2020.05.002

El-Shafei, K., Elshaghabee, F. M. F., El-Sayed, H. S., and Kassem, J. M. (2018). Assessment the viability properties of *Lactobacillus casei* strain using labneh as a carrier. *Acta Scientiarum Polonorum Technol. Alimentar.* 17, 267–276. doi: 10.17306/J.AFS.0583

Fayed, B., Abood, A., El-Sayed, H. S., Hashem, A. M., and Mehanna, N. S. H. (2018). A synbiotic multiparticulate microcapsule for enhancing inulin intestinal release and Bifidobacterium gastro-intestinal survivability. *Carbohydrate Polyme.* 193, 137–143. doi: 10.1016/j.carbpol.2018.03.068

Fayed, B., El-Sayed, H. S., Abood, A., Hashem, A. M., and Mehanna, N. S. (2019). The application of multi-particulate microcapsule containing probiotic bacteria and inulin nanoparticles in enhancing the probiotic survivability in yoghurt. *Biocatal. Agric. Biotechnol.* 22, 101391. doi: 10.1016/j.bcab.2019.101391

Francis, H. M., Stevenson, R. J., Chambers, J. R., Gupta, D., Newey, B., et al. (2019). A brief diet intervention can reduce symptoms of depression in young adults – A randomised controlled trial. *PLoS ONE.* 14, e0222768. doi: 10.1371/journal.pone.0222768

Francisco, C. V., Ruiz-Fernández, V., Lahera, F., Lago, J., and Pino, L. S. (2019). Natural molecules for healthy lifestyles: Oleocanthal from extra virgin olive oil. *J. Agric. Food Chem.* 67, 3845–3853. doi: 10.1021/acs.jafc.8b06723

Gallardo, G., Guida, L., Martinez, V., López, M. C., Bernhardt, D., Blasco, R., et al. (2013). Microencapsulation of linseed oil by spray drying for functional food application. *Food Res. Int.* 52, 473–482. doi: 10.1016/j.foodres.2013.01.020

Gilliland, S. E., and Walker, D. K. (1990). Factors to consider when selecting a culture of *Lactobacillus acidophilus* as a dietary adjunct to produce a hypocholesterolemic effect in humans. *J. Dairy Sci.* 73, 905–911. doi: 10.3168/jds.S0022-0302(90)78747-4

Hamed, S. F., Hashim, A. F., Abdel Hamid, H., Abd-Elsalam, K. A., Golonka, I., Musia,ł, W., et al. (2020). Edible alginate/chitosan-based nanocomposite microspheres as delivery vehicles of omega-3 rich oils. *Carbohydr. Poly.* 239, 116201. doi: 10.1016/j.carbpol.2020.116201

IDF, (1997). *International Dairy Federation.* Dairy starter cultures of lactic acid bacteria (LAB) standard of identity, IDF Standard No. 149A. Brussels.

IOC (2015). "Trade standard applying to olive oils and olive pomace oils", in: *International Olive Council,* COI/T.15/NC No 3/Rev. 8

Ismail, S. A., El-Sayed, H. S., and Fayed, B. (2020). Production of prebiotic chitooligosaccharide and its nano/microencapsulation for the production of functional yoghurt. *Carbohydr. Poly.* 234, 115941. doi: 10.1016/j.carbpol.2020.115941

Jafari, S. M., Assadpoor, E., He, Y., and Bhandari, B. (2008). Encapsulation efficiency of food flavours and oils during spray drying. *Drying Technol.* 26, 816–835. doi: 10.1080/07373930802135972

Kailasapathy, K. (2006). Survival of free and encapsulated probiotic bacteria and their effect on the sensory properties of yoghurt. *LWT-Food Sci. Technol.* 39, 1221–1227. doi: 10.1016/j.lwt.2005.07.013

Kailasapathy, K., and Chin, J. (2000). Survival and therapeutic potential of probiotic organisms with reference to *Lactobacillus acidophilus* and *Bifidobacterium* spp. *Immunol. Cell Biol.* 78, 80–88. doi: 10.1046/j.1440-1711.2000.00886.x

Koç, M., Güngör, Ö., Zungur, A., Yalçin, B., Selek, I., Ertekin, F. K., et al. (2015). Microencapsulation of extra virgin olive oil by spray drying: effect of wall materials composition, process conditions, and emulsification method. *Food Bioprocess Technol.* 8, 301–318. doi: 10.1007/s11947-014-1404-9

Ladokun, O., and, Oni, S., (2014). Fermented milk products from different milk types. *Food Nutr. Sci.* 5, 1228–1233. doi: 10.4236/fns.2014.513133

Li, S., Jiang, C., Chen, X., Wang, H., and Lin, J. (2014). Lactobacillus casei immobilized onto montmorillonite: survivability in simulated gastrointestinal conditions, refrigeration and yogurt. *Food Res. Int.* 64, 822–830. doi: 10.1016/j.foodres.2014.08.030

Ling, E. R. (1963). "*A Text Book of Dairy Chemistry, vol.2, practical (3rd ed.)*", London: Chapman and Hall Ltd. p. 58–65.

Lotfipour, F., Mirzaeei, S., and Maghsoodi, M. (2012). Preparation and characterization of alginate and psyllium beads containing *Lactobacillus acidophilus*. *Sci. World J.* 2012, 1–8. doi: 10.1100/2012/680108

Madene, A., Jacquot, M., Scher, J., and Desobry, S. (2006). Flavourencapsulation and controlled release- a review. *Int. J. Food Sci. Technol.* 41, 1–21. doi: 10.1111/j.1365-2621.2005.00980.x

Mahmoud, M., Abdallah, N. A., El-Shafei, K., Tawfik, N. F., and El-Sayed, H. S. (2020). Survivability of alginate-microencapsulated *Lactobacillus plantarum* during storage, simulated food processing and gastrointestinal conditions. *Heliyon.* 6, e03541. doi: 10.1016/j.heliyon.2020.e03541

Marefati, A., Pitsiladis, A., Oscarsson, E., Ilestam, N., and Bergenståhl, B. (2021). Encapsulation of *Lactobacillus reuteri* in W1/O/W2 double emulsions: formulation, storage and in vitro gastro-intestinal digestion stability. *LWT.* 146, 111423. doi: 10.1016/j.lwt.2021.111423

McClements, D. J. (2005). "*Food Emulsions: Principles, Practice, and Techniques*", Boca Raton, FL: CRC Press.

Mcclements, D. J. (2007). Critical review of techniques and methodologies for characterization of emulsion stability. *Crit. Rev. Food Sci. Nutr.* 47, 611–649. doi: 10.1080/10408390701289292

Min, M., Bunt, C. R., Mason, S. L., and Hussain, M. A. (2019). Non-dairy probiotic food products: an emerging group of functional foods. *Crit. Rev. Food Sci. Nutr.* 59, 2626–2641. doi: 10.1080/10408398.2018.1462760

Moghanjougi, Z. M., Bari, M. R., Khaledabad, M. A., Amiri, S., and Almasi, H. (2021). Microencapsulation of *Lactobacillus acidophilus* LA-5 and Bifidobacterium animalis BB-12 in pectin and sodium alginate: a comparative study on viability, stability, and structure. *Food Sci. Nutr.* 9, 5103–5111 doi: 10.1002/fsn3.2470

Morelli, L., and Capurso, L. (2012). FAO/WHO guidelines on probiotics: 10 years later. *J. Clin Gastroenterol.* 46, S1–S2. doi: 10.1097/MCG.0b013e318269fdd5

Oliveira, A., and Pintado, M. (2015). Stability of polyphenols and carotenoids in strawberry and peach yoghurt throughout in vitro gastrointestinal digestion. *Food Function.* 6, 1611–1619. doi: 10.1039/C5FO00198F

Paim, D. R., Costa, S. D., Walter, E. H., and Tonon, R. V. (2016). Microencapsulation of probiotic jussara (Euterpe edulis M.) juice by spray drying. *LWT.* 74, 21–25. doi: 10.1016/j.lwt.2016.07.022

Pang, Y., Duan, X., Ren, G., and Liu,.W. (2017). Comparative study on different drying methods of fish oil microcapsules. *J. Food Quality.* 2017, 7. doi: 10.1155/2017/1612708

Paredes, A. J., Asensio, C. M., Llabot, J. M., Allemandi, D. A., and Palma, S. D. (2016). Nanoencapsulation in the food industry: manufacture, applications and characterization. *J. Food Bioeng. Nanoprocess.* 1, 56–79. Available online at: http://hdl.handle.net/11336/64263

Pimentel-Gonza'leza, D. J., Campos-Montielb, R. G., Lobato-Callerosc, C., Pedroza-Islasd, R., and Vernon-Carter, E. J. (2009). Encapsulation of *Lactobacillus rhamnosus* in double emulsions formulated with sweet whey as emulsifier and survival in simulated gastrointestinal conditions. *Food Res. Int.* 42, 292–297. doi: 10.1016/j.foodres.2008.12.002

Pourjafar, H., Noori, N., Gandomi, H., Basti, A. A., and Ansari, F. (2020). Viability of microencapsulated and non-microencapsulated Lactobacilli in a commercial beverage. *Biotechnol. Rep.* 25, e00432. doi: 10.1016/j.btre.2020.e00432

Raghuwanshiet, S., Misra, S., Sharma, R., and Bisen, P. (2018). Probiotics: nutritional therapeutic tool. *J. Probiotics Health.* 6, 2. doi: 10.4172/2329-8901.1000194

Razavi, S., Janfaza, S., Tasnim, N., Gibson, D. L., and Hoorfar, M. (2021). Microencapsulating Polymers for Probiotics Delivery Systems: Preparation, Characterization, and Applications. *Food Hydrocoll.* 120, 106882. doi: 10.1016/j.foodhyd.2021.106882

Ribeiro, M. C. E., Chaves, K. S., Gebara, C., Infante, F. N., Grosso, C. R., and Gigante, M. L. (2014). Effect of microencapsulation of *Lactobacillus acidophilus* LA-5 on physicochemical, sensory and microbiological characteristics of stirred probiotic yoghurt. *Food Res. Int.* 66, 424–431. doi: 10.1016/j.foodres.2014.10.019

SAS (2004). *Statistical Analyses Systems*. SAS, User Guide Statistics. SAS. Institute Inc, Cary, NC.

Shah, N. P., Lankaputhra, W. E., Britz, M. L., and Kyle, W. S. (1995). Survival of *Lactobacillus acidophilus* and *Bifidobacterium bifidum* in commercial yoghurt during refrigerated storage. *Int. Dairy J.* 5, 515–521. doi: 10.1016/0958-6946(95)00028-2

Singha, S., and Hedenqvist, M. S. (2020). A review on barrier properties of poly (lactic acid)/Clay nanocomposites. *Polymers.* 12, 1095. doi: 10.3390/polym12051095

Tavakoli, H., Hosseini, O., Jafari, S. M., and Katouzian, I. (2018). Evaluation of physicochemical and antioxidant properties of yogurt enriched by olive leaf phenolics within nanoliposomes. *J. Agric. Food Chem.* 66, 9231–9240. doi: 10.1021/acs.jafc.8b02759

Terpou, A., Papadaki, A., Lappa, I. K., Kachrimanidou, V., Bosnea, L. A., and Kopsahelis, N. (2019). Probiotics in food systems: Significance and emerging strategies towards improved viability and delivery of enhanced beneficial value. *Nutrients.* 11, 1591. doi: 10.3390/nu11071591

Tonon, R. V., Grosso, C. R. F., and Hubinger, M. D. (2011). Influence of emulsion composition and inlet air temperature on the microencapsulation of flaxseed oil by spray drying. *Food Res. Int.* 44, 282–289. doi: 10.1016/j.foodres.2010.10.018

Tripathi, M. K., and Giri, S. K. (2014). Probiotic functional foods: Survival of probiotics during processing and storage. *J. Funct. Foods* 9, 225–241. doi: 10.1016/j.jff.2014.04.030

Yoon, S. J., Park, J. M., Gu, J. G., Lee, J. S., An, J. H., Kim, S. H., et al. (2013). Establishment of quality criteria and estimate of shelf-life for yogurt beverage and stirred-type yogurt in Korea. *Food Sci. Biotechnol.* 22, 477–483. doi: 10.1007/s10068-013-0104-y

Zhang, H., Shi, Y., Xu, X., Zhang, M., and Ma, L. (2020). Structure regulation of bentonite-alginate nanocomposites for controlled release of imidacloprid. *ACS Omega.* 5, 10068–10076. doi: 10.1021/acsomega.0c00610

Conflict of Interest: The authors declare that the research was conducted in the absence of any commercial or financial relationships that could be construed as a potential conflict of interest.

frontiers | Frontiers in Microbiology

ORIGINAL RESEARCH
published: 31 May 2022
doi: 10.3389/fmicb.2022.923526

Improved Production of ε-Poly-L-Lysine in *Streptomyces albulus* Using Genome Shuffling and Its High-Yield Mechanism Analysis

*Yongjuan Liu[1,2,3,4], Kaifang Wang[2], Long Pan[2,5] and Xusheng Chen[2]**

[1]Shandong Provincial Key Laboratory of Synthetic Biology, Qingdao Institute of Bioenergy and Bioprocess Technology, Chinese Academy of Sciences, Qingdao, China, [2]The Key Laboratory of Industrial Biotechnology, Ministry of Education, School of Biotechnology, Jiangnan University, Wuxi, China, [3]Shandong Energy Institute, Qingdao, China, [4]Qingdao New Energy Shandong Laboratory, Qingdao, China, [5]College of Biological Engineering, Henan University of Technology, Zhengzhou, China

OPEN ACCESS

Edited by:
Chun Cui,
South China University of Technology, China

Reviewed by:
Jiasong Jiang,
Lonza, United States
Fengyu Du,
Qingdao Agricultural University, China
Fuming Zhang,
Rensselaer Polytechnic Institute, United States

***Correspondence:**
Xusheng Chen
chenxs@jiangnan.edu.cn

Specialty section:
This article was submitted to Food Microbiology, a section of the journal Frontiers in Microbiology

Received: *19 April 2022*
Accepted: *09 May 2022*
Published: *31 May 2022*

Citation:
Liu Y, Wang K, Pan L and Chen X (2022) Improved Production of ε-Poly-L-Lysine in Streptomyces albulus Using Genome Shuffling and Its High-Yield Mechanism Analysis. Front. Microbiol. 13:923526. doi: 10.3389/fmicb.2022.923526

ε-Poly-L-lysine (ε-PL), a natural food preservative, has recently gained interest and mainly produced by *Streptomyces albulus*. Lacking of efficient breeding methods limit ε-PL production improving, knockout byproducts and increase of main product flux strategies as a logical solution to increase yield. However, removing byproduct formation and improving main product synthesis has seen limited success due to the genetic background of ε-PL producing organism is not clear. To overcome this limitation, random mutagenesis continues to be the best way towards improving strains for ε-PL production. Recent advances in Illumina sequencing opened new avenues to understand improved strains. In this work, we used genome shuffling on strains obtained by ribosome engineering to generate a better ε-PL producing strain. The mutant strain SG-86 produced 144.7% more ε-PL than the parent strain M-Z18. Except that SG-86 displayed obvious differences in morphology and ATP compared to parent strain M-Z18. Using Illumina sequencing, we mapped the genomic changes leading to the improved phenotype. Sequencing two strains showed that the genome of the mutant strain was about 2.1 M less than that of the parent strain, including a large number of metabolic pathways, secondary metabolic gene clusters, and gene deletions. In addition, there are many SNPs (single nucleotide polymorphisms) and InDels (insertions and deletions) in the mutant strain. Based on the results of data analysis, a mechanism of ε-PL overproduction in *S. albulus* SG-86 was preliminarily proposed. This study is of great significance for improving the fermentation performance and providing theoretical guidance for the metabolic engineering construction of ε-PL producing strains.

Keywords: ε-poly-L-lysine, *Streptomyces albulus*, mutation breeding, genome shuffling, comparative genomics, high yield mechanism

INTRODUCTION

ε-Poly-l-lysine (ε-PL) is a poly-cationic peptide with 25–35 L-lysine residues, and the peptide is connected through amide bond between α-carboxy group and ε-amino group (Najjar et al., 2007). ε-PL has antimicrobial activities against a wide spectrum of microorganisms including Gram-positive and Gram-negative bacteria, yeasts, and molds. It inhibits the growth of microorganisms by destroying the cell membrane structure, causing interruption of material, energy, and information transmission of cells, and ultimately leading to cell death (Melo et al., 2009; Ye et al., 2013; Santos et al., 2018; Zhang et al., 2018). Furthermore, ε-PL are water-soluble, edible, biodegradable, and nontoxic towards humans and the environment, as they degrade into lysine without any side effects (Shukla et al., 2012; Chheda and Vernekar, 2015). Based on its strong antibacterial activity and low toxicity, ε-PL is used as a natural food preservative in Japan, South Korea, United States and China, and it has been currently used in many foods including soft drinks, cheese, egg-based dishes, salad dressings, fish, sauces and potato-based foods (Fadli et al., 2012). Besides its use in the food industry, ε-PL has numerous applications in the pharmaceutical industry as drug carriers, nanoparticles, gene carriers, liposomes, interferon inducers, lipase inhibitors, hydrogels, coating materials, etc. (Bankar and Singhal, 2013).

Nowadays, plenty of efforts and methods have been committed to enhancing ε-PL-producing strains. The most successful one was screening for mutants with S-(2-aminoethyl)-L-cysteine (AEC) plus glycine resistance after nitrosoguanidine treatment and ultraviolet mutagenesis (Hiraki et al., 1998). Moreover, atmospheric and room temperature plasma (ARTP) mutagenesis combined with AEC resistance screening as well as genome shuffling were reported to improve the production of ε-PL (Li et al., 2012; Zong et al., 2012). However, the above methods are quite expensive on account AEC, which is about $180 per gram and rather inefficient. Recently, modern metabolic engineering breeding technology also has been applied in ε-PL production promotion. Xu et al. (2015) established a genetic system to integrate *Vitreoscilla* hemoglobin (VHb) gene into the chromosome of *Streptomyces albulus* PD-1 and Gu et al. (2016) inserted heterologous VHb gene and SAM (S-adenosylmethionine) synthetase gene into the *S. albulus* NK660 chromosome to improve the ε-PL biosynthesis. These methods for improving ε-PL production, ranging from classical random approaches to metabolic engineering, are either costly or labor-intensive. In our lab, Wang et al. (2015, 2017) combined ARTP mutagenesis with streptomycin resistance to obtain a high-yield strain *S. albulus* AS3-14, combined genome shuffling with gentamicin-resistance to achieve the promotion of ε-PL productivity of *S. albulus* W-156 and induced double antibiotic-resistant mutations in *S. albulus*. Despite their efficiency, these methods still present a number of problems, particularly the difficulty in determining the reasons for high yield, due to the complex mutagenesis background.

Genome shuffling (GS) has been extensively used in industry to obtain improved strains, particularly in high GC content microorganisms (Leja et al., 2011). GS combines the advantages of multi-parental crossing facilitated by DNA exchange allowing to access foreign DNA, which facilitates improved phenotypes over traditional random mutagenesis (Stratigopoulos and Cundliffe, 2002). It does not need to know the genetic background of the strain and has the advantage of rearranging the genomes of unknown organisms directly (Zhang et al., 2002). It has become an efficient method of microbial breeding. The first application of GS was the production of tylosin in *Streptomyces fradiae* (Zhang et al., 2002). Subsequently, *Bacillus subtilis*, as riboflavin-producing bacteria, was improved by GS in the laboratory (Chen et al., 2004). GS has become increasingly popular in recent years. Other scholars have successfully selected high-yield enzyme (Liang and Guo, 2007), drug (Gong et al., 2007), food additive (Hida et al., 2007), acid-resistant (Gos and Raszeja, 1993), ethanol-resistant (Macnab, 1996) strains by this method. All these studies used random mutagenesis to generate phenotypic diversity and then recombine with the parental strain by fusing protoplasts.

In this work, we used GS and distinct strains of *S. albulus* obtained by Streptomycin resistance to improve ε-PL production. The mutant strain SG-86 displayed obvious differences in morphology, ε-PL production, and ATP compared to parent strain M-Z18. Illumina sequencing was then used to analyze these two strains and identify novel/unique regions leading to the improved phenotype of recombination strain SG-86. These two strains were sequenced and analyzed and the genome of the recombination strain was about 2.1 M less than that of the parent strain, including a large number of metabolic pathways, secondary metabolic gene clusters, and gene deletions. Using comparative genome analysis, single nucleotide polymorphism (SNPs), insertions and deletions (InDels) analysis (Cingolani et al., 2012), we showed that changes in the genome correspond to InDel and SNP mutations in regions of high recombination probability. Bioinformatics analyses and functional characterizations indicated that the proteins encoded by these mutant genes may be related to ε-PL synthesis. Finally, a mechanism of ε-PL overproduction in *S. albulus* SG-86 was preliminarily constructed by comparative genomics.

MATERIALS AND METHODS

Strains and Media

Streptomyces albulus M-Z18 was used as parent strain, whose ε-PL yield was 1.7 g/L in shake-flask fermentation and stored in our lab (Li et al., 2013). *Streptomyces albulus* M-Z18 was isolated from soil as described by Nishikawa and Ogawa (2002) and has been subjected to ultraviolet and nitrosoguanidine mutagenesis as described by Hiraki et al. (1998). Recombination strain *S. albulus* SG-86 was obtained by ribosome engineering and GS. The solid medium (BTN), seed culture medium (M3G), and fermentation medium (YH) were described previously (Liu et al., 2019a). Liquid regeneration medium consisted of 118 g/L sucrose, 25 g/L glucose, 10 g/L $MgCl_2{\cdot}6H_2O$, 0.4 g/L $CaC1_2{\cdot}2H_2O$, trace element 2 ml/L, and 10 ml/L TES buffer (pH 7.5). The pH was adjusted to 7.0 with 2 mol/L sterile NaOH after autoclaving. Solid regeneration medium was prepared by adding

20 g agar in 1 L liquid regeneration medium and sterilized at 115°C for 20 min, the pH was adjusted to 7.0 with 2 mol/L NaOH.

Preparation of the Starting Mutants Through Ribosome Engineering for Genome Shuffling

Spores' suspension (10^5 CFU/ml) of *S. albulus* M-Z18 with 120–500 μl was spread on BTN plates containing 0–10 μg/ml streptomycin and incubated at 30°C for 8–10 days. For the primary and secondary screening of mutant strains, multi-well plate fermentation and 250 ml shake-flask fermentation tests were performed as described in our previous study (Liu et al., 2017) and YH was used as fermentation medium. Colonies with abundant spores were inoculated into 24-deep-well microtiter plates containing 2 ml YH medium for 4 days. The mutants with higher ε-PL production were continually inoculated on BTN medium and cultivated for 8–10 days at 30°C until spores mature. Three loops of spores were transferred to 40 ml of M3G medium in a 250 ml flask and subsequently incubated in a rotary shaker (HYL-C, Qiangle Laboratory Equipment Co., Taicang, China) at 200 rpm, 30°C for 24 h. Then, 8.0% (v/v) of seed culture was transferred to fresh YH medium and incubated at 30°C with 200 rpm shaking for 72 h. Five mutants with the highest ε-PL production determined in shake-flask fermentation were chosen as starting strains using 0–45 μg/ml streptomycin to further improve the production of ε-PL (Liu et al., 2019b).

Protoplast Formation, Fusion, and Regeneration

Ten-milliliter mycelia of strains with high ε-PL production obtained by ribosome engineering were harvested from the logarithmic growth phase, respectively. Then centrifuged (4,500 × *g*) and washed successively with aseptic water and PB buffer. The obtained mycelia were subsequently treated with 5 ml PB buffer and 800 μl lysozyme (50 mg/ml) at 30°C for 2 h, during which the mixed solution is inverted about every 10 min. Protoplasts formation was observed by microscopy and washed twice with PB buffer to remove the lysozyme. Subsequently, 5–6 ml protoplast was inactivated by ultraviolet radiation for 80 min at a distance of 8 W ultraviolet lamp 30 cm in a sterile culture dish with a diameter of 9 cm. The other 5–6 ml protoplasts were inactivated in a 70°C water bath. Protoplasts inactivated by ultraviolet radiation and heat were mixed and centrifuged for 5–10 min at 1,000 rpm. Protoplast fusion was carried out at 38°C–40°C to add 3 ml PEG 6000 for 15 min. The fusions of 180 μl were added in a 5 ml liquid regeneration medium and spread on solid regeneration medium plates. ε-PL productivities of shuffled colonies were evaluated in 24-deep-well microtiter plates and shaking-flask fermentation.

Morphological Characterization of Strain by Scanning Electron Microscopy

Scanning electron microscopy (SEM) was used to observe the mycelia and spores of *S. albulus* M-Z18 and SG-86 according to Liu et al. (2019a). In brief, cut agar blocks were washed twice in phosphate-buffered saline solution and then immersed in 5% glutaraldehyde. After that, the samples were immobilized with 1% osmium acid (0.1 M PBS, pH 7.2) and then washed with 0.1 M PBS. Then an ethanol gradient dehydration, samples were taken at the critical point dried, and pasted on the sample table of the ion sputtering instrument (SCD 005, BAL-TEC, California, United States) was coated and scanned under the scanning electron microscope (Quanta 200, FEI, Hillsboro, United States).

Measurement of Intracellular ATP and Proteins

Intracellular ATP was determined as described by Wu et al. (2012) and Wang et al. (2020). And protein synthesis activity *in vivo* according to Myronovskyi et al. (2011) with slight modification. The plasmid PIB139-gusA* was introduced into *Escherichia coli* strain ET12567/pUZ8002 and then transferred into *S. albulus* M-Z18 and SG-86 by intergeneric conjugation to generate M-Z18-GUS and SG-86-GUS, respectively. Mycelia were harvested by centrifugation, washed once with distilled water, and resuspended in lysis buffer [50 mM phosphate buffer (pH 7.0), 5 mM dithiothreitol (DTT), 0.1% Triton X-100, 1 mg/ml lysozyme]. Lysis was performed at 37°C for 15 min. Lysates were centrifuged at 4,000 *g* for 10 min. Then, 0.5 ml of lysate was mixed with 0.5 ml of dilution buffer [50 mM phosphate buffer (pH 7.0), 5 mM DTT, 0.1% Triton X-100] supplemented with 5 ml 0.2 M p-nitrophenyl-b-d-glucuronide. The optical density at 415 nm was measured after 20 min of incubation at 37°C. As a reference, a 1:1 mixture of lysate and dilution buffer was used (Liu et al., 2019a).

Sequencing and *de novo* Assembly

Total DNA of *S. albulus* M-Z18 and *S. albulus* SG-86 at 30 h during fermentation were extracted and purified by DNA extraction kit (DP302, TIANGEN, Beijing, China) following the manufacturer's instructions. The quality of the DNA was assessed by gel electrophoresis. And the genome of M-Z18 and SG-86 were sequenced using a PacBio RS II platform at Beijing Genomics Institute (BGI, Shenzhen, China). Four SMRT cells Zero-Mode Waveguide arrays of sequencing were used by the PacBio platform to generate the subreads set. PacBio subreads (length < 1 kb) were removed. The program Pbdagcon was used for self-correction. Draft genomic unitigs, which are uncontested groups of fragments, were assembled using the Celera Assembler against a high-quality corrected circular consensus sequence subreads set. To improve the accuracy of the genome sequences, GATK and SOAP tool packages (SOAP2, SOAPsnp, and SOAPindel) were used to make single-base corrections. To trace the presence of any plasmid, the filtered Illumina reads were mapped using SOAP to the bacterial plasmid database.

Gene Prediction and Annotation

Putative protein-coding sequences (CDSs) were predicted by Glimmer 3.02 software (Delcher et al., 1999; Olano et al., 2008). tRNA, rRNA, and sRNAs recognition made use of tRNA scan-SE (Lowe and Eddy, 1997), RNAmmer, and the Rfam

database. The tandem repeats annotation was obtained using the Tandem Repeat Finder, and the minisatellite DNA and microsatellite DNA were selected based on the number and length of repeat units. CDS annotation was based on the BLASTP program with NR, COG, and KEGG databases. The tRNA genes were directly predicted by tRNAscan-SE (Lowe and Eddy, 1997). The single nucleotide variations (SNPs), InDels, and secondary metabolic gene clusters were identified by Mummer, Mauve, antiSMASH 6.0.1, and BLASTP programs.

Analytical Methods

The withdrawn fermentation broth was centrifuged at 4,500 *g* for 10 min, the supernatant was used to determine the ε-PL concentration using the methyl orange precipitation method according to Itzhaki (1972). In brief, an equal volume of sample with 0.06–0.12 g/L ε-PL diluted with 0.07 mM phosphate buffer (pH 6.90) and 0.7 mM methyl orange solution were mixed together, which were reacted at 30°C with shaking for 30 min. The ε-PL concentration can be estimated from the absorbance at 465 nm of the methyl orange remaining in the supernatant solution through standard curve calculation.

Statistical Analysis

All described experiments were performed in independent biological triplicates unless stated otherwise. Presented data in the graphs are the averages of the replicates ± the SD.

RESULTS AND DISCUSSION

Screening for Improved ε-PL Producing Strains

Genome shuffling amplifies the genetic diversity within a selected mutant population through extensive homologous recombination. Thus, the starting strains for genome shuffling require a population of improved mutants with diverse genetic sequences (Zhang et al., 2002; Hida et al., 2007). In this work, streptomycin resistance was used for mutation treatment to screen high ε-PL producing strains. As shown in **Figure 1**, after low streptomycin resistance (0–10 μg/ml streptomycin) five high-yield mutants (S-99, S-107, S-28, S-37, and S-23) were isolated for the secondary screening. The ε-PL productivity of these five mutants in shake flask was 2.45, 2.45, 2.48, 2.55, and 2.59 g/L, respectively. In order to fully release the potential of streptomycin in increasing ε-PL production of *S. albulus*, spores of the high-yield mutants S-99, S-107, S-28, S-37, and S-23 were mixed and spread onto plates containing high streptomycin resistance (0–45 μg/ml streptomycin). Similarly, five high-yield mutants (SS-35, SS-51, SS-19, SS-62, and SS-31) were identified in shake-flask fermentation. The ε-PL productivity of these five mutants in shake flask was 2.81, 2.93, 2.97, 3.00, and 3.04 g/L, respectively. Further genome shuffling SS-35, SS-51, SS-19, SS-62, and SS-31 were used as starting strains. Two successive rounds of genome shuffling were carried out with the mutants. From the first to second rounds of genome shuffling, 324 and 116 colonies appeared on the agar plates, respectively. A 4.16 g/L ε-PL recombinant, SG-86, was obtained after the second round of protoplast fusion, which was 144.7% higher than that of the parent strain M-Z18.

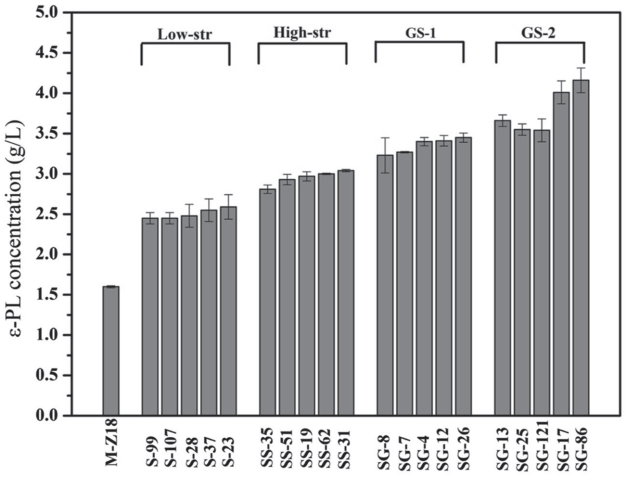

FIGURE 1 | The ε-poly-L-lysine (ε-PL) production of mutants obtained by streptomycin resistance and genome shuffling (low-str, low streptomycin resistance; high-str, high streptomycin resistance; GS-1, first round of genome shuffling; and GS-2: second round of genome shuffling).

Phenotypic Difference Between the Wild-Type of *Streptomyces albulus* M-Z18 and *Streptomyces albulus* SG-86

Even though *S. albulus* M-Z18 and *S. albulus* SG-86 share a close relationship, they show obvious differences in morphology except for ε-PL production. **Figure 2** shows the macroscopic and microscopic photographs of M-Z18 and SG-86. M-Z18 colonies were smooth and its spores were brown (**Figures 2A1**,**3**), while SG-86 colonies had a volcanic rock shape with a central depression and were radiation and their spores were greyish green (**Figures 2B5**,**7**). SEM analysis showed the hyphae of SG-86 appeared full and abundant as the parent strain M-Z18, but the vesicles became small and the existence of dried mycelium was observed in SG-86 (**Figures 2A2**,**B6**). Further, SG-86's spores were bigger and had more spines than the parent strain M-Z18. What's interesting was that the vesicles became as large as the mycelium of M-Z18 (**Figures 2A4**,**B8**). It is of great value to recognize changes in the cultivation characteristics of high-yielding strain for industrial application (Ren et al., 2015; Wang et al., 2016).

ATP Levels and Protein Synthesis of *Streptomyces albulus* M-Z18 and *Streptomyces albulus* SG-86

The process of ε-PL biosynthesis is influenced by energy provision (Yamanaka et al., 2010; Zeng et al., 2014). To understand the intracellular energy, we determined intracellular ATP levels at 24, 48, and 72 h. **Figure 3A** displayed the results, which represented ATP production from the TCA cycle. SG-86 presented

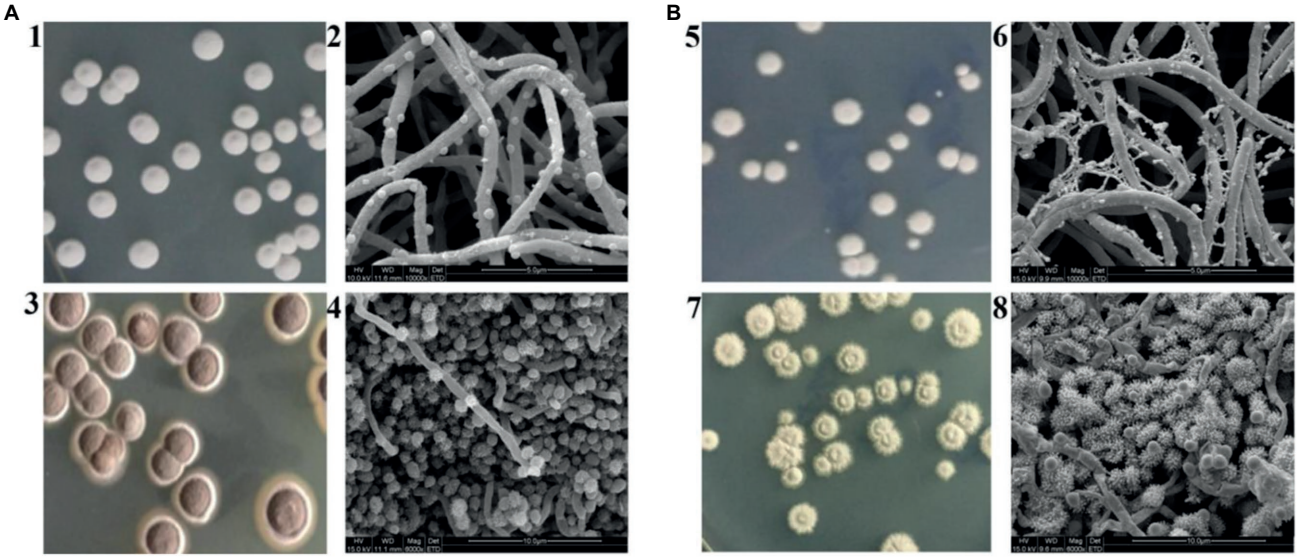

FIGURE 2 | Cultivation characteristics of M-Z18 and SG-86 in solid culture. **(A)** M-Z18 and **(B)** SG-86. 1, 3, 5, 7: colony characterized and spore colour by a camera and 2, 4, 6, 8: hypha and spore characterized by scanning electron microscope (SEM).

high ATP levels at 48 and 72 h. Especially at 72 h, the intracellular ATP level of SG-86 was 1.31-fold higher than parent strain *S. albulus* M-Z18. We also determined the relationship between protein synthesis and ε-PL production in the parental strain and mutant to use a reporter gene assay based on the glucuronidase gene (Myronovskyi et al., 2011). The glucuronidase activity was measured at 24, 48, and 72 h after inoculation. As shown in **Figure 3B**, glucuronidase activity displayed no significant difference between mutant SG-86 and parental strain at 48 and 72 h. It indicated that the high-level ε-PL production was not caused by accelerated protein synthesis.

Illumina Sequencing, Gene Prediction, and Function Annotation

To understand the genetic basis underlying phenotypic differences, especially the apparent differences in the yield of ε-PL and the morphology, between the wild-type *S. albulus* M-Z18 and the high-yield strain *S. albulus* SG-86, the whole genome of *S. albulus* M-Z18 and *S. albulus* SG-86 were sequenced. The complete genome sequence of M-Z18 and SG-86 were determined by *de novo* assemble.

The genomic sequences of the two strains were all composed of two contigs and one plasmid. Similar to the other sequenced *S. albulus*, M-Z18 has a linear chromosome of 9,556,033 bp with an average 72.22% G + C content. A total of 8,897 protein-coding sequences (CDS), 68 tRNA, 52 sRNA, 7 16S-23S-5SrRNA operons, 1707 tandem repeats, 1,159 Minisatellite DNA Numbers, and 232 Microsatellite DNA Numbers were determined by Glimmer 3.02. The chromosome of SG-86 was 7,471,099 bp with an average 72.42% GC content. There were 6,792 CDS, 53 tRNA, 4 16S-23S-5SrRNA operons with a total length of 6,466,035 bp, 1,481 tandem repeats, 1,022 Minisatellite DNA Numbers, and 189 Microsatellite DNA Numbers (**Table 1**). Moreover, gene prediction and functional annotation by 13 databases including COG, GO, KEGG, NR, and so on. And the proportion of each database is different (**Supplementary Table 1**).

Genome Variation Analysis of *Streptomyces albulus* M-Z18 and *Streptomyces albulus* SG-86

To elucidate the relationship between phenotype and genotype, we performed a systematic genomic comparison between M-Z18 and SG-86. A gene–gene comparison suggests that M-Z18 has 2,122 unique genes and SG-86 has 246 unique genes (*E*-value < 0.0001; **Figure 4A**). As a major difference, M-Z18 and SG-86 were not highly conserved gene content and gene order, and there is rearrangement and inversion (**Figure 4B**). Compared with M-Z18, the chromosome size of SG-86 is 2.1 M smaller and the plasmid size of SG-86 is just 19 bp less than M-Z18 (**Table 1**). The results showed that the reduced 2.1 M of the SG-86 genome was almost on the chromosome, including metabolic pathways, secondary metabolic gene clusters, and genes. In addition to this large deletion, a total of 142 insertions, 16 deletions, and 33 single nucleotide mutations (SNP) were confirmed. These large deletions, InDels, and SNP will be described in detail below.

Intragenic InDels Analysis of *Streptomyces albulus* SG-86

Compared with M-Z18, 16 deletion sites and 142 insertion sites were found in SG-86, including 74 intragenic InDels (**Supplementary Table 2**). Besides the putative and unknown proteins, the proteins encoded by these genes mainly include membrane proteins, ABC transporters, cytochrome P450, and DNA polymerase. In addition, there are two histidine kinases,

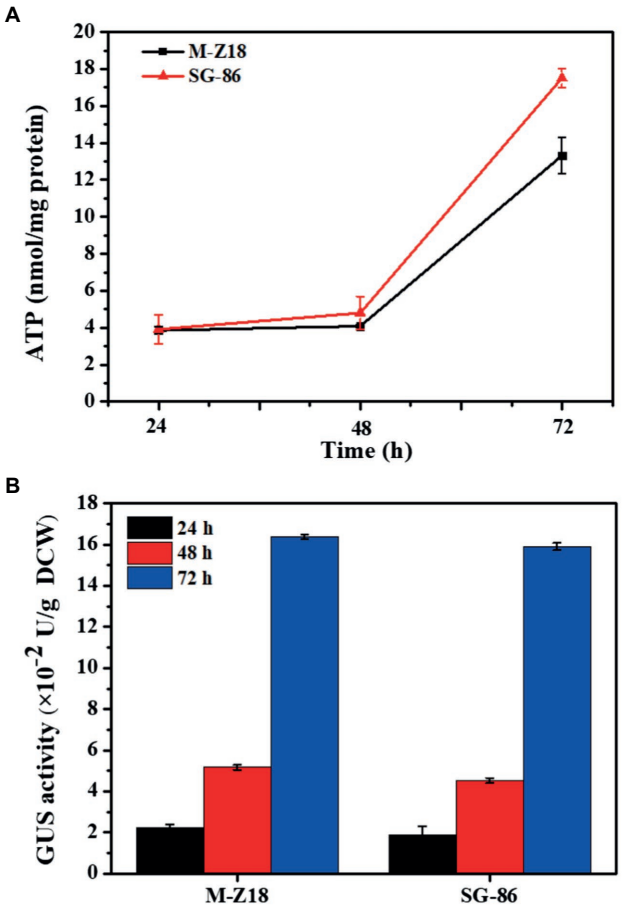

FIGURE 3 | Time-dependent changes of ATP involved in ε-PL biosynthesis in *S. albulus* M-Z18 and mutants SG-86 during shake flask fermentation **(A)**. Detection of b-glucuronidase activity. Glucuronidase activity was measured in cell lysates of parental strain *S. albulus* M-Z18 and mutant SG-86 from fermentation broth at 24, 48, and 72 h, respectively **(B)**.

two types I PKS and one NRPS. The functions of membrane proteins are multifaceted. Membrane proteins play a very important role in many life activities of organisms, such as cell proliferation and differentiation, energy conversion, signal transduction, and material transport. It is estimated that about 60% of the drug targets are membrane proteins (Santos et al., 2016). Besides membrane proteins, some mutations related to transporters were also found, such as 2961361G, 2961427C, and 5685423C. The biological transport system helps cells obtain the required nutrients, excrete harmful products, and the combined function of transporters enables cells to maintain sustainable growth and development. In particular, ABC transporters can increase the availability of nutrients or reduce the number of toxic elements in cells. Transporters are an important factor in anti-phenotypic characteristics including prokaryotes (Padan, 2009). Moreover, transporters can improve acid tolerance. For example, arginine/ornithine reverse transporter is used to introduce decarboxylase reverse transporter of glutamate in arginine deaminase pathway γ-aminobutyrate. Therefore, it is speculated that transporter

TABLE 1 | General features of genomes of *Streptomyces albulus* M-Z18 and *Streptomyces albulus* SG-86.

	***S. albulus* M-Z18**	***S. albulus* SG-86**
Genome size(bp)	9,556,033	7,471,099
GC content (%)	72.22	72.42
Gene number	8,897	6,792
Gene total length (bp)	8,282,598	6,466,035
gene length/genome (%)	86.67	86.55
tRNA	68	66
rRNA	7×(16S-23S-5S)	7×(16S-23S-5S)
sRNA	52	33
Tandem repeat number	1,707	1,481
Minisatellite DNA number	1,159	1,022
Microsatellite DNA number	232	189
Prophage number	2	2
Plasmid	1	1
Plasmid size (bp)	36,936	36,955
Plasmid GC content in %	68.91	68.92

mutations play a key role in improving pH tolerance (Guan et al., 2013).

Histidine kinase is an important part of the two-component system. The two-component system is a very important regulatory factor, which is responsible for regulating physiological metabolic processes such as cell growth, differentiation, and metabolism, especially closely related to morphological differentiation and secondary metabolite synthesis in Streptomyces (Mendes et al., 2007). Interestingly, four mutations encoding cytochrome P450 were also found. Research shows that P450 is a key participant in the biosynthesis pathway of natural products. Natural products are the most chemically and structurally diverse small molecules known, requiring a large number of P450 (Girvan and Munro, 2016). *Streptomyce avermitilis* and *Streptomyces coelicolor* sequencing found 33 and 18 P450, respectively, accounting for 0.2% and 0.4% of all coding sequences. P450 is usually related to secondary metabolism or biotransformation. The number and diversity of P450 in Streptomyces may affect the biosynthetic potential of natural products (Rudolf et al., 2017). In addition, two genes encoding type I PKS and one NRPS were found to be mutated. The functions of these proteins are unknown, but the results show that they do not affect the yield of ε-PL. It may be beneficial to the synthesis of ε-PL in some way.

Intergenic InDels Analysis of *Streptomyces albulus* SG-86

As shown in **Supplementary Table 3**, there are 84 intergenic InDels in SG-86, of which 44 mutations are unknown and hypothetical proteins, accounting for 59.5%. The remaining gene mutations are mainly related to DNA polymerase, transporter, transcription regulatory protein, and methyltransferase. In addition, there are three mutations related to anti macrophage protein, anti-bleomycin protein, and cyclase, respectively. DNA polymerase is associated with genome rearrangement, homologous recombination, gene transformation, or DNA repair (Roth et al., 1996; McVean et al., 2002; Luna-Flores et al., 2017).

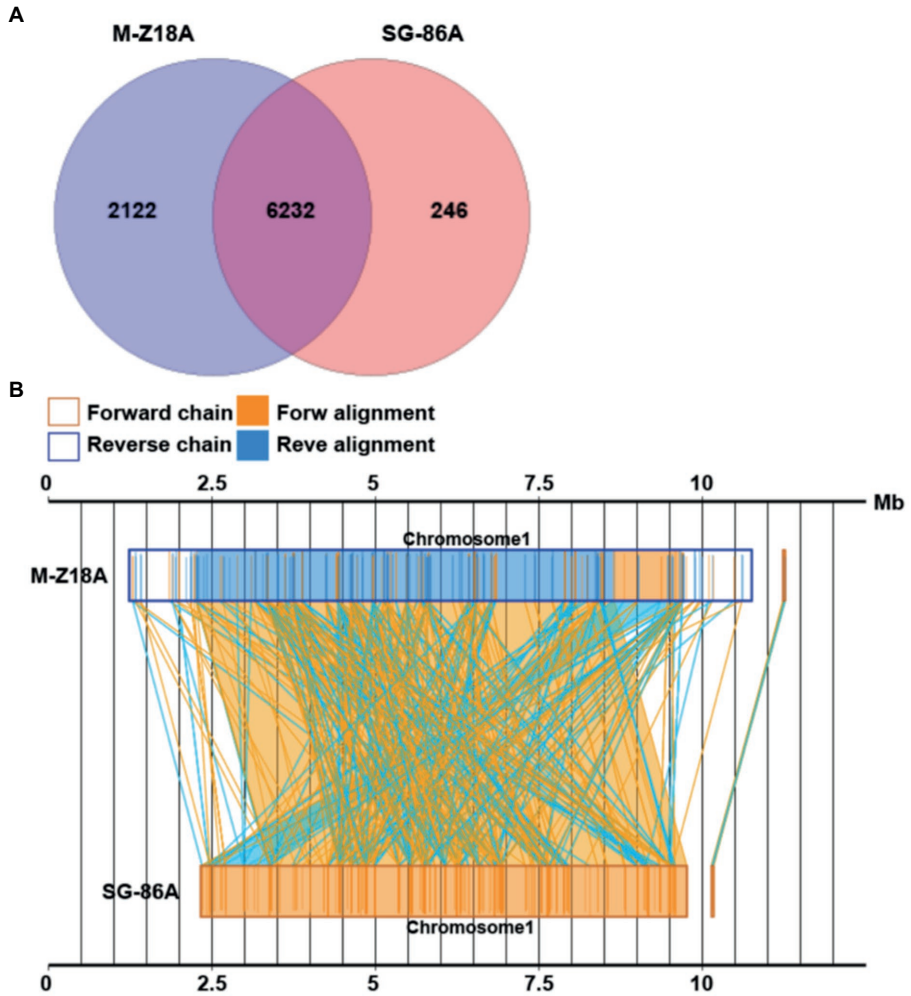

FIGURE 4 | Venn diagram showing the number of core genes and pan genes for two strains **(A)**. Syntenic dot plot of two strains **(B)**.

Mutation-related transporters are mainly ABC transporters, such as ABC transporter ATP binding protein, sugar ABC transporter, and iron carrier ABC transporter. ABC transporters are a class of primary active transporters, including endotransporters and efflux proteins. Endotransporters are mainly responsible for the intake of nutrients and efflux proteins are responsible for transporting substances from intracellular to extracellular. They are mainly related to the efflux of toxic substances such as antibiotics. In Streptomyces, secondary metabolites are secreted extracellularly mainly through ABC transporters (Méndez and Salas, 2001). In addition, ABC transporter is also related to mycelial differentiation and antibiotic synthesis in Streptomyces, which is the link between carbon source utilization, mycelial differentiation, and secondary metabolite synthesis. Hillerich and Westpheling (2006) found that agl3EFG can respond to the signal of glucoside, thus affecting the morphological differentiation and antibiotic synthesis of *S. coelicolor*. Therefore, it is indicated that the mutations related to the transporter may improve ε-PL production of the SG-86 strain.

Mutations are also found in transcription factors. These transcription factors interact with genetics to regulate gene expression. The interaction between protein and DNA may also contribute to new regulatory systems. For example, the transcriptional regulatory TrmB has an insertion mutation. TrmB has been widely studied in archaeococcus, which is closely related to sugar transport and metabolism (Lee et al., 2008). In addition, three mutations are related to transferase, which can catalyze various chemical functional groups except for hydrogen (transfer from one substrate to another), and also play a role in peptide chain extension in protein synthesis. Pisciotta et al. (2018) also found that SCO1731 methyltransferase can regulate the production of actinomycin and morphological differentiation in *Streptomyces coeruleus* A3(2). Whether it plays the same role in SG-86 needs to be further verified.

SNP Mutation Analysis of *Streptomyces albulus* SG-86

In addition to these InDel mutations, 33 SNP were identified between the two genomes, including 25 intragenic SNPs and 5 intergenic SNPs (**Table 2**). The intragenic SNPs included

11 synonymous mutations, 1 nonsense mutation, 15 nonsynonymous mutations. In addition to the putative proteins, these 15 nonsynonymous mutations consisted of oxidoreductase, keto acid-reducing isomerase, peptidase, cytochrome P450, transcriptional regulators, transporters, and membrane proteins. Except for anti-σ factor and AfsR family transcription regulatory proteins, the roles of most other proteins have been described before. σ factor is a non-specific protein that acts as a cofactor of all RNA polymerases and it is an inherent component of DNA-dependent RNA polymerase. It recognizes the common sequence of promoters and binds to holoenzyme. σ factor itself cannot bind to DNA, but the interaction with the core enzyme will activate its DNA binding region. Anti-σ factors are regulated by direct interactions between proteins (anti-σ factors and σ factor; Wang et al., 2020). AfsR family regulatory proteins are global regulatory proteins, and AfsK-AfsR can regulate secondary metabolites globally (Horinouchi, 2003). In addition, Sohng (2009) showed that heterologous expression of AfsR homologous genes in other Streptomyces will increase the yield of corresponding antibiotics.

Metabolic Pathway and Gene Deletion Analysis of *Streptomyces albulus* SG-86

According to KEGG analysis, both M-Z18 and SG-86 have complete EMP (glycolytic pathway), PPP (pentose phosphate pathway), TCA (tricarboxylic acid cycle), and DAP (diaminopimelate pathway) metabolic pathways, and have efficient material and energy metabolism in the fermentation process. However, SG-86 has a large number of gene deletions among these metabolic pathways, including the deletion of metabolic pathways. **Supplementary Table 4** shows that SG-86 lacks four metabolic pathways, namely sterol synthesis, phosphatidylinositol signaling system, Salmonella infection, and sterol biosynthesis. These pathways have nothing to do with ε-PL synthesis, which indicated that genome rearrangement removes many metabolic pathways unrelated to ε-PL synthesis in SG-86, reduces the

TABLE 2 | Single nucleotide mutation of recombinant strain.

Gene ID	Base change	Code change	Change of amino acids	Mutate type	Gene name
Intergenic	T→C				
Intergenic	G→T				
M-Z18AGL001581	G→A	CGG→CGA	R→R	Synonymous	Amidohydrolase
M-Z18AGL001707	C→G	TCC→TGC	S→C	Nonsynonymous	Hypothetical protein
M-Z18AGL001926	T→C	TAC→CAC	Y→H	Nonsynonymous	Oxidoreductase
M-Z18AGL002480	G→T	GCC→GCA	A→A	Synonymous	Acyl-CoA dehydrogenase
M-Z18AGL002891	T→G	GAG→GCG	E→A	Nonsynonymous	Ketol-acid reductoisomerase
M-Z18AGL002996	G→A	GCG→GCA	A→A	Synonymous	Two-component sensor histidine kinase
M-Z18AGL003566	G→C	GGC→GCC	T→A	Nonsynonymous	Peptidase
Intergenic	G→A				
M-Z18AGL003702	C→T	GAG→AAG	E→K	Nonsynonymous	Cytochrome P450
M-Z18AGL003817	G→A	AAG→AAA	K→K	Synonymous	Hypothetical protein
M-Z18AGL004063	A→T	TCA→ACA	S→T	Nonsynonymous	Anti-sigma factor antagonist
M-Z18AGL004389	C→T	CTC→CTT	L→L	Synonymous	Membrane protein
M-Z18AGL004492	C→T	GAA→AAA	E→K	Nonsynonymous	AfsR family transcriptional regulator
M-Z18AGL004926	G→A	CTG→CTA	L→L	Synonymous	Hypothetical protein K530_49370
M-Z18AGL004926	G→A	GCG→ACG	A→T	Nonsynonymous	Hypothetical protein K530_49370
M-Z18AGL004963	T→A	CAG→CTG	Q→L	Nonsynonymous	Transcriptional regulator
Intergenic	C→T				
M-Z18AGL005160	G→A	CCG→CCA	P→P	Synonymous	Hypothetical protein
M-Z18AGL005326	T→C	GTC→GCC	V→A	Nonsynonymous	Membrane protein
M-Z18AGL005622	C→G	CGG→CCG	R→P	Nonsynonymous	6-Phospho-beta-glucosidase
M-Z18AGL005910	C→T	GTG→GTA	V→V	Synonymous	DNA-binding protein
M-Z18AGL006102	G→A	GCC→ACC	A→T	Nonsynonymous	Transporter
M-Z18AGL006129	T→A	CTC→CAC	L→H	Nonsynonymous	Tryptophan synthase subunit alpha
M-Z18AGL006373	C→T	CGG→CGA	R→R	Synonymous	Protease
M-Z18AGL007131	C→T	GCC→GCT	A→A	Synonymous	Oxidoreductase
M-Z18AGL007294	C→T	CTG→TTG	L→L	Synonymous	Type I polyketide synthase
M-Z18AGL007603	T→G	CTC→CGC	L→R	Nonsynonymous	Cyclase
M-Z18AGL007672	G→A	CAG→TAG	Q→X	Nonsense	Transporter
M-Z18AGL008875	C→T	GGG→AGG	G→R	Nonsynonymous	Transcriptional regulator
Intergenic	T→G				
Intergenic	G→T				

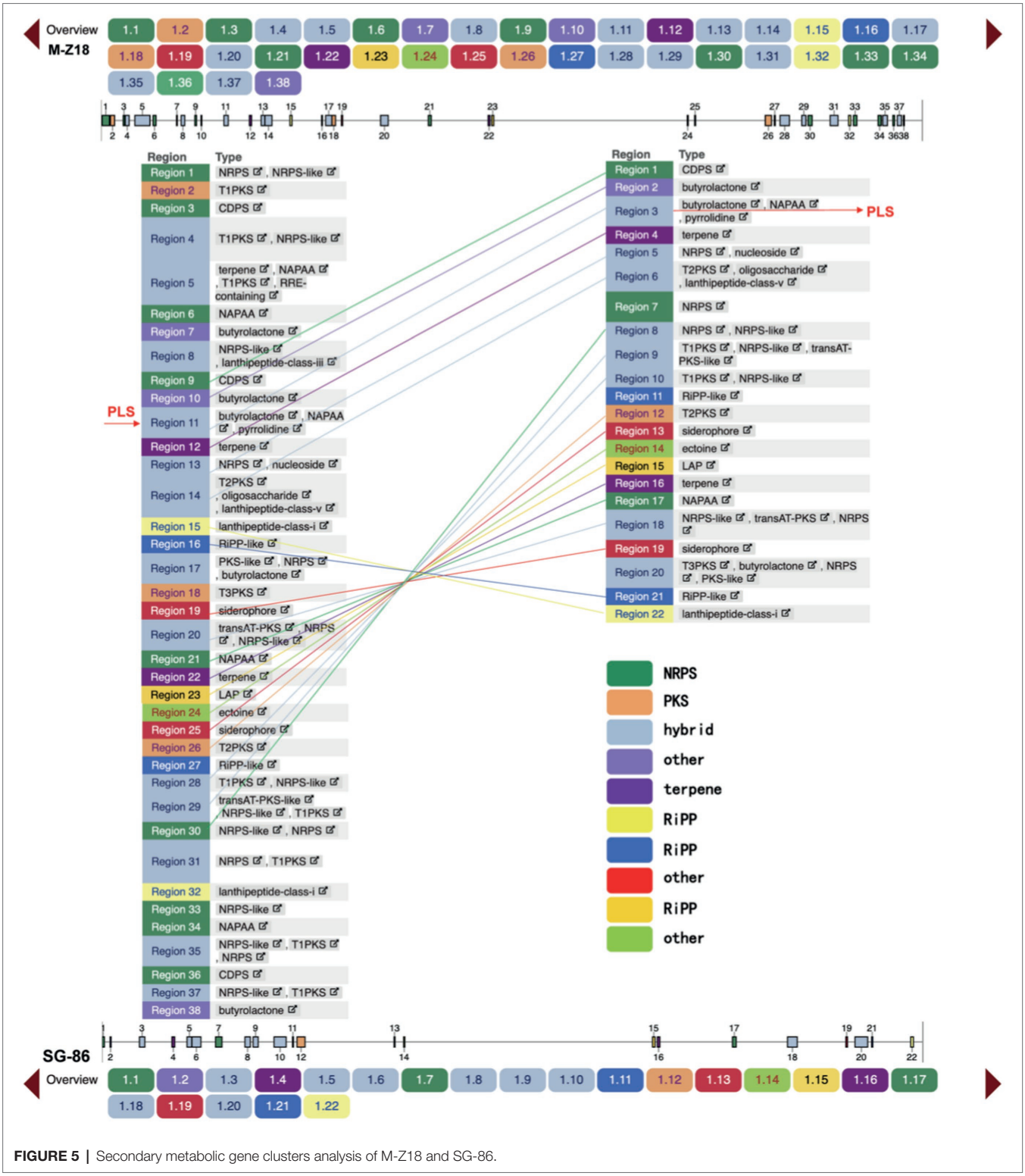

FIGURE 5 | Secondary metabolic gene clusters analysis of M-Z18 and SG-86.

genome of SG-86, and may improve the efficiency of intracellular ε-PL synthesis. In addition, there are gene deletions in alanine and glutamate (racD), glycine, serine and threonine (Gatm), arginine and proline (E3.5.2.10), histidine (DDC), tyrosine (moaA), tryptophan (DDC) metabolic pathways, and valine, leucine, and isoleucine (IVD, scoB) degradation pathways (**Supplementary Table 4**). The loss of these by-product metabolism and degradation pathway genes reduces the synthesis of by-products, and more metabolic flow flows to the precursor of ε-PL, which may improve the production of ε-PL.

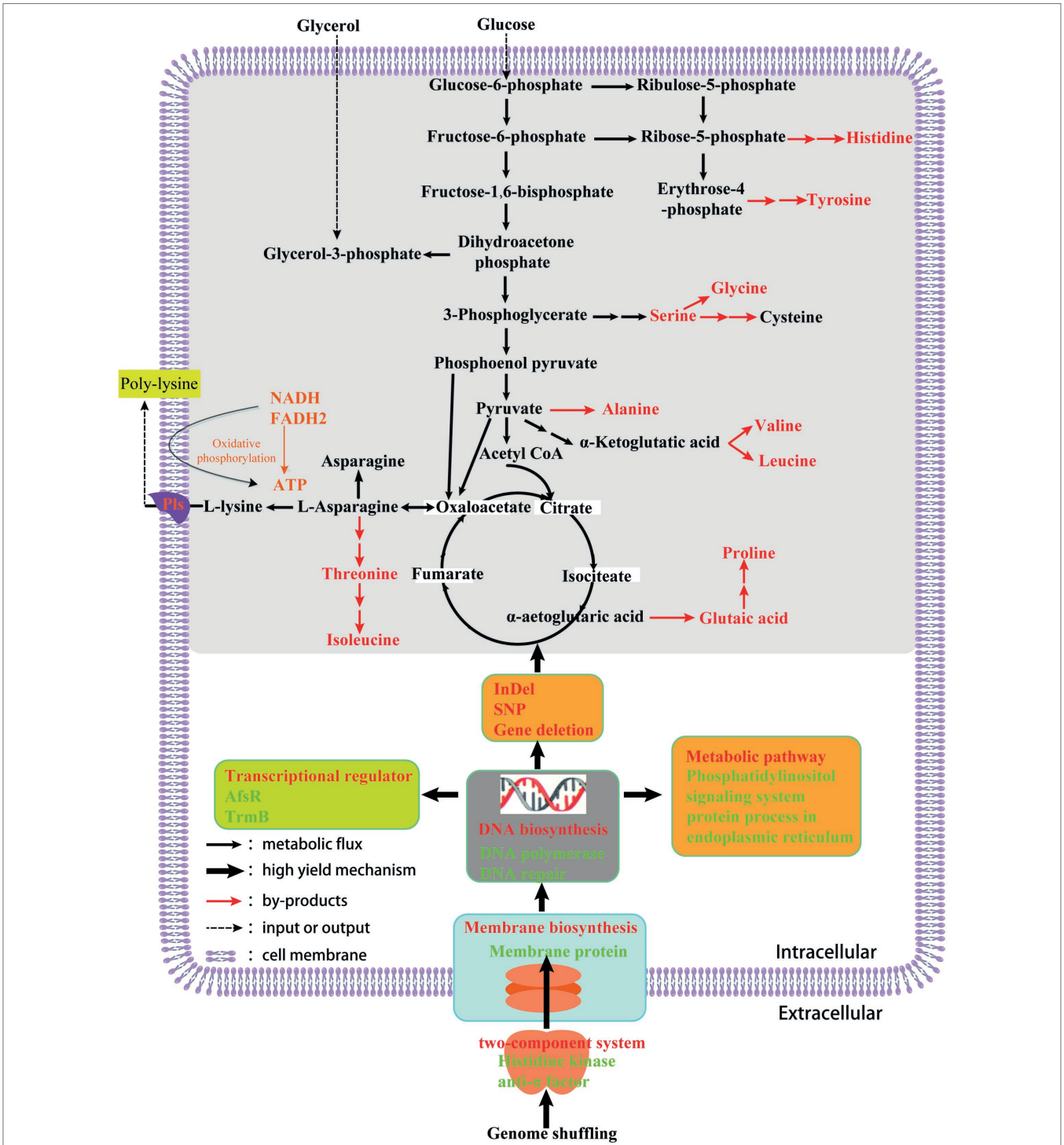

FIGURE 6 | High-yielding mechanism of ε-PL from *S. albulus* using genome shuffling.

Secondary Metabolic Gene Clusters Deletion Analysis of *Streptomyces albulus* SG-86

We predicted the secondary metabolic gene clusters of the two strains by antiSMASH 6.0.1 and the results showed that there were 38 secondary metabolic gene clusters in M-Z18, including nine non-ribosomal peptide synthetase (NRPS), three polyketide synthase (PKS; T1PKS, T2PKS, and T3PKS), 13 hybrid gene clusters, three terpenes, four Ripp (Other unspecified ribosomally synthesized and post-translationally modified peptide product cluster) and seven other secondary metabolic gene clusters. However, only 22 secondary metabolic gene clusters

were found in SG-86, including three NRPS, one type II PKS, eight hybrid synthetase, two terpenes, four Ripp, and four other secondary metabolic gene clusters. SG-86 had six NRPS, two PKS, five hybrid gene clusters, one terpene, and three other secondary metabolic gene clusters less than M-Z18. After comparison, it was found that these missing gene clusters were at both ends and far away from ε-PL synthase (PLS) in M-Z18 (**Figure 5**). In Actinomycetes, the synthesis of secondary metabolites is catalyzed by a variety of enzymes, the most important of which are PKS and NRPS, while the missing PKS and NRPS in SG-86 do not affect ε-PL yield. On the contrary, the deletion of secondary metabolic gene clusters makes some other compounds no longer produced, and more energy and carbon metabolism flow may flow to ε-PL production.

CONCLUSION

Based on the above results, an ε-PL high yield mechanism of *S. albulus* was preliminarily proposed (**Figure 6**). In this work, we used genome shuffling on strains obtained by ribosome engineering to obtain an ε-PL high yield mutant strain. The mutant strain SG-86 displayed obvious differences in morphology, ε-PL production, and ATP compared to parent strain M-Z18. Except that the two-component system histidine kinase and anti-σ factor mutated after GS. Anti-σ factor blocking the interaction between σ factor and RNA polymerase core enzyme leads to the increase of transcription level of genes related to peptidoglycan synthesis, to guide the correct synthesis of the cell wall. Meanwhile, the selective permeability of the cell membrane was changed. Four genes encoding membrane proteins have InDels. Membrane proteins play a very important role in many life activities of organisms, such as cell proliferation and differentiation, energy conversion, signal transduction, and material transport. Besides, DNA synthesis and repairability changed. The gene encoding DNA polymerase and DNA polymerase subunit is mutated, but DNA replication is normal, which indicates that the enzyme has little relationship with DNA replication and plays an important role in DNA repair. The level of transcriptional regulation changed. For example, TrmB, AfsK, and other genes are mutated. AfsK can globally regulate secondary metabolites, and these transcriptional regulators interact with genetic materials to regulate gene expression, which may also contribute to a new regulatory system. In addition, GS leads to a large number of deletions in genes, secondary metabolic gene clusters, and metabolic pathways. Genome "shrink" not only removes some redundant genes, but also leads to the reduction of the synthesis of metabolic by-products such as alanine, glutamate, glycine, serine, threonine, arginine, and histidine. And we predicted more metabolic may flow to the precursor of ε-PL. Then, the production of ε-PL was eventually promoted. More importantly, the analysis of ε-PL high yield mechanism provides theoretical guidance for metabolic engineering transformation to further improve the production of ε-PL.

DATA AVAILABILITY STATEMENT

The original contributions presented in the study are included in the article/**Supplementary Material**, further inquiries can be directed to the corresponding author.

AUTHOR CONTRIBUTIONS

XC conceived the project and supervised the research. XC and YL designed the experiments, analyzed all data, and wrote the manuscript. YL, KW, and LP performed the experiments. All authors contributed to the article and approved the submitted version.

FUNDING

This work was financially supported by the National Key R&D Program of China (2020YFA0907700), the National Natural Science Foundation of China (31901622 and 32100049), and the Natural Science Foundation of Jiangsu Province (BK20191332 and BK20190585).

SUPPLEMENTARY MATERIAL

The Supplementary Material for this article can be found online at: https://www.frontiersin.org/articles/10.3389/fmicb.2022.923526/full#supplementary-material

REFERENCES

Bankar, S. B., and Singhal, R. S. (2013). Panorama of poly-ε-lysine. *RSC Adv.* 3, 8586–8603. doi: 10.1039/C3RA22596H

Chen, T., Wang, J. Y., Zhou, S. Q., Chen, X., Ban, R., and Zhao, X. M. (2004). Trait improvement of riboflavin producing *Bacillus subtilis* by genome shuffling and metabolic flux analysis. *J. Chem. Ind. Eng.* 55, 1842–1848.

Chheda, A., and Vernekar, M. (2015). A natural preservative ε-poly-L-lysine: fermentative production and applications in food industry. *Int. Food Res. J.* 22, 23–30.

Cingolani, P., Patel, V. M., Coon, M., Nguyen, T., Land, S. J., Ruden, D. M., et al. (2012). Using *Drosophila melanogaster* as a model for genotoxic chemical mutational studies with a new program, SnpSift. *Front. Genet.* 3:35. doi: 10.3389/fgene.2012.00035

Delcher, A. L., Harmon, D., Kasif, S., White, O., and Salzberg, S. L. (1999). Improved microbial gene identification with GLIMMER. *Nucleic Acids Res.* 27, 4636–4641. doi: 10.1093/nar/27.23.4636

Fadli, M., Saad, A., Sayadi, S., Chevalier, J., Mezrioui, N.-E., Pagès, J.-M., et al. (2012). Antibacterial activity of *Thymus maroccanus* and *Thymus broussonetii* essential oils against nosocomial infection–bacteria and their synergistic potential with antibiotics. *Phytomedicine* 19, 464–471. doi: 10.1016/j.phymed.2011.12.003

Girvan, H. M., and Munro, A. W. (2016). Applications of microbial cytochrome P450 enzymes in biotechnology and synthetic biology. *Curr. Opin. Chem. Biol.* 31, 136–145. doi: 10.1016/j.cbpa.2016.02.018

Gong, G. L., Sun, X., Liu, X. L., Hu, W., Cao, W. R., Liu, H., et al. (2007). Mutation and a high-throughput screening method for improving the production of epothilones of sorangium. *J. Ind. Microbiol. Biotechnol.* 34, 615–623. doi: 10.1007/s10295-007-0236-2

Gos, T., and Raszeja, S. (1993). Postmortem activity of lactate and malate dehydrogenase in human liver in relation to time after death. *Int. J. Legal Med.* 106, 25–29. doi: 10.1007/BF01225020

Gu, Y., Wang, X., Yang, C., Geng, W., Feng, J., Wang, Y., et al. (2016). Effects of chromosomal integration of the vitreoscilla hemoglobin gene (vgb) and S-adenosylmethionine synthetase gene (metK) on [epsilon]-poly-l-lysine synthesis in *Streptomyces albulus* NK660. *Appl. Biochem. Biotechnol.* 178, 1445–1457. doi: 10.1007/s12010-015-1958-7

Guan, N., Liu, L., Shin, H. D., Chen, R. R., Zhang, J., Li, J., et al. (2013). Systems-level understanding of how *Propionibacterium acidipropionici* respond to propionic acid stress at the microenvironment levels: mechanism and application. *J. Biotechnol.* 167, 56–63. doi: 10.1016/j.jbiotec.2013.06.008

Hida, H., Yamada, T., and Yamada, Y. (2007). Genome shuffling of *Streptomyces* sp. U121 for improved production of hydroxycitric acid. *Appl. Microbiol. Biotechnol.* 73, 1387–1393. doi: 10.1007/s00253-006-0613-1

Hillerich, B., and Westpheling, J. (2006). A new GntR family transcriptional regulator in *Streptomyces coelicolor* is required for morphogenesis and antibiotic production and controls transcription of an ABC transporter in response to carbon source. *J. Bacteriol.* 188, 7477–7487. doi: 10.1128/JB.00898-06

Hiraki, J., Hatakeyama, M., Morita, H., and Izumi, Y. (1998). Improved epsilon-poly-L-lysine production of an S-(2-aminoethyl)-L-cysteine resistant mutant of *Streptomyces albulus*. *Seibutsu-kogaku Kaishi* 76, 487–493.

Horinouchi, S. (2003). AfsR as an integrator of signals that are sensed by multiple serine/threonine kinases in *Streptomyces coelicolor* A3(2). *J. Ind. Microbiol. Biotechnol.* 30, 462–467. doi: 10.1007/s10295-003-0063-z

Itzhaki, R. F. (1972). Colorimetric method for estimating polylysine and polyarginine. *Anal. Biochem.* 50, 569–574. doi: 10.1016/0003-2697(72)90067-X

Lee, S. J., Surma, M., Hausner, W., Thomm, M., and Boos, W. (2008). The role of TrmB and TrmB-like transcriptional regulators for sugar transport and metabolism in the hyperthermophilic archaeon *Pyrococcus furiosus*. *Arch. Microbiol.* 190, 247–256. doi: 10.1007/s00203-008-0378-2

Leja, K., Myszka, K., and Czaczyk, K. (2011). Genome shuffling: a method to improve biotechnological processes. *Biotechnology* 4, 345–351. doi: 10.5114/bta.2011.46551

Li, S., Chen, X., Dong, C., Zhao, F., Tang, L., and Mao, Z. (2013). Combining genome shuffling and interspecific hybridization among *Streptomyces* improved epsilon-poly-L-lysine production. *Appl. Biochem. Biotechnol.* 169, 338–350. doi: 10.1007/s12010-012-9969-0

Li, S., Li, F., Chen, X.-S., Wang, L., Xu, J., Tang, L., et al. (2012). Genome shuffling enhanced ε-poly-l-lysine production by improving glucose tolerance of *Streptomyces graminearus*. *Appl. Biochem. Biotechnol.* 166, 414–423. doi: 10.1007/s12010-011-9437-2

Liang, H. Y., and Guo, Y. (2007). Whole genome shuffling to enhance activity of fibrinolytic enzyme-producing strains. *Chin. Biotechnol.* 27, 39–43.

Liu, Y., Chen, X., Pan, L., and Mao, Z. (2019a). Differential protein expression of a streptomycin-resistant *Streptomyces albulus* mutant in high yield production of ε-poly-l-lysine: a proteomics study. *RSC Adv.* 9, 24092–24104. doi: 10.1039/C9RA03156A

Liu, Y., Chen, X., Zhao, J., Li, Q., and Mao, Z. (2019b). Improvement of ε-poly-L-lysine production of *Streptomyces albulus* by continuous introduction of streptomycin resistance. *Process Biochem.* 82, 10–18. doi: 10.1016/j.procbio.2019.04.006

Liu, Y., Chen, X., Zhao, J., Pan, L., and Mao, Z. (2017). Development of microtiter plate culture method for rapid screening of ε-poly-L-lysine-producing strains. *Appl. Biochem. Biotechnol.* 183, 1209–1223. doi: 10.1007/s12010-017-2493-5

Lowe, T. M., and Eddy, S. R. (1997). tRNAscan-SE: a program for improved detection of transfer RNA genes in genomic sequence. *Nucleic Acids Res.* 25, 955–964. doi: 10.1093/nar/25.5.955

Luna-Flores, C. H., Palfreyman, R. W., Kromer, J. O., Nielsen, L. K., and Marcellin, E. (2017). Improved production of propionic acid using genome shuffling. *Biotechnol. J.* 12:1600120. doi: 10.1002/biot.201600120

Macnab, R. (1996). *Escherichia coli and Salmonella: Cellular and Molecular Biology.* ASM Press, 1458–1496.

McVean, G., Awadalla, P., and Fearnhead, P. (2002). A coalescent-based method for detecting and estimating recombination from gene sequences. *Genetics* 160, 1231–1241. doi: 10.1093/genetics/160.3.1231

Melo, M. N., Ferre, R., and Castanho, M. A. (2009). Antimicrobial peptides: linking partition, activity and high membrane-bound concentrations. *Nat. Rev. Microbiol.* 7, 245–250. doi: 10.1038/nrmicro2095

Mendes, M. V., Tunca, S., Anton, N., Recio, E., Sola-Landa, A., Aparicio, J. F., et al. (2007). The two-component phoR-phoP system of *Streptomyces natalensis*: inactivation or deletion of phoP reduces the negative phosphate regulation of pimaricin biosynthesis. *Metab. Eng.* 9, 217–227. doi: 10.1016/j.ymben.2006.10.003

Méndez, C., and Salas, J. A. (2001). The role of ABC transporters in antibiotic-producing organisms-drug secretion and resistance mechanisms. *Res. Microbiol.* 152, 341–350. doi: 10.1016/s0923-2508(01)01205-0

Myronovskyi, M., Welle, E., Fedorenko, V., and Luzhetskyy, A. (2011). β-Glucuronidase as a sensitive and versatile reporter in actinomycetes. *Appl. Environ. Microbiol.* 77, 5370–5383. doi: 10.1128/AEM.00434-11

Najjar, M. B., Kashtanov, D., and Chikindas, M. (2007). ε-Poly-l-lysine and nisin A act synergistically against gram-positive food-borne pathogens *Bacillus cereus* and *Listeria monocytogenes*. *Lett. Appl. Microbiol.* 45, 13–18. doi: 10.1111/j.1472-765X.2007.02157.x

Nishikawa, M., and Ogawa, K. (2002). Distribution of microbes producing antimicrobial epsilon-poly-L-lysine polymers in soil microflora determined by a novel method. *Appl. Environ. Microbiol.* 68, 3575–3581. doi: 10.1128/AEM.68.7.3575-3581

Olano, C., Lombó, F., Méndez, C., and Salas, J. A. (2008). Improving production of bioactive secondary metabolites in actinomycetes by metabolic engineering. *Metab. Eng.* 10, 281–292. doi: 10.1016/j.ymben.2008.07.001

Padan, E. (2009). Bacterial membrane transport: superfamilies of transport proteins. *eLS.* doi: 10.1002/9780470015902.a0003743.pub2

Pisciotta, A., Manteca, A., and Alduina, R. (2018). The SCO1731 methyltransferase modulates actinorhodin production and morphological differentiation of *Streptomyces coelicolor* A3(2). *Sci. Rep.* 8:13686. doi: 10.1038/s41598-018-32027-8

Ren, X., Xu, Y., Zeng, X., Chen, X., Tang, L., and Mao, Z. (2015). Microparticle-enhanced production of ε-poly-l-lysine in fed-batch fermentation. *RSC Adv.* 5, 82138–82143. doi: 10.1039/c5ra14319e

Roth, J. R., Benson, N., Galitski, T., Haack, K., Lawrence, J. G., and Miesel, L. (1996). "Rearrangements of the bacterial chromosome: formation and applications," in *Escherichia coli and Salmonella. 2nd Edn.* ed. F. C. Neidhardt (Washington DC: ASM Press), 2256–2276.

Rudolf, J. D., Chang, C. Y., Ma, M., and Shen, B. (2017). Cytochromes P450 for natural product biosynthesis in *Streptomyces*: sequence, structure, and function. *Nat. Prod. Rep.* 34, 1141–1172. doi: 10.1039/c7np00034k

Santos, J. C., Sousa, R. C., Otoni, C. G., Moraes, A. R., Souza, V. G., Medeiros, E. A., et al. (2018). Nisin and other antimicrobial peptides: production, mechanisms of action, and application in active food packaging. *Innov. Food Sci. Emerg.* 48, 179–194. doi: 10.1016/j.ifset.2018.06.008

Santos, R., Ursu, O., Gaulton, A., Bento, A. P., Donadi, R. S., Bologa, C. G., et al. (2016). A comprehensive map of molecular drug targets. *Nat. Rev. Drug Discov.* 16, 19–34. doi: 10.1038/nrd.2016.230

Shukla, S. C., Singh, A., Pandey, A. K., and Mishra, A. (2012). Review on production and medical applications of ε-polylysine. *Biochem. Eng. J.* 65, 70–81. doi: 10.1016/j.bej.2012.04.001

Sohng, J. K. (2009). Identification and functional characterization of an afsR homolog regulatory gene from *Streptomyces venezuelae* ATCC 15439. *J. Microbiol. Biotechnol.* 19, 121–128. doi: 10.4014/jmb.0803.223

Stratigopoulos, G., and Cundliffe, E. (2002). Expression analysis of the tylosin-biosynthetic gene cluster_ pivotal regulatory role of the tylQ product. *Chem. Biol.* 9, 71–78. doi: 10.1016/s1074-5521(01)00095-3

Wang, L., Chen, X., Wu, G., Li, S., Zeng, X., Ren, X., et al. (2015). Improved ε-poly-l-lysine production of *Streptomyces* sp. FEEL-1 by atmospheric and room temperature plasma mutagenesis and streptomycin resistance screening. *Ann. Microbiol.* 65, 2009–2017. doi: 10.1007/s13213-015-1039-8

Wang, L., Chen, X., Wu, G., Li, S., Zeng, X., Ren, X., et al. (2017). Enhanced ε-poly-l-lysine production by inducing double antibiotic-resistant mutations in *Streptomyces albulus*. *Bioprocess Biosyst. Eng.* 40, 271–283. doi: 10.1007/s00449-016-1695-5

Wang, L., Chen, X., Wu, G., Zeng, X., Ren, X., Li, S., et al. (2016). Genome shuffling and gentamicin-resistance to improve ε-poly-l-lysine productivity of *Streptomyces albulus* W-156. *Appl. Biochem. Biotechnol.* 180, 1601–1617. doi: 10.1007/s12010-016-2190-9

Wang, C., Ren, X., Yu, C., Wang, J., Wang, L., Zhuge, X., et al. (2020). Physiological and transcriptional responses of *Streptomyces albulus* to acid stress in the biosynthesis of ε-poly-L-lysine. *Front. Microbiol.* 11:1379. doi: 10.3389/fmicb.2020.01379

Wu, C., Zhang, J., Chen, W., Wang, M., Du, G., and Chen, J. (2012). A combined physiological and proteomic approach to reveal lactic-acid-induced alterations in *Lactobacillus casei* Zhang and its mutant with enhanced lactic acid tolerance. *Appl. Microbiol. Biotechnol.* 93, 707–722. doi: 10.1007/s00253-011-3757-6

Xu, Z., Bo, F., Xia, J., Sun, Z., Li, S., Feng, X., et al. (2015). Effects of oxygen-vectors on the synthesis of epsilon-poly-lysine and the metabolic characterization of *Streptomyces albulus* PD-1. *Biochem. Eng. J.* 94, 58–64. doi: 10.1016/j.bej.2014.11.009

Yamanaka, K., Kito, N., Imokawa, Y., Maruyama, C., Utagawa, T., and Hamano, Y. (2010). Mechanism of ε-poly-l-lysine production and accumulation revealed by identification and analysis of an ε-poly-l-lysine-degrading enzyme. *Appl. Environ. Microbiol.* 76, 5669–5675. doi: 10.1128/AEM.00853-10

Ye, R., Xu, H., Wan, C., Peng, S., Wang, L., Xu, H., et al. (2013). Antibacterial activity and mechanism of action of ε-poly-l-lysine. *Biochem. Biophys. Res. Commun.* 439, 148–153. doi: 10.1016/j.bbrc.2013.08.001

Zeng, X., Chen, X.-S., Ren, X.-D., Liu, Q.-R., Wang, L., Sun, Q.-X., et al. (2014). Insights into the role of glucose and glycerol as a mixed carbon source in the improvement of ε-poly-l-lysine productivity. *Appl. Biochem. Biotechnol.* 173, 2211–2224. doi: 10.1007/s12010-014-1026-8

Zhang, Y., Perry, K., Vinci, V. A., Powell, K., Stemmer, W. P., and del Cardayré, S. B. (2002). Genome shuffling leads to rapid phenotypic improvement in bacteria. *Nature* 415, 644–646. doi: 10.1038/415644a

Zhang, X., Shi, C., Liu, Z., Pan, F., Meng, R., Bu, X., et al. (2018). Antibacterial activity and mode of action of ε-polylysine against *Escherichia coli* O157: H7. *J. Med. Microbiol.* 67, 838–845. doi: 10.1099/jmm.0.000729

Zong, H., Zhan, Y., Li, X., Peng, L., Feng, F., and Li, D. (2012). A new mutation breeding method for *Streptomyces albulus* by an atmospheric and room temperature plasma. *Afr. J. Microbiol. Res.* 6, 3154–3158. doi: 10.5897/AJMR11.1251

Conflict of Interest: The authors declare that the research was conducted in the absence of any commercial or financial relationships that could be construed as a potential conflict of interest.

Publisher's Note: All claims expressed in this article are solely those of the authors and do not necessarily represent those of their affiliated organizations, or those of the publisher, the editors and the reviewers. Any product that may be evaluated in this article, or claim that may be made by its manufacturer, is not guaranteed or endorsed by the publisher.

frontiers | Frontiers in Microbiology

ORIGINAL RESEARCH
published: 14 June 2022
doi: 10.3389/fmicb.2022.923656

In vivo Protein Interference: Oral Administration of Recombinant Yeast-Mediated Partial Leptin Reduction for Obesity Control

Feng Yue†, Lihong Du†, Ruyu Wang, Baoquan Han, Xiaojun Zhang, Zhangzhang Yao, Wenqiang Zhang, Chang Cai, Zhiying Zhang and Kun Xu**

College of Animal Science and Technology, Northwest A&F University, Shaanxi, China

OPEN ACCESS

Edited by:
Yu Xia,
Jiangnan University, China

Reviewed by:
Long Zhang,
Xi'an Jiaotong University, China
Tingting Zhang,
Shanxi University, China
Qixiao Zhai,
Jiangnan University, China

***Correspondence:**
Zhiying Zhang
zhangzhy@nwafu.edu.cn
Kun Xu
xukunas@nwafu.edu.cn

† These authors have contributed equally to this work and share first authorship

Specialty section:
This article was submitted to Food Microbiology, a section of the journal Frontiers in Microbiology

Received: *19 April 2022*
Accepted: *17 May 2022*
Published: *14 June 2022*

Citation:
Yue F, Du L, Wang R, Han B, Zhang X, Yao Z, Zhang W, Cai C, Zhang Z and Xu K (2022) In vivo Protein Interference: Oral Administration of Recombinant Yeast-Mediated Partial Leptin Reduction for Obesity Control. Front. Microbiol. 13:923656. doi: 10.3389/fmicb.2022.923656

Obesity-related diseases are always the major health problems that concern the whole world. Serial studies have reported that obesity development is closely related to the out-of-control leptin encoded by the obesity gene (*ob*). The latest report declaimed "Less Is More," a model explaining that partial leptin reduction triggers leptin sensitization and contributes to obesity control. Here, we came up with a novel concept, *in vivo* protein interference (iPRTi), an interesting protein knock-down strategy for *in vivo* partial leptin reduction. First, the specific immune response against leptin induced by the oral administration of *ob* recombinant yeast was confirmed. Subsequentally, leptin resistance was observed in diet-induced obese mice, and oral administration with *ob* recombinant yeast declined the circulating leptin and reduced significantly the body weight gain. To further investigate whether the iPRTi strategy is capable of obesity management, the diet-induced obese mice were administrated with *ob* recombinant yeast. All the indexes examined including the circulating leptin, triglyceride, and total cholesterol, as well as food intake and weight gain, demonstrated a positive effect of the iPRTi strategy on obesity control. In short, this study provides a novel strategy for the potential application of recombinant yeast for the therapy of obese individuals with leptin resistance.

Keywords: protein interference, protein knock-down, leptin resistance, partial leptin reduction, obesity control, oral administration, recombinant yeast

HIGHLIGHTS

- Oral administration of *ob* recombinant yeast induces *in vivo* specific immune response.
- Oral administration of diet-inducing obese mice with *ob* recombinant yeast relieves leptin resistance and reduces body weight gain.
- Oral administration of diet-induced obese mice with *ob* recombinant yeast contributes to obesity control.

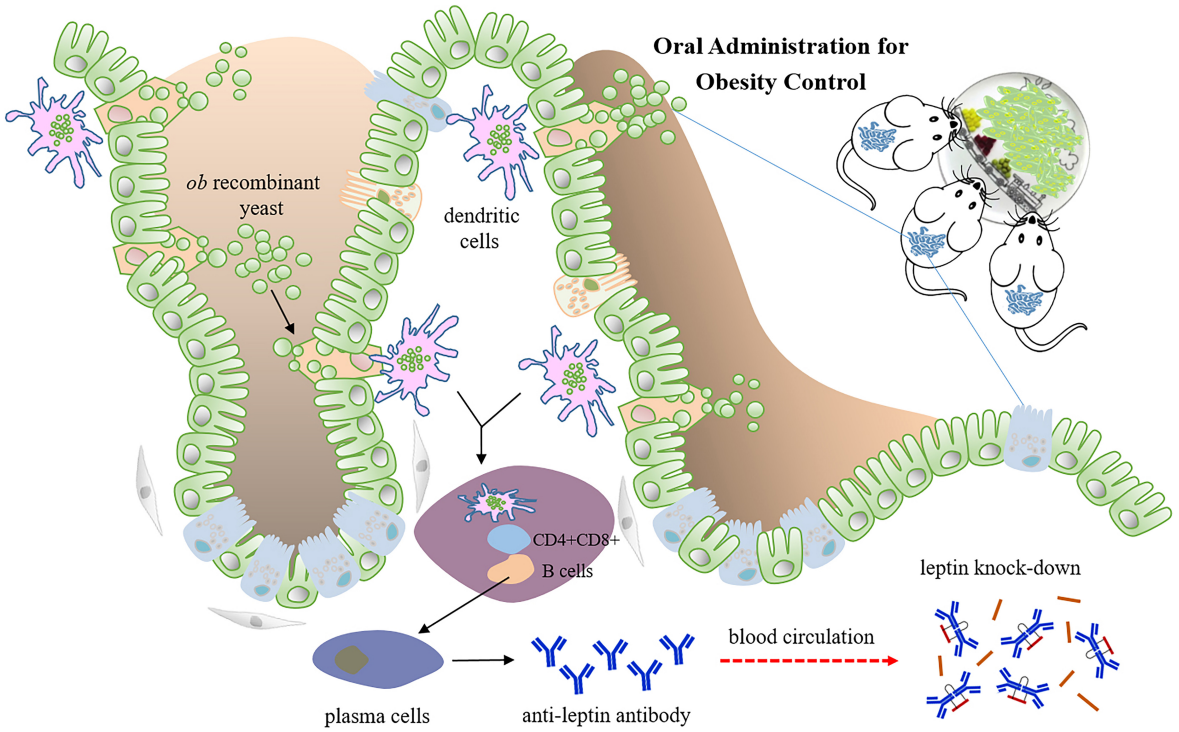

GRAPHICAL ABSTRACT | Oral administration of *ob* recombinant yeast mediated partial leptin reduction for diet-induced obesity control. When the whole yeast is uptaken by phagocytic cells in the gut, for example, dendritic cells, it is supposed to be lysed within the cells. The recombinant DNA vaccine cassette can be released, expressed, and further presented to lymphocytes, thereby activating the immune response.

INTRODUCTION

Obesity mainly characterized by excess body fat is one of the prominent risks causing chronic diseases, including type 2 diabetes, atherosclerosis, cardiovascular disease, cancer, and other related diseases It has become a major health problem covering the world. Although numerous efforts have been made for obesity control, including lifestyle change, surgical treatment, medical therapy, and so on, the weight loss effects often fail to meet the demand of obese individuals. What's more, pharmacological leptin therapy for the treatment of diet-induced obesity has been reported to be ineffective, which is the famed "leptin resistance" phenomenon (Zhao et al., 2020a).

Leptin, encoded by the obese gene (*ob*), is known as an adipocyte hormone that controls energy expenditure, and acts as an afferent negative feedback signal to the central nervous system, maintaining homeostatic control of adipose tissue mass and regulating appetite and metabolism (Zhang et al., 1994). Leptin is secreted primarily by white adipose tissue and its secretion is proportional to adipocytes (Maffei et al., 1995). Many studies have revealed that increased leptin secretion is a significant predictor of altered blood lipid profiles and glucose–insulin homeostasis (Frederich et al., 1995; Laforest et al., 2015). In the context of conventional obesity, obese individuals do not lack leptin; rather, they display higher levels of circulating leptin. However, the oversecreted leptin will not contribute to energy expenditure, diet control, and weight loss, which is known as leptin resistance and is caused by impaired leptin signaling in the brain (Zelissen et al., 2005; Knight et al., 2010; Flier and Maratos-Flier, 2017).

Therefore, "Less Is More," partial leptin reduction has been raised recently as an insulin sensitization and weight loss strategy (Zhao et al., 2020a). The latest studies have demonstrated that insulin sensitization and weight loss could be achieved by reducing circulating leptin through an immunological approach in an obesogenic environment (Zhao et al., 2019, 2020b; Hankir and Seyfried, 2020). Neutralizing antibody injection triggers an immune response to endogenous oversecreted leptin, and maintaining lower circulating leptin is highly beneficial to obesity control in diet-induced obese mice (Zhao et al., 2020b).

Inspired by the idea to trigger the immune response to endogenous oversecreted leptin for obesity control, we proposed in the current study to develop an oral yeast vaccine for leptin knock-down based on our previous studies and came up with a novel concept *in vivo* protein interference (iPRTi).

MATERIALS AND METHODS

Strains and Plasmids

Saccharomyces cerevisiae JMY31 strain (*MATα, ade2-1; ura3-1; his3-11; trp1-1; leu2-3,112; can1-100*) and *Escherichia coli* JM109 and Rosetta (DE3) strains, as well as the JMB84 plasmid, all came from the lab storage as we previously used (Han et al., 2019;

Zakria et al., 2019). JMB84 is a yeast-bacteria shuttle vector harboring replication origins and selecting marker genes intent for both yeast and *Escherichia coli* transformation. It was used as the backbone and the negative control in the current study. The JMY31 strain for the construction of recombinant yeast vaccines was grown and kept in a YPD medium. The JM109 strain for the construction of recombinant plasmids and The Rosetta (DE3) strain for leptin prokaryotic expression were grown and kept in an LB medium.

Construction of Vectors

To establish the iPRTi and verifying system, a series of plasmid vectors as shown in **Figure 1A** was constructed by recombinant DNA technology using JM109 competent cells. The coding sequence (CDS) of the mouse *ob* gene (NM_008493.3) was first cloned from the adipose tissue cDNA by RT-PCR. The yeast shuttle vector JMB84-CMV-ob and the prokaryotic expression vector pET32a-ob were generated, respectively, by replacing the *MSTN* CDS of the JMB84-CMV-MSTN (Zakria et al., 2019) and pET32a-MSTN (Zhang et al., 2011) vectors with the *ob* CDS. Based on the JMB84-CMV-ob vector, the *OVA* CDS and the *T2A-GFP* open reading frame were cloned up- and downstream of the *ob* CDS successively to generate the JMB84-CMV-OVA-ob and JMB84-CMV-OVA-ob-T2A-GFP vectors. Similar to what we previously did (Han et al., 2019), the ovalbumin (OVA) was introduced to enhance the immunogenicity, and the green fluorescent protein (GFP) was used to verify the expression of the *ob* DNA vaccine cassette in mammalian cells.

Verification of the *ob* Recombinant Cassette in Mammalian Cells

Mammalian 293T cells were maintained in Dulbecco's modified Eagle's medium (DMEM; GIBCO) supplemented with 10% fetal bovine serum (FBS; BI), 100 U/ml penicillin, and 100 mg/ml streptomycin in a 37°C humidified atmosphere with 5% CO_2 incubation. The cells were seeded into 12-well plates and were transfected with the JMB84-CMV-OVA-ob-T2A-GFP plasmid DNA by Lipofectamine 2000 (Invitrogen) according to the manufacturer's protocol. After 48 h of the transfection, the cells were observed to confirm the expression of the CMV-OVA-ob-T2A-GFP recombinant cassette and were photographed with a fluorescence microscope.

Preparation of the Recombinant Whole Yeast Vaccines

Yeast JMY31 cells were transformed using the LiAc method (Gietz, 2014), respectively, with the shuttle vectors JMB84-CMV-ob and JMB84-CMV-OVA-ob, as well as the control empty vector JMB84. Different transformant clones were selected using plates with SD/-Ura medium (Clontech) incubated at 30°C for 3 days and were further expanded in liquid SD/-Ura medium with shaking for another 3 days. The yeast transformant cells were harvested, resuspended in PBS with the density of 2×10^8 cfu/ml and heat-inactivated at 56°C for 1 h (Kiflmariam et al., 2013). The resuspended and inactivated yeast transformant cells were then aliquoted and stored at −80°C until the oral administration.

Prokaryotic Expression of Leptin

Escherichia coli Rosetta (DE3) transformants with the recombinant plasmid pET32a-ob were selected using LB plates with ampicillin supplemented. The transformant cells were seeded and expanded in liquid LB/+Amp medium at 37°C with shaking. When the optical density at 600 nm (OD_{600}) reached up to 0.6, the expression was induced with 0.5 Mm IPTG supplemented for 4 h. Then, the bacterial cells were harvested, resuspended in PBS, and subjected to sonication. The protein purification of recombinant leptin was conducted using the AKTA protein chromatography system with Ni-NTA Kit (BaiHui, China) according to the manufacturer's protocol. The purified recombinant leptin was stored at −80°C for the subsequent detection of serumal anti-leptin antibodies.

Mice and Oral Immunization

A total of 96 5-week-old female Kunming mice were purchased from the Breeding and Research Centre of Xi'an Jiaotong University, China. All mice were housed and handled according to the guidelines for the Welfare and Moral Inspection of Experimental Animals in China (No. 2 Order of State Science and Technology Commission of the PRC) and were approved by the Animal Ethics Committee of Northwest A&F University (approval number NWAFU-DK2020046). Generally, the mice were raised with a 12-h light/12-h dark cycle and in a temperature-controlled environment (22 ± 2°C) and had *ad libitum* access to food and water.

For the oral immunization experiment (as shown in **Figures 2A–C**), all the mice were acclimated to the new environment for 1 week after arrival and were randomly divided into the normal chow (NC) group and the high-fat diet (HFD) groups. The HFD groups included the diet-inducing obesity (DIOing) group maintained with continuous D12492 high-fat feeding and the diet-induced obesity (DIOed) group with NC after high-fat feeding induction (**Figure 2C**). Each group was further divided into four treatments (as shown in **Table 1**) with oral administration of different recombinant yeast and control PBS solution. The experiment mice for each treatment were housed in two cages and were orally administrated with recombinant yeast 100μl once per mouse every 4 days for a total of 60 days. Blood samples were collected by tail vein sampling before, during, and after the immunization (Day0, Day30, and Day60). The samples of the same time from different individuals of each treatment were mixed for antiserum preparation.

Body Weight and Food Intake Measurement

In order to measure the changes in the body weight and food intake of the mice in the HFD groups, the mice of different treatments were acclimated for at least 1 week to reduce the anxiety effects, and the initial body weight before oral immunization was measured. Then, the body weight and food intake during the experiment were measured every week. The data for food intake was represented as a daily average. The body weights of the mice from different treatments were measured

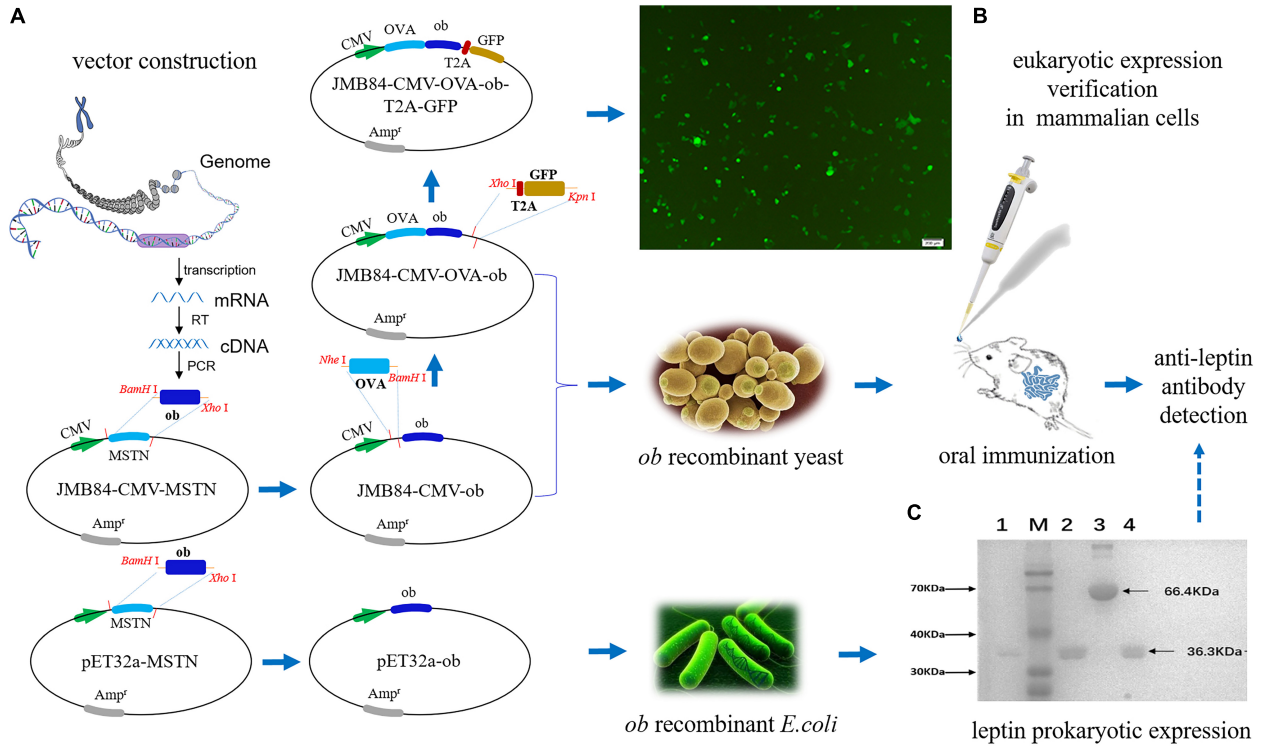

FIGURE 1 | Schematic diagram of the experiment design and vector verification. **(A)** Flow chart for the construction of the plasmid vectors. **(B)** Fluorescence observation of the 293T cells transfected with the JMB84-CMV-OVA-ob-T2A-GFP vector. The GFP expression suggested the recombinant CMV-OVA-*ob* cassette, as a DNA vaccine, could be expressed successfully in mammalian cells. **(C)** SDS-PAGE electrophoresis result of the purified leptin protein. Line 1, 2, and 4: purified leptin proteins expressed by different *E. coli* Rosetta (DE3) transformants. Line 3, the bull serum albumin (BSA) control. M: Blue Plus II protein marker.

every week, and the average body weight gain was calculated at the end of oral immunization.

Western Blotting Assay

The western blotting (WB) assay was conducted for the preliminary qualitative validation of anti-leptin antibodies in the antiserum from immunized mice. The purified recombinant leptin protein prepared above by prokaryotic expression was used as an antigen for the WB detection. The antiserums (Day60) from immunized mice of different treatments served as the primary antibodies at a 1:50 dilution. A goat-anti-mouse secondary antibody labeled with HRP was used at the dilution 1:2,000. The results were visualized with chemiluminescence by the ChemiDoc XRS imaging system (Bio-Rad, United States).

Enzyme-Linked Immunosorbent Assay

The Enzyme-linked immunosorbent assay (ELISA) for tittering the anti-leptin antibodies in the antiserums was performed as we previously did (Zakria et al., 2019). 96-well EIA/RIA plates were coated overnight at 4°C with the purified recombinant leptin protein (100 μl, 5 ng/μl) and blocked for 2 h at 37°C with 5% non-fat milk. After washed with PBS 3 times, serial diluted antiserums (Day60, 1:20; 1:40; 1:80; 1:160; 1:320; 1:640; 1:1280) were added and incubated for overnight at 4°C. Subsequently, the plates were washed with PBS and incubated for 2 h with a goat anti-mouse HRP-conjugated antibody (Beyotime, China). The immunoreactions were developed with TMB substrates (Tiangen, China) and stopped by the addition of 2 M sulfuric acid before the plate was read at 450 nm. The circulating leptin in the antiserums (Day0, Day30, and Day60) was also detected using a commercial ELISA kit according to the user manual and the results were calculated by standard curve (Solarbio, China). Each antiserum mixture was assayed with at least three technical repeats.

Total Cholesterol and Triglyceride Tests

Total cholesterol and triglyceride test kits were purchased from Nanjing Jiancheng Bioengineering Institute[1] and the tests were performed according to the proposal. The reagent was mixed with the antiserum and incubated at 37°C for 10 min before the plates were read at 510 nm by a micro plate spectrophotometer. Each antiserum mixture was assayed with at least three technical repeats.

Liver Histology

Liver tissues from different immunized mice of the DIOing group were excised and fixed overnight in 4% paraformaldehyde and were thereafter switched to 50% ethanol for long-time storage. Then the liver tissues were paraffin embedded, sectioned,

[1]www.njjcbio.com

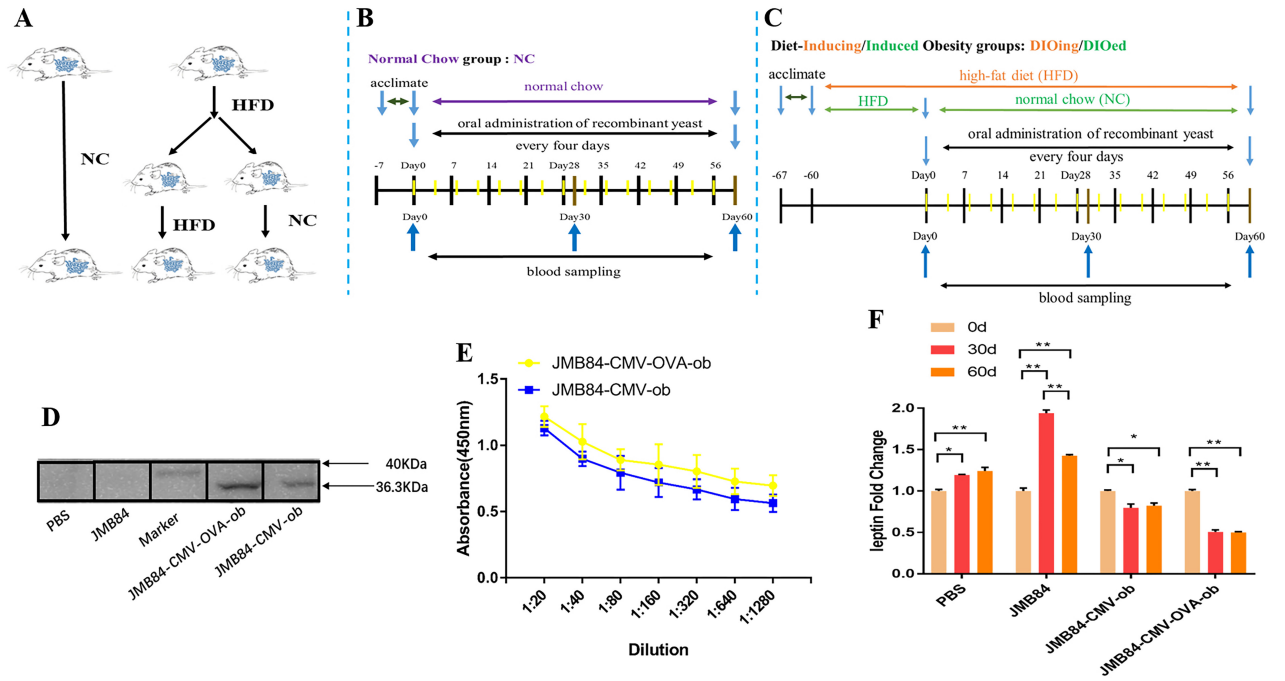

FIGURE 2 | Oral immunization groups and timelines, preliminary immune response induced by oral administration of *ob* recombinant yeast in NC mice. **(A)** Oral immunization groups. **(B)** The feeding, oral immunization, and blood sampling timeline for the NC group. **(C)** The feeding, immunization, and sampling timeline for the DIOing and DIOed groups. **(D)** WB assay result with purified leptin recombinant protein as the antigen and different antiserums (Day60) from different treatments as the primary antibodies. **(E)** ELISA result for anti-leptin antibody titering in the antiserums (Day60) from the oral immunized mice by *ob* recombinant yeast. **(F)** The changes in circulating leptin were detected by ELISA in the antiserums (Day0, Day30, and Day60) from different treatments. The * sign indicates statistical significance at a *P* value of < 0.05; ** represents $P < 0.01$.

and sliced at 8 mm per slide. The slices were stained with hematoxylin-eosin (HE) and then visualized under a microscope (OLYMPUS CKX53).

Statistical Analysis

Statistical analysis was evaluated with ANOVA by IBM SPSS Statistics 21. Data were expressed as mean ± standard error of mean (SEM). $^{*}p < 0.05$ and $^{**}p < 0.01$ were regarded as statistically significant, and ns as no significance.

RESULTS

Experiment Design and Vector Verification

In general, to establish the iPRTi and verifying system, the yeast shuttle vector JMB84-CMV-ob and the prokaryotic expression vector pET32a-ob were first constructed based on previous vectors (**Figure 1A**). The vector JMB84-CMV-OVA-ob was next constructed with OVA introduced to enhance the immunogenicity as we previously did (Han et al., 2019). JMB84-CMV-OVA-ob-T2A-GFP was further constructed with GFP introduced to verify the expression of the *ob* DNA vaccine cassette in mammalian cells. As OVA-ob was expressed as a fusion and JMB84-CMV-OVA-ob was constructed based on JMB84-CMV-ob with the same expression pattern, hence mammalian-expression observed from JMB84-CMV-OVA-ob-T2A-GFP by green fluorescence could prove the expression of both the CMV-OVA-ob and CMV-ob cassettes.

The whole experiment design was divided into three parts, respectively, mammalian expression verification, oral yeast immunization, and antigen prokaryotic expression. Firstly, 293T cells were transfected with the JMB84-CMV-OVA-ob-T2A-GFP plasmid DNA to confirm the functional expression of the CMV-OVA-ob-T2A-GFP cassette. The green fluorescence (**Figure 1B**) suggested the recombinant CMV-OVA-ob and CMV-ob cassettes, as DNA vaccines, which were the core components in this study, could be expressed successfully in mammalian cells. Secondly, yeast JMY31 cells were transformed with the shuttle vectors JMB84-CMV-ob and JMB84-CMV-OVA-ob, as well as the control empty vector JMB84. The corresponding transformants were selected, identified, and expanded for subsequent oral immunization. Meanwhile, *E. coli* Rosetta (DE3) transformants harboring pET32a-ob were used for the prokaryotic expression of leptin protein. As displayed in **Figure 1C**, the recombinant leptin was successfully expressed and purified, which would serve as the antigen in the WB and ELISA assays for the detection of serumal anti-leptin antibodies. As for the immunization, when the oral administrated whole yeast is uptaken by phagocytic cells in the gut, for example,

TABLE 1 | Oral administration treatments for each experiment group.

Treatment	Oral administration	Density	Dosage	Function
PBS	–	–	100 μl	Blank control
JMY31 (JMB84)	Whole yeast	2×10^8 cfu/ml	100 μl	Carrier control
JMY31 (JMB84-CMV-ob)	Whole yeast (*ob*)	2×10^8 cfu/ml	100 μl	Vaccine group
JMY31 (JMB84-CMV-OVA-ob)	Whole yeast (*OVA-ob*)	2×10^8 cfu/ml	100 μl	Vaccine group

dendritic cells (DCs), it is supposed to be lysed within the cells. The recombinant CMV-OVA-ob or CMV-ob cassettes can be released, expressed, and further presented to lymphocytes, thereby activating the immune response. Here, the recombinant CMV-OVA-ob or CMV-ob cassettes function as DNA vaccines and the yeast cell acts as the carrier.

Oral Administration of *ob* Recombinant Yeast Induces a Specific Immune Response

To conduct the oral immunization experiment, all the mice were randomly divided into the NC group and HFD groups (**Figure 2A**), and the HFD groups were further termed as the DIOing and DIOed groups characterized by different high-fat feeding patterns. The feeding, oral immunization, and blood sampling timelines for the three groups are shown in **Figures 2B,C**.

Preliminary, to confirm specific immune response could be induced by oral *ob* recombinant yeast, the NC group mice were first orally administrated with different recombinant yeast. WB assay was first conducted for the qualitative validation of anti-leptin antibodies in the antiserums after the oral immunization. The result clearly demonstrated specific anti-leptin antibodies could be induced by the oral administration of both JMY31 (CMV-ob) and JMY31 (CMV-OVA-ob) yeast transformants (**Figure 2D**). ELISA assay was subsequently conducted for anti-leptin antibody titering, and the result (**Figure 2E**) shows that the anti-leptin antibody titer was slightly higher for the JMY31 (CMV-OVA-ob) treatment, suggesting introducing the *OVA* gene into a DNA vaccine could contribute to improving the specific immune effect. The circulating leptin detection result (**Figure 2F**) further demonstrated partial leptin reduction, which we would like to term as leptin knock-down or iPRTi, did can be achieved by the oral *ob* recombinant yeast. The knock-down effect was obviously more significant for the JMY31 (CMV-OVA-ob) treatment, which reached an exciting 50% after the 30- and 60-day intermittent immunizations. Besides, we noticed that the circulating leptin was increased for the control PBS and JMY31 (JMB84) treatments, which was supposed due to the potential overnutrition of "NC die" that we used.

Oral Administration of *ob* Recombinant Yeast Relieves Leptin Resistance in DIOing Mice

To investigate whether the oral recombinant yeast meditated iPRTi strategy could contribute to leptin resistance remission, the mice of the DIOing group were administrated continuously with HFD feed before and during the oral immunization (**Figure 2C**). Leptin resistance could be induced routinely by a 60-day HFD induction, and continuous HFD feeding during the oral immunization was supposed to maintain the induction.

The WB and ELISA assay results both demonstrated again that specific immune response could be induced by oral *ob* recombinant yeast and JMY31 (CMV-OVA-ob) performed much better (**Figures 3A,B**). Further detection of the circulating leptin (**Figure 3C**) demonstrated firstly no significant increase during the oral immunization for the control treatments, indicating probably a highest level was reached after the 60-day HFD induction and leptin resistance were successfully induced, and secondly oral administration of the JMY31 (CMV-OVA-ob) recombinant yeast could reduce the circulating leptin effectively to about 75% in the context of continuous HFD induction.

In addition, the mice from the JMY31 (CMV-OVA-ob) treatment grew much more slowly than those from the control treatments (**Figure 3D**), and the corresponding body weight gain was reasonably the lowest (**Figure 3E**). The average daily feed intake of the mice from the JMY31 (CMV-OVA-ob) treatment was decreased compared to other treatments (**Figure 3F**), which was supposedly due to the leptin sensitization successfully triggered as expected by its partial reduction. Correspondingly, the blood total cholesterol and triglyceride were both downregulated significantly after the 60-day oral administration of the recombinant yeast JMY31 (CMV-OVA-ob; **Figures 3G,H**). HFD feeding usually affects tissue in a negative manner, especially liver, and we observed a marked reduction in hepatic steatosis after the 60-day oral administration of the *ob* recombinant yeast (**Figure 3I**).

Oral Administration of *ob* Recombinant Yeast Contributes to Diet-Induced Obesity Control

In view that diet-induced obese individuals are not always fed with high-fat food and a normal diet is usually preferred when one is planning to lose weight, to further investigate whether the iPRTi strategy is capable practically for obesity management, we also conducted the DIOed group experiment with the diet-induced mice administrated with NC and *ob* recombinant yeast (**Figure 2C**).

Same as above, the specific anti-leptin antibodies induced by oral *ob* recombinant yeast were first qualitatively and quantitatively confirmed by WB and ELISA, respectively (**Figures 4A,B**). Encouragingly, a dramatic reduction of the circulating leptin, which was knocked-down by more than

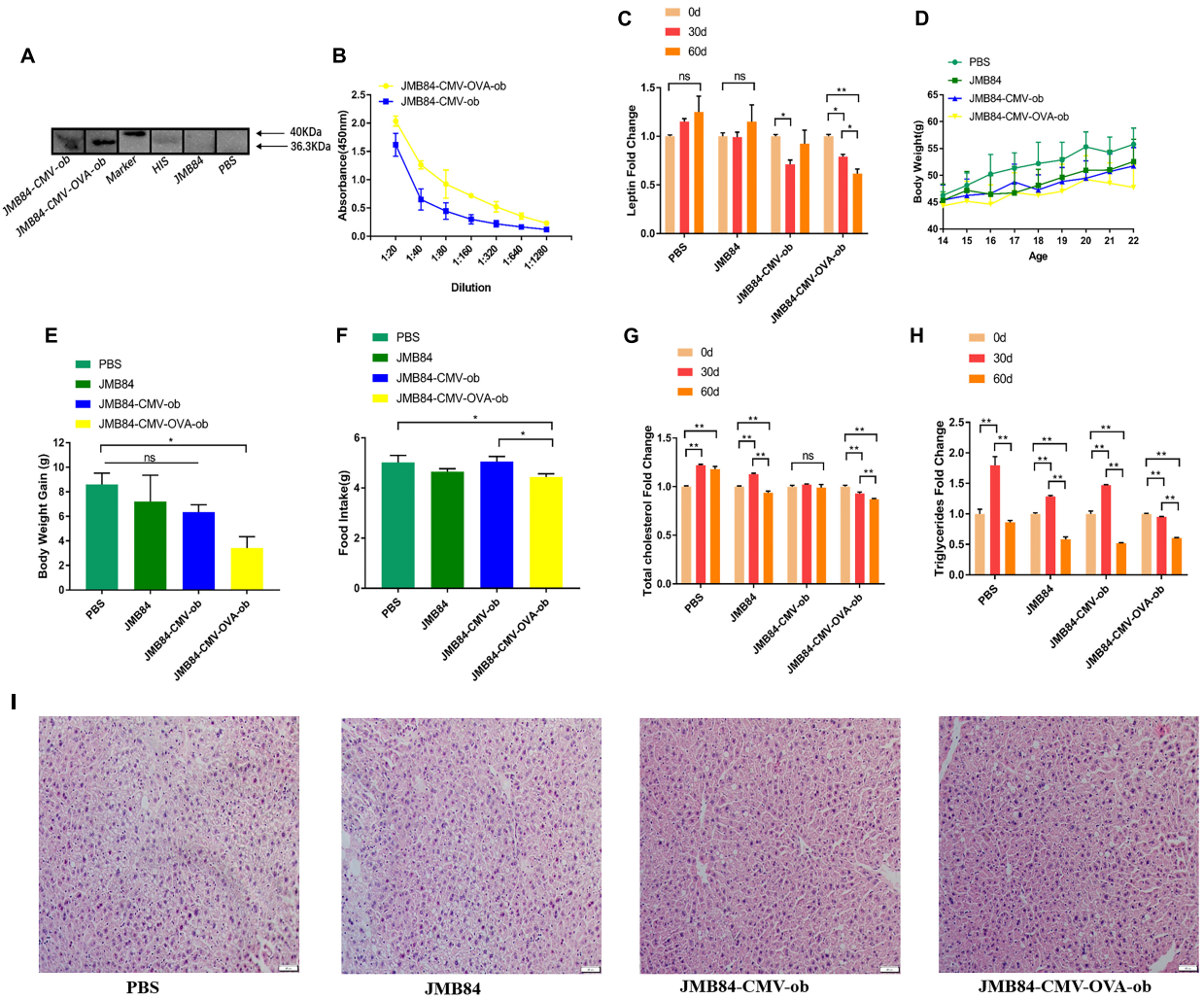

FIGURE 3 | Oral administration of *ob* recombinant yeast relieves leptin resistance in DIOing mice. **(A)** WB assay result for the qualitative detection of anti-leptin antibodies in different antiserums (Day60) from different treatments. **(B)** ELISA result for anti-leptin antibody titering in the antiserums (Day60) from the oral immunized mice by *ob* recombinant yeast. **(C)** The changes of circulating leptin detected by ELISA in the antiserums (Day0, Day30, and Day60) from different treatments. **(D)** The weekly average body weight of the mice from different treatments. The age was indicated as weeks, and the mice were orally immunized at 14-week-old. **(E)** The comparison of the average body weight gain of the mice from different treatments at the end of oral immunization (Day60). **(F)** The comparison of the average daily feed intake of the mice from different treatments during the oral immunization. **(G,H)** The changes in total cholesterol and triglyceride were detected in the antiserums (Day0, Day30, and Day60) from different treatments. **(I)** Histological analysis of mice liver from different treatments. The "ns" indicates statistical significance at a P value of > 0.05; * represents $P < 0.05$; ** represents $P < 0.01$.

75%, was again detected after both 30- and 60-day oral administration of the recombinant yeast JMY31 (CMV-OVA-ob). The body weight of the mice from the JMY31 (CMV-OVA-ob) treatment was decreased 4 weeks (at the 18-week-old) after the oral immunization (**Figures 4D,E**), and the average daily feed intake was also decreased significantly (**Figure 4F**). Surprisingly, the blood total cholesterol was downregulated dramatically in all the treatments (**Figure 4G**), which was supposedly due to the diet changing to NC after HFD induction. We also observed an interesting rise-fall pattern for the blood triglyceride (**Figure 4H**), indicating a long-term 60-day oral immunization is necessary for diet-induced obesity management.

DISCUSSION

Yeast exhibits many particulate features of immunostimulatory complexes, and its cell-wall components, especially β-1,3-D-glucan and mannan, possess naturally immunologic adjuvant potential (Lee et al., 2021). The whole recombinant yeast vaccine, which was first put forward by Stubbs et al. (2001), can activate DCs to elicit protective cell-mediated immunity. DCs are the most powerful antigen-presenting cells in the body, and a little amount of DCs can stimulate a robust immune response (Palucka and Banchereau, 2012; Nava et al., 2021). In addition to the recombinant antigen, it has been reported that yeast does not induce any antibody response against its native

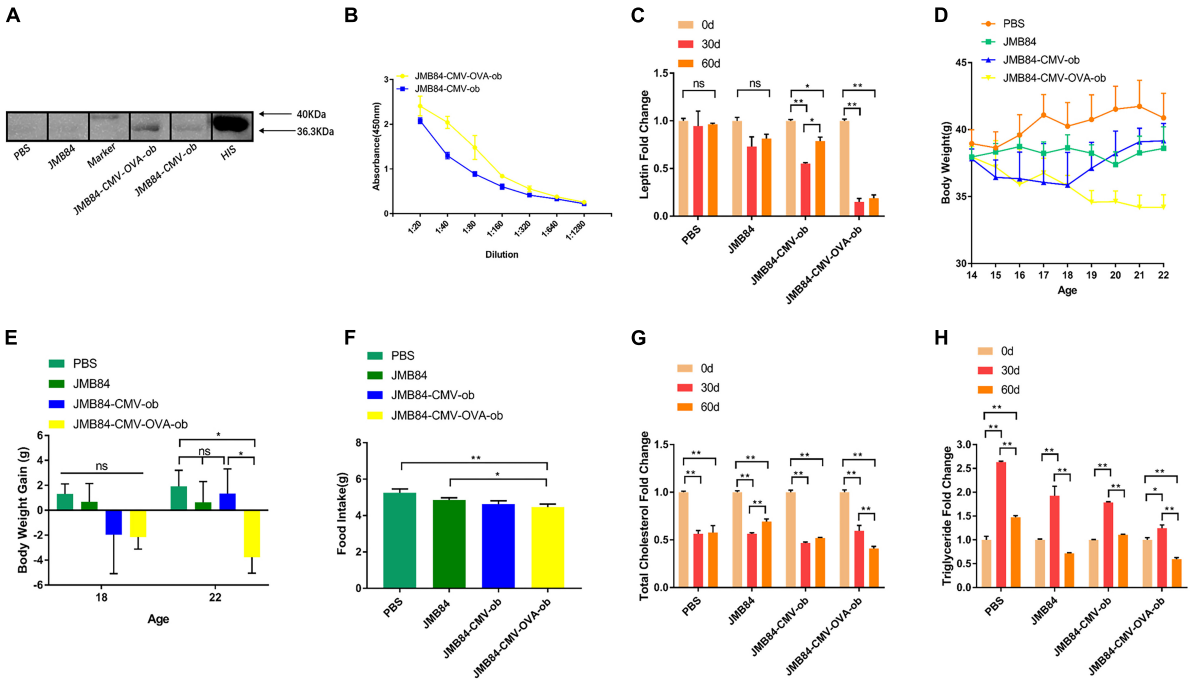

FIGURE 4 | Oral administration of *ob* recombinant yeast contributes to obesity control of DIOed mice. **(A)** WB assay result for the qualitative detection of anti-leptin antibodies in different antiserums (Day60) from different treatments. **(B)** ELISA result for anti-leptin antibody titering in the antiserums (Day60) from the oral immunized mice by *ob* recombinant yeast. **(C)** The changes in circulating leptin were detected by ELISA in the antiserums (Day0, Day30, and Day60) from different treatments. **(D)** The weekly average body weight of the mice from different treatments. The age was indicated as weeks, and the mice were orally immunized at 14-week-old. **(E)** The comparison of the average body weight gain of the mice from different treatments at the middle (Day28, 18-week-old) and the end (Day56, 22-week-old) of oral immunization. **(F)** The comparison of the average daily feed intake of the mice from different treatments during the oral immunization. **(G,H)** The changes of total cholesterol and triglyceride were detected in the antiserums (Day0, Day30, and Day60) from different treatments. The "ns" indicates statistical significance at a P value of > 0.05; * represents $P < 0.05$; ** represents $P < 0.01$.

proteins (Hudson et al., 2016). A lot of attention have been paid to the whole recombinant yeast vaccine for the potential application in the immunological therapy of cancer diseases (Miquel-Clopes et al., 2019).

On this basis, our laboratory has been devoted to the development of the oral yeast vaccine in the last decades. The whole recombinant yeast vaccine by oral administration was supposed to target M cells and DCs in the intestinal mucosal immune system. Targeted delivery to intestinal DCs of *in situ* expressed protein antigens (Zhang et al., 2011, 2012; Liu et al., 2016) and recombinant DNA vaccines (Kiflmariam et al., 2013; Yan et al., 2015; Han et al., 2019), as well as functional shRNA expression cassettes (Zhang et al., 2014; Xu et al., 2016; Zakria et al., 2019), were all achieved by oral administration of recombinant yeast in our previous studies.

Oral vaccine can induce systemically as well as mucosal immunity and is more attractive than an injectable vaccine for the pain-free vaccination route. However, gastrointestinal barriers and antigen degradation are the major concerns when developing oral vaccines (Gonzalez-Cruz and Gill, 2021). Yeast cell-wall, in addition to its natural adjuvant potential, can also play as a perfect immune protectant against gastrointestinal digestion. What's more, our previous studies have demonstrated that the oral recombinant yeast vaccine is capable to trigger the immune response to not only exogenous antigens (Kiflmariam et al., 2013; Han et al., 2019), but also to endogenous factors such as myostatin (MSTN; Zhang et al., 2011; Zakria et al., 2019). Hence, the novel iPRTi strategy by oral administration of recombinant yeast vaccine was proposed in the current study and was further proved to be effective for *in vivo* partial leptin reduction.

Another major concern for oral vaccines is their relatively low efficiency. OVA was introduced in our previous studies to enhance the immunogenicity of oral recombinant yeast mediated both *in situ* protein vaccine (Zhang et al., 2011) and recombinant DNA vaccine (Han et al., 2019). The results in the present study further demonstrated clearly that the introduction of the *OVA* gene into a DNA vaccine cassette can improve its immune effect significantly. It has been also reported functional shRNA and miRNA could be delivered to the intestinal immune system by oral administration of recombinant yeast (Zhang et al., 2014, 2020, 2021). Another study we did previously further suggested that oral recombinant yeast vaccine could be enhanced by coupling with an shRNA for modulating DC-mediated immune response (Zakria et al., 2019). On the other hand, yeast cell surface β-glucan modification by genetic engineering, as well as antigen or/and ligand surface display, may be alternative strategies for improving the efficiency of oral recombinant yeast vaccines (Lei et al., 2020; Lee et al., 2021; Trentelman et al., 2021).

To guarantee the immune effect in this study, a 60-day long-term intermittent oral immunization was applied for all three experimental groups. First, in the NC group mice, the leptin knock-down effect was almost the same on Day30 and Day60 after the immunization initiation (**Figure 2F**). Secondly, in the context of continuous HFD induction (DIOing group), the whole 60-day immunization was demonstrated to be necessary for efficient leptin knock-down (**Figure 3C**), and the body weight growth was slowed down but not lost (**Figure 3D**). Finally, in the DIOed group mice administrated with NC diet after HFD induction, dramatical leptin knock-down (**Figure 4C**), as well as body the weight loss (**Figure 4D**), were observed in the JMY31 (JMB84-CMV-OVA-ob) treatment at both Day30 and Day60. Taken together, we conclude that oral administration of *ob* recombinant yeast can contribute to diet-induced obesity control, and synergetic dietary control is still necessary.

In conclusion, we present a novel iPRTi strategy for *in vivo* protein knockdown by oral administration of recombinant yeast, which was demonstrated to be effective for partial leptin reduction and diet-induced obesity control.

DATA AVAILABILITY STATEMENT

The original contributions presented in the study are included in the article/**Supplementary Material**, further inquiries can be directed to the corresponding author/s.

ETHICS STATEMENT

The animal study was reviewed and approved by Animal Ethics Committee of Northwest A&F University (approval number NWAFU-DK2020046).

AUTHOR CONTRIBUTIONS

KX, ZZ, and FY contributed to the study design and data interpretation. FY was the principal investigator and wrote the draft. LD and KX contributed to the manuscript revising and figure drawing. All other authors contributed to partial experiment conduction and data analysis. All authors read and approved the final manuscript.

FUNDING

This study was supported by grants from Science and Technology Department of Shaanxi Province-China (Shaanxi Key R&D Program, No.2021NY-027; Key Project of Natural Science Basic Research, No.2019JZ-07) and State Key Laboratory of Plateau Ecology and Agriculture of Qinghai University-China (Open Fund Project, No.2020-KF-006).

ACKNOWLEDGMENTS

The authors would like to thank all the colleagues in ZZ's lab from Northwest A&F University (China) for their excellent technical assistance and helpful discussions.

SUPPLEMENTARY MATERIAL

The Supplementary Material for this article can be found online at: https://www.frontiersin.org/articles/10.3389/fmicb.2022.923656/full#supplementary-material

REFERENCES

Flier, J. S., and Maratos-Flier, E. (2017). Leptin's physiologic role: does the emperor of energy balance have no clothes? *Cell Metab.* 26, 24–26. doi: 10.1016/j.cmet.2017.05.013

Frederich, R. C., Hamann, A., Anderson, S., Lollmann, B., Lowell, B. B., and Flier, J. S. (1995). Leptin levels reflect body lipid content in mice: evidence for diet-induced resistance to leptin action. *Nat. Med.* 1, 1311–1314. doi: 10.1038/nm1295-1311

Gietz, R. D. (2014). Yeast transformation by the LiAc/SS carrier DNA/PEG method. *Methods Mol. Biol.* 1163, 33–44.

Gonzalez-Cruz, P., and Gill, H. S. (2021). Demystifying particle-based oral vaccines. *Expert Opin. Drug Deliv.* 18, 1455–1472. doi: 10.1080/17425247.2021.1946511

Han, B., Xu, K., Liu, Z., Ge, W., Shao, S., Li, P., et al. (2019). Oral yeast-based DNA vaccine confers effective protection from *Aeromonas hydrophila* infection on *Carassius auratus*. *Fish Shellfish Immunol.* 84, 948–954.

Hankir, M. K., and Seyfried, F. (2020). Partial leptin reduction: an emerging weight loss paradigm. *Trends Endocrinol. Metab.* 31, 395–397. doi: 10.1016/j.tem.2020.03.001

Hudson, L. E., Mcdermott, C. D., Stewart, T. P., Hudson, W. H., Rios, D., Fasken, M. B., et al. (2016). Characterization of the probiotic yeast *Saccharomyces boulardii* in the healthy mucosal immune system. *PLoS One* 11:e0153351. doi: 10.1371/journal.pone.0153351

Kiflmariam, M. G., Yang, H., and Zhang, Z. (2013). Gene delivery to dendritic cells by orally administered recombinant *Saccharomyces cerevisiae* in mice. *Vaccine* 31, 1360–1363. doi: 10.1016/j.vaccine.2012.11.048

Knight, Z. A., Hannan, K. S., Greenberg, M. L., and Friedman, J. M. (2010). Hyperleptinemia is required for the development of leptin resistance. *PLoS One* 5:e11376. doi: 10.1371/journal.pone.0011376

Laforest, S., Labrecque, J., Michaud, A., Cianflone, K., and Tchernof, A. (2015). Adipocyte size as a determinant of metabolic disease and adipose tissue dysfunction. *Crit. Rev. Clin. Lab. Sci.* 52, 301–313. doi: 10.3109/10408363.2015.1041582

Lee, C., Verma, R., Byun, S., Jeun, E. J., Kim, G. C., Lee, S., et al. (2021). Structural specificities of cell surface beta-glucan polysaccharides determine commensal yeast mediated immuno-modulatory activities. *Nat. Commun.* 12:3611. doi: 10.1038/s41467-021-23929-9

Lei, H., Xie, B., Gao, T., Cen, Q., and Ren, Y. (2020). Yeast display platform technology to prepare oral vaccine against lethal H7N9 virus challenge in mice. *Microb. Cell Fact.* 19:53. doi: 10.1186/s12934-020-01316-1

Liu, Z., Zhou, G., Ren, C., Xu, K., Yan, Q., Li, X., et al. (2016). Oral administration of myostatin-specific recombinant *Saccharomyces cerevisiae* vaccine in rabbit. *Vaccine* 34, 2378–2382. doi: 10.1016/j.vaccine.2016.03.036

Maffei, M., Halaas, J., Ravussin, E., Pratley, R. E., Lee, G. H., Zhang, Y., et al. (1995). Leptin levels in human and rodent: measurement of plasma leptin and ob RNA in obese and weight-reduced subjects. *Nat. Med.* 1, 1155–1161. doi: 10.1038/nm1195-1155

Miquel-Clopes, A., Bentley, E. G., Stewart, J. P., and Carding, S. R. (2019). Mucosal vaccines and technology. *Clin. Exp. Immunol.* 196, 205–214. doi: 10.1111/cei.13285

Nava, S., Lisini, D., Frigerio, S., and Bersano, A. (2021). Dendritic cells and cancer immunotherapy: the adjuvant effect. *Int. J. Mol. Sci.* 22:12339.

Palucka, K., and Banchereau, J. (2012). Cancer immunotherapy via dendritic cells. *Nat. Rev. Cancer* 12, 265–277.

Stubbs, A. C., Martin, K. S., Coeshott, C., Skaates, S. V., Kuritzkes, D. R., Bellgrau, D., et al. (2001). Whole recombinant yeast vaccine activates dendritic cells and elicits protective cell-mediated immunity. *Nat. Med.* 7, 625–629. doi: 10.1038/87974

Trentelman, J. J. A., Tomas-Cortazar, J., Knorr, S., Barriales, D., Hajdusek, O., Sima, R., et al. (2021). Probing an *Ixodes ricinus* salivary gland yeast surface display with tick-exposed human sera to identify novel candidates for an anti-tick vaccine. *Sci. Rep.* 11:15745. doi: 10.1038/s41598-021-92538-9

Xu, K., Liu, Z., Zhang, L., Zhang, T., and Zhang, Z. (2016). SiRNA in vivo-targeted delivery to murine dendritic cells by oral administration of recombinant yeast. *Methods Mol. Biol.* 1364, 165–181. doi: 10.1007/978-1-4939-3112-5_14

Yan, N., Xu, K., Li, X., Liu, Y., Bai, Y., Zhang, X., et al. (2015). Recombinant *Saccharomyces cerevisiae* serves as novel carrier for oral DNA vaccines in *Carassius auratus*. *Fish Shellfish Immunol.* 47, 758–765. doi: 10.1016/j.fsi.2015.10.020

Zakria, H. M., Han, B., Yue, F., Mu, L., Fang, Y., Li, X., et al. (2019). Significant body mass increase by oral administration of a cascade of shIL21-MSTN yeast-based DNA vaccine in mice. *Biomed. Pharmacother.* 118:109147. doi: 10.1016/j.biopha.2019.109147

Zelissen, P. M., Stenlof, K., Lean, M. E., Fogteloo, J., Keulen, E. T., Wilding, J., et al. (2005). Effect of three treatment schedules of recombinant methionyl human leptin on body weight in obese adults: a randomized, placebo-controlled trial. *Diabetes Obes. Metab.* 7, 755–761. doi: 10.1111/j.1463-1326.2005.00468.x

Zhang, L., Peng, H., Feng, M., Zhang, W., and Li, Y. (2021). Yeast microcapsule-mediated oral delivery of IL-1beta shRNA for post-traumatic osteoarthritis therapy. *Mol. Ther. Nucleic Acids* 23, 336–346. doi: 10.1016/j.omtn.2020.11.006

Zhang, L., Peng, H., Zhang, W., Li, Y., Liu, L., and Leng, T. (2020). Yeast cell wall particle mediated nanotube-RNA delivery system loaded with miR365 antagomir for post-traumatic osteoarthritis therapy via oral route. *Theranostics* 10, 8479–8493. doi: 10.7150/thno.46761

Zhang, L., Zhang, T., Wang, L., Shao, S., Chen, Z., and Zhang, Z. (2014). In vivo targeted delivery of CD40 shRNA to mouse intestinal dendritic cells by oral administration of recombinant *Sacchromyces cerevisiae*. *Gene Ther.* 21, 709–714. doi: 10.1038/gt.2014.50

Zhang, T., Sun, L., Xin, Y., Ma, L., Zhang, Y., Wang, X., et al. (2012). A vaccine grade of yeast *Saccharomyces cerevisiae* expressing mammalian myostatin. *BMC Biotechnol.* 12:97. doi: 10.1186/1472-6750-12-97

Zhang, T., Yang, H., Wang, R., Xu, K., Xin, Y., Ren, G., et al. (2011). Oral administration of myostatin-specific whole recombinant yeast Saccharomyces cerevisiae vaccine increases body weight and muscle composition in mice. *Vaccine* 29, 8412–8416. doi: 10.1016/j.vaccine.2011.08.007

Zhang, Y., Proenca, R., Maffei, M., Barone, M., Leopold, L., and Friedman, J. M. (1994). Positional cloning of the mouse obese gene and its human homologue. *Nature* 372, 425–432.

Zhao, S., Kusminski, C. M., Elmquist, J. K., and Scherer, P. E. (2020a). Leptin: less is more. *Diabetes* 69, 823–829. doi: 10.2337/dbi19-0018

Zhao, S., Li, N., Zhu, Y., Straub, L., Zhang, Z., Wang, M. Y., et al. (2020b). Partial leptin deficiency confers resistance to diet-induced obesity in mice. *Mol. Metab.* 37:100995. doi: 10.1016/j.molmet.2020.100995

Zhao, S., Zhu, Y., Schultz, R. D., Li, N., He, Z., Zhang, Z., et al. (2019). Partial leptin reduction as an insulin sensitization and weight loss strategy. *Cell Metab.* 30, 706–719. doi: 10.1016/j.cmet.2019.08.005

Conflict of Interest: The authors declare that the research was conducted in the absence of any commercial or financial relationships that could be construed as a potential conflict of interest.

Publisher's Note: All claims expressed in this article are solely those of the authors and do not necessarily represent those of their affiliated organizations, or those of the publisher, the editors and the reviewers. Any product that may be evaluated in this article, or claim that may be made by its manufacturer, is not guaranteed or endorsed by the publisher.

frontiers | Frontiers in Microbiology

TYPE Original Research
PUBLISHED 27 July 2022
DOI 10.3389/fmicb.2022.934696

OPEN ACCESS

EDITED BY
Yu Xia,
Jiangnan University, China

REVIEWED BY
Beizhong Han,
China Agricultural University, China
Jiasong Jiang,
Lonza, United States
Changwei Ao,
Agricultural University of Hebei, China

*CORRESPONDENCE
Ruifang Li
lrf@haut.edu.cn

SPECIALTY SECTION
This article was submitted to Food Microbiology, a section of the journal Frontiers in Microbiology

RECEIVED 02 May 2022
ACCEPTED 30 June 2022
PUBLISHED 27 July 2022

CITATION
Hou X, Hui M, Sun Z, Li X, Shi X, Xiao R, Wang J, Pan C and Li R (2022) Comparative analysis of the microbiotas and physicochemical properties inside and outside medium-temperature *Daqu* during the fermentation and storage. *Front. Microbiol.* 13:934696. doi: 10.3389/fmicb.2022.934696

Comparative analysis of the microbiotas and physicochemical properties inside and outside medium-temperature *Daqu* during the fermentation and storage

Xiaoge Hou[1], Ming Hui[1], Zhongke Sun[1], Xuesi Li[2], Xin Shi[1], Ran Xiao[1], Junfei Wang[3], Chunmei Pan[2] and Ruifang Li[1,4]*

[1]School of Biological Engineering, Henan University of Technology, Zhengzhou, China, [2]School of Food and Biological Engineering, Henan University of Animal Husbandry and Economy, Zhengzhou, China, [3]College of Science, Henan University of Technology, Zhengzhou, China, [4]Key Laboratory of Functional Molecules for Biomedical Research, Henan University of Technology, Zhengzhou, China

Medium-temperature *Daqu* (MT-*Daqu*), a saccharification-fermentation agent and aroma-producing agent, is used to produce Chinese strong-flavor *Baijiu*. Many related studies have been published; however, less is known about microbial community and quality properties inside and outside the MT-*Daqu* from fermentation to storage. Here, along with determining the physicochemical index, the microbial community of MT-*Daqu* was investigated using both culture-dependent and culture-independent methods during 31 days of fermentation and 4 months of storage. Volatile compounds of mature MT-*Daqu* were analyzed using headspace solid-phase microextraction (HS-SPME) combined with gas chromatography-mass spectrometry (GC–MS). The results indicated obvious variation in the microbial community due to the changes in environmental conditions, and the physicochemical indices shifted from fluctuations in the fermentation period to relative stability after storage for 3 months. Moreover, the microbial counts and physicochemical indices of the inner layers of MT-*Daqu* differed from those of the outer layers. The dominant communities, including the bacterial phyla *Firmicutes*, *Proteobacteria*, and *Actinobacteria* and the fungal phyla *Ascomycota* and *Mucoromycota*, showed different abundances in the two parts of the mature MT-*Daqu*, and different microbial communities were enriched in both parts. Additionally, pyrazines and alcohols were the most abundant volatile aroma compounds in the mature MT-*Daqu*.

KEYWORDS

MT-*Daqu*, microbial community, physicochemical indices, volatile compounds, fermentation, mature

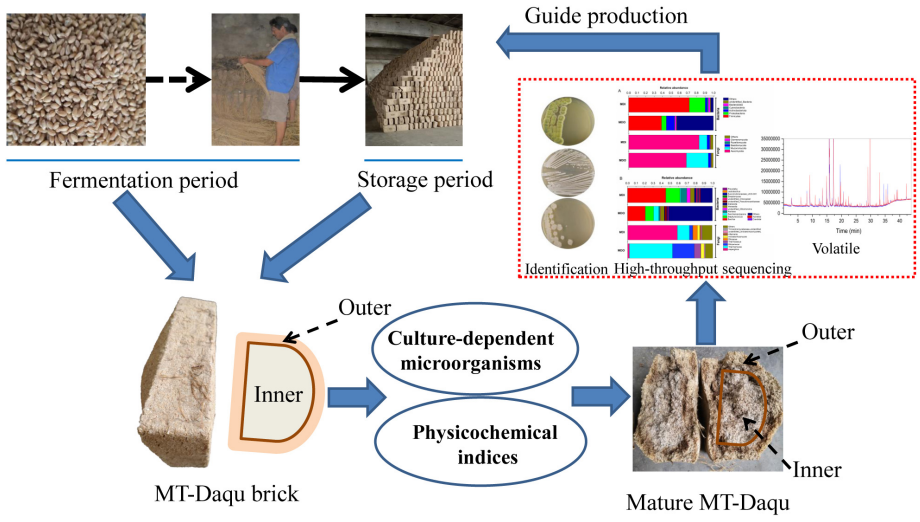

GRAPHICAL ABSTRACT

Introduction

Baijiu is one of the six well-known distillates worldwide (Jin et al., 2017; He et al., 2019), and *Daqu* was used as a saccharification and fermentation agent and aroma-producing agent for *Baijiu* production (Wang et al., 2017). Thus, *Daqu* constituents exert a direct effect on the final distilled *Baijiu*. Due to the abundant accumulation of microorganisms, enzymes and flavor compounds are formed during an open spontaneous solid-state fermentation process (Cai et al., 2021; Deng et al., 2021). According to the highest fermenting temperature, *Daqu* is mainly classified into three types: high-temperature *Daqu* (60–70°C), medium-temperature *Daqu* (50–60°C), and low-temperature *Daqu* (40–50°C) (Deng et al., 2020; Cai et al., 2021; Hu et al., 2021; Wang et al., 2021). These three types of *Daqu* have been employed to produce *Jiang*-flavor, strong-flavor, and light-flavor *Baijiu*, which are the three most popular *Baijiu* products on the Chinese market (Hu et al., 2021; Zhang H. et al., 2021).

Strong-flavor *Baijiu*, with ethyl caproate as the main aroma, has the characteristics of a fragrant flavor, soft mouthfeel, and long-lasting aftertaste and is the most famous type of *Baijiu*, with an annual output of more than 70% of all Chinese liquor (Xu et al., 2017; Zou et al., 2018; Deng et al., 2021). The generation of the flavor of strong-flavor *Baijiu* is closely linked to MT-*Daqu*. As a saccharifying starter for 1000 of years and as raw material, MT-*Daqu* is combined with approximately 20% raw grains for strong-flavor *Baijiu* fermentation (Xu et al., 2017; Zou et al., 2018). MT-*Daqu* is produced by solid fermentation using a wheat or wheat mixture as raw materials, and the process involves three phases: material mixing and shaping, spontaneous solid-state fermenting, and maturing (**Supplementary Figure 1**; Zou et al., 2018). During MT-*Daqu* production, the fermentation phase is crucial and proceeds through five stages, namely, the *Anqu*, *Peijun*, *Dinghuo*, *Huanluo*, and *Dalong* phases (Yan et al., 2019). As a result, numerous microorganisms, such as *Bacillus*, *Acetobacter*, *Pseudomonas*, *Weissella*, *Alternaria*, *Aspergillus*, *Mucor*, *Saccharomyces*, and *Hansenula*, inhabited the fermentation broth, and enzymes, such as liquefaction enzymes, saccharifying enzymes, proteases, and esterifying enzymes, accumulated through microbial metabolism. Flavor compounds, such as organic acids, alcohols, esters, aldehydes, and ketones, contributing to the generation of flavor of *Baijiu* are also enriched in this period (Yan et al., 2013a, 2019; Liu et al., 2018; Deng et al., 2021). Additionally, fresh *Daqu* must mature for 3–6 months to exclude undesirable microorganisms and balance metabolic compounds (Fan et al., 2019; Yang et al., 2021). Only mature *Daqu* can be used for *Baijiu* brewing. Therefore, understanding the rule of microbial succession and metabolism in the MT-*Daqu* production process might contribute to the stability and quality of *Daqu*.

However, the microbial composition and physicochemical indices in *Daqu* undergo continuous succession during production due to environmental factors (Fu et al., 2021). Meanwhile, different microbiotas and physicochemical properties have been observed in different parts of the same *Daqu* brick due to the difficulty in transferring heat, water, and oxygen (Jin et al., 2019; Chen et al., 2020; Zhang Y. et al., 2021). The aforementioned results all affect the quality of *Daqu*. At present, the criteria that are accepted by *Baijiu* industry have clearly specified the organoleptic requirement and predominant physicochemical index requirement for a

fermentation MT-*Daqu* that is mature (People's Republic of China Light Industry Professional Standard., 2011b), QB/T 4259-2011, 2011; (Shangdong Province Local Standard, 2009, in China, DB37/T 1231-2009, 2009). The microorganism and the physicochemical property indices inside and outside the strong flavor *Daqu* are not included in the industrial criteria. Therefore, analyzing the microbiotas and physicochemical indices inside and outside the *Daqu* during production might provide a scientific theory for establishing a relatively comprehensive method to evaluate the quality and control the process of *Daqu*. Some studies on these have been performed (Jin et al., 2019; Chen et al., 2020; Zhang Y. et al., 2021). Jin et al. (2019) revealed that the dominant microbes and volatile flavors on the surface and the core of soy-flavor *Daqu* had different distribution characteristics and found that microbial interactions were stronger in the core than on the surface (Jin et al., 2019). Thereafter, Zhang Y. et al. (2021) explored the microbiota, enzymes, and metabolites in different parts of fresh and mature soy-flavor *Daqu*, and the dominant enzymes varied significantly and identified the predominant microbial community migrated between the two parts of *Daqu* during production (Zhang Y. et al., 2021). In addition to *Jiang*-flavor *Daqu*, studies on differences in microbiota and physicochemical indices between surface and central parts of special-flavor *Baijiu Daqu* were reported, and the microbial distribution and physicochemical indices in the two parts were significantly different (Chen et al., 2020). These findings potentially provide a theoretical basis for microbial resources and quality control of *Daqu* (Wang et al., 2021). However, Chinese flavor *Baijiu* brewing enterprises are widely distributed over South China and North China and have their own unique ecological environments and diverse regulations for the production of *Daqu*. Therefore, a comprehensive understanding of the mechanisms underlying the composition of *Daqu* might contribute to better control of the *Daqu* process and standardize local *Baijiu* production (Xu et al., 2017; Liu et al., 2018). Currently, studies that examine different parts or different types of *Daqu* mainly focus on high-temperature or low-temperature *Daqu* (Chen et al., 2020; Cai et al., 2021; Wang et al., 2021; Zhang Y. et al., 2021), and a comprehensive study of the microbial compositions and the quality characteristics of different parts of MT-*Daqu* have not yet been conducted.

In this study, the bacterial and fungal communities in different parts of strong-flavor *Daqu* from the fermentation period to the mature period were investigated using a culture-dependent method, and the changes in the physicochemical properties throughout the production process were also explored. Based on these results, the maturity period of MT-*Daqu* was evaluated, and the analysis of microbial composition, physicochemical indices, and volatile compounds of different parts of mature MT-*Daqu* using the Illumina MiSeq platform and headspace solid-phase microextraction (HS-SPME)-GC–MS was the main focus. This study provides guidance for the determination of the mature stage, for the process control of MT-*Daqu*, and for improving the quality of strong-flavor *Baijiu*.

Materials and methods

Production of medium-temperature-*Daqu* and sample collection

Medium-temperature-*Daqu* samples were obtained from Songhe Co., Ltd., in Henan, China (longitude 115.48°E and latitude 33.86°N), a typical distillery that produces strong-flavor *Baijiu* in Henan Province. MT-*Daqu* was produced by traditional solid-state fermentation in summer (**Supplementary Figure 1**). The same batch of MT-*Daqu* bricks was removed from the fermentation room on days 1, 5, 9, 13, 17, 21, 26, and 31 and from the storage room at 0.5, 1, 1.5, 2, 3, and 4 months. The *Daqu* samples were collected as described in the previous reports (Yan et al., 2019). A total of three *Daqu* bricks were randomly selected from the top, middle, and bottom of stacked layers. Subsequently, each *Daqu* brick was divided into two parts based on the fire-circle strategy (Wang et al., 2020): the 0.5–2-cm thick outer layer (named MDO) and the inner layer of the remaining part (named MDI). Then, the same parts (equal weight) of each *Daqu* brick were mixed into one sample and separated into two parts for subsequent testing. Samples were collected during two parallel batches of MT-*Daqu* production, and four biological replicates of each sample were obtained. Approximately 50 g of the sample was immediately brought to the laboratory to analyze the microbial community, 100 g of sample was stored at −20°C for the analysis of physicochemical indices and volatile compounds, and 50 g of sample was sealed in sterile bags and stored at −80°C for Illumina MiSeq sequencing.

Analysis of environmental factors and physicochemical indices

During the MT-*Daqu* fermentation period, the temperature and humidity in the fermentation room and the interior of *Daqu* bricks were measured using thermometers and hygrometers, respectively (Li et al., 2016). The physicochemical indices were determined according to the industrial general standard methods with a slight modification (People's Republic of China Light Industry Professional Standard., 2011a), QB/T 4257-2011, 2011; Shangdong Province Local Standard in China, DB37/T (1231-2009). Moisture (g/g,%) was measured as the weight loss of the samplers after drying at 105°C for 3–5 h until constant weight. The total acidity (mmol/10 g) was determined by titrating with 0.1 M NaOH to pH 8.2. Liquefying activity (g/g● h) was determined by the reaction

time (minutes) with a mixture of iodine solution and starch solution. Saccharifying activity (mg/g•h) was measured using Fehling's solution titration method (Xiao et al., 2017). The esterifying activity (mg/g•100 h) was determined using the saponification method and reported as the amount of ethyl caproate synthesized from caproic acid and ethanol per 100 h by 1 g of dried *Daqu*. Fermenting activity (gCO_2/g•72 h) was determined by the weight loss of sorghum saccharifying solution incubated with 0.5 g of *Daqu*, and it was reported as the amount of CO_2 released in 72 h by 1 g dried *Daqu*.

Culture-dependent analysis of representative microorganisms in medium-temperature-*Daqu*

Microbial enumeration using culture-dependent methods has described in the previous study (Hu et al., 2017).

About 10 g of *Daqu* sample was mixed with 90 ml of sterile saline (0.85% w/v sodium chloride) in a-250 ml sterile conical flask and shaken at 25°C for 30 min at 120 rpm to obtain homogenized samples. After allowing the mixture to stand for a few minutes, the supernatant was diluted 10-folds. Next, 0.2 ml of the diluted suspension was spread in triplicate on the surface of plate count agar medium (Oxoid CM0325) and cultured at 37°C for 24 h to enumerate total aerobic bacteria and spread on potato dextrose agar medium (Oxoid CM0139) and Czapek Dox medium containing 0.1 g/L ampicillin and cultured at 30°C for 3 days to enumerate yeasts and molds (Wang et al., 2018). For the estimation of spore-forming bacteria, a 10% (w/v) sample suspension was heated at 80°C for 10 min and then spread on plate count agar medium, followed by incubation at 55°C for 72 h (Zheng et al., 2012). Colony-forming units (CFUs) per gram of fresh weight sample were calculated based on their morphological features.

Considering the application of the mature MT-*Daqu* for *Baijiu* production, the strains from the mature MT-*Daqu* were isolated and identified. A total of five to ten colonies with the square root of the total number of colonies were picked randomly from each plate for purification using the successive streak plate method (Yang et al., 2022). Genomic DNA was used as a template for PCR to amplify the bacterial 16S rDNA using the universal primer pairs 27F and 1492R, the mold 18S rDNA using the primers NS1(5′-GTAGTCATATGCTTGTCTC-3′) NS6 (5′-GCATCACAGACCTGTTATTGCCTC-3′), and the yeast internal transcribed spacer (ITS) regions using the universal primers ITS1/ITS4 (Zhang H. et al., 2021). Then, purified PCR products were sequenced by Sangon Biotech Co., Ltd. (Shanghai, China), and the sequences were submitted to GenBank for comparison with those in the NCBI GenBank database using the BLAST search tool for the identification of the strains.

Culture-independent analysis of the microbial community in mature medium-temperature-*Daqu*

Mature MT-*Daqu* samples were removed for Illumina sequencing. Metagenomic DNA was extracted using the CTAB/SDS method, and DNA concentration and purity were monitored on 1% agarose gels. According to the concentration, DNA was diluted to 1 ng/μl using sterile water (Xiao et al., 2017). Variable regions V4 of the bacterial 16S rRNA gene were amplified with degenerate PCR primers: 515F (5′-GTGCCAGCMGCCGCGGTAA-3′) and 806R (5′-GGACTACHVGGGTWTCTAAT-3′). ITS1 of the ITS region was amplified with degenerate PCR primers: ITS1F (CTTGGTCATTTAGAGGAAGTAA) and ITS2R (GCTGCGTTCTTCATCGATGC). The PCR products were purified with a Qiagen Gel Extraction Kit (Qiagen, Germany), sent to Novogene Co., Ltd. (Beijing, China), and sequenced using the Illumina NovaSeq platform. The raw 16S rRNA and ITS gene sequencing reads were merged using FLASH version 1.2.7, quality-filtered using the QIIME (v1.9.1) quality control process, and the effective tags were finally obtained by removing chimera sequences using the UCHIME algorithm (UCHIME Algorithm). The sequence analysis was performed using UPARSE v7.0.1001, and sequences with ≥97% similarity were assigned to the same OTUs. Rarefaction curves were obtained by comparing the richness and evenness of OTUs among samples. A representative sequence for each OTU was screened for annotation using the Silva Database (Release 138) for bacteria and the Unite Database (Release 8.0) for fungi. The species diversity, including alpha diversity and beta diversity, was analyzed using QIIME (1.9.1) software and displayed with R software (version 2.15.3). The original sequence was deposited in the NCBI Sequence Read Archive (SRA, PRJNA815814).

Analyses of volatile compounds in mature medium-temperature-*Daqu* using headspace solid-phase microextraction gas chromatography-mass spectrometry

Volatile compounds in mature MT-*Daqu* were analyzed using HS-SPME-GC–MS. Using a 50/30 μm DVB/CAR/PDMS fiber (Supelco, Bellefonte, PA, United States) preconditioned in the GC injection port at 250°C for 30 min, volatile extraction was performed using a published method with a minor modification (He et al., 2019). Briefly, 2.0 g of *Daqu* powder and 5 μl internal standard (2-octanol, 0.0722 g/L, Sigma-Aldrich, St. Louis, MO, United States) were placed into a 20-ml headspace vial containing 5 ml of saturated sodium chloride solution. Then, the vial was placed in a thermostatic block stirrer to

equilibrate for 10 min at 50°C and subsequently extracted for 45 min with stirring at 500 r/min. After extraction, the SPME fiber was withdrawn into the needle and immediately inserted into the injection port of the Thermo Fisher Scientific GC–MS system coupled with a trace TR-WAX fused silica capillary column (30 m × 0.25 mm i.d., 0.25-μm film thickness, Thermo Fisher Scientific, United States). Ultrahigh-purity helium was used as the carrier gas at a constant flow velocity of 1 ml/min, and the temperature of the injector and detector was maintained at 250°C. Split injection (10:1) was used. The oven temperature was programmed as follows: 35°C for 2 min, 5°C/min ramp to 110°C for 5 min, and 7°C/min ramp to 230°C for 7 min. The temperatures of the interface and ion source were 250 and 240°C, respectively. The electron impact (EI) ionization energy was 70 eV. EI spectra were recorded in the 30–450 amu range in full scan acquisition mode. Volatile compounds were identified by comparison with the MS spectral database library of the National Institute for Standards and Technology (NIST 2.3, 2017) and were required to fit logically with respect to the retention time in the chromatograms. Semiquantitative determination of the compounds was conducted using a reported method (Tang H. L. et al., 2019).

Statistical and bioinformatic analyses

The biomass of every group of microbes was determined by counting viable colonies on agar in plates with appropriately diluted samples and calculated with the formula LogCFU/g using EXCEL2016. The statistical significance of differences between the samples was determined using SPSS Statistics 16.0 software with one-way ANOVA followed by Duncan's test, and significant differences were defined as $p < 0.05$ or $p < 0.01$. The linear relationship between predominant physiochemical indices was analyzed by calculating the Pearson correlation coefficient using SPSS 16.0 software. Principal coordinates analysis (PCoA) was applied to explore the possible differences between the samples based on Bray–Curtis distances *via* ANOSIM using R (version 3.3.1). The linear discriminant analysis (LDA) effect size (LEfSe) method was used to identify significant variations among different parts of MT-*Daqu* samples (LDA > 3.5, $p < 0.05$).

Results

Dynamics of environmental factors and physicochemical indices

The core temperature of MT-*Daqu* reached 60°C after 7 days, maintained 60°C for 7 days, and then decreased gradually until 24 days (**Supplementary Figure 2**). The relative humidity of fermentation room was close to saturation (100%) after 5 days. As shown in **Table 1**, the moisture of MDO significantly decreased to 14.18% in the first 9 days ($p < 0.05$), while that of MDI began to decrease from 34.20%, and the moisture in MDI was higher than that in MDO from 5 days to 75 days; then, the moisture content of both sections reached a plateau (<13%) after storage for 2 months. Similarly, the acidity of MDI was higher than that of MDO before 3 months, whereas the acidity of MDO changed slightly, but that of MDI increased sharply in the first 5 days ($p < 0.05$), peaked (2.10 mmol/10 g) on the 5th day, and then gradually decreased to a relatively stable value (1.0 mmol/10 g). In contrast, the liquefying activity and saccharifying activity of MDO were both higher than those of MDI after fermentation for 5 days ($p < 0.05$). The saccharifying activity in MDI decreased substantially from 722.50 mg/g•h to 22.50 mg/g•h in the early stage of fermentation, then increased slightly, and finally exhibited a relatively stable range from 222 to 450 mg/g•h. The saccharifying activity and liquefying activity in MDO increased to relatively stable ranges of 852 to 925 mg/g•h and 3.10 to 3.92 g/g•h after 5 days, respectively. The esterifying activity in the two parts of MT-*Daqu* exhibited a relatively high value during storage and tended to be consistent after 75 days (> 12.0 mg/g•100 h). The fermenting activity in both MDI and MDO underwent similar changes: increasing within 1–5 days, decreasing gradually within 5–31 days, and then plateauing at approximately 1.50 gCO_2/g•72 h until the end of storage.

Dynamics of culture-dependent microorganisms

The aerobic bacteria (**Figure 1A**, the upper y-coordinate) and yeast counts (**Figure 1B**, the upper y-coordinate) in MDI showed a similar pattern in the 31-day fermentation: reaching the minimum value on the 17th day. The aerobic bacteria in MDO (**Figure 1A**, the bottom of the *y*-axis) decreased rapidly in the first 9 days, then increased slowly to reach the maximum at 45 days, and subsequently decreased and stabilized at 90 days. The total yeast in MDO (**Figure 1B**, the bottom y-coordinate) decreased rapidly to reach the minimum value on the 17th day, then was restored to its original counts on the 45th day, and continued to decrease during storage. The total spore-forming bacteria counts in both parts of *Daqu* showed no obvious difference and similarly increased during the fermentation period and remained stable in the storage period (**Figure 1A**). In the fermentation period, the changes in mold in MDI (**Figure 1B**, the upper y-coordinate) were similar to those in spore-forming bacteria in MDI, whereas the mold in MDO increased rapidly in the first 5 days and remained stable thereafter (**Figure 1B**, the bottom of the *y*-axis).

As shown in **Figure 2**, during storage, the microbial counts, except those of molds, in the MDI were significantly higher than those in the MDO ($p < 0.05$) in the first 2 months, whereas counts of the four groups of microbial in the MDI were close

TABLE 1 Differences in physicochemical indices of samples during MT-*Daqu* production.

MT-*Daqu* sample	Phase	Time (days)	Moisture (%)	Acidity (mmol/10 g)	Liquifying activity (g/g·h)	Saccharifying activity (mg/g·h)	Esterifying activity (mg/g·100h)	Fermenting activity (gCO_2/g·72 h)
MDI	Fermentation	1	33.85 ± 1.41^{a}	0.40 ± 0.08^{h}	0.25 ± 0.15^{cde}	722.50 ± 10.61^{a}	5.71 ± 0.22^{e}	1.79 ± 0.49^{ab}
		5	34.40 ± 0.00^{a}	2.10 ± 0.07^{a}	0.29 ± 0.03^{cde}	22.50 ± 10.61^{f}	5.49 ± 1.46^{e}	2.02 ± 0.11^{a}
		9	34.20 ± 1.13^{a}	1.90 ± 0.03^{a}	0.18 ± 0.10^{de}	52.50 ± 3.54^{f}	8.61 ± 0.98^{cd}	1.75 ± 0.08^{abc}
		13	29.65 ± 1.06^{b}	1.40 ± 0.00^{b}	0.18 ± 0.06^{e}	95.00 ± 7.07^{f}	8.14 ± 0.79^{cd}	1.64 ± 0.19^{abc}
		17	23.70 ± 1.97^{c}	1.30 ± 0.14^{bc}	0.45 ± 0.15^{b}	260.00 ± 14.14^{de}	6.78 ± 1.00^{de}	1.31 ± 0.03^{cd}
		21	17.98 ± 0.45^{d}	1.1 ± 0.07^{de}	0.50 ± 0.09^{b}	335.00 ± 91.92^{cd}	$8.930 \pm 0.80c$	0.95 ± 0.01^{d}
		26	16.45 ± 0.14^{de}	1.00 ± 0.00^{ef}	0.55 ± 0.03^{b}	222.50 ± 53.03^{e}	8.67 ± 1.00^{cd}	0.98 ± 0.01^{d}
		31	18.17 ± 0.88^{d}	1.20 ± 0.00^{cd}	1.33 ± 0.06^{a}	440.00 ± 84.85^{bc}	13.95 ± 0.50^{ab}	0.95 ± 0.02^{d}
	Storage	45	15.5 ± 0.50^{ef}	0.90 ± 0.14^{ef}	0.37 ± 0.02^{bc}	287.50 ± 60.10^{de}	12.45 ± 0.80^{b}	1.79 ± 0.31^{ab}
		60	12.68 ± 0.32^{f}	1.00 ± 0.07^{ef}	0.38 ± 0.07^{bc}	284.00 ± 36.77^{de}	13.15 ± 0.80^{ab}	1.45 ± 0.10^{bc}
		75	13.295 ± 0.12^{f}	1.00 ± 0.07^{ef}	0.20 ± 0.11^{bc}	317.50 ± 24.75^{de}	13.65 ± 0.06^{ab}	1.62 ± 0.09^{bc}
		90	12.09 ± 0.30^{f}	0.90 ± 0.07^{f}	0.40 ± 0.05^{bc}	351.13 ± 15.73^{bcd}	12.09 ± 0.04^{b}	1.49 ± 0.12^{bc}
		120	12.12 ± 1.24^{f}	1.00 ± 0.03^{ef}	0.45 ± 0.10^{bc}	450.00 ± 42.43^{b}	13.88 ± 0.49^{ab}	1.31 ± 0.10^{cd}
		150	12.13 ± 0.78^{f}	0.70 ± 0.05^{f}	0.50 ± 0.08^{bc}	424.00 ± 50.91^{bc}	14.86 ± 0.40^{a}	$1.54 \pm 0.06b^{c}$
MDO	Fermentation	1	34.80 ± 0.28^{a}	0.63 ± 0.09^{cd}	0.20 ± 0.00^{d}	725.00 ± 7.07^{a}	5.91 ± 0.90^{g}	$2.00 \pm 0.24b^{c}$
		5	22.50 ± 0.35^{b}	0.80 ± 0.00^{b}	3.10 ± 0.14^{c}	855.00 ± 7.07^{b}	4.82 ± 0.59^{g}	2.29 ± 0.15^{a}
		9	14.18 ± 2.01^{c}	0.70 ± 0.00^{bcd}	3.64 ± 0.06^{ab}	852.50 ± 3.53^{b}	12.27 ± 1.94^{abc}	2.22 ± 0.10^{ab}
		13	12.38 ± 0.25^{d}	0.70 ± 0.00^{bcd}	3.92 ± 0.11^{a}	852.50 ± 17.67^{b}	8.01 ± 0.40^{e}	1.84 ± 0.12^{cd}
		17	11.23 ± 0.67^{d}	0.75 ± 0.07^{bc}	3.33 ± 0.32^{bc}	855.00 ± 35.35^{b}	7.76 ± 1.21^{ef}	1.43 ± 0.15^{e}
		21	12.43 ± 0.18^{d}	0.70 ± 0.00^{bc}	3.64 ± 0.29^{ab}	925.00 ± 14.14^{b}	9.78 ± 0.35^{de}	1.14 ± 0.08^{h}
		26	13.95 ± 0.49^{cde}	0.65 ± 0.06^{c}	3.32 ± 0.16^{bc}	920.00 ± 21.21^{b}	8.56 ± 0.57^{e}	1.15 ± 0.02^{h}
		31	14.08 ± 0.74^{c}	0.75 ± 0.07^{bc}	3.44 ± 0.18^{bc}	887.50 ± 67.17^{b}	11.92 ± 0.81^{bc}	1.26 ± 0.08^{gh}
	Storage	45	13.50 ± 0.49^{ef}	0.60 ± 0.00^{d}	3.37 ± 0.08^{bc}	882.50 ± 17.68^{b}	11.22 ± 1.15^{cd}	1.50 ± 0.12^{efg}
		60	11.32 ± 0.40^{f}	0.75 ± 0700^{bc}	3.25 ± 0.21^{bc}	875.00 ± 7.07^{b}	11.16 ± 1.03^{cd}	1.32 ± 0.05^{gh}
		75	12.40 ± 0.69^{f}	0.80 ± 0.00^{b}	3.44 ± 0.19^{bc}	888.50 ± 44.54^{b}	12.57 ± 0.01^{abc}	1.59 ± 0.09^{def}
		90	12.05 ± 0.43^{f}	0.75 ± 0.07^{bc}	3.32 ± 0.14^{bc}	901.00 ± 41.01^{b}	12.79 ± 0.32^{abc}	1.67 ± 0.08^{cde}
		120	12.05 ± 0.00^{f}	0.95 ± 0.07^{a}	3.30 ± 0.13^{bc}	850.00 ± 42.43^{b}	13.52 ± 0.70^{ab}	1.72 ± 0.04^{cde}
		150	12.55 ± 0.57^{f}	1.00 ± 0.00^{a}	3.21 ± 0.06^{c}	915.00 ± 21.20^{b}	14.24 ± 0.58^{a}	$1.57 \pm 0.18d^{efg}$

Values are means of quadruplicates ± SD. The different letters (a–g) after value are significantly different ($p < 0.05$). MDI, the inner layers of MT-*Daqu*; MDO, the outer layers of MT-*Daqu*.

to those of MDO after 3 months of storage. Furthermore, all microbial counts in the MDO remained relatively constant after 1 month of storage.

Composition of representative bacteria and fungi in mature medium-temperature-*Daqu*

A total of eighty-two bacterial isolates were obtained from the mature samples. Based on the analysis of the 16S rRNA gene sequence, 6 bacterial genera (15 species) were identified (**Supplementary Table 1**). Of these, *Bacillus* and *Staphylococcus* accounted for 70.7 and 13.4% of the bacterial community, respectively, at the genus level. A total of fifty fungal isolates were selected for identification by ITS region sequencing and 18S rRNA gene sequence analysis. A total of nine fungal species were identified, including *Wickerhamomyces anomalus* (12 strains), *Pichia jadinii* (8 strains), *Aspergillus awamori* (13 strains), *Aspergillus ustus* (4 strains), *Penicillium purpurogenum* (7 strains), *Penicillium sp.* (1 strain), *Alternaria alternata* (4 strains), and *Lichtheimia corymbifera* (1 strain) (**Supplementary Table 2**). *W. anomalus* and *A. awamori* mainly appeared in MDI, whereas other fungal species exhibited a similar distribution in both parts of MT-*Daqu*.

Analysis of the microbial community of mature medium-temperature-*Daqu* using Illumina sequencing

Illumina sequencing of the bacterial 16S rRNA genes and fungal ITS gene generated a total of 283,896 and 520,350 effective sequences, respectively. After clustering all the

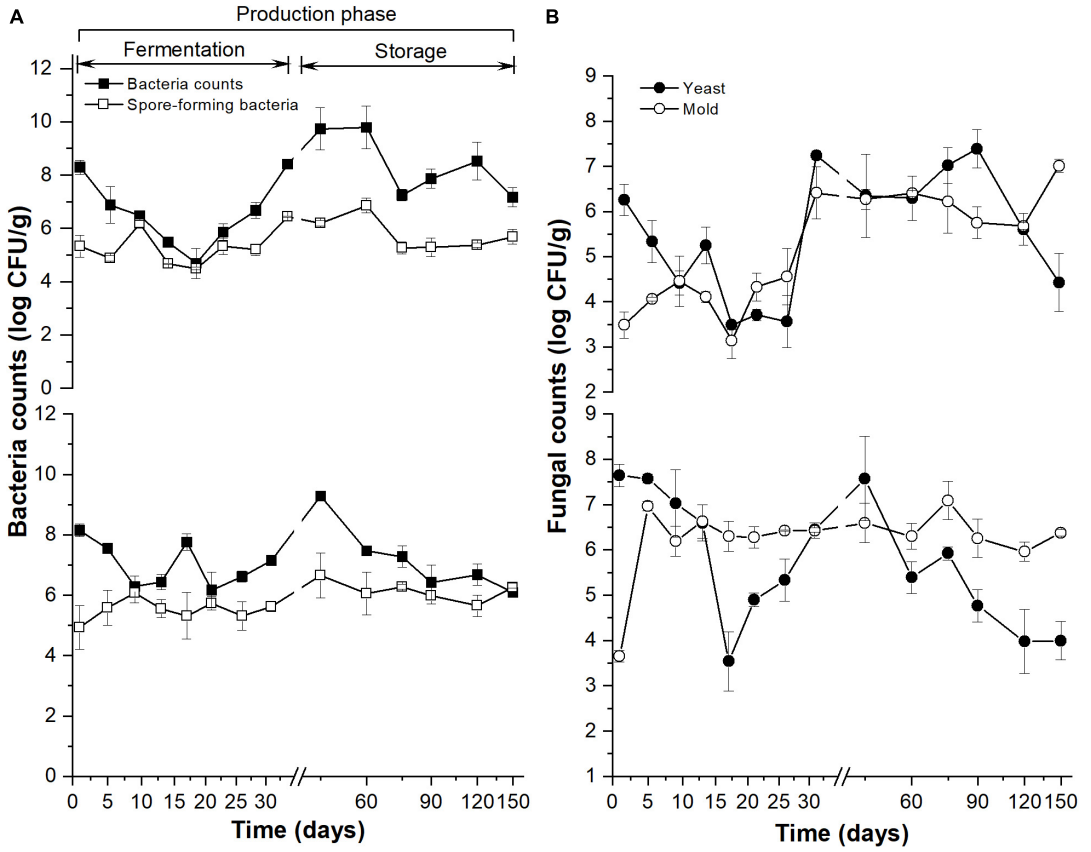

FIGURE 1
Dynamics of culture-dependent bacteria **(A)** and fungi **(B)** in MT-*Daqu* during entire production, including 31-day fermentation period and 4 months storage. The upper and lower *y*-axis indicate the microbial counts in MDI (the inner layers of MT-*Daqu*) and MDO (the outer layers of MT-*Daqu*), respectively.

sequences, 597-632 and 625-773 OTUs of observed species in the outer layer and inner layer of MT-*Daqu* were obtained, respectively. The community diversity of either bacteria or fungi in the MDI was greater than that in the MDO, whereas the number of bacterial OTUs (observed species) was less than that of fungal OTUs (**Supplementary Table 3**). At the phylum level (**Figure 3A**), the three dominant bacterial phyla were *Firmicutes* (75.68%), *Proteobacteria* (17.27%), and *Actinobacteria* (2.72%) in MDI. In MDO, *Firmicutes* and *Proteobacteria* were still dominant, but at lower percentages, e.g., only 39.26 and 5.74%, respectively. Moreover, the two dominant fungal phyla were *Ascomycota* and *Mucoromycota*, and the former was the predominant type, which accounted for 82.20 and 65.79% of the total sequences in MDI and MDO, respectively. At the genus level (**Figure 3B**), bacteria were dominated by *Bacillus*, *Staphylococcus*, *Pantoea*, *Weissella*, *Saccharopolyspora*, *Klebsiella,* and *Prevotella*. *Bacillus* and *Staphylococcus* were highly abundant (>9.83%) in the MDI and MDO samples, whereas *Bacillus* was relatively more abundant in MDI (47.02%) than in MDO (21.07%), and *Saccharopolyspora* was much less abundant in MDI (0.79%) than in MDO (6.11%). For fungi, *Thermomyces*, *Aspergillus*, *Rhizomucor*, *Thermoascus*, *Rhizopus*, *Archaeorhizomyces,* and *Alternaria* were the predominant genera in both parts of MT-*Daqu*. The abundances of *Aspergillus* and *Rhizopus* in MDI (58.88 and 5.34%, respectively) were higher than in MDO (20.05 and 0.14%). However, the abundances of *Thermomyces*, *Rhizomucor*, and *Thermoascus* in the MDI (13.56, 3.82, and 0.60%, respectively) were less than in MDO (50.67, 25.72, and 7.51%, respectively).

Analysis of community structure in different parts of mature medium-temperature-*Daqu*

Principal coordinates analysis showed that the cumulative contribution of the first two principal coordinates was 89.16% for bacterial communities (**Figure 4A**) and 89.92% for fungal communities (**Figure 4B**). Moreover, the two PCoA plots showed that the samples of the same part of MT-*Daqu* clustered together, and PERMANOVA revealed that the differences were significant ($p = 0.034 < 0.05$). LEfSe indicated that as many

10.3389/fmicb.2022.934696

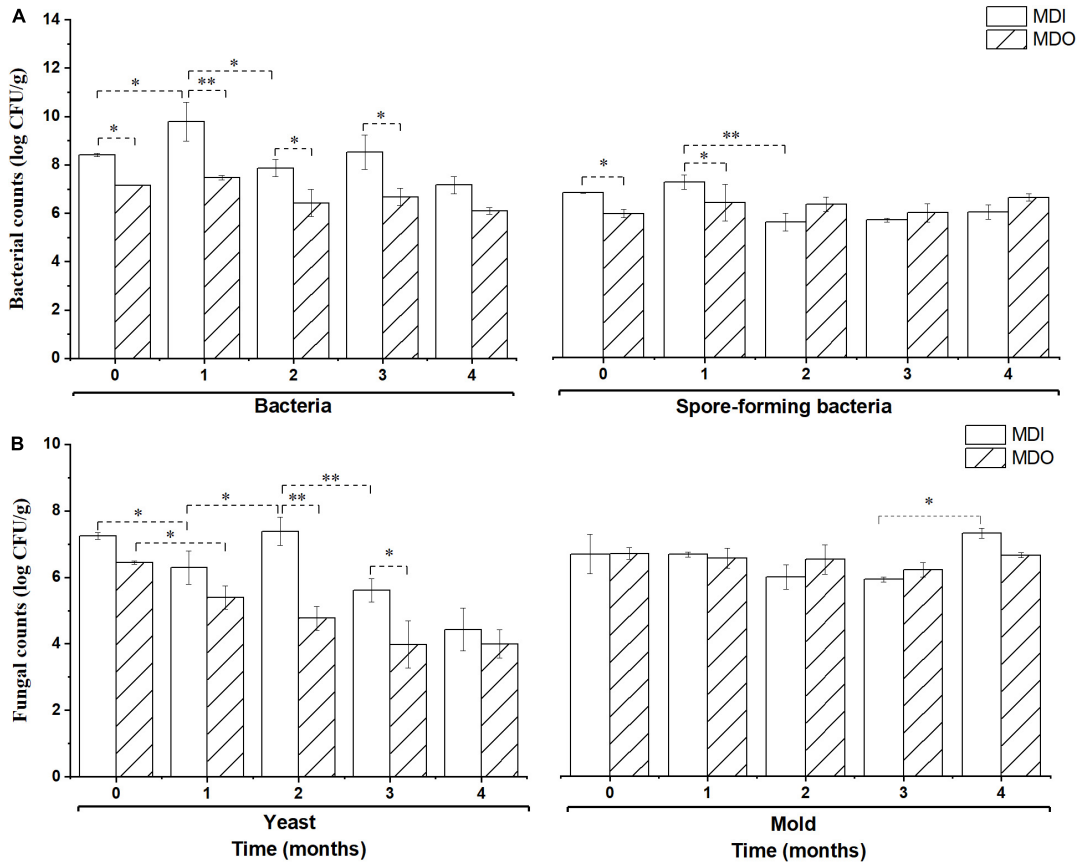

FIGURE 2
Comparison of the bacteria **(A)** and fungi **(B)** in the MDI and MDO samples during storage. Significant differences are noted by * ($p < 0.05$) and ** ($p < 0.01$).

as 30 bacteria (Figure 4C) and 29 fungi (Figure 4D) exhibited significant differences ($p < 0.05$) in different parts of MT-*Daqu* samples. *Bacillus*, *Klebsiella, Cronobacter,* and *Pantoea* were the most significantly enriched bacterial genera in MDI, whereas *Saccharopolyspora,* unclassified or no rank *Pseudonocardiaceae,* and unclassified *Bacteria* were enriched in MDO. A total of eighteen taxa and 11 taxa exerted significant effects ($p < 0.05$) on fungal community structure in the MDI and MDO samples, respectively. Furthermore, *Aspergillus*, *Alternaria,* and *Rhizopus* were enriched fungal genera in the MDI but *Thermomyces*, *Thermoascus,* and *Rhizomucor* were enriched in the MDO. At the genus level, the different types of samples contained a higher proportion of type-specific microorganisms.

Analyses of volatile compounds in different parts of mature medium-temperature-*Daqu*

A total of sixty-five volatile compounds, including 17 alcohols, 10 esters, 13 aldehydes, 7 ketones, 10 pyrazines, and 8 other compounds, were identified and semiquantified (Supplementary Table 4). Of these, isoamyl alcohol, hexanol, 2,3-butanediol, benzyl alcohol, phenylethyl alcohol, ethylhexanoate, ethylpalmitate, ethyllinoleate hexanal, benzaldehyde, geranylacetone, and tetramethylpyrazine were dominant in mature MT-*Daqu*. The contents of six species of volatile compounds are shown in Figure 5. The contents of alcohols and pyrazines were the highest in all samples, and only the alcohol content in the MDI (699.05 μg/kg) was significantly higher than that in the MDO (348.88 μg/kg). In the MDI sample, no significant difference was observed between the contents of alcohols and pyrazines, whereas in the MDO sample, the content of pyrazines at 590.96 μg/kg was the highest, which was 25 times higher than the lowest content of ketones (23.57 μg/kg).

Discussion

The investigation of the culture-dependent microbial abundance and physicochemical properties of Daqu provided

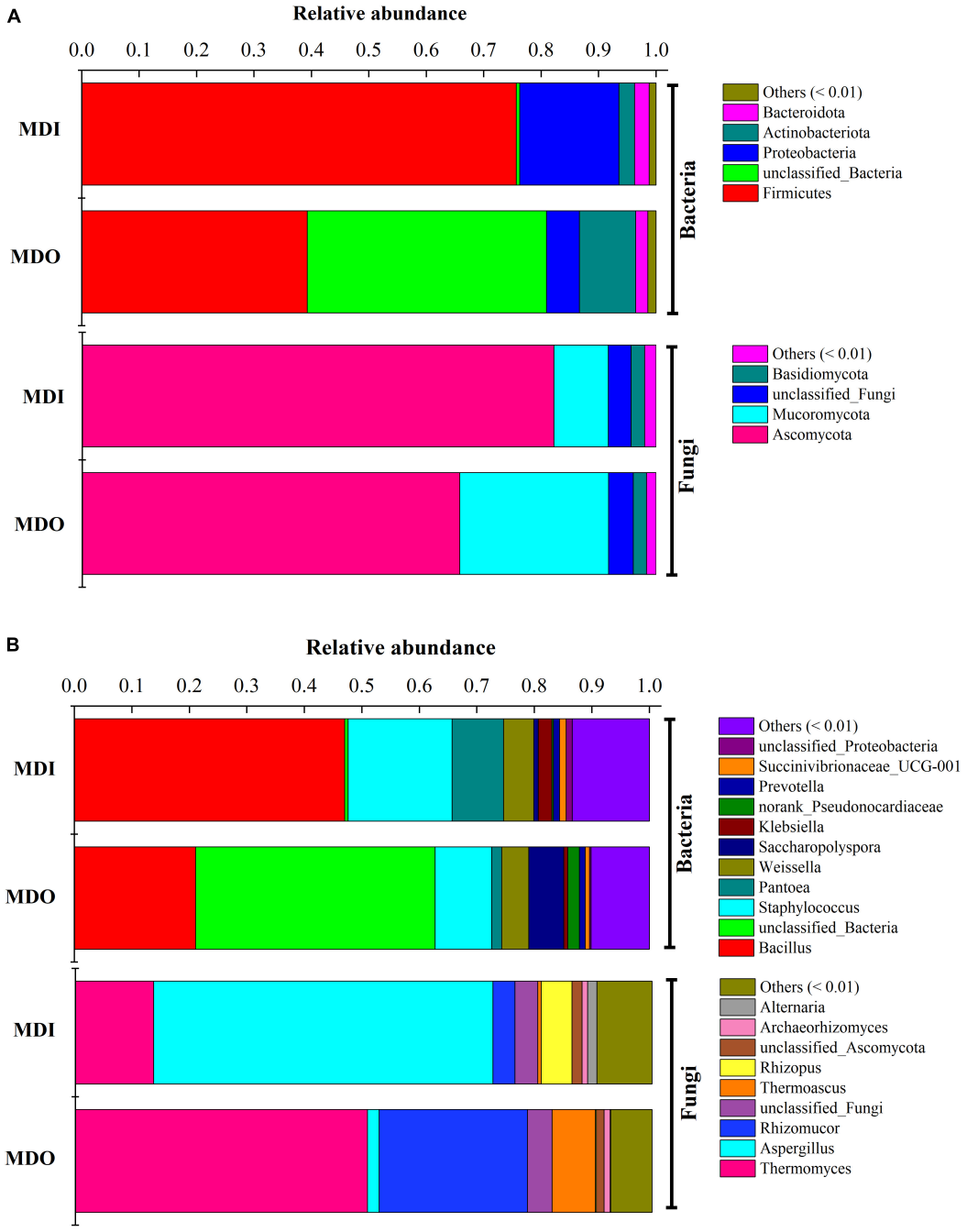

FIGURE 3
Microbial composition in different parts of the mature MT-*Daqu*. **(A)** Bacterial and fungal composition at the phylum level (more than 0.5%); **(B)** bacterial and fungal composition at the genus level (more than 0.5%). MDI, inner layers of MT-*Daqu*; MDO, outer layers of MT-*Daqu*.

the first insight into the microbial composition and metabolic changes, which provides a basis for further omics analyses (Huang et al., 2020) and might be used to initially evaluate the maturity of *Daqu*. Despite the high workload and incomplete coverage, culture-dependent methods isolate cultivable strains that can be used as functional starters with contributions to the quality of ferment liquor and foods (Zheng et al., 2012; Lv et al., 2015; Yang et al., 2022). Considering bacteria, yeasts and molds as the three major types of microbiota in *Daqu* (Cai et al., 2021) and spore-forming bacteria, especially *Bacillus* as producers of enzymes and aroma compounds that contribute to *Daqu* flavor and quality (Yan et al., 2013b; He et al., 2019), two groups of bacteria, namely, aerobic bacteria and spore-forming bacteria and two groups of fungi, namely, yeast

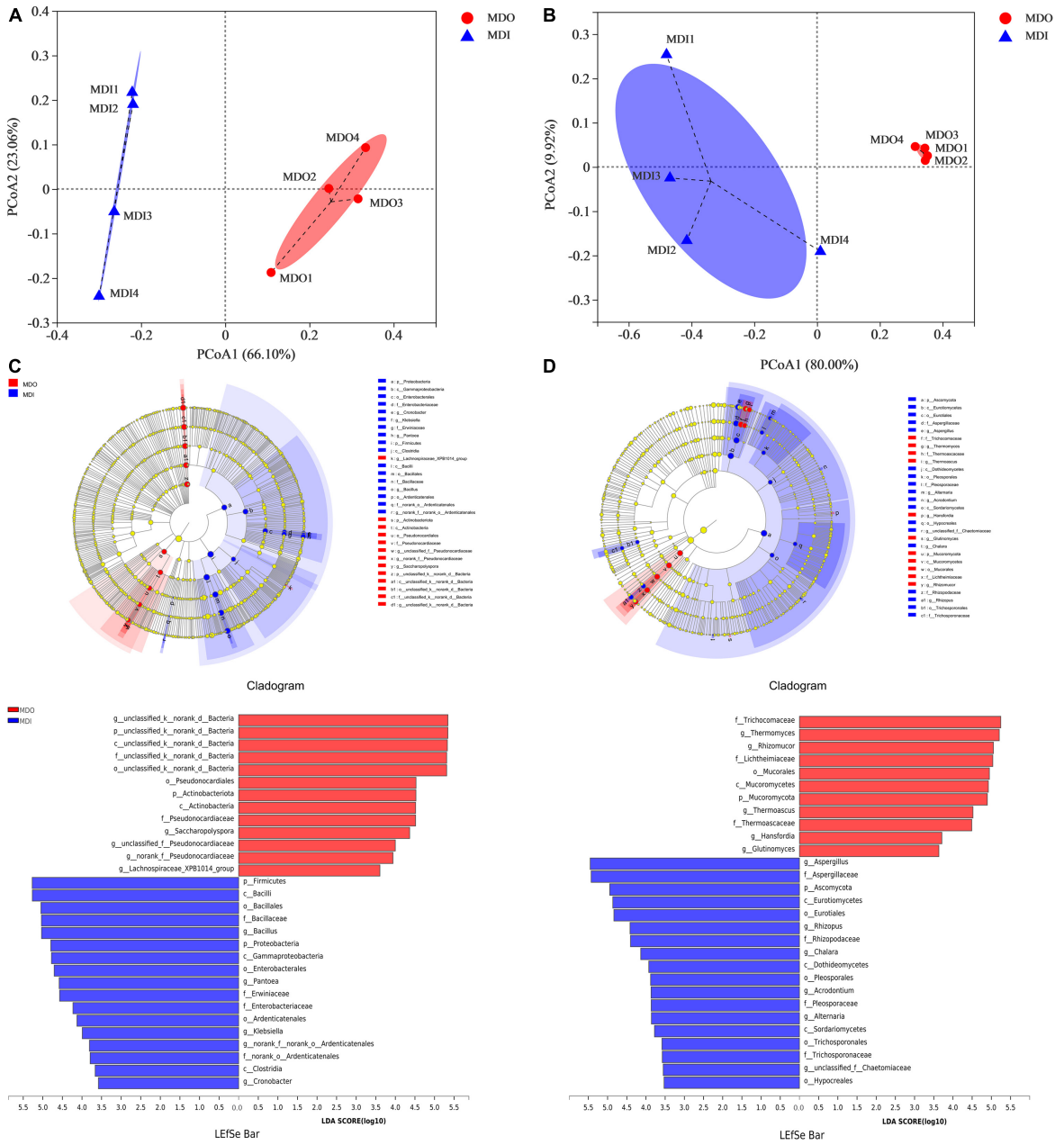

FIGURE 4
Principal coordinates analysis score plots of microbial β-diversity based on Bray–Curtis distance ($p < 0.05$) and LEfSe analysis of the MDI and MDO samples (LDA > 3.5, $p < 0.05$). Bacterial **(A,C)** and fungal **(B,D)** taxa showed significantly different abundances.

and mold, were analyzed using culture-dependent methods during MT-*Daqu* production. In the fermentation period, the counts of aerobic bacteria in MDI and yeast in both parts of MT-*Daqu* rapidly decreased to the minimum values at 17 days (**Figures 1A,B**) as the temperature increased to 60°C (**Supplementary Figure 2**) and then increased until the end of fermentation, consistent with previous findings (Li et al., 2016; Yan et al., 2019). This result might be attributed to the decrease in non-thermotolerant bacterial genera, such as lactic acid bacteria (LAB), and fungal genera, such as *Pichia*, which was restrained when the temperature was higher than 40°C (Li P. et al., 2015). The counts of spore-forming bacteria and molds in both parts of MT-*Daqu* increased rapidly in the first 9 days during the *Peijun* stage and then decreased slowly from 9 days to 17 days at the *Dinghuo* stage, thereafter increasing gradually or remaining stable until the end of fermentation. In the *Peijun* and *Dinghuo* stages, thermotolerant spore-forming bacteria, such as *Bacillus,* and filamentous fungi, such as

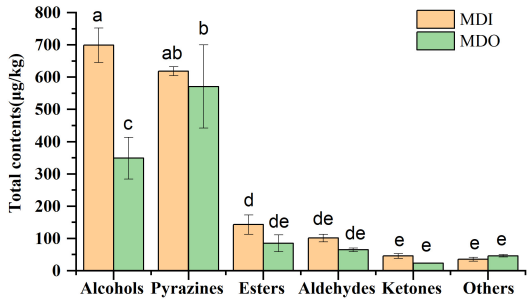

FIGURE 5
Relative abundance of six categories of volatile compounds in MDI and MDO samples of the mature MT-*Daqu*. Different letters indicate significant differences ($p < 0.05$).

Aspergillus, *Rhizopus*, *Rhizomucor,* and *Amylomyces,* survived and were commonly involved in solid-state fermentation with increasing temperature and decreasing moisture and increasing environmental relative humidity (**Supplementary Figure 2**; Li P. et al., 2015; Shanqimuge et al., 2015; Yan et al., 2019). This finding was confirmed by the changes in the total aerobic bacteria in MDI. The counts of total aerobic bacteria were essentially coincident with those of spore-forming bacteria from 9 days to 17 days, showing that the spore-forming bacteria are capable of producing endospores that are highly resistant to unfavorable environmental conditions of heat and desiccation, and thus, they were predominant among the total aerobic bacteria in this stage (Shanqimuge et al., 2015). Additionally, the cell counts of the four microbial groups in MDO were higher than those in MDI from 5 days to 21 days, which is fairly consistent with the results of previous studies (Zheng et al., 2012). The explanation for this observation may be that less access to water and air and a higher temperature MDI were not suitable for the growth of bacteria, except spore-forming bacteria, whereas the interface containing abundant air and nutrient substances easily formed in MDO, leading to the promotion of microbial growth (Li et al., 2013; Zhang Y. et al., 2021).

Consistent with previous studies, the cell counts of aerobic bacteria and yeasts in MDI and MDO samples were significantly different before and after the samples were stored for 3 months, and a similar difference was observed in the counts of spore-forming bacteria before 2 months (Li et al., 2013; Jin et al., 2019). These results supported the hypothesis that these environmental conditions promote three groups of microorganisms to propagate further in the inner layers. After at least 3 months of storage, the microbial counts in both parts of MT-*Daqu* were not significantly different ($p > 0.05$) because the changes in the environmental conditions, including temperature, moisture, and acidity, during storage, and drove the microorganisms in both parts of MT-*Daqu* to become similar and eventually form a stable system (Zhang Y. et al., 2021). Overall, culture-dependent microorganisms are stabilized after 3 months of storage.

The acidity of both parts quickly peaked in the early stage of fermentation, and the value of MDI was higher than that of MDO before 3 months (**Table 1**). Acidity was regarded as the most significant factor correlated with the composition of the microbial communities in the early stage of *Daqu* fermentation, and some *Lactobacillus* species were detected at higher percentages in the central part (Li et al., 2013), leading to the continuous synthesis of numerous organic acids (Shanqimuge et al., 2015). The liquefying activity and the saccharifying activity of *Daqu* are the two major contributors to liquefaction and saccharification in *Baijiu* production. Therefore, the two activities in different parts of *Daqu* showed similar changes throughout production (**Table 1**), and the two indices in MDI after fermenting 5 days and in MDO during production exhibited significantly positive correlations (Pearson correlation coefficient $\rho = 0.58$, $p < 0.05$ and $\rho = 0.81$, $p < 0.01$). The results might be attributed to the thermal stability of amylase and glucoamylase at high incubation temperatures of approximately 60°C (Li P. et al., 2015). Moreover, changes in both activities in the MDI and the MDO samples were similar to the counts of mold and spore-forming bacteria, respectively. A few studies have reported that some mold species, such as *Thermoascus*, *Aspergillus*, and *Rhizomucor*, and spore-forming bacterial species, such as *B. licheniformis*, *B. subtilis*, and *B. cereus*, which were identified as the core genera in *Daqu* production, produce various hydrolytic enzymes for starch liquefication and saccharification (Li Z. M. et al., 2015; Wang et al., 2018; Yan et al., 2019). Esterifying activity mainly contributes to the synthesis of esters that are the prominent flavor of *Baijiu* (Guan et al., 2021). In this study, along with the decrease in yeast counts, esterifying activity remained at a lower range until complete fermentation. Similar to acidity, the fermenting activity, especially in MDO, increased in the early fermentation period but did not change significantly in storage, mainly due to the higher counts of yeasts in the early phase (Fan et al., 2020).

Consistent with previous reports (Fan et al., 2020; Guan et al., 2021), we showed that storage for at least 3 months is necessary for MT-*Daqu* to reach a stable state in **Figure 2**. Moreover, we found that five main bacterial phyla, *Firmicutes*, *Proteobacteria*, *Actinobacteria*, *Cyanobacteria*, and *Bacteroidetes*, and two dominant fungal phyla, *Ascomycota* and *Mucoromycota*, were identified in both parts of MT-*Daqu*. These dominant microbial communities in MT-*Daqu* have been reported in other studies (Guan et al., 2021), and the same discovery was documented in both low-temperature and high-temperature *Daqu* (Li et al., 2013; Jin et al., 2019). *Bacillus*, *Klebsiella,* and *Pantoea* might represent potential biomarkers for MDI and *Saccharopolyspora* for MDO. The result that *Saccharopolyspora* were dominant outside of MT-*Daqu* is consistent with a previous study, and the study indicated

that they were derived from the environment or raw materials to provide the initial microbiota (Zhang Y. et al., 2021). In addition, large amounts of *Bacillus*, *Staphylococcus,* and *Weissella* emerged in both samples. This finding was consistent with the analysis in terms of the predominance of *Bacillus* and *Staphylococcus* isolated and identified using culture-dependent methods (**Supplementary Table 1**). This study also showed that fungal communities in MT-*Daqu* were mainly comprised of *Aspergillus*, *Thermomyces*, *Rhizomucor*, *Thermoascus,* and *Rhizopus*, and *Aspergillus* and *Rhizopus* were dominant in MDI, whereas *Thermomyces*, *Rhizomucor*, and *Thermoascus* were predominant in MDO. The same composition of molds at the genus level in MT-*Daqu* was observed in liquor industries of South China, such as Sichuan and Jiangsu, which are the dominant regions producing strong-flavor *Baijiu* (Guan et al., 2021). Additionally, LEfSe revealed that the fungal genera *Aspergillus*, *Alternaria,* and *Rhizopus* were enriched in the MDI, whereas *Thermomyces*, *Thermoascus,* and *Rhizomucor* were enriched in the MDO. Unlike their abundances in high-temperature *Daqu*, *Byssochlamys*, and *Fusarium* were predominant in the inner and outer parts of high-temperature *Daqu*, respectively, and *Thermoascus* possessed an absolutely dominant position in both positions (Zhang Y. et al., 2021). In MT-*Daqu*, we did not detect *Byssochlamys* and only detected a low abundance of *Fusarium* (0.013%). These results may be due to the different production processes for different types of *Daqu* or different regional environments (Cai et al., 2021). Therefore, MT-*Daqu* has a specific fungal community structure. *Aspergillus*, *Alternaria,* and *Rhizopus* might be considered as biomarkers for MDI, whereas *Thermomyces*, *Thermoascus,* and *Rhizomucor* may be considered as biomarkers for MDO of MT-*Daqu* (Hu et al., 2021). The dominant fungal community comprised of molds was discovered in high-temperature and MT-*Daqu* (Hu et al., 2017; Wang et al., 2018), whereas the fungal composition with a high proportion of yeasts, such as *Wickerhamomyces*, *Saccharomycopsis*, and *Pichia*, was detected in low-temperature *Daqu* because of its fermentation at a lower temperature (Cai et al., 2021; Hu et al., 2021). Therefore, the special fungal composition of MT-*Daqu* is different from that of low-temperature *Daqu* but close to that of high-temperature *Daqu*, which potentially explains why the strong-flavor *Daqu* has its own unique flavor and physiological–biochemical characteristics.

Flavors in *Daqu* play an important role in the flavor classification of Chinese *Baijiu* (Zhang et al., 2011; Wang et al., 2020). In this study, isoamyl alcohol, hexanol, 2,3-butanediol, benzyl alcohol, phenylethyl alcohol, ethylhexanoate, ethylpalmitate, ethyllinoleate, hexanal, benzaldehyde, geranylacetone, and tetramethylpyrazine were detected as the predominant flavors in mature MT-*Daqu* (**Supplementary Table 4**), consistent with the findings of *Luzhou-Daqu* (Sichuan, China) (Zhang et al., 2011; He et al., 2019) and *Yingjia-Daqu* (Anhui, China) (Yan et al., 2019). Of these compounds, tetramethylpyrazine was present the highest relative abundance in both parts of MT-*Daqu*, followed by phenylethyl alcohol and benzaldehyde. Pyrazines, which are nitrogen-containing compounds, are the important volatile compounds of Chinese *Baijiu* that provide baked, roasted, and nutty notes (Fan and Qian, 2006) and are reported to be the key active compounds of Jiang-flavor *Baijiu* (Jin et al., 2019). A total of ten pyrazines were also identified in our samples, five of which were detected in "*Wuliangye*" and "*Jiannanchun*" strong-flavored *Baijiu* (Fan and Qian, 2006). He et al. (2019) reported that 10 pyrazines were identified in *Luzhoulaojiao-Daqu*, and the relatively high content of tetramethylpyrazine was consistent with the high abundance of *Bacillus* in fortified MT-*Daqu* inoculation with *Bacillus velezensis* and *Bacillus subtilis* (He et al., 2019). According to Jin et al. (2019), *Bacillales*, *Thermoactinomyces*, and *Aspergillus* are the principal contributors to pyrazines (Jin et al., 2019). We found that alcohols were also the most dominant flavor compounds and total alcohols were detected at the highest abundance in MDI (**Figure 5**). Alcohols, as important precursors of acids and esters, comprise the largest group of compounds, and most of them have been detected in Chinese liquor, which often impart fruity, floral, green, and alcoholic odors and contribute to the flavor of Chinese liquor (Zhang et al., 2011). Phenethyl alcohol, imparting floral components, such as rose and fruity notes, was the main constituent in alcohols in MT-*Daqu* (Yang et al., 2021) and was the second most abundant compound in this study. In addition to phenethyl alcohol, isoamyl alcohol, hexanol, and S-2,3-butanediol were present at high contents in all samples, and their contents in MDI were higher than those in MDO. These higher alcohols might be formed from amino acid catabolism *via* the Ehrlich metabolic pathway or from lipid oxidation by some microbial strains, such as *Enterobacter*, *Acinetobacter*, *Aspergillus*, *Rhizopus,* and *Alternaria* (Zhang et al., 2011; Tang Q. X. et al., 2019; Yang et al., 2022). In addition, geranylacetone, which was present at an intermediate content, was first identified in MT-*Daqu*, and its function and source in *Daqu* are still unknown and require further exploration.

Conclusion

This study provided a comprehensive understanding of the microbial community and physicochemical properties inside and outside the MT-*Daqu* used for strong-flavor *Baijiu* production from the fermentation period to the mature period. Both culture-dependent and culture-independent methods provided a view of changes in the microbial community during production and discrepancies in the different parts of the MT-*Daqu*. The physicochemical property indices in both parts of MT-*Daqu* shifted from the fermentation period to a relatively

stable range after storage for 3 months, and a difference between the inner layers and the outer layers was also observed. The findings provide theoretical evidence for industrial process control and evaluating the mature period of MT-*Daqu*. This study also investigated the predominant bacterial and fungal composition and volatile compounds inside and outside the mature MT-*Daqu*. The results will assist in quality judgments of the mature MT-*Daqu* and identifying the functional microbial sources to apply in *Baijiu* brewing.

Data availability statement

The original contributions presented in the study are included in the article/**Supplementary material**, further inquiries can be directed to the corresponding author.

Author contributions

XH conducted all the experiments and wrote the initial manuscript. RL and MH conceived and designed the experiments. ZS and JW revised and proofread the manuscript. XS and RX analyzed the experimental data. XL and CP contacted the liquor manufacturer and participated in the partial production experiment. All authors read and approved the manuscript.

Funding

This work was supported by the Major Special Subproject of Henan Province (181100211400-8), the Key Project of Scientific and Technological Research in Henan Province (182102110008), and the Innovative Funds Plan of Henan University of Technology (2020ZKCJ23).

Acknowledgments

We thank Fuqiang Li, Zihong Liu, and Peixue Yan at the Henan Songhe Distillery Co., Ltd., for their contribution to the sampling of MT-*Daqu*.

Conflict of interest

The authors declare that the research was conducted in the absence of any commercial or financial relationships that could be construed as a potential conflict of interest.

Publisher's note

Supplementary material

The Supplementary Material for this article can be found online at: https://www.frontiersin.org/articles/10.3389/fmicb.2022.934696/full#supplementary-material

References

Cai, W., Wang, Y., Ni, H., Liu, Z., Liu, J., Zhong, J., et al. (2021). Diversity of microbiota, microbial functions, and flavor in different types of low-temperature Daqu. *Food Res. Int.* 150:110734. doi: 10.1016/j.foodres.2021.110734

Chen, Y., Li, K., Liu, T., Li, R., Fu, G., Wan, Y., et al. (2020). Analysis of difference in microbial community and physicochemical indices between surface and central parts of Chinese special-Flavor Baijiu Daqu. *Front. Microbiol.* 11:592421. doi: 10.3389/fmicb.2020.592421

Deng, L., Mao, X., Liu, D., Ning, X. Q., Shen, Y., Chen, B., et al. (2020). Comparative analysis of physicochemical properties and microbial composition in High-Temperature Daqu with different colors. *Front. Microbiol.* 11:588117. doi: 10.3389/fmicb.2020.588117

Deng, Y., Huang, D., Han, B., Ning, X., Yu, D., Guo, H., et al. (2021). Correlation: between autochthonous microbial diversity and volatile metabolites during the fermentation of Nongxiang Daqu. *Front. Microbiol.* 12:688981. doi: 10.3389/fmicb.2021.688981

Fan, G. S., Fu, Z. L., Sun, B. G., Zhang, Y. H., Wang, X. L., Xia, Y. Q., et al. (2019). Roles of aging in the production of light-flavored Daqu. *J. Biosci. Bioeng.* 127, 309–317. doi: 10.1016/j.jbiosc.2018.08.005

Fan, G. S., Fu, Z. L., Teng, C., Liu, P. X., Wu, Q. H., Rahman, M. K. R., et al. (2020). Effects of aging on the quality of roasted sesame-like flavor Daqu. *BMC Microbiol.* 20:67. doi: 10.1186/s12866-020-01745-3

Fan, W. L., and Qian, M. C. (2006). Characterization of aroma components of Chinese "Wuliangye" and "Jiannanchuan" liquors by aroma extracr dilution analysis. *J. Agric. Food Chem.* 54, 2695–2704. doi: 10.1021/jf052635t

Fu, G. M., Deng, M. F., Chen, K. D., Chen, Y. R., Cai, W. Q., Wu, C. F., et al. (2021). Peak-temperature effects of starter culture (Daqu) on microbial community succession and volatile substances in solid-state fermentation (Jiupei) during traditional Chinese special-flavour Baijiu production. *Lwt* 152:112132. doi: 10.1016/j.lwt.2021.112132

Guan, T. W., Yang, H., Ou, M. Y., and Zhang, J. X. (2021). Storage period affecting dynamic succession of microbiota and quality changes of strong-flavor Baijiu Daqu. *Lwt* 139:110544. doi: 10.1016/j.lwt.2020.110544

He, G. Q., Dong, Y., Huang, J., Wang, X. J., Zhang, S. Y., Wu, C. D., et al. (2019). Alteration of microbial community for improving flavor character of Daqu by inoculation with *Bacillus velezensis* and *Bacillus subtilis*. *Lwt* 111, 1–8. doi: 10.1016/j.lwt.2019.04.098

Hu, Y. L., Dun, Y. H., Li, S. A., Fu, B., Xiong, X. M., Peng, N., et al. (2017). Changes in microbial community during fermentation of high-temperature Daqu used in the production of Chinese 'Baiyunbian' liquor. *J. Ins. Brew.* 123, 594–599. doi: 10.1002/jib.455

Hu, Y. N., Huang, X. N., Yang, B., Zhang, X., Han, Y., Chen, X. X., et al. (2021). Contrasting the microbial community and metabolic profile of three types of light-flavor Daqu. *Food Biosci.* 44:101395. doi: 10.1016/j.fbio.2021.101395

Huang, X., Fan, Y., Lu, T., Kang, J., Pang, X., Han, B., et al. (2020). Composition and metabolic functions of the microbiome in fermented grain during light-flavor Baijiu fermentation. *Microorganisms* 8:1281. doi: 10.3390/microorganisms8091281

Jin, G. Y., Zhu, Y., and Xu, Y. (2017). Mystery behind Chinese liquor fermentation. *Trends Food Sci. Technol.* 63, 18–28. doi: 10.1016/j.tifs.2017.02.016

Jin, Y., Li, D., Ai, M., Tang, Q., Huang, J., Ding, X., et al. (2019). Correlation between volatile profiles and microbial communities: a metabonomic approach to study Jiang-flavor liquor Daqu. *Food Res. Int.* 121, 422–432. doi: 10.1016/j.foodres.2019.03.021

Li, P., Liang, H., Lin, W. T., Feng, F., and Luo, L. (2015). Microbiota Dynamics Associated with Environmental Conditions and Potential Roles of Cellulolytic Communities in Traditional Chinese Cereal Starter Solid-State Fermentation. *Appl. Environ. Microbiol.* 81, 5144–5156. doi: 10.1128/AEM.01325-15

Li, Z. M., Chen, L., Bai, Z. H., Wang, D. L., Gao, L. P., and Hui, B. D. (2015). Cultivable bacterial diversity and amylase production in two typical light-flavor Daqus of Chinese spirits. *Front. Life Sci.* 8, 264–270. doi: 10.1080/21553769.2015.1041188

Li, P., Lin, W., Liu, X., Wang, X., and Luo, L. (2016). Environmental factors affecting microbiota dynamics during traditional solid-state fermentation of Chinese Daqu starter. *Front. Microbiol.* 7:1237. doi: 10.3389/fmicb.2016.01237

Li, X. R., Ma, E. B., Yan, L., Meng, Z. H., Du, X. W., and Quan, Z. X. (2013). Bacterial and fungal diversity in the starter production process of Fen liquor, a traditional Chinese liquor. *J. Microbiol.* 51, 430–438. doi: 10.1007/s12275-013-2640-9

Liu, J., Chen, J., Fan, Y., Huang, X., and Han, B. (2018). Biochemical characterisation and dominance of different hydrolases in different types of Daqu – a Chinese industrial fermentation starter. *J. Sci. Food Agric.* 98, 113–121. doi: 10.1002/jsfa.8445

Lv, X. C., Chen, Z. C., Jia, R. B., Liu, Z. B., Zhang, W., Chen, S. J., et al. (2015). Microbial community structure and dynamics during the traditional brewing of Fuzhou Hong Qu glutinous rice wine as determined by culture-dependent and culture-independent techniques. *Food Control* 57, 216–224. doi: 10.1016/j.foodcont.2015.03.054

People's Republic of China Light Industry Professional Standard. (2011b). *Strong Flavour Daqu (QB/T 4259-2011), Ministry of Industry and Information Technology of the People's Republic of China*. Beijing: China Light Industry Press, 1–4.

People's Republic of China Light Industry Professional Standard. (2011a). *General Methods of Analysis for Daqu (QB/T 4257-2011), Ministry of Industry and Information Technology of the People's Republic of China*. Beijing: China Light Industry Press, 1–3.

Shangdong Province Local Standard. (2009). *General Technical Conditions of Daqu (DB37/T 1231-2009)*. China: Shangdong Province Bureau of Quality and Technical Supervision, 1–15.

Shanqimuge, Liang, H., Zhang, C., Shao, C., Peng, X., Liang, L., et al. (2015). A DGGE marker-mediated mast monitoring of bacterial diversity and comprehensive identification of high-temperature Daqu starter. *J. Food Sci.* 80:M1519–M1525. doi: 10.1111/1750-3841.12903

Tang, H. L., Liang, H. B., Song, J. K., Lin, W. F., and Luo, L. X. (2019). Comparison of microbial community and metabolites in spontaneous fermentation of two types Daqu starter for traditional Chinese vinegar production. *J. Biosci. Bioeng.* 128, 307–315. doi: 10.1016/j.jbiosc.2019.03.011

Tang, Q. X., He, G. Q., Huang, J., Wu, C. D., Jin, Y., and Zhou, R. Q. (2019). Characterizing relationship of microbial diversity and metabolite in Sichuan Xiaoqu. *Front. Microbiol.* 10:696. doi: 10.3389/fmicb.2019.00696

Wang, P., Wu, Q., Jiang, X. J., Wang, Z. Q., Tang, J. L., and Xu, Y. (2017). *Bacillus licheniformis* affects the microbial community and metabolic profile in the spontaneous fermentation of Daqu starter for Chinese liquor making. *Int. J. Food Microbiol.* 250, 59–67. doi: 10.1016/j.ijfoodmicro.2017.03.010

Wang, X. D., Ban, S. D., and Qiu, S. Y. (2018). Analysis of the mould microbiome and exogenous enzyme production in Moutai-flavor Daqu. *J. Ins. Brew.* 124, 91–99. doi: 10.1002/jib.467

Wang, Y., Cai, W., Wang, W., Shu, N., Zhang, Z., Hou, Q., et al. (2021). Analysis of microbial diversity and functional differences in different types of high-temperature Daqu. *Food Sci. Nutr.* 9, 1003–1016. doi: 10.1002/fsn3.2068

Wang, Z. M., Wang, C. T., Shen, C. H., Wang, S. T., Mao, J. Q., Li, Z., et al. (2020). Microbiota stratification and succession of amylase-producing *Bacillus* in traditional Chinese Jiuqu (fermentation starters). *J. Sci. Food Agric.* 100, 3544–3553. doi: 10.1002/jsfa.10405

Xiao, C., Lu, Z. M., Zhang, X. J., Wang, S. T., Ao, L., Shen, C. H., et al. (2017). Bio-Heat Is a Key Environmental Driver Shaping the Microbial Community of Medium-Temperature Daqu. *Appl. Environ. Microbiol.* 83:e01550–17. doi: 10.1128/AEM.01550-17

Xu, Y. Q., Sun, B. G., Fan, G. S., Teng, C., Xiong, K., Zhu, Y. P., et al. (2017). The brewing process and microbial diversity of strong flavour Chinese spirits: a review. *J. Ins. Brew.* 123, 5–12. doi: 10.1002/jib.404

Yan, S. B., Tong, Q. Q., and Guang, J. Q. (2019). Yeast dynamics and changes in volatile compounds during the fermentation of the traditional Chinese strong-flavor Daqu. *Lwt* 106, 57–63. doi: 10.1016/j.lwt.2019.02.058

Yan, Z., Zheng, X. W., Chen, J. Y., Han, J. S., and Han, B. Z. (2013a). Effect of different *bacillus* strains on the profile of organic acids in a liquid culture of Daqu. *J. Ins. Brew.* 119, 78–83. doi: 10.1002/jib.58

Yan, Z., Zheng, X. W., Han, B. Z., Han, J. S., Nout, M. J., and Chen, J. Y. (2013b). Monitoring the ecology of *Bacillus* during Daqu incubation, a fermentation starter, using culture-dependent and culture-independent methods. *J. Microbiol. Biotechnol.* 23, 614–622. doi: 10.4014/jmb.1211.11065

Yang, H. Y., Peng, Q., Zhang, H. B., Sun, J. Q., Shen, C., and Han, X. Y. (2022). The volatile profiles and microbiota structures of the wheat Qus used as traditional fermentation starters of Chinese rice wine from Shaoxing region. *Lwt* 154:112649. doi: 10.1016/j.lwt.2021.112649

Yang, Y., Wang, S. T., Lu, Z. M., Zhang, X. J., Chai, L. J., Shen, C. H., et al. (2021). Metagenomics unveils microbial roles involved in metabolic network of flavor development in medium-temperature Daqu starter. *Food Res. Int.* 140:110037. doi: 10.1016/j.foodres.2020.110037

Zhang, C. L., Ao, Z. H., Chui, W. Q., Shen, C. H., Tao, W. Y., and Zhang, S. Y. (2011). Characterization of the aroma-active compounds in Daqu: a tradition Chinese liquor starter. *Eur. Food Res. Technol.* 234, 69–76. doi: 10.1007/s00217-011-1616-4

Zhang, H., Wang, L., Tan, Y., Wang, H., Yang, F., Chen, L., et al. (2021). Effect of *Pichia* on shaping the fermentation microbial community of sauce-flavor Baijiu. *Int. J. Food Microbiol.* 336:108898. doi: 10.1016/j.ijfoodmicro.2020.108898

Zhang, Y., Shen, Y., Cheng, W., Wang, X., Xue, Y., Chen, X., et al. (2021). Understanding the shifts of microbial community and metabolite profile from wheat to mature Daqu. *Front. Microbiol.* 12:714726. doi: 10.3389/fmicb.2021.714726

Zheng, X. W., Yan, Z., Han, B. Z., Zwietering, M. H., Samson, R. A., Boekhout, T., et al. (2012). Complex microbiota of a Chinese "Fen" liquor fermentation starter (Fen-Daqu), revealed by culture-dependent and culture-independent methods. *Food. Microbiol.* 31, 293–300. doi: 10.1016/j.fm.2012.03.008

Zou, W., Zhao, C., and Luo, H. (2018). Diversity and Function of Microbial Community in Chinese Strong-Flavor Baijiu Ecosystem: A Review. *Front. Microbiol.* 9:671. doi: 10.3389/fmicb.2018.00671

frontiers | Frontiers in Microbiology

TYPE Original Research
PUBLISHED 10 August 2022
DOI 10.3389/fmicb.2022.979079

OPEN ACCESS

EDITED BY
Chun Cui,
South China University of Technology, China

REVIEWED BY
Xiao-Jun Ji,
Nanjing Tech University, China
Shang-Tian Yang,
The Ohio State University, United States
Xuefeng Wu,
Hefei University of Technology, China

*CORRESPONDENCE
Xian Zhang
zx@jiangnan.edu.cn
Zhiming Rao
raozhm@jiangnan.edu.cn

SPECIALTY SECTION
This article was submitted to Food Microbiology, a section of the journal Frontiers in Microbiology

RECEIVED 27 June 2022
ACCEPTED 20 July 2022
PUBLISHED 10 August 2022

CITATION
Hu M, Liu F, Wang Z, Shao M, Xu M, Yang T, Zhang R, Zhang X and Rao Z (2022) Sustainable isomaltulose production in *Corynebacterium glutamicum* by engineering the thermostability of sucrose isomerase coupled with one-step simplified cell immobilization. *Front. Microbiol.* 13:979079. doi: 10.3389/fmicb.2022.979079

Sustainable isomaltulose production in *Corynebacterium glutamicum* by engineering the thermostability of sucrose isomerase coupled with one-step simplified cell immobilization

Mengkai Hu, Fei Liu, Zhi Wang, Minglong Shao, Meijuan Xu, Taowei Yang, Rongzhen Zhang, Xian Zhang* and Zhiming Rao*

Key Laboratory of Industrial Biotechnology, Ministry of Education, School of Biotechnology, Jiangnan University, Wuxi, China

Sucrose isomerase (SI), catalyzing sucrose to isomaltulose, has been widely used in isomaltulose production, but its poor thermostability is still resisted in sustainable batches production. Here, protein engineering and one-step immobilized cell strategy were simultaneously coupled to maintain steady state for long-term operational stabilities. First, rational design of *Pantoea dispersa* SI (PdSI) for improving its thermostability by predicting and substituting the unstable amino acid residues was investigated using computational analysis. After screening mutagenesis library, two single mutants (PdSIV280L and PdSIS499F) displayed favorable characteristics on thermostability, and further study found that the double mutant PdSIV280L/S499F could stabilize PdSIWT better. Compared with PdSIWT, PdSIV280L/S499F displayed a 3.2°C-higher T_m, and showed a ninefold prolonged half-life at 45°C. Subsequently, a one-step simplified immobilization method was developed for encapsulation of PdSIV280L/S499F in food-grade *Corynebacterium glutamicum* cells to further enhance the recyclability of isomaltulose production. Recombinant cells expressing combinatorial mutant (RCSI2) were successfully immobilized in 2.5% sodium alginate without prior permeabilization. The immobilized RCSI2 showed that the maximum yield of isomaltulose by batch conversion reached to 453.0 g/L isomaltulose with a productivity of 41.2 g/l/h from 500.0 g/L sucrose solution, and the conversion rate remained 83.2% after 26 repeated batches.

KEYWORDS

thermostability, isomaltulose, sucrose isomerase, one-step simplified immobilization, repeated batches

Introduction

Currently, excessive sugar intake has led to people's weight gain and its associated health problems such as hyperlipidemia, hypertension, and diabetes (Olszewski et al., 2019). Exploring low-calorie functional sweeteners for food ingredients and additives has become a research hotspot (Novotny et al., 2019; Van Laar et al., 2021). Isomaltulose, an isomer of sucrose, is a reducing disaccharide. It exists in natural molasses in a small amount and has 45 percent of the sweetness of sucrose, but is non-toxic and non-cariogenic (Barea-Alvarez et al., 2014). Therefore, isomaltulose is an ideal sucrose substitute and is a Food Drug Administration certified healthy sugar, and its addition and consumption are not restricted (Linaa et al., 2002). In addition, isomaltulose has many beneficial healthcare functions and physiological properties, including inhibiting elevated blood sugar levels (Maresch et al., 2017), inhibiting fat accumulation (Lee et al., 2020), improving anti-fatigue ability (Stevenson et al., 2017), and maintaining the intestinal micro ecological balance (Kendall et al., 2018). However, the process of chemically synthesizing isomaltulose produces by-products and chemical waste, increasing the cost of product separation and wastewater treatment (Zhang et al., 2017). Therefore, the preparation of isomaltulose by biotransformation technology has been widely investigated in recent years (Liu et al., 2020).

Sucrose isomerase (SI, EC 5.4.99.11), be known as isomaltulose synthase, converts sucrose into isomaltulose or trehalulose along with glucose and fructose (Mu et al., 2014). Current investigations of SI are mainly in the mining of novel genes and property characterizations of SIs. Those currently-reported SIs showed limited thermostability during the biocatalysis process, such as the SI of *Klebsiella* sp. LX3, which has a 1.8 min half-life at 50°C (Li et al., 2011), SI of *Klebsiella pneumonia* lost its 40% relative activity after incubating at 50°C for 20 min (Aroonnual et al., 2007), and SI of Erwinia sp was completely inactivated after 24 h incubation at 30°C (Kawaguti and Harumi Sato, 2010). Based on our comparative analysis, PdSI from *Pantoea dispersa* have strong ability to converting sucrose to isomaltulose, and the reaction conditions are more suitable for industrial production than others sources, but its thermostability is still unsatisfactory in the industrial applications (Li et al., 2017; Zhang et al., 2019; Zheng et al., 2019). Therefore, modification at the molecular level to improve the thermostability of PdSI should be further investigated.

Protein engineering has been shown to be an effective approach to enhance the thermostability of enzymes and is subdivided into directed evolution, semi-rational design, and rational design (Stepankova et al., 2013). Although the irrational and semi-rational designs were powerful in enzyme modification at elevated temperatures (Tizei et al., 2016; Arnold, 2019), they are time-consuming and laborious. In contrast, rational design based on computer-aided has greatly accelerated scientific research's speed and success rate (Cui et al., 2020). Fold X, one of the most reliable computational design predictors, has been developed to predict beneficial substitutions related to thermal stability by rapidly evaluating the Gibbs free energy difference ($\Delta\Delta G$) (Guerois et al., 2002; Schymkowitz et al., 2005). Recently, FoldX has been used to improve the thermostability of many enzymes. Luo et al. (2016) obtained the best variant PoOPH$_{M9}$ with thermostability (T_{50}^{15}) of 67.6°C via hierarchical iteration mutagenesis. Bi et al. (2020) engineered thermophilic pullulanase using FoldX predictor, the T_m of mutant G692M increased by 3.8°C, and the half-life is 2.1-fold longer than the wild-type at 70°C. Wang et al. (2020) constructed a mutant (S142A/D217V/Q239F/S250Y) based on the FoldX algorithm, and the half-life of the combination mutant increased 41.7-fold at 60°C. Thus, *in silico* energy calculations (FoldX) may provide a clear guide for the molecular engineering of SI.

Besides, the production method of isomaltulose also affects the thermostability of SI to a certain extent. Immobilized enzymes or cells have become the main biocatalytic route for isomaltulose production, but immobilized enzymes still face high cost and tedious operation steps such as cell disruption and protein purification (Wu et al., 2015; Zhang et al., 2019). In contrast, immobilized cells have become an alternative approach. However, endotoxin or toxic cell wall pyrogens of non-food-grade hosts would be an obstacle to the green synthesis of isomaltulose. To solve the potential safety hazards, some researchers have introduced SIase genes into non-pathogenic hosts, including *Lactococcus lactis* MG1363 (Park et al., 2010), *Bacillus subtilis* WB800 (Wu et al., 2017), *Saccharomyces cerevisiae* (Lee et al., 2011), and *Yarrowia lipolytica* S47 (Zhang et al., 2018). However, *L. lactis* MG1363 (Park et al., 2010) exhibited a low expression level of SI (100 μg/mL), and *S. cerevisiae* (Lee et al., 2011) and *Y. lipolytica* (Zhang et al., 2018) grew slowly (48–96 h). *Corynebacterium glutamicum* ATCC13032 is listed as a "generally recognized as safe" microorganism and has been successfully used as a host for producing food compounds efficiently, like amino acids, vitamins, organic acids, and rare sugars (Shin et al., 2016). As far as we know, *C. glutamicum* has currently been used as a food-grade expression platform to produce the rare sugars and sugar alcohols, such as D-Tagatose (Shin et al., 2016), D-allulose (Yang et al., 2019), D-mannitol (Baumchen and Bringer-Meyer, 2007) and so on. However, due to the rigid cell wall structure of Gram-positive bacteria such as *C. glutamicum* and *Lactobacillus*, the catalytic efficiency is often affected by the transmembrane transport of substrates or products. Traditionally, cells need to be permeabilized before immobilization (Shin et al., 2016; Bober and Nair, 2019), but this process can cause cell lysis and waste time to prepare immobilized cells. Therefore, development of a one-step

simplified immobilized cell method has also become particularly important.

Herein, in order to obtain robust SI from a small mutation library via rational design, computational design software (FoldX5) combined with conservation analysis and functional region assessment was employed to predict potential candidates. Then, Differential Scanning Fluorimetry (DSF) and molecular dynamic simulation (MD) were used to evaluate the changes in the thermostability and elucidate the mechanism, respectively. Finally, the best variant was intracellularly overexpressed in the food-grade strain *C. glutamicum*, and recombinant cells were further immobilized by one-step simplified immobilization method for the sustainable production of isomaltulose. Taken together, combined strategies involving computational-aided design, rational engineering and immobilized cells in this work provide a strategy to improve its performance in industrial applications. As far as we know, this is the first report of the maximum batches of isomaltulose production using an immobilized engineered food-grade host.

Materials and methods

Reagents and enzymes

Sucrose, isomaltulose, and high-performance liquid chromatography (HPLC)-grade acetonitrile were bought from Aladdin (Shanghai, China). PrimSTAR Max DNA Polymerase, restriction enzymes, protein markers, and *Dpn*I were purchased from TaKaRa (Dalian, China). Isopropyl-β-D-thiogalactopyranoside and chloramphenicol were supplied by Yuanye Bio-Technology (Shanghai, China). Plasmid Mini Preparation Kit was provided by Beyotime (Shanghai, China). Other reagents were purchased from Sinopharm Chemical Reagent (Shanghai, China) unless otherwise noted.

Plasmids, strains, and medium

All plasmids and strains used in this study could be found in **Supplementary Table 1**. The original sequence of SI gene from the *Pantoea dispersa* UQ68J (*Pdsi*) (GenBank accession number: AY223549) without signal peptide was synthesized and sequenced by Suzhou GENEWIZ Company, and the C-terminal's 6xHis tag of *Pdsi* was used for protein purification. The *Pdsi* gene was incorporated between *Hind*III and *Eco*RI sites of the *Escherichia coli*/*C. glutamicum* shuttle plasmid pXMJ19 to generate pXMJ19-*pdsi*. *E. coli* strain JM109 was used as a gene cloning host to construct recombinant plasmids. *C. glutamicum* was used as an expression host to characterize enzymatic properties, and whole cells were used as biocatalysts for cell immobilization. *E. coli* cells were grown in LB medium at 37°C. *C. glutamicum* cells were grown on BHI medium at 30°C. Chloramphenicol was added if necessary to the final concentration of 25 μ g/mL.

Computational prediction for sucrose isomerase thermostability

As a starting point, the structure of wild-type (PdSIWT) and other mutants were modeled using the ERSI from *Erwinia rhapontici* NX5 (PDB: 4hph.1.A) as a template with 74.10% sequence identity by SWISS-MODEL (Xu et al., 2013), MolProbity (Chen et al., 2010) and PROCHECK (Laskowski et al., 1993) were applied for model evaluation, and evaluation results of PdSIWT are presented as Ramachandran plot (**Supplementary Figure 1**). Candidates for site-directed mutagenesis were identified based on ΔΔG changes. FoldX 3.0 algorithm was utilized to estimate the folding free energy of PdSIWT. A standardized script written in python was performed to change all positions of the protein sequence to other 19 amino acids. The relative folding free energy changes ($\Delta\Delta G = \Delta G_{Mut} - \Delta G_{WT}$) was calculated after each residue was mutated into the other amino acids.

Site-directed mutagenesis PCR

The plasmid pXMJ19-*pdsi* was used as an amplification template to construct the SI mutants by using overlap extension PCR. The primers used could be found in **Supplementary Table 2**. Final amplification fragments were digested by the endonuclease *Dpn* I at 37°C for 1.5 h. Then the PCR mixture was chemically transformed into *E. coli* JM109. The sequenced plasmids were transformed into *C. glutamicum* cells by electroporation for protein expression.

Expression and purification

The recombinant *C. glutamicum* strains were first cultivated into 10 mL BHI liquid medium supplemented with 25 μg/mL chloramphenicol at 30°C for overnight, and then 2% inoculation volume were transferred to 100 mL BHI medium. When the optical density at 600 nm was approximately 1.5, the expression of SI was induced with 0.5 mM IPTG at 30°C for another 20 h.

The cells were centrifuged (8,000 × *g*, 4°C) for 5 min, washed twice, and then resuspended in 10 mL of 50 mM citric acid-Na_2HPO_4 buffer (pH 6.0). Cells in suspension were sonicated for 20 min and centrifuged to remove cell debris. Subsequently, the soluble supernatant fractions were loaded onto a 1 mL Ni affinity column (GE Healthcare, HisTrap

HP) after filtration, and the column was pre-equilibrated with 50 mM wash buffer (20 mM Tris and 500 mM NaCl, pH 7.4) before loading samples. Finally, the target protein was eluted using an elution buffer (20 mM Tris, 500 mM NaCl, and 300 mM imidazole, pH 7.4) with a linear gradient. Sodium dodecyl sulfate-polyacrylamide gel electrophoresis (SDS-PAGE) was used to analyze purified protein. The concentration of protein was determined through the Bradford method.

Determination of enzyme activity

The isomaltulose-forming activity of PdSIWT and mutants was measured using 525 mM sucrose as substrate (pH 6.0). Specifically, 100 μL purified enzyme was incubated with 900 μL sucrose (584 mM) in 50 mM citric acid-Na_2HPO_4 buffer (pH 6.0), the reaction mixture was performed at 30°C for 10 min and was stopped by boiling at 100°C for 5 min. One unit (U) of SI activity was defined as the amount of SI required to catalyze the formation of 1 μmol isomaltulose per 1 min under the above conditions.

Determination of optimal pH and temperature

The optimal pH value for enzyme activity was assayed in 50 mM citric acid- Na_2HPO_4 buffer (pH 4.0–8.0) at 30°C. The optimal temperature was determined between 20 and 50°C in buffer (pH 6.0). Purified enzyme of PdSIWT and mutants were incubated at 45°C to determine thermostability. Samples were taken at 20 min intervals and the residual activity was then determined. The original activity before incubating at 45°C was taken as 100%. Each assay was repeated three times.

Determination of kinetic parameters

Kinetic parameters of purified enzymes were determined under standard assay conditions with sucrose as a substrate. The sucrose substrate concentrations were as follows: 14.6, 29.2, 58.4, 102.0, 146.0, 234.0, 292.0, and 584.0 mM, respectively. Then, V_{max} and K_m values were determined through regression fitting of experimental data using GraphPad Prism 8.0.

Differential scanning fluorescence assay

The DSF procedure used in this research was slightly modified (Bi et al., 2020). T_m values were determined by monitoring the maximum relative fluorescence intensity after incubating the purified protein and SYPRO Orange dye together in PCR tubes at elevated temperatures in the real-time PCR machine. T_m values were measured at 1°C/min rate over the range of 25 ~ 95°C. Three parallel samples were determined.

Bioinformatics analysis

Molecular dynamic simulations (MD) were performed by using YASARA software[1]. Specifically, PdSIWT and mutant's thermal fluctuations were analyzed using an Amber03 force field, and SI was surrounded by H_2O containing 0.29% NaCl with pH 6.0 in a dodecahedron box. ConSurf Server was employed to identify proteins' functional Regions (Berezin et al., 2004). Residue Interaction Network Generator was used to recognize various kinds of interactions introduced by the mutation in this study (Piovesan et al., 2016). ESPript 3.0 was mainly employed to analyze alignment sequence (Robert and Gouet, 2014).

Batch culture

RCSI was cultivated into 200 mL of seed medium in a 1 L shake flask and grown at 30°C for 15 h with shaking at 220 rpm. The seed medium (g/L) consisted of 0.4 $MgSO_4{\cdot}7H_2O$, 0.5 KH_2PO_4, 1.0 urea, 1.5 K_2HPO_4, 10.0 $(NH_4)_2SO_4$, 50.0 corn syrup, 10.0 angel yeast, 40.0 glucose, and the initial pH of the seed medium was 7.0. The seed culture (200 mL) was inoculated into 1.8 L sterilized fermentation medium (g/L) [150.0 glucose, 5.0 corn syrup, 20.0 angel yeast, 30.0 $(NH_4)_2SO_4$, 2.0 KH_2PO_4, 1.0 urea, 1.0 KCl, 0.5 $MgSO_4{\cdot}7H_2O$, 0.02 $ZnSO_4{\cdot}7H_2O$, 0.02 $FeSO_4{\cdot}7H_2O$, and 0.02 $MnSO_4{\cdot}H_2O$] of a 5 L fermenter (DIBIER, Shanghai, China). The temperature and pH were maintained at 30°C, 7.0, respectively. The final concentration of 0.5 mM IPTG was added to the fermenter to induce PDSI when the optical density reached 20 at 600 nm. The DO was kept at 30% (v/v) by coupling with the agitation speed. The 50% (V/V) ammonia solution was used to adjust the pH of the medium.

Preparation of immobilized *C. glutamicum* cells by a one-step simplified immobilization method

For the immobilization of the recombinant *C. glutamicum* cells (RCSI), approximately 150 g cells (wet weight) were mixed in 1 L of 2.5% sodium alginate solution containing 0.1% Triton X-100. After thoroughly mixing, the mixture was slowly dropped into 8% (w/v) $CaCl_2$ solution containing

1 http://www.yasara.org

25% sucrose to form 3.75 mm immobilized pellets using a needle. The pellets are stored at 4°C overnight in this solution, and then were washed with sterile distilled water to remove $CaCl_2$. Immobilized *C. glutamicum cells* were then used for the production of isomaltulose. In addition, parameters related to cell immobilization, such as the concentration of sodium alginate and $CaCl_2$ were optimized, mechanical strength was used to verify the hardness of immobilized pellets. Mechanical strength (g/cm^2) was measured by pressing 20 immobilized particles on an electronic balance and reading the maximum pressure they can withstand when they were broken.

Biosynthesis of isomaltulose using immobilized *C. glutamicum* cells in a 5 L fermenter

For biotransformation, immobilized *C. glutamicum* cells pellets (130 g/L) were washed three times with 50 mM citric acid-Na_2HPO_4 buffer (pH 6.0). The *C. glutamicum* cells pellets were then transferred into the 1.5 L reaction solution containing 500 g/L sucrose (pH 6.0, citric acid-Na_2HPO_4 buffer). The whole reaction process was carried out at 35°C for 11 h, and the speed is adjusted to 40 rpm to stir the reaction liquid in the catalytic process. Samples were collected at different time and further tested by HPLC. After each biotransformation, immobilized *C. glutamicum* cells pellets were recycled with simple centrifugation for the next batch.

High-performance liquid chromatography analysis

Samples were determined by HPLC (Agilent 1260, United States) system equipped with a refractive index detector (RID) and separated by an NH_2 column (DIKMA, platisil 5 μm NH_2, 250 mm × 4.6 mm). The mobile phase was 80% acetonitrile at a flow rate of 1.0 $mL{\cdot}min^{-1}$ at 30°C, and RID temperature was controlled at 35°C. The amounts of sugar concentration were calculated via peak areas.

Results and discussion

Selection of the mutagenesis sites for improving thermostability of sucrose isomerase

To rationally design the most promising mutants, FoldX was used to screen variant PdSI by calculating the relative folding free energy changes ($\Delta\Delta G$). When $\Delta\Delta G > 0$, it means that the structure of the mutant is more unstable than that of the wild type. While $\Delta\Delta G < 0$, the structure of the mutant is more stable. After calculation, $\Delta\Delta G$ values of all 10,982 single point mutations were obtained, and the mutation sites with $\Delta\Delta G < 0$ were selected as the candidates. To further improve the prediction accuracy by the FoldX algorithm, an additional conservation analysis was performed to avoid point mutation of amino acids at conserved positions resulting in loss of enzyme activity (Li et al., 2018). The Consurf Server, as an essential tool for evolutionary conservation analyses, can automatically estimate the conserved degree of amino acids in homologous sequences of SI (Berezin et al., 2004). When the amino acid is marked with the letter "f" or "s," it means that the amino acid is highly conserved in critical functional domains, that is, the residue is not suitable as a candidate for thermal stability modification. When the amino acid is marked with the letter "e" or "b," the amino acid is variable in functional domains and then the residue can be considered as a candidate for thermal stability modification (**Supplementary Figure 2**). Finally, ten mutations were selected for the subsequent experimental study after computation-aided engineering: PdSIE76R, PdSIA100E, PdSIG152P, PdSII205M, PdSIV280L, PdSIS328F, PdSIS499F, PdSIS563R, PdSIS563L, and

TABLE 1 The $\Delta\Delta G$ values of candidate mutants computed by FoldX, and special activity of mutants.

Position	Original amino acid	Mutant amino acid	$\Delta\Delta G$ value ($Kcal{\cdot}mol^{-1}$)	Specific activity ($U\ mg^{-1}$)
76	E	R	−1.94251	613 ± 3.3
100	A	E	−1.17737	620 ± 4.2
152	G	P	−2.26873	606 ± 3.7
205	I	M	−1.43737	438 ± 3.9
280	V	L	−1.68313	616 ± 3.5
328	S	F	−2.41961	533 ± 4.1
499	S	F	−1.57516	618 ± 2.7
563	S	L	−1.53936	282 ± 4.2
563	S	R	−1.57516	501 ± 4.2
578	N	M	−1.41972	595 ± 3.7

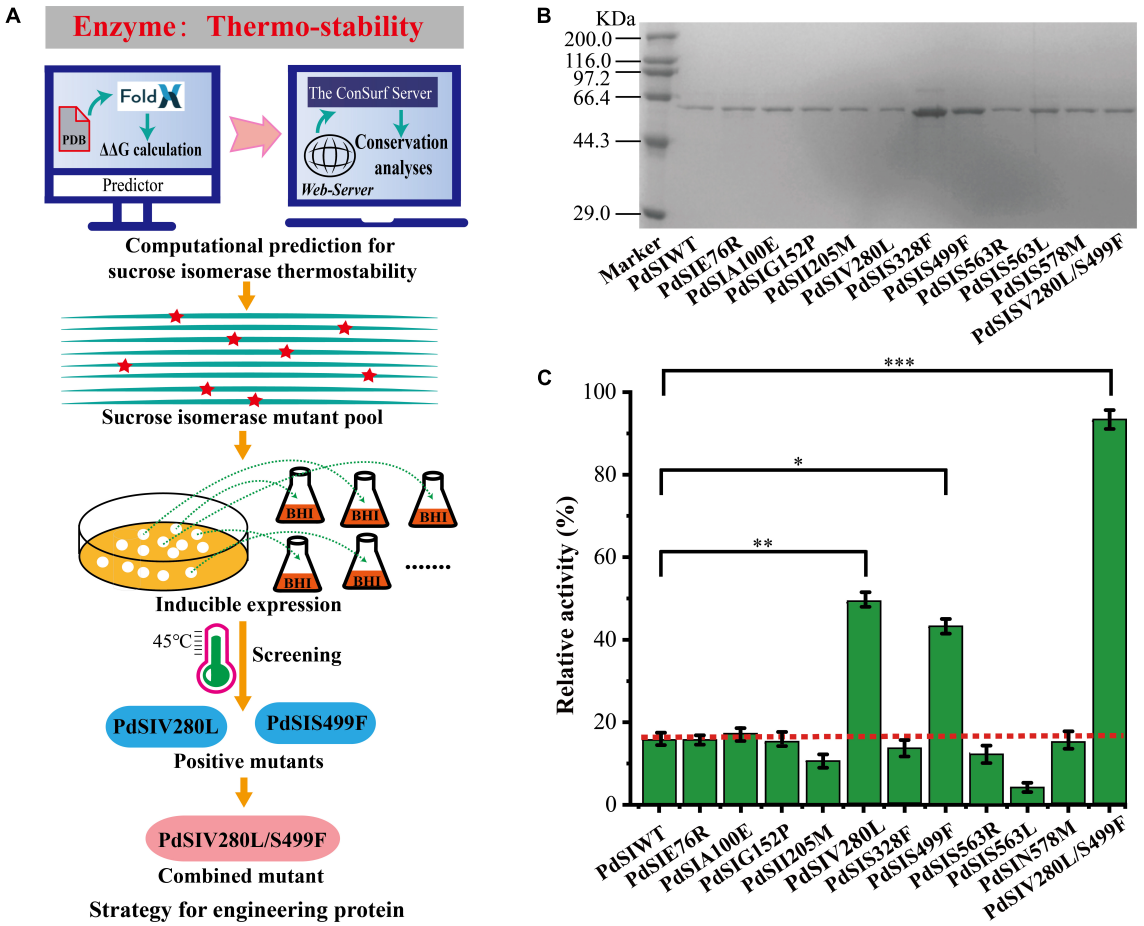

FIGURE 1
(A) The Flowchart for engineering sucrose isomerase. **(B)** SDS-PAGE shows the expression of mutants. **(C)** The residual activity of PdSIWT and its mutants after incubation at 45°C for 20 min. *p*-values are represented as follow: $^{*}P < 0.05$, $^{**}P < 0.01$, $^{***}P < 0.001$.

PdSIN578M (Table 1). The strategy of engineering SI thermostability is shown in Figure 1A.

Each single point mutation was individually expressed in *C. glutamicum* to test whether these substitution mutations improved the thermostability of PdSIWT (Figure 1B). To obtain positive mutants quickly, the thermostability of mutants was evaluated by determining the residual activity after heat treatment at 45°C for 20 min. As shown in Figure 1C, PdSIWT retained 15.7% (98.4 U/mg) of its initial activity, whereas two positive mutants PdSIV280L and PdSIS499F retained 49.1% (302.5 U/mg) and 43.2% (267.0 U/mg) of their original activity (Table 1), respectively. However, thermostability of other mutants did not change or decrease significantly. These results demonstrated that PdSIV280L and PdSIS499F show better thermostability than PdSIWT. To assess the possible interaction between these two single points, double mutant PdSIV280L/S499F was constructed and investigated. PdSIV280L/S499F retained 93.3% (581.3 U/mg) of its initial activity after incubating at 45°C for 20 min.

Enzymatic properties and kinetic analysis of PdSIV280L, PdSIS499F, and PdSIV280L/S499F

The thermostabilities and catalytic properties of the PdSIWT and positive mutants PdSIV280L, PdSIS499F, and PdSIV280L/S499F were further characterized. The optimal pH value of the three mutants was 5.5, similar to that of the PdSIWT (Figure 2A). Consistent with PdSIWT, these three positive mutants' optimal temperature was 30°C, while they exhibited higher relative activity at the same temperature (Figure 2B). At 45°C, PdSIWT retained 58.1% of its maximum activity, whereas mutants PdSIV280L, PdSIS499F, and PdSIV280L/S499F retained 61.8, 59.4, and 74.1% of its maximum activities, respectively.

Then, changes in thermostability of these three mutants and PdSIWT were assessed by determining residual activities after different incubation times at 45°C. As shown in Figure 2C, the thermostability of mutants was significant

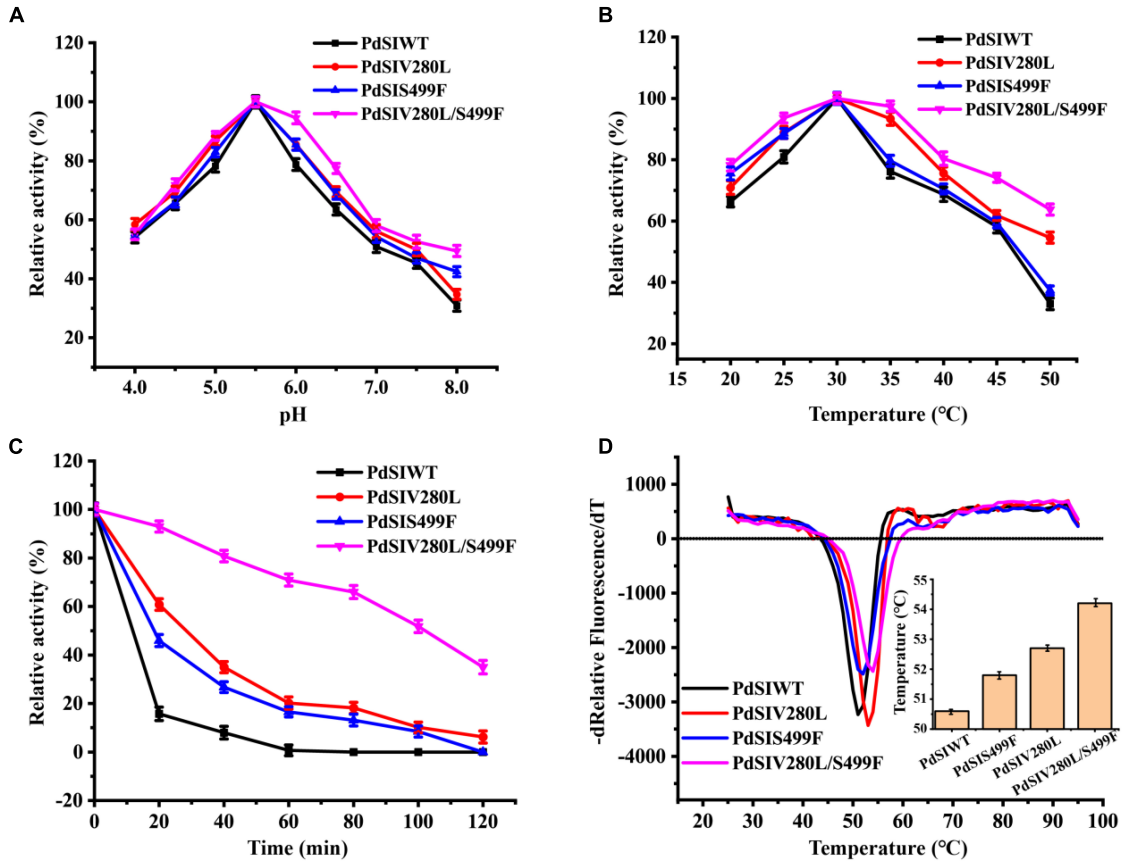

FIGURE 2
Effects of pH and temperature on the enzyme activity of PdSIWT and mutants. **(A)** The optimal reaction pH. **(B)** The optimal reaction temperature. **(C)** The thermostability of PdSIWT and positive mutants PdSIV280L, PdSIS499F, and PdSIV280L/S499F at 45°C. **(D)** The T_m of PdSIWT and mutants measured by DSF.

than that of PdSIWT, and PdSIV280L/S499F displayed the most significant improvement. At 45°C, the $t_{1/2}$ of PdSIWT was only 11.2 min. In contrast, the $t_{1/2}$ of PdSIV280L, PdSIS499F, and PdSIV280L/S499F were 25.4, 21.5, and 100.0 min, 2.3, 1.9, and 8.9 times better than PdSIWT. These findings thus indicated that two amino acid substitutions (V280L and S499F) were beneficial to improve the thermostability of PdSIWT.

To further evaluate the thermodynamic stability of PdSIWT and its variants, the melting temperature (T_m) was measured by DSF. As shown in Figure 2D, the T_m of PdSIWT was 50.6°C, while the T_m values of PdSIV280L, PdSIS499F, and PdSIV280L/S499F mutants were 52.7, 51.8, and 54.2°C, respectively. These results are consistent with the thermostability studies of the three positive mutants.

Kinetic parameters of the PdSIWT and its mutants were measured using different concentrations of sucrose as substrate. As listed in Table 2, three mutants showed slight differences in catalytic activity with PdSIWT. K_m and k_{cat}/K_m of these mutants also changed slightly, indicating that point mutations have little influence on enzyme properties while improving the thermostability.

TABLE 2 Comparison of wild-type (WT) PDSI and mutants enzymatic properties.

Enzyme	K_m (mM)	K_{cat} (S^{-1})	K_{cat}/K_m (S^{-1} mM^{-1})	T_m (°C)	$t_{1/2}$(min) (45°C)	Special activity (U mg^{-1})
WT PDSI	42.1 ± 1.8	712 ± 6.1	16.7 ± 1.2	50.6 ± 0.1	11.2	627 ± 2.1
V280L	44.1 ± 2.1	698 ± 7.2	15.8 ± 0.9	52.7 ± 0.2	25.4	616 ± 3.5
S499F	43.2 ± 1.5	701 ± 6.8	16.2 ± 1.1	51.8 ± 0.1	21.5	618 ± 2.7
V280L/S499F	42.8 ± 1.7	708 ± 6.5	16.5 ± 0.9	54.2 ± 0.3	100.0	623 ± 1.9

Structure analysis and molecular dynamic simulation of mutant enzymes for improving thermostability

To analyze the conformational change of the mutations caused by each substituted residue, the 3D structure of PdSIWT and mutants were modeled with the Swiss-Model protein automated modeling program. The tight packing of protein interiors plays a vital role in protein stability for the burial of both polar and non-polar groups, and one -CH_2- group buried on folding contributes 1.1 ± 0.5 kcal/mol of energy to protein stability (Nick Pace et al., 2014). As shown in **Figure 3B**, a single -CH_2- group was added to the side chain after mutating the amino acid Val to Leu at position 280. This seems to reveal that the introduction of alanine's bulky non-polar side chain may be responsible for improving the stability. In addition, an inspection of the structure model of the V280L showed that L280 was located in the α-helix (**Figure 3A**), and V280L substitution also generated two Vander Waals forces (VDW) bonds with Q329 and T330 of the other α-helix. Therefore, the two newly introduced VDW may also stabilize the local stability, thereby facilitating the geometry more stable. The thermostability of *Bacillus thermoleovorans* pullulanase was also successfully improved via the same strategy (Bi et al., 2020). Interestingly, all the amino acids at 280 sites from other sources were L except for V from the *P. dispersa* UQ68J through multiple sequence alignment (**Figure 3E**). Therefore, the increased thermostability of V280L mutant may also be related to the evolutionary conservatism of the enzyme (Pinney et al., 2021).

Previous studies have pointed out that molecular interactions, including hydrogen bonds, disulfide bonds, VDW, aromatic–aromatic interaction, and hydrophobic interaction, are the major structural factors that affect protein thermostability. In all of these factors, the contribution of hydrophobic interaction to protein stability accounts for about 60% (Gromiha et al., 2013). As shown in **Figure 3D**, a new

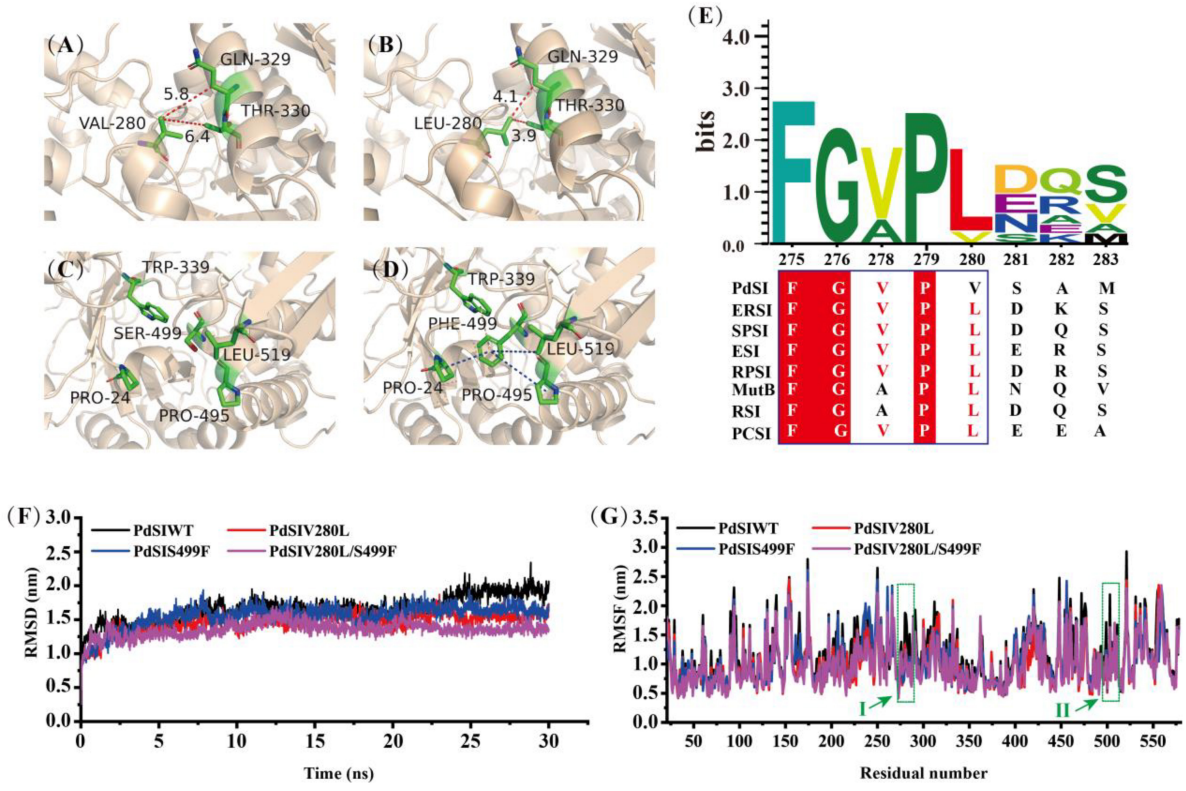

FIGURE 3
Structure analysis and Molecular dynamics simulations. **(A)** V280 was located in α-helix, forming two new VDWs with Q329 and W330 in mutant L280. **(B)** Reddish dashed lines refer to VDWs. **(D)** A new hydrophobic network including F499 and other residues (P24, W339, P495, and L519) was formed in S499 **(C)**, the hydrophobic interactions are shown as a blue dashed line, π-cation stacked interaction between Trp339 and Phe499 is shown as magentas line. **(E)** Multiple sequence alignment of Slases from different species. ERSI, *Erwinia rhapontici* NCPPB 1578; *Pantoea dispersa* UQ68J, PdSI; *Serratia plymuthica* PAMC26656, SPSI; ESI, *Enterobacter* sp. FMB-1; RPSI, *Raoultella planticola* UQ14S; MutB, *Pseudomonas mesoacidophila* MX-45; RSI, *Rhizobium* sp. MX-45 (M1E1F7); PCSI, *Pectobacterium carotovorum*. **(F)** The RMSD values of all backbone atoms for PdSIWT and mutants. **(G)** The RMSF values of each amino acid residue for PdSIWT and mutants. Letters I, II represent the amino acid position at site 280 and 499, respectively.

hydrophobic network formed for substituted residue from hydrophilic S (Figure 3C) to strong hydrophobic F at site 499, which contains four residues (P24, W339, P495, and L519) within 5 angstroms. Therefore, residue 499 greatly changed the hydrophobic stacking around the mutation, enhancing the hydrophobic interaction effect. In addition, a cation–π interaction between F499 and W339 was found after mutation, which may further improve the thermostability of PdSIS499F. In summary, the improved thermostability of mutant PdSIS499F may result from the hydrophobic interactions and cation–π interaction. Moreover, no new molecular interactions were introduced into the double mutant PdSIV280L/S499F. Maybe the synergistic effect of these two single point mutations further promoted the improvement of stability of the double mutant.

In order to further clarify the overall structural rigidity of the enzyme and the fluctuation changes of each amino acid residue, we conducted MD of PdSIWT and three mutants (PdSIV280L, PdSIS499F, and PdSIV280L/S499F) at 318K for 30 ns in this study. Root mean square deviation (RMSD) and root mean square fluctuation (RMSF) represents the degree of molecular structure change and freedom of movement of individual atoms in a molecule, respectively. As shown in Figure 3F, the RMSD of all systems no longer fluctuates drastically after 13 ns, and then RMSD varied around 1.5 nm. After equilibration at 318 K, the average values of PdSIWT was 1.659 nm, whereas the average values of three mutants (PdSIV280L, PdSIS499F, and PdSIV280L/S499F) declined to 1.457, 1.520, and 1.353 nm, respectively. Since the thermostability of protein is not positively correlated with its RMSD value, the lower RMSD value of mutants indicated the mutated structure was relatively stable than that of the PdSIWT.

Similarly, RMSF could also reflect the local flexibility of the protein. One region has a higher RMSF value, indicates that the conformation of this region was more unstable. As shown in Figure 3G, some regions around residue V280, S499 showed significant fluctuations in RMSF values of PdSIWT at 318 K. Generally, these amino acids were thought to be thermo-unstable. On the contrary, RMSF of three mutants (PdSIV280L, PdSIS499F, and PdSIV280L/S499F) showed mild fluctuations in the same areas of PdSIWT mentioned above. In conclusion, mutations in these sites (V280 and S499) contribute significantly to improving the stability of PdSIWT.

Development of a one-step simplified immobilization method for *C. glutamicum* cells

To develop an economically feasible immobilization method for *C. glutamicum* cells, several different immobilization methods were investigated in this work. As shown in Figure 4A, the traditional immobilization of *C. glutamicum* cells usually requires centrifugation followed by permeabilization, which is cumbersome in industrial production (a). Therefore, reducing the operation steps of immobilization is more in line with the requirements of industrial production (b). After research and comparison (Figure 4B), it was found that shortening the process of immobilization did not affect the catalytic effect, and even the catalytic efficiency was better than that of traditional immobilization. The relative activity of the control (without permeabilization) and a (pre-permeabilization) reached 73.3 and 97.2%, respectively, compared to the b (without pre-permeabilization) in this study.

To further optimize the preparation of immobilized *C. glutamicum* cells, we further optimized the concentration of sodium alginate and $CaCl_2$. As shown in Figure 4C, an increase of initial sodium alginate concentrations from 2.0 to 2.5% increased the conversion rate and mechanical strength (435 g/cm^2). However, the mechanical strength (435 g/cm^2) stopped increasing and the conversion rate began to decline, when the initial sodium alginate concentrations exceeded 2.5%. Also, the concentration of $CaCl_2$ plays a huge role. As shown in Figure 4D, the mechanical strength is greatly affected by the concentration of $CaCl_2$, increasing concentrations of $CaCl_2$ from 4.0 to 8.0% markedly increased the conversion rate and mechanical strength. At 8.0%, the conversion rate and mechanical strength (485 g/cm^2) are optimal. Thus, the subsequent preparation of immobilized *C. glutamicum* cells was carried out under this condition.

Optimization of reaction conditions for the immobilized RCSI1 and RCSI2 biotransformation

To optimize the biocatalytic conditions for isomaltulose production, the influence of temperature, pH as variables were explored using immobilized RCSI1 (recombinant cells expressing wild-type SI) and RCSI2. As shown in Figure 5A, the optimum pH of immobilized RCSI1 and RCSI2 was pH 6.0, no noticeable changes were detected in the optimum pH conditions. However, shift in the optimal temperature was observed between immobilized RCSI1 and RCSI2, the relative activity of RCSI1 was highest at 30°C, while the maximum catalytic activity of RCSI2 was at 35°C (Figure 5B). At the same time, we also observed that immobilized RCSI2 exhibited a broad catalytic capacity in the range of 25–35°C. Therefore, the phenomenon may be attributed to the differences in the micro-environment after encapsulating the engineered thermostable PdSIV280L/S499F into immobilized recombinant *C. glutamicum* cells.

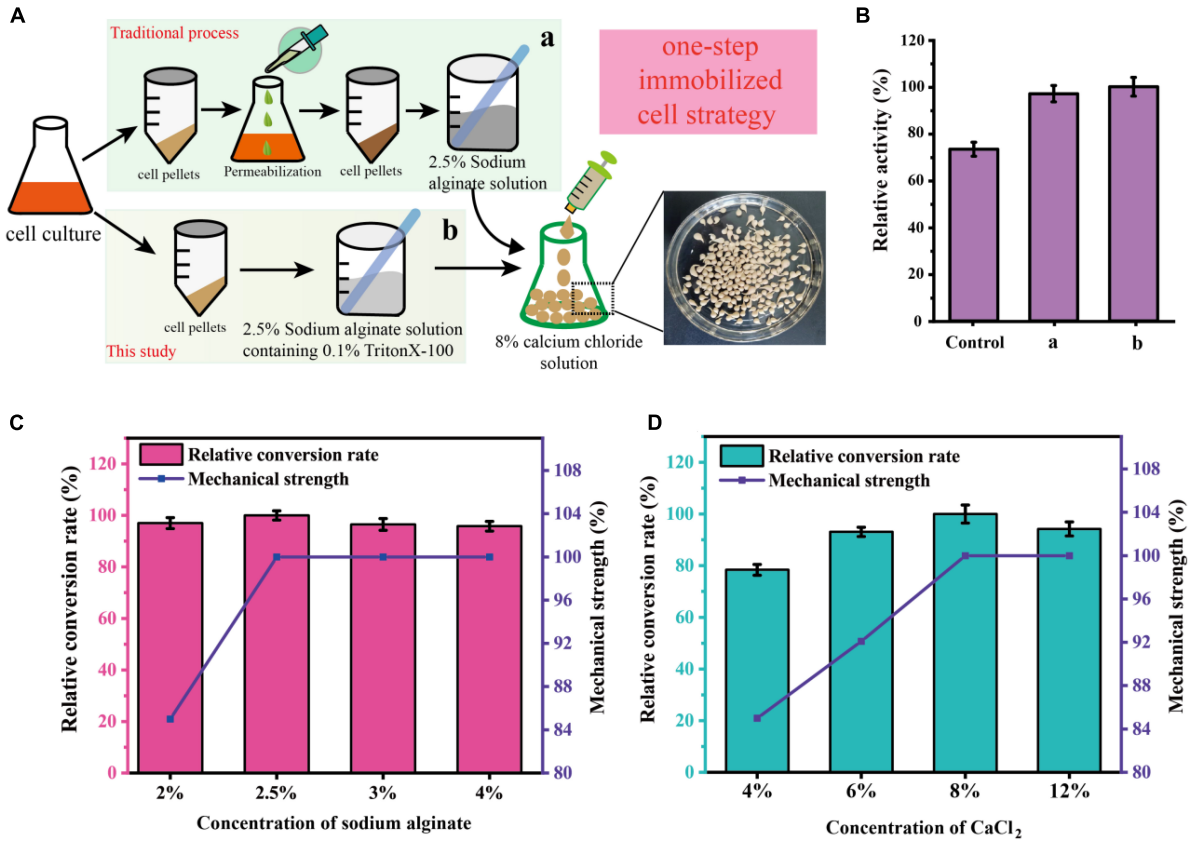

FIGURE 4
Schematic representation of the immobilization of *C. glutamicum* cells using a one-step simplified method. **(A)** Procedures for immobilization of *C. glutamicum* cells. **(B)** Comparison of different immobilization methods. [Control: without cell permeabilization, (a) cell pre-permeabilization with 0.1% triton-X100 before immobilization, (b) 2.5% Sodium alginate solution containing 0.1% triton-X100 was used for cell immobilization]. **(C)** Effect of different sodium alginate concentrations on sucrose conversion and mechanical strength of immobilized pellets. **(D)** Effect of different $CaCl_2$ concentrations on sucrose conversion and mechanical strength of immobilized pellets.

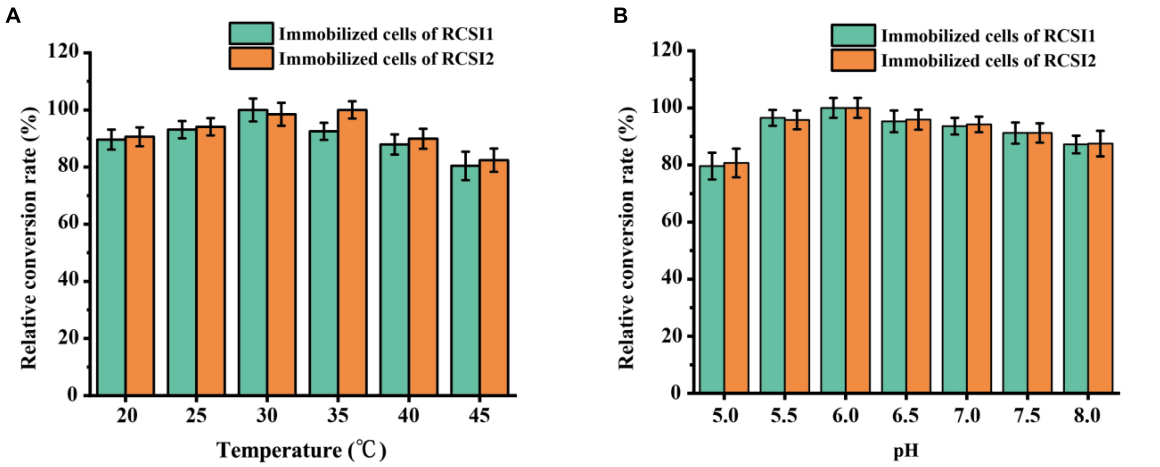

FIGURE 5
Optimization of biotransformation conditions for isomaltulose production using immobilized *C. glutamicum* cells. **(A)** Effect of temperature. **(B)** Effect of pH.

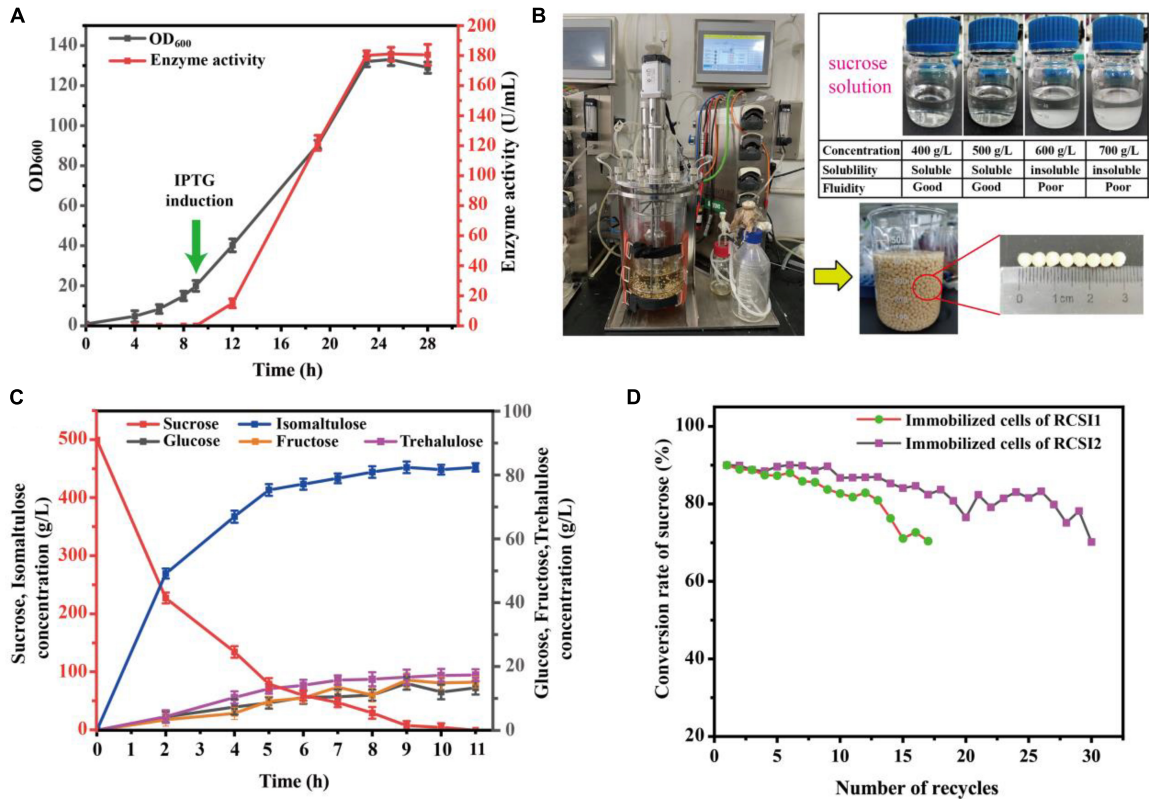

FIGURE 6
Batch culture and biotransformation were performed in a 5 L fermenter. **(A)** Batch culture of strain RCSI2 in a 5 L bioreactor. **(B)** Efficient production of isomaltulose using immobilized *C. glutamicum* cells in 5 L fermenter. **(C)** Time course of the isomaltulose production from the sucrose in 5 L fermenter. **(D)** Sustainable synthesis of isomaltulose using immobilized *C. glutamicum* cells.

TABLE 3 Comparison of isomaltulose yield in different food grade strains.

Strains	Concentration of sucrose (g/L)	Yield of isomaltulose (g/L)	Productivity (g/l/h)	Number of rescue	Conversion rate	References
Immobilized Enzyme						
Y Yarrowia lipolytica XY	–	–	–	13	~80%	Zhang et al., 2019
Whole-cell						
Yarrowia lipolytica S47	600	572.1	23.83	1	95%	Zhang et al., 2018
B. subtilis	230.1	221.6	36.9	12	~80%	Wu et al., 2017
Yarrowia lipolytica CGMCC7326	500	460	32.8	12	~80%	Li et al., 2017
S. cerevisiae	50	<4	0.09	1	<0.08	Lee et al., 2011
L. lactis	50	36	0.75	1	72%	Park et al., 2010
Corynebacterium glutamicum	500	453	41.2	26	83.2%	This study

Batch culture of RCSI2 and sustainable synthesis of isomaltulose in a 5 L fermenter

Batch culture of strain RCSI2 was tested in a 5 L fermentor. The DO was controlled at 30% during the whole process by coupling the rotation. As shown in Figure 6A, the cell density of OD_{600} increased to 19.3 in initially 9 h, and then IPTG was supplemented to the bioreactor at a final concentration of 0.5 mM to induce the expression of SI at this time. Subsequently, the biomass increases rapidly, OD_{600} increased to 132.2 and the total enzyme activity reaches 180.2 U/mL in 23 h. After 28 h, the cell density of OD_{600} started to drop to 129.5, and the enzyme activity (180.2 U/mL) no longer

increased at this time. Finally, the cells were centrifuged for subsequent immobilization.

Based on the above results, one-batch biocatalysis process was applied to transform sucrose to isomaltulose in a 5 L fermenter using immobilized RCSI2 cells. However, limited by the solubility of the substrate (**Figure 6B**), 500.0 g/L sucrose was selected for isomaltulose production in this study. As shown in **Figure 6C**, the reaction time-course curves, consisting of isomaltulose production and by-product glucose and fructose accumulation, are illustrated. The concentration of isomaltulose increased rapidly for the first 6 h and gradually reached a plateau after 11 h. To be specific, the maximum yield of isomaltulose reached 453.0 g/L in 11 h with a conversion rate of 90.6% (w/w) and a productivity of 41.2 g/L/h. At the same time, 13.3g/L glucose, 15.1 g/L fructose and 17.3 g/L trehalulose were produced as byproduct during the reaction.

To increase isomaltulose productivity and save the cost of culturing bacteria, the sustainable catalytic reaction of immobilized cells was evaluated. As depicted in **Figure 6D**, the immobilized RCSI2 exhibited robust and excellent operational stability with a total reaction batches up to 30 and maintained more than 83.2% of the initial isomaltulose productivity even after 26 batches of repeated utilization. However, the conversion rate of RCSI1 decreased to 71.1% after 15 batches. Therefore, we successfully obtained a recombinant GRAS strain with the highest operational stability. The productivity was also the highest reported among the food-grade strains (**Table 3**), still 1.1 times higher than the highest previous study on recombinant *B. subtilis* strains.

Conclusion

The outstanding thermostability of SI has always been pursued in successful industrial manufacturing bioprocess for isomaltulose, as even a slight enhancement can improve long-term activity under reaction conditions and increase the ability to remain high activity in the biotransformation. In this work, the thermal stability of SI from *P. dispersa* UQ 68J toward sucrose isomerization was greatly improved via rational engineering utilizing computer-aided design and conservation analysis and functional region assessment. We gained a robust variant PdSIV280L/S499F, which displayed a 3.6°C increase in apparent melting temperature and about ninefold longer half-life at 45°C compared to PdSIWT. More importantly, we characterized the reason underlying increased thermostability systemically. These results showed that the comprehensive strategy is a versatile and efficient method to improve the thermostability of enzymes without extensive experiment. In addition to the properties of the enzyme itself, the catalytic method is equally important. Immobilized cell transformation is the most promising catalytic method for industrial production of isomaltulose, which cannot only improve long-term activity under optimum conditions, but also facilitates sustainable production. However, immobilization of Gram-positive bacterial cells is still complicated and tedious. Therefore, we also developed a one-step simplified cell immobilization, the immobilized RCSI2 catalyst exhibits robustness and continuous operational stability in isomaltulose production, the conversion rate remained at 83.2% even after 26 continuous rounds of biocatalysis. In conclusion, protein engineering coupled with a one-step immobilized cell strategy provides an effective method to enhance the high yield of isomaltulose in this study.

Data availability statement

The datasets presented in this study can be found in online repositories. The names of the repository/repositories and accession number(s) can be found in the article/**Supplementary material**.

Author contributions

MH designed and performed the experiments and wrote manuscript. ZW and FL analyzed bioinformatics data. MS, MX, TY, and RZ performed investigation and resources. XZ edited and revised the manuscript. ZR provided project administration and funding acquisition. All authors contributed to the article and approved the submitted version.

Funding

This work was supported by the National Key Research and Development Program of China (No. 2021YFC2100900), National Natural Science Foundation of China (Nos. 32171471 and 32071470), the Postgraduate Research & Practice Innovation Program of Jiangsu Province (KYCX21_2026), and Key Research and Development Project of Shandong Province, China (No. 2019JZZY020605).

Conflict of interest

The authors declare that the research was conducted in the absence of any commercial or financial relationships that could be construed as a potential conflict of interest.

Publisher's note

All claims expressed in this article are solely those of the authors and do not necessarily represent those

of their affiliated organizations, or those of the publisher, the editors and the reviewers. Any product that may be evaluated in this article, or claim that may be made by its manufacturer, is not guaranteed or endorsed by the publisher.

Supplementary material

The Supplementary Material for this article can be found online at: https://www.frontiersin.org/articles/10.3389/fmicb.2022.979079/full#supplementary-material

References

Arnold, F. H. (2019). Innovation by evolution: bringing new chemistry to life (Nobel Lecture). *Angew. Chem. Int. Ed. Engl.* 58, 14420–14426. doi: 10.1002/anie.201907729

Aroonnual, A., Nihira, T., Seki, T., and Panbangred, W. (2007). Role of several key residues in the catalytic activity of sucrose isomerase from *Klebsiella pneumoniae* NK33-98-8. *Enzyme Microbial Technol.* 40, 1221–1227. doi: 10.1016/j.enzmictec.2006.09.011

Barea-Alvarez, M., Benito, M. T., Olano, A., Jimeno, M. L., and Moreno, F. J. (2014). Synthesis and characterization of isomaltulose-derived oligosaccharides produced by transglucosylation reaction of *Leuconostoc mesenteroides* dextransucrase. *J. Agric. Food Chem.* 62, 9137–9144. doi: 10.1021/jf5033735

Baumchen, C., and Bringer-Meyer, S. (2007). Expression of glf Z.m. increases D-mannitol formation in whole cell biotransformation with resting cells of *Corynebacterium glutamicum*. *Appl. Microbiol. Biotechnol.* 76, 545–552. doi: 10.1007/s00253-007-0987-988

Berezin, C., Glaser, F., Rosenberg, J., Paz, I., Pupko, T., Fariselli, P., et al. (2004). ConSeq: the identification of functionally and structurally important residues in protein sequences. *Bioinformatics* 20, 1322–1324. doi: 10.1093/bioinformatics/bth070

Bi, J., Chen, S., Zhao, X., Nie, Y., and Xu, Y. (2020). Computation-aided engineering of starch-debranching pullulanase from *Bacillus thermoleovorans* for enhanced thermostability. *Appl. Microbiol. Biotechnol.* 104, 7551–7562. doi: 10.1007/s00253-020-10764-z

Bober, J. R., and Nair, N. U. (2019). Galactose to tagatose isomerization at moderate temperatures with high conversion and productivity. *Nat. Commun.* 10:4548. doi: 10.1038/s41467-019-12497-12498

Chen, V. B., Arendall, W. B. III, Headd, J. J., Keedy, D. A., Immormino, R. M., Kapral, G. J., et al. (2010). MolProbity: all-atom structure validation for macromolecular crystallography. *Acta Crystallogr. D. Biol. Crystallogr.* 66(Pt 1), 12–21. doi: 10.1107/S0907444909042073

Cui, H., Cao, H., Cai, H., Jaeger, K. E., Davari, M. D., and Schwaneberg, U. (2020). Computer-Assisted recombination (CompassR) teaches us how to recombine beneficial substitutions from directed evolution campaigns. *Chemistry* 26, 643–649. doi: 10.1002/chem.201903994

Gromiha, M. M., Pathak, M. C., Saraboji, K., Ortlund, E. A., and Gaucher, E. A. (2013). Hydrophobic environment is a key factor for the stability of thermophilic proteins. *Proteins* 81, 715–721. doi: 10.1002/prot.24232

Guerois, R., Nielsen, J. E., and Serrano, L. (2002). Predicting changes in the stability of proteins and protein complexes: a study of more than 1000 mutations. *J. Mol. Biol.* 320, 369–387. doi: 10.1016/s0022-2836(02)00442-444

Kawaguti, H. Y., and Harumi Sato, H. (2010). Effect of concentration and substrate flow rate on isomaltulose production from sucrose by *Erwinia sp.* cells immobilized in calcium-alginate using packed bed reactor. *Appl. Biochem. Biotechnol.* 162, 89–102. doi: 10.1007/s12010-009-8899-y

Kendall, F. E., Marchand, O., Haszard, J. J., and Venn, B. J. (2018). The comparative effect on satiety and subsequent energy intake of ingesting sucrose or isomaltulose sweetened trifle: a randomized crossover trial. *Nutrients* 10:1504. doi: 10.3390/nu10101504

Laskowski, R. A., MacArthur, M. W., Moss, D. S., and Thornton, J. M. (1993). PROCHECK - a program to check the stereochemical quality of protein structures. *J. App. Cryst.* 26, 283–291. doi: 10.1006/jmbi.1996.0663

Lee, G. Y., Jung, J. H., Seo, D. H., Hansin, J., Ha, S. J., Cha, J., et al. (2011). Isomaltulose production via yeast surface display of sucrose isomerase from *Enterobacter sp* FMB-1 on *Saccharomyces cerevisiae*. *Bioresour. Technol.* 102, 9179–9184. doi: 10.1016/j.biortech.2011.06.081

Lee, S. J., Yu, W. K., Park, H. R., Kim, H., Kim, J. H., Park, J., et al. (2020). Improved effect of palatinose syrup bioconverted from sucrose on hyperglycemia and regulation of hepatic lipogenesis in male C57BL/6J mice. *J. Food Biochem.* 44:e13201. doi: 10.1111/jfbc.13201

Li, L. J., Wang, H. W., Cheng, H. R., and Deng, Z. X. (2017). Isomaltulose production by yeast surface display of sucrose isomerase from Pantoea dispersa on *Yarrowia lipolytica*. *J. Funct. Foods* 32, 208–217. doi: 10.1016/j.jff.2017.02.036

Li, R., Wijma, H. J., Song, L., Cui, Y., Otzen, M., Tian, Y., et al. (2018). Computational redesign of enzymes for regio- and enantioselective hydroamination. *Nat. Chem. Biol.* 14, 664–670. doi: 10.1038/s41589-018-0053-50

Li, S., Cai, H., Qing, Y., Ren, B., Xu, H., Zhu, H., et al. (2011). Cloning and characterization of a sucrose isomerase from *Erwinia rhapontici* NX-5 for isomaltulose hyperproduction. *Appl. Biochem. Biotechnol.* 163, 52–63. doi: 10.1007/s12010-010-9015-z

Linaa, B. A. R., Jonkera, D., and Kozianowskib, G. (2002). Isomaltulose (Palatinose1): a review of biological and toxicological studies. *Food Chem. Toxicol.* 40, 1375–1381.

Liu, L., Bilal, M., Luo, H., Zhao, Y., and Duan, X. (2020). Studies on biological production of isomaltulose using sucrose isomerase: current status and future perspectives. *Catalysis Lett.* 151, 1868–1881. doi: 10.1007/s10562-020-03439-x

Luo, X. J., Zhao, J., Li, C. X., Bai, Y. P., Reetz, M. T., Yu, H. L., et al. (2016). Combinatorial evolution of phosphotriesterase toward a robust malathion degrader by hierarchical iteration mutagenesis. *Biotechnol. Bioeng.* 113, 2350–2357. doi: 10.1002/bit.26012

Maresch, C. C., Petry, S. F., Theis, S., Bosy-Westphal, A., and Linn, T. (2017). Low glycemic index prototype isomaltulose-update of clinical trials. *Nutrients* 9:381. doi: 10.3390/nu9040381

Mu, W. M., Li, W. J., Wang, X., Zhang, T., and Jiang, B. (2014). Current studies on sucrose isomerase and biological isomaltulose production using sucrose isomerase. *Appl. Microbiol. Biotechnol.* 98, 6569–6582. doi: 10.1007/s00253-014-5816-5812

Nick Pace, C., Scholtz, J. M., and Grimsley, G. R. (2014). Forces stabilizing proteins. *FEBS Lett.* 588, 2177–2184. doi: 10.1016/j.febslet.2014.05.006

Novotny, O., Dufosse, T., and Davidek, T. (2019). Unexpected potential of iso-oligosaccharides in the generation of important food odorants. *J. Agric. Food Chem.* 67, 2954–2962. doi: 10.1021/acs.jafc.8b07100

Olszewski, P. K., Wood, E. L., Klockars, A., and Levine, A. S. (2019). Excessive consumption of sugar: an insatiable drive for reward. *Curr. Nutr. Rep.* 8, 120–128. doi: 10.1007/s13668-019-0270-275

Park, J. Y., Jung, J. H., Seo, D. H., Ha, S. J., Yoon, J. W., Kim, Y. C., et al. (2010). Microbial production of palatinose through extracellular expression of a sucrose isomerase from *Enterobacter sp*. FMB-1 in *Lactococcus lactis* MG1363. *Bioresour Technol.* 101, 8828–8833. doi: 10.1016/j.biortech.2010.06.068

Pinney, M. M., Mokhtari, D. A., Akiva, E., Yabukarski, F., Sanchez, D. M., Liang, R., et al. (2021). Parallel molecular mechanisms for enzyme temperature adaptation. *Science* 371:eaay2784. doi: 10.1126/science.aay2784

Piovesan, D., Minervini, G., and Tosatto, S. C. (2016). The RING 2.0 web server for high quality residue interaction networks. *Nucleic Acids Res.* 44, W367–W374. doi: 10.1093/nar/gkw315

Robert, X., and Gouet, P. (2014). Deciphering key features in protein structures with the new ENDscript server. *Nucleic Acids Res.* 42, W320–W324. doi: 10.1093/nar/gku316

Schymkowitz, J., Borg, J., Stricher, F., Nys, R., Rousseau, F., and Serrano, L. (2005). The FoldX web server: an online force field. *Nucleic Acids Res.* 33, W382–W388. doi: 10.1093/nar/gki387

Shin, K. C., Sim, D. H., Seo, M. J., and Oh, D. K. (2016). Increased production of food-grade d-tagatose from d-galactose by permeabilized and immobilized cells of *Corynebacterium glutamicum*, a GRAS host, expressing d-galactose isomerase

from *Geobacillus thermodenitrificans*. *J. Agric. Food Chem.* 64, 8146–8153. doi: 10.1021/acs.jafc.6b03588

Stepankova, V., Bidmanova, S., Koudelakova, T., Prokop, Z., Chaloupkova, R., and Damborsky, J. (2013). Strategies for stabilization of enzymes in organic solvents. *ACS Catalysis* 3, 2823–2836. doi: 10.1021/cs400684x

Stevenson, E. J., Watson, A., Theis, S., Holz, A., Harper, L. D., and Russell, M. (2017). A comparison of isomaltulose versus maltodextrin ingestion during soccer-specific exercise. *Eur. J. Appl. Physiol.* 117, 2321–2333. doi: 10.1007/s00421-017-3719-3715

Tizei, P. A., Csibra, E., Torres, L., and Pinheiro, V. B. (2016). Selection platforms for directed evolution in synthetic biology. *Biochem. Soc. Trans.* 44, 1165–1175. doi: 10.1042/BST20160076

Van Laar, A. D. E., Grootaert, C., and Van Camp, J. (2021). Rare mono- and disaccharides as healthy alternative for traditional sugars and sweeteners? *Crit. Rev. Food Sci. Nutr.* 61, 713–741. doi: 10.1080/10408398.2020.1743966

Wang, R., Wang, S., Xu, Y., and Yu, X. (2020). Enhancing the thermostability of Rhizopus chinensis lipase by rational design and MD simulations. *Int. J. Biol. Macromol.* 160, 1189–1200. doi: 10.1016/j.ijbiomac.2020.05.243

Wu, L., Wu, S., Qiu, J., Xu, C., Li, S., and Xu, H. (2017). Green synthesis of isomaltulose from cane molasses by Bacillus subtilis WB800-pHA01-palI in a biologic membrane reactor. *Food Chem.* 229, 761–768. doi: 10.1016/j.foodchem.2017.03.001

Wu, L. T., Liu, Y., Chi, B., Xu, Z., Feng, X. H., Li, S., et al. (2015). An innovative method for immobilizing sucrose isomerase on epsilon-poly-L-lysine modified mesoporous TiO2. *Food Chem.* 187, 182–188. doi: 10.1016/j.foodchem.2015.04.072

Xu, Z., Li, S., Li, J., Li, Y., Feng, X., Wang, R., et al. (2013). The structural basis of *Erwinia rhapontici* isomaltulose synthase. *PLoS One* 8:e74788. doi: 10.1371/journal.pone.0074788

Yang, J., Tian, C., Zhang, T., Ren, C., Zhu, Y., Zeng, Y., et al. (2019). Development of food-grade expression system for d-allulose 3-epimerase preparation with tandem isoenzyme genes in *Corynebacterium glutamicum* and its application in conversion of cane molasses to D-allulose. *Biotechnol. Bioeng.* 116, 745–756. doi: 10.1002/bit.26909

Zhang, P., Wang, Z. P., Liu, S., Wang, Y. L., Zhang, Z. F., Liu, X. M., et al. (2019). Overexpression of secreted sucrose isomerase in *Yarrowia lipolytica* and its application in isomaltulose production after immobilization. *Int. J. Biol. Macromol.* 121, 97–103. doi: 10.1016/j.ijbiomac.2018.10.010

Zhang, P., Wang, Z. P., Sheng, J., Zheng, Y., Ji, X. F., Zhou, H. X., et al. (2018). High and efficient isomaltulose production using an engineered *Yarrowia lipolytica* strain. *Bioresour. Technol.* 265, 577–580. doi: 10.1016/j.biortech.2018.06.081

Zhang, W., Zhang, T., Jiang, B., and Mu, W. (2017). Enzymatic approaches to rare sugar production. *Biotechnol. Adv.* 35, 267–274. doi: 10.1016/j.biotechadv.2017.01.004

Zheng, Y., Wang, Z., Ji, X., and Sheng, J. (2019). Display of a sucrose isomerase on the cell surface of *Yarrowia lipolytica* for synthesis of isomaltulose from sugar cane by-products. *3 Biotech* 9:179. doi: 10.1007/s13205-019-1713-1719

frontiers | Frontiers in Microbiology

TYPE Original Research
PUBLISHED 11 January 2023
DOI 10.3389/fmicb.2022.1107092

OPEN ACCESS

EDITED BY
Yu Xia,
Jiangnan University,
China

REVIEWED BY
Shuangping Liu,
Jiangnan University,
China
Teodora Coldea,
University of Agricultural Sciences and Veterinary Medicine of Cluj-Napoca,
Romania

*CORRESPONDENCE
Ming Hui
huiming@haut.edu.cn

SPECIALTY SECTION
This article was submitted to Food Microbiology, a section of the journal Frontiers in Microbiology

RECEIVED 24 November 2022
ACCEPTED 19 December 2022
PUBLISHED 11 January 2023

CITATION
Xiao R, Liu M, Tian Q, Hui M, Shi X and Hou X (2023) Physical and chemical properties, structural characterization and nutritional analysis of kefir yoghurt. *Front. Microbiol.* 13:1107092. doi: 10.3389/fmicb.2022.1107092

Physical and chemical properties, structural characterization and nutritional analysis of kefir yoghurt

Ran Xiao[1], Ming Liu[1], Qing Tian[1], Ming Hui[1,2]*, Xin Shi[1] and Xiaoge Hou[1]

[1]College of Biological Engineering, Henan University of Technology, Zhengzhou, Henan, China, [2]Industrial Microorganism Preservation and Breeding Henan Engineering Laboratory, Zhengzhou, Henan, China

Scanning electron microscopy (SEM), Confocal laser scanning microscopy (CLSM) and low field nuclear magnetic resonance (LF-NMR) were used to analyse the relationship between the chemical, texture, rheology, microstructure and water distribution of kefir (yeast, acetic acid bacteria and *Lactobacillus plantarum*) yoghurt fermented by mixed bacteria and *L. plantarum* L_1 fermented yoghurt. This work was conducted to prepare a real champagne yoghurt and explore the difference between it and ordinary yoghurt. The nutritional evaluation of the two treatment groups was carried out by amino acid analysis, and the volatile flavour substances of the two treatment groups were detected by solid phase microextraction (SPME)–gas chromatograph (GC)–mass spectrometry (MS). Results showed that the addition of acetic acid bacteria and yeast increased the water content of kefir, resulting in a decrease in its water-holding rate. Moreover, the increase in acidity weakened the connection between the protein networks, the flocculent protein structure was not more densely stacked than the L_1 group, and the internal bonds were unstable. The rheological results showed that the apparent viscosity decreased faster with the increase in shear force. The CLSM and LF-NMR showed that the hydration and degree of freedom of kefir yoghurt protein decreased, resulting in an increased protein network density. The SEM showed that the cross-linking between kefir casein clusters was considerably tight to form small chains, the pore distribution was uneven, and a weak cheese structure was formed. In addition, the volatile flavour substances in the kefir group increased the phenylethyl alcohol, isobutanol, and isoamyl alcohol compared with those in the L_1 group, with a slight refreshing taste brought by alcohol and special soft malt alcohol aroma and rose aroma not found in ordinary yoghurt, which was more in line with the characteristics and taste of traditional kefir champagne yoghurt.

KEYWORDS

kefir, SEM, CLSM, flavour, amino acid

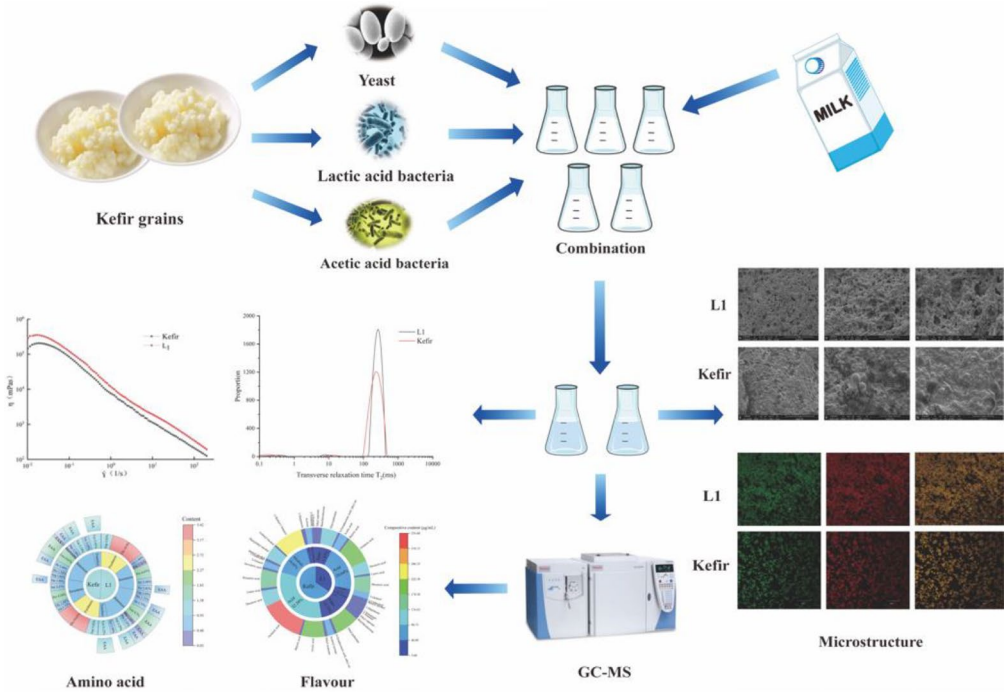

GRAPHICAL ABSTRACT

1. Introduction

Kefir originated in the Caucasus and is made from cow's and goat's milk that has been naturally fermented in sheepskin bags (Petrova et al., 2021). Kefir is widely consumed and popular in many countries, including Europe, Asia, South America and North America (Sadiye, 2020). Moreover, kefir has been consumed for thousands of years because of its health benefits and holds a significant role in food. Kefir is different from yoghurt and other types of fermented dairy products. Yoghurt is fermented from milk and bacteria (yogurt cultures), while kefir is an acidic, low-alcohol probiotic drink derived from a complex mixture of metabolites of bacteria (including *Lactobacillus*, *Lactococcus* and *Acetate*) and yeast (Lynch et al., 2021; Baniasadi et al., 2022). In addition, kefir differs from other fermented dairy products, which is known as 'champagne yoghurt'. Given that kefir contains complex symbiotic relationships (lactic acid and acetic acid-producing bacteria, lactose fermentation and alcoholic yeast), such a complex microecological environment allows the lactose, protein and fat in milk to be degraded into galactose, lactic acid, exopolysaccharides, vitamins, free amino acids, free fatty acids, volatile alcohols, aldehydes, ketones and esters, which compounds create kefir's unique flavour (Souza and Dias, 2017; Sharma et al., 2021). A number of studies have reported the beneficial properties of kefir, such as lowering blood pressure (Silva-Cutini et al., 2019), anti-cancer (Sharifi et al., 2017), anti-viral (Hamida et al., 2021), cholesterol-lowering (Lim et al., 2017), anti-diabetic (Salari et al., 2021), anti-inflammatory (Chen et al., 2020) and immunity-boosting and anti-oxidant (Chen et al., 2020; Patil et al., 2021).

The most abundant flora in kefir granules is lactic acid bacteria, which provides a certain acidity and viscosity of yoghurt. Many lactic acid bacteria are probiotics and have a health-promoting effect (Gezginç et al., 2022). Yeast is the main feature that distinguishes kefir yoghurt from other types of yoghurt. The addition of yeast adds ethanol and carbon dioxide to kefir yoghurt and increases the flavour of yoghurt (Şahingil, 2019). However, an excessive amount yeast can give the yoghurt a yeasty taste and affect the flavour of the product (Farag et al., 2020). Meanwhile, a certain amount of acetic acid bacteria can provide acetic acid for kefir and combine with alcohols to form esters, which also has a certain positive effect on product flavour (Lynch et al., 2019). Natural fermenters are more appropriate for fermenting kefir because the strain of kefir grain is easy to change in the fermentation process (Wang et al., 2016). Currently, kefir grain fermented yoghurt is difficult to replicate and cannot be standardised for production (Nielsen et al., 2014). Accordingly, many researchers have isolated these three types of typical dominant strains for process compounding to find the appropriate amount of co-fermented milk to produce kefir to standardise the production of kefir yoghurt. These researchers have chosen the right method to enrich the volatile components, determine the flavour substances and organoleptically evaluate them to ensure that the right ratio of strains can be determined for subsequent experiments (Xing et al., 2017; Duran et al., 2022). However, few articles on structural characterisation in kefir yoghurt have been published. The three pillars of *Lactobacillus plantarum* L_1, yeast TN_1 and acetic acid bacteria A_3 were selected for the

fermentation of kefir yoghurt to find the reason for the change in the structure of kefir yoghurt after the addition of different acetic acid bacteria and yeasts. The physical and chemical indexes, microstructural observation, rheology and texture of kefir yoghurt and single lactic acid bacteria fermented yoghurt were determined, and the nutritional flavour was analysed. This study aims to explore the changes in the structure of kefir yoghurt after the addition of yeast and acetate and to discover the pattern of the unique flavour and structure of kefir yoghurt, which will provide a theoretical basis for the development and quality control of kefir products.

2. Materials and methods

2.1. Materials

Saccharomyces cerevisiae (TN_1), *L. plantarum* (L_1) and *Acetobacter tropicalis* (A_3) were provided by our laboratory. Meanwhile, the milk was purchased from Mengniu Co., Ltd.

2.2. Yoghurt fermentation

(1) Strain activation: The A_3 and L_1 strains were activated with MRS liquid medium. TN_1 strain was activated by using YPD liquid medium. (2) Fermentation experiments: Approximately 50 ml of pure milk and 2.5 g of white granulated sugar were added to several 100 ml yoghurt bottles. After pasteurisation (62°C, 30 min), the strains were cooled, inoculated with 7% (*V/V*) of the fermentation agent, mixed and cultured at 37°C for 12 h until the fermentation was completed. Thereafter, the strains were transferred to the 4°C refrigerator and cooked overnight.

2.3. pH and titratable acidity (TA)

The pH of the yoghurt was measured with an analyser (Qiu et al., 2021), whilst that of kefir and L_1 fermented milk was measured with a digital pH meter (*FE28*-Standard, METTLER TOLEDO, America). The titration method adapted from Chouchouli et al. (2013) was applied to determine the TA of the yoghurt samples. Briefly, 10 g of yoghurt was mixed with 20 ml of distilled water and titrated with NaOH (0.1 mol/l) in the presence of phenolphthalein. The results were expressed as a percentage of lactic acid. The determination was carried out in triplicate.

2.4. Water-holding capacity (WHC) and syneresis

WHC was determined by using the method previously reported (Nguyen et al., 2017) and slightly modified. he dehydration shrinkage in yoghurt samples was measured with an Eppendorf centrifuge (5810R, Eppendorf, Germany) at 3800 g at 4°C for 30 min for 20 g of yoghurt. Specifically, a 15 g yoghurt sample was centrifuged at 12,000 g at 4°C for 20 min. After centrifugation, the clear supernatant was poured out, weighed and used to determine the percentage of dehydration shrinkage (W/W). All measurements were repeated three times.

$$\mathrm{WHC}(\%) = \frac{\text{weight of drained gels}(\mathrm{g})}{\text{weight of yoghurt}(\mathrm{g})} \times 100 \quad (1)$$

$$\text{Syneresis}(\%) = \frac{\text{weight of whey}(\mathrm{g})}{\text{weight of yoghurt}(\mathrm{g})} \times 100 \quad (2)$$

2.5. Textural analysis

The kefir and L_1 samples were taken out after ripening overnight in a 4°C refrigerator for comparative analysis. A TA-XT plus texture analyser (Stable Micro System Co., Britain) was used to determine the texture parameters of the samples. During the TPA mode test, P/50 probe is used, the test distance is 25 mm, the trigger point is 5.0 g, the pre-test speed is 2 mm/s, the test speed is 2 mm/s, and the post-test speed is 6 mm/s. The indicators include: hardness, elasticity, cohesion, stickiness and resilience.

2.6. Rheological analysis

Before the test, the yoghurt sample was placed at room temperature for 15 min, and the apparent viscosity was measured by using haake rheometer (MARS 60, Thermo Fisher Scientific, American). The selected rotor model was P60/Ti-02150138. Fixture for the test plate (diameter 25 mm) test spacing of 500 μm, 1 ml of yoghurt sample was tested on the surface, and the excess samples were removed. Calibration was performed at 25°C for 1 min, with 30 points at 0.1–200 s^{-1} shear rate (γ) for testing to create a dynamic viscosity curve.

2.7. Confocal laser scanning microscopic (CLSM) analysis

A CLSM (FV3000, OLYMPUS, Japan) was used to study the microstructure of yoghurt. Approximately 3 ml of fermented milk was taken, and 30 μl of 0.125% Nile red dye solution (the excitation and emission wavelengths were 580–630 nm) was used to stain the lipid. After colour development, 10 μl of 0.1% *Fast Green* solution (the excitation and emission wavelengths were 641–741 nm) was used to stain the protein for 20 min (Laiho et al., 2017; Wang et al., 2019). Furthermore, 150 μl slides containing the dye mixture were placed under CLSM for observation. Nile Red was used to excite and observe the fat in the yoghurt at 561 nm. *Fast Green* was used to excite and observe the protein in the yoghurt at 640 nm.

2.8. Determination of microstructure scanning electron microscopy (SEM)

The microstructure of the yoghurt samples was observed by SEM (Quanta 250FEG, FEI, America). The sample preparation for SEM is performed according to the method described (Bensmira and Jiang, 2012; Pan et al., 2019). The two groups of fermented milk were cut from the middle of the sample square curd and placed in 2% glutaraldehyde solution at 4°C for more than 12 h. After fixation, the samples were washed three times with PBS (pH 7.2) for 5 min each time. Moreover, 50, 70, 80 and 90% gradient ethanol were dehydrated for 10 min after cleaning and dehydrated twice with 100% ethanol for 10 min each. After dehydration with tert-butanol replacement 2 times, each 15 min. After the operation is completed, put in-80°C refrigerator frozen overnight, using vacuum freeze-drying samples, with a blade to cut off the dry part, the debris installed in the aluminum SEM short rod, and sputtering cup pad coated with vacuum gold. Following the examination of the sample's microstructure by vacuum SEM, a gold film was coated on the surface of the sample with platinum. The final voltage was 15 kV, with magnifications of 5,000 and 20,000 times observed by SEM.

2.9. LF-NMR analysis

The L_1 single bacteria fermented yoghurt and kefir fermented milk were placed into the special sample tube of nuclear magnetic resonance and detected in the nuclear magnetic resonance sample pool. The main parameters of the instrument are set as follows: Micro MR-CL-I low-field NMR analyser (Micro MR-CL-I, Niumag Electronic Technology Co., Ltd., Shanghai, China), 1–10 mm magnet probe and 20 MHz proton resonance frequency. The Carr–Purcell–Meiboom–Gill pulse sequence was applied to collect the T2 relaxation time. The other major parameters were set as follows: the waiting time (WT) was 7,000 ms, the time to echo (TE) was 0.200 ms, the number of echoes (NECH) was 9,000, and the number of scans (NS) was 16. The signal attenuation curve of the transverse relaxation time was obtained.

2.10. Determination of free amino acid content

The single free amino acid content (mg/g) was determined with an amino acid analyser (S433D, Sykam, Germany). Chromatographic column: LCA106//Na detection wavelength: 570 mm + 440 mm mobile phase: sodium citrate A = 0.12 N, pH 3.45; b = 0.2 N, pH 10.85. Temperature: 58°C–74°C. Gradient temperature control flow rate: elution pump 0.45 ml/min + derivative pump 0.25 ml/min. Pressure: 30–60 bar (Yang et al., 2021).

2.11. GC–MS analysis

The treatment group at the end of fermentation was taken to detect flavour components. Headspace extraction was performed through solid phase microextraction (SPME). Each sample (3 g) of 20 μl of 0.009 g/l 2-octanol was placed in a 20 ml vial as an internal standard for subsequent quantitative analysis. Determination was carried out by using SPME combined with GC–MS. After exposure of the SPME fibres to the top space at 45°C for 45 min for sampling, the SPME fibres were introduced into a GC syringe and allowed to stand for analysis for 3 min for the thermal desorption of the analytes (Shi et al., 2022).

GC–MS was performed with a Thermo Scientific Trace 1,300 gas chromatograph connected to a Thermo Scientific ISO7000 single quadrupole mass spectrometer selective detector (Trace1300-ISQ7000, Thermo Fisher Scientific, Waltham, MA, United States). A DB-WAX chromatographic column was used (30 m × 0.25 mm inner diameter and 0.25 μm film thickness, J&W Scientific, United States). An ultra-high purity helium was used as the carrier gas at a constant flow rate of 1 ml/min. The separation ratio was 20:1. The column temperature was raised from room temperature to 40°C for 1 min. The temperature was raised to 150°C at 5°C/min and to 210°C at 10°C/min for 5 min. The MS conditions were as follows: 280°C ion source temperature, 215°C transmission line temperature, 70 eV ionisation mode EI and 35–450 u mass-charge (m/z) scan range (Ding et al., 2015). The compounds were identified through MS library searches (NIST/EPA/NIH version 2.0 (1995) and MS data in the Wiley registry) and the MS spectral database library of the National Institute of Standards and Technology.

2.12. Statistical analysis

All the experiments were carried out three times. Origin 2018 software was used for data mapping and statistical analysis. IBM SPSS Statistics 26 software was utilised for significance analysis. The significance level of 5% was used and data were shown as mean ± standard error of the mean.

3. Results and discussion

3.1. Strains observed under an SEM

The initial strain was observed under an electron microscope. The three strains used to ferment yoghurt are shown in Figure 1. A is *L. plantarum* L_1, B is *S. cerevisiae* TN_1, and C is *A. tropicalis* A_3.

3.2. Chemical properties

At the end of fermentation, the pH value and TA of the kefir group were higher than those of the L_1 group (Table 1). This condition is due to the co-fermentation of the lactic and acetic

FIGURE 1
(A) L_1 morphology under the scanning electron microscope. **(B)** TN_1 morphology under the scanning electron microscope. **(C)** A_3 morphology under the scanning electron microscope.

TABLE 1 Comparison of physicochemical indexes of different yoghurt groups.

Type	pH	TA(°T)	WHC (%)	Syneresis (%)
L_1	4.50 ± 0.01^a	72.00 ± 2.65^b	65.72 ± 2.83^a	50.28 ± 0.20^b
Kefir	4.52 ± 0.02^a	77.67 ± 2.08^a	44.13 ± 2.85^b	60.23 ± 1.71^a

Different letters in the same column indicate significant differences ($p < 0.05$).

TABLE 2 Effects of L_1 and kefir groups on the texture of yoghurt.

Type	L_1	Kefir
Hardness	127.11 ± 6.65^b	180.72 ± 3.26^a
Elasticity	0.97 ± 0.008^a	0.67 ± 0.06^b
Cohesiveness	0.59 ± 0.016^a	0.49 ± 0.048^b
Stickiness	110.47 ± 3.21^b	155.74 ± 4.20^a
Resilience	0.03 ± 0.00^b	0.09 ± 0.01^a

Different letters in the same row indicate significant differences ($p < 0.05$).

acid bacteria, resulting in the excessive production of lactic and acetic acid. The water holding rate of the L_1 group was the highest, and the whey separating rate was lower than that of the kefir group. The decrease in the kefir group may be due to the destruction of the casein network structure by the ethanol produced by the fermented lactose in the yeast group, resulting in a decrease in the stability of the fermented milk gel and the water holding rate. The whey precipitation rate is a bad characteristic of yoghurt. The whey precipitation rate of kefir group is larger, which may be due to the rich variety of organic acids in mixed fermentation. The high pH and titration acidity indicate that the acidity is considerably high. The isoelectric point of casein is easier to approach, which results in coagulation and excessive whey precipitation. As the results of previous studies have shown. Khan et al. (2014) reports that higher acid concentrations cause milk protein denaturation, which significantly affects the binding between them, resulting in milk protein loss as fine particles.

The WHC of the kefir group was 32.85% lower than that of the L_1 group. Firstly, yeast will produce ethanol by alcohol fermentation under anaerobic conditions due to the addition of yeast and acetic acid bacteria in the kefir group. The acetic acid bacteria will use ethanol to produce water. Water and whey are not easy to separate in yoghurt, which will also result in a lower water holding rate. In addition, the sensitivity of kefir to dehydration did not decrease because the fermentation time of the kefir sample was less than 18 h, which was 19.78% higher than that of the L_1 group. The kefir treatment group showed low WHC and high levels of dehydration shrinkage, which were consistent with the results of Bensmira and Jiang (2012). Yoghurt prepared at low temperatures had a higher WHC than that at high temperatures, and the dehydration rate of the samples fermented at high temperatures was significantly increased.

3.3. Texture analysis

The texture of the kefir and L_1 fermented milk was compared and analysed. The evaluation indexes mainly included hardness, elasticity, cohesion and so on. Table 2 shows that the hardness of the kefir group was 42.18% higher than that of the L_1 group, and the viscosity was increased by 40.9%. This condition may be related to the electrostatic interaction between the protein matrix and TN_1 and A_3, forming an electrostatic complex, resulting in a dense network (Wang et al., 2022). The kefir group also significantly reduced the elasticity (30.93%) and cohesiveness (16.95%) of yoghurt ($p < 0.05$). This phenomenon may be caused by the addition of acetic acid bacteria after the yoghurt's acidity increased, resulting in the disintegration of the gel structure. The addition of yeast resulted in reduced cohesion and viscosity, and decarboxylation has a certain effect on the texture and physical properties.

In addition, the higher hardness and adhesion of the kefir group may be related to the fermentation temperature. Haque et al. (2001) pointed out that increasing the fermentation

temperature would result in a systematic increase in the hardness, adhesion, and deformation resistance of the kefir milk. Second, the acetic acid bacteria will produce acetic acid acidification reaction (Bensmira and Jiang, 2012), which will result in cheese, and the hardness will be significantly improved. The hardness may also be related to the use of a high protein concentration of milk fermentation. Following a comprehensive evaluation, the addition of yeast and acetic acid bacteria will change the structure of yoghurt, in accordance with the characteristics of kefir yoghurt beverage.

3.4. Rheology analysis

The apparent viscosity of the two groups of yoghurt in the shear range of 0.1–200 s^{-1} showed a shear dilution phenomenon with the increase in shear rate (Figure 2), and it gradually decreased. This shear thinning behaviour may be due to the destruction of intramolecular and intermolecular associations in the yoghurt system (Duboc and Mollet, 2001). The initial viscosity of the single strain L_1 treatment group was slightly larger than that of the kefir treatment group. At a high shear rate, the apparent viscosity of the L_1 fermented milk was always greater than that of kefir fermented milk, and the final viscosity was better. The L_1 treatment group had a large number of lactic acid bacteria and strong metabolic activity, thereby promoting the binding of casein micelles by reducing the pH value, with better viscosity and less water loss in the matrix space.

No significant difference was observed between the curve of the kefir treatment group and the single strain L_1 group. However, the greater viscosity consumption may be related to the increase in hardness during fermentation. This phenomenon may be due to the hydrolysis of casein leading to the plasticisation of water and the associated decrease in mechanical force viscosity (Alinovi et al., 2018), which weakens the resistance of yoghurt gels to breakdown. Meanwhile, this phenomenon is the result of the interaction of milk proteins

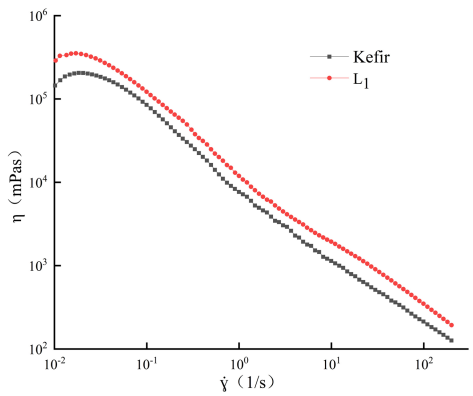

FIGURE 2
Analysis of rheological properties.

adsorbed on the fat droplets. The degree of fat globule dispersion is large, and the number of free casein units that can form a network is reduced because the commercial milk after homogenisation is used. Moreover, the acidity of this group is high due to the addition of acetic acid bacteria. Thus, the protein structure is more easily destroyed.

3.5. Confocal laser scanning microscope (CLSM)

The microstructural difference between the kefir fermented milk and the L_1 fermented milk was observed by CLSM (Figure 3). Fat (green) and casein clusters (red), yellow for the superposition of fat and protein renderings. Significant differences in the casein cluster structure can be observed between the L_1 and the kefir groups. Both treatment groups showed a continuous flocculent protein structure. The flocculent protein structure of the kefir group was not as dense as that of the L_1 group, the gap of the branch protein network was larger, the distribution was more dispersed, and the connection between groups was weaker. This condition may be related to the ability of the fat globules to positively interact with casein matrix and whey protein. Yoghurt gels with high whey protein ratio have a more discontinuous structure with larger pores, and the presence of large whey protein aggregates promotes the formation of coarse gel microstructures characterised by large gaps (Krzeminski et al., 2011). There are research reports that yeast and acetic acid bacteria co-ferment and decompose proteins in the substrate to produce vitamin B6, consume oxygen in the system to produce anaerobic environment, and produce acetic acid to reduce the pH of the system, thereby activating some lactic acid bacteria to ferment lactose and produce extracellular polysaccharides (Tao et al., 2022). In addition, The kefir group produces a cheese similar to the original kefir grains with increased acidity and more whey precipitation due to the synergistic action of multiple strains (Karim and Aider, 2022). The microstructure of low-fat yoghurt with a smaller gap of L_1 protein cluster, higher proportion of whey protein and increased aggregation of whey protein was mainly a granular network. The gels with a high casein-to-whey ratio observed finer protein chains, smaller particle sizes, more uniform distribution, and stronger inter-group linkages (Figure 3B). This situation also explains the reason why the L_1 group yoghurt has a higher WHC. Such a protein network structure is more conducive to increasing the WHC of the gel. The kefir group (Figure 3E) has a large gap, and the dispersed microstructure arrangement will lead to a weaker ability of the protein to intercept water molecules, low water holding capacity and increased dehydration capacity. This situation is also related to texture and rheology, and the gel is easier to loosen. The kefir group observed in SEM that casein is tightly cross-linked but does not have a stronger internal bond-stabilised complex, which may result in protein rearrangement during storage and an unstable casein network,

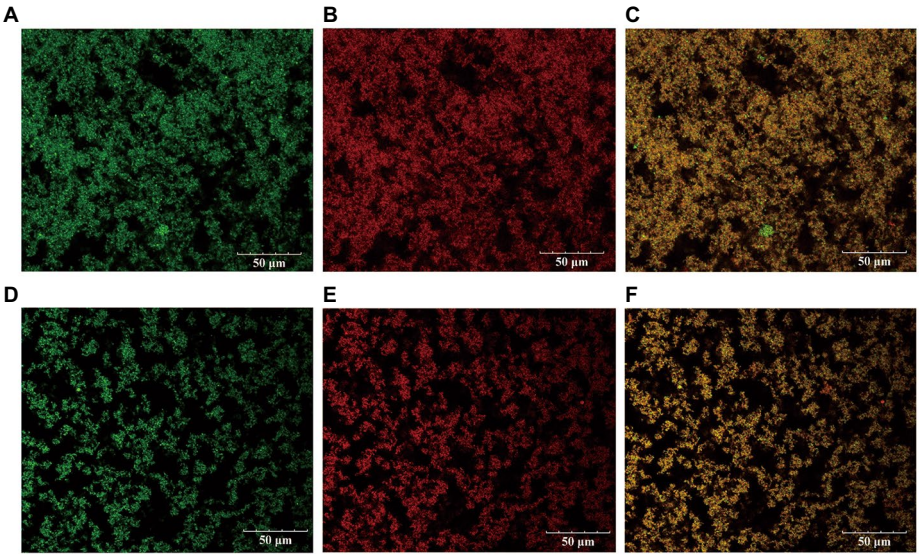

FIGURE 3
The distribution of protein and fat in L_1 fermented milk and kefir fermented milk under laser scanning confocal. (**A** represents the fat distribution in L_1, **B** represents the protein distribution in L_1, and **C** is the superimposed effect of the two. **D** represents the fat distribution in kefir, **E** represents the protein distribution in kefir, and **F** is the superimposed effect of the two).

which is also related to the rapid decrease in apparent viscosity in rheological properties.

3.6. SEM analysis of the yoghurt microstructure

The microstructure of set yoghurt system was observed by scanning electron microscopy (SEM). The results are shown in Figure 4. The SEM revealed a smaller and more compact protein network in the two groups, which may be related to the use of milk with higher protein content before fermentation.

In the structure of the L_1 group, the density of the gel network and molecular stacking increased, the pore size was continuous, the whey pores were evenly distributed, and the size was uniform. This condition is attributed to the aggregation of casein and denatured proteins on the micelle surface that results in the formation of clusters during the acidification of milk, thereby forming a 3D network (Ozcan-Yilsay et al., 2007). *L. plantarum* L_1 appears on the protein surface between the fat and the protein layers or is suspended in yoghurt. The single-strain L_1 group fermented under anaerobic fermentation conditions showed stronger WHC and finer structure, which is consistent with the study.

Evident differences can be observed in the microstructure between the kefir and the L_1 groups. The surface of the kefir group was a dense membrane composed of irregularly interconnected chains of a casein micelle protein matrix structure. SEM shows an analogue of biofilm. A previous study showed that Lactobacillus and Acetobacter are important strains which produce kefir polysaccharides and form biofilms, while yeast plays a role in connecting and promoting this complex interphase network structure and environment. In addition, some bacteria that secrete biofilm polysaccharides, such as Lactobacillus, are attached to the surface of small molecule particles (Dong et al., 2018). The extracellular polysaccharides secreted by them can adhere to other microorganisms, bacteria and fungi can adhere and co-exist through direct interaction and interact with the components (proteins) in the fermentation substrate, eventually forming a relatively sealed space (Fontán et al., 2006). The physicochemical properties showed that kefir had higher acidity, resulting in thicker protein networks, smaller and irregular gaps and larger clumps (Figure 4F). On the one hand, the more balanced the binding of casein micelles to whey protein, the fewer network voids observed because of the higher the protein content. Inhomogeneous structures and large pores were observed in gels containing large protein aggregates and bound to whey protein-encapsulated casein micelles, which is consistent with the results observed by CLSM and surface observation (Vasbinder et al., 2004). On the other hand, the kefir-treated group appears to be more tightly packed, with smaller gaps and a protein network similar to that of cheese. Accordingly, less water is retained inside, and the dehydration rate increases (Ahmed and Bajwa, 2019). The chain in the figure denotes the aggregation and growth of individual particles, which may also be caused by the aggregation of adjacent chains. In addition, casein micelle fusion intolerant protein particles may also result in an obscured micelle profile. Bensmira and Jiang (2012) noted that kefir histones were more tightly fused together, and clusters became denser and thicker as the fermentation temperature increased above 32°C, forming a relatively concentrated structure (Figure 3D) and more tightly crosslinked structure and promoting dehydration. These properties affected the texture of kefir (Table 1). In addition, the ability of the protein in the kefir group to intercept water molecules became weaker, and the dehydration shrinkage rate

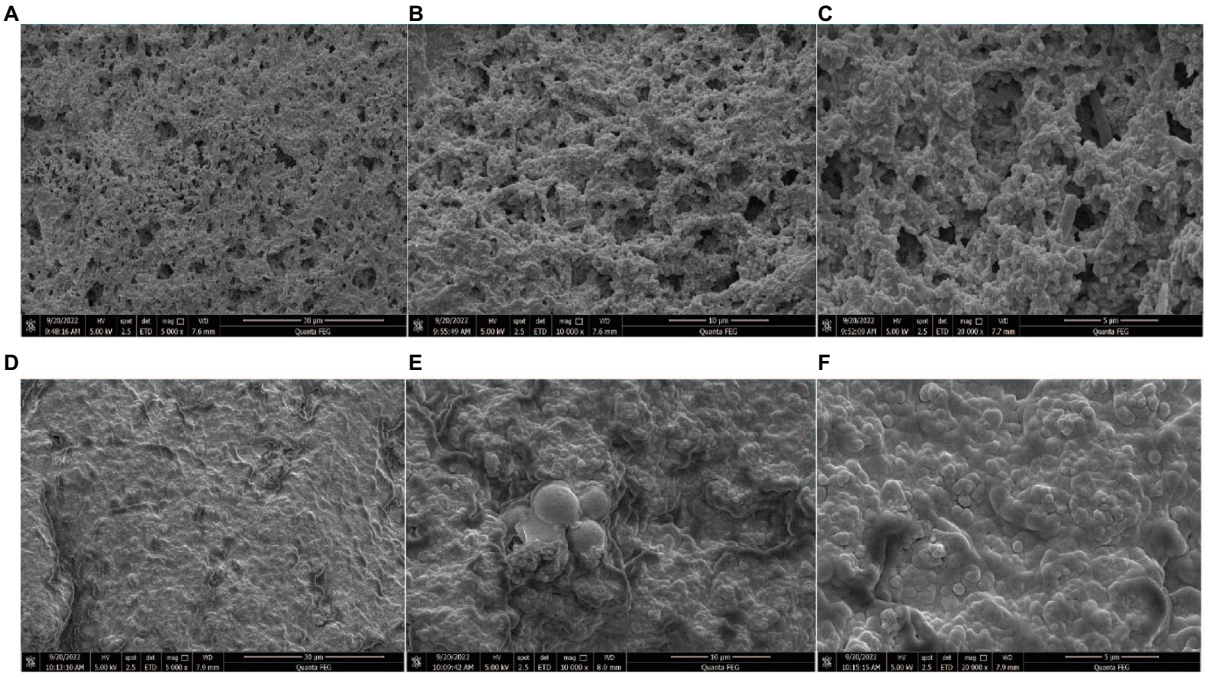

FIGURE 4
The SEM micrographs of yogurt L_1 and kefir at different magnifications (**A,B,C** represents L_1 yogurt magnification of 5.00 kx, 10.00 kx, and 20.00 kx. **D,E,F** represents kefir magnification of 5.00 kx, 10.00 kx, and 20.00 kx).

became higher. The honeycomb holes can be evidently seen from the outside, which can also explain that the protein cross-linking is closer, but the dehydration is stronger. The high content of acidic ions changed the phenomenon of protein interaction, which had an important influence on the final structure and quality of yoghurt.

TABLE 3 LF-NMR data of Kefir and L_1.

Samples	Relaxation time(ms)			Peak area
	T_{21}	T_{22}	T_{23}	T_{23}
L_1	0.633	9.479	304.661	18970.52
Kefir	0.478	20.996	409.786	17552.83

3.7. Lf-NMR

The relaxation time T_2 of yoghurt fermented by different probiotics was obtained based on the T_2 relaxation time distribution map of the LF-NMR (Table 3). Relative signal intensities (T_{21}, T_{22} and T_{23}) represent bound water, semi-bound water and free water, respectively. The transverse relaxation time T_2 of the two yoghurt treatment groups is shown in Figure 5. The LF-NMR transverse relaxation time T_2 is divided into three regions: the T_{21} region with relaxation time between 0 ms and 3 ms represents the relaxation of hydrogen protons in the water molecule layer tightly bound to polar groups (i.e., bound water), which has the smallest fluidity; the T_{22} region with relaxation time between 5 ms and 30 ms represents immobile water. The T_{23} region with relaxation time between 100 ms and 500 ms represents free water (Liu et al., 2018; Xu et al., 2022).

The results of relaxation time T_{22} showed that the relaxation time of the kefir group was longer than that of the L_1 group. Table 3 illustrates that the kefir group had the smallest water distribution area and the lowest free water content in the T_{23}

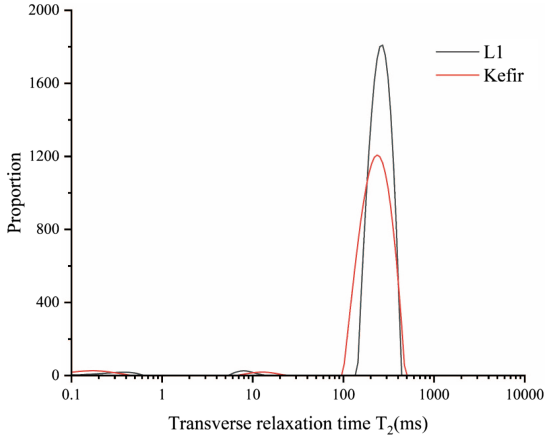

FIGURE 5
Distribution of T_2 relaxation times on set yoghurts at L_1 and kefir by LF-NMR.

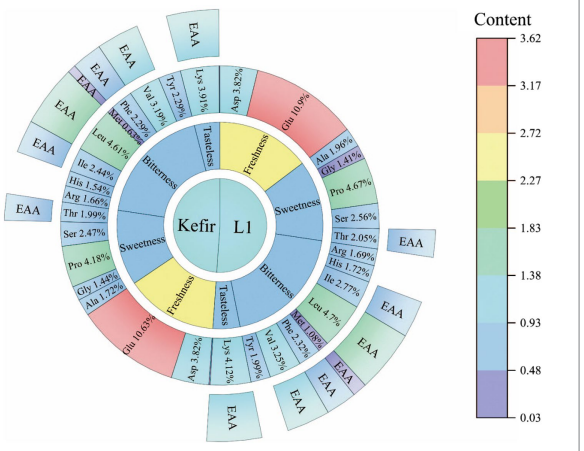

FIGURE 6
Sunburst diagram of amino acids of L_1 and kefir.

free water region, and the area of free water could reflect the water retention capacity of the protein gel structure (Xu et al., 2019). The kefir group may be due to the synergistic effect of yeast and acetic acid bacteria after the addition of yeast and acetic acid bacteria, which decomposes macromolecules, such as protein and fat, into small peptides and small lipid particles, fills the pores of the yoghurt gel structure, makes the pores smaller and forms a dense network structure that closely combines water molecules, similar to Wang et al. (2018). The free water in the kefir group retained less structure than the L_1 group and was physically less capable of capturing water molecules. The LF NMR detection results are consistent with the experimental results of the microstructure, water retention and dehydration.

3.8. Amino acid analysis

Protein and amino acids are among of the important indicators of yoghurt. These indicators provide essential or non-essential amino acids and other nutrients to be utilised by the body (Day et al., 2021). Amino acids are also precursors of aromatic compounds in yoghurt, which give yoghurt different flavours (Celik et al., 2021). Yoghurt retains its freshness due to aspartic and glutamic acid. Threonine, serine, glycine, proline and alanine give yoghurt a pleasant sweetness. Leucine, isoleucine, phenylalanine and arginine exhibit bitterness (Cautela et al., 2021). In this study, 17 amino acids were detected in milk, yoghurt L_1 and kefir. The results are shown in Figure 6. Glutamic acid is the most abundant amino acid in milk and yoghurt. A previous study reported that glutamic acid combines with ammonia in the body to form non-toxic glutamine, which reduces blood ammonia and the symptoms of hepatic coma (Jiang et al., 2022). Proline, aspartic acid, leucine, valine and lysine were the next most abundant. Amongst these amino acids, leucine and valine, which act as branched-chain amino acids, promote the release of insulin and growth hormone (Jung et al., 2021). Moreover, lysine, as an essential amino acid, can promote human growth and development and fat oxidation and enhance immunity, which has positive nutritional significance in many aspects (Ruocco et al., 2021).

TABLE 4 The contents of free acid in Kefir and L_1 fermented yoghurt.

Classification	Content(mg/g)		FC	Change
	L_1	Kefir		
EAA	6.74 ± 0.18^a	6.34 ± 0.16^b	0.94	–
NEAA	10.24 ± 0.21^a	9.91 ± 0.19^b	0.97	–
TAA	16.99 ± 0.39^a	16.24 ± 0.35^b	0.96	–
EAA/ NAA	$65.82\%^a$	$63.98\%^b$	0.97	–
EAA/TAA	$39.70\%^a$	$39.01\%^a$	0.98	–

The data are the means of three independent experiments ± standard deviations ($n = 3$). EAA is essential amino acid. NEAA is non-essential amino acid. TAA is total amino acid. FC represents the ratio of amino acid content of kefir and L1 in yoghurt. ^{a,b}Values in the same row with different superscript letters differ significantly ($p < 0.05$).

The analysis found that the amino acid content of all yoghurts significantly changed compared with milk. Alanine, proline, threonine, isoleucine, methionine and lysine in kefir yoghurt were significantly lower than those in L_1. The significant decrease in alanine, proline, isoleucine and methionine as hydrophobic amino acids was due to the addition of acetic acid bacteria and yeast, which may produce different flavour substances. However, whether this is the reason why the kefir yoghurt structure becomes a dense pore structure remains to be further studied. The amounts of glycine and tyrosine in kefir yoghurt increased by 1.02 and 1.15 times compared with those in L_1. Glycine is a constituent amino acid of the endogenous oxidant glutathione (Rom et al., 2022). Liu et al. (2021) found that glycine improves the growth and proliferation of the neonatal pig intestinal epithelial cells and the ability to resist oxidative stress. In addition, the essential and non-essential amino acid content of the two yoghurts are shown in Table 4. Although the content of EAA in kefir is 0.94 times lower than that of L_1, its EAA/NEAA exceeds 60%, and EAA/TAA reaches 39%, which is also a nutritional standard for high-quality protein.

3.9. Analysis of a flavour substance

A total of 33 flavour substances were detected by GC–MS, mainly esters, acids, ketones, aldehydes and alcohols. These substances include 12 esters, 6 ketones and aldehydes, 6 alcohols and 9 acids. Kefir had 6 more flavour substances than L1. The substance and relative content are shown in Table 5.

Flavour substances are produced by proteins, lactose and lipids through a series of metabolic pathways such as lipid decomposition, proteolysis and glycolysis (McAuliffe et al., 2019). The protein and fat in dairy products are metabolised by the enzyme system of the bacteria to produce flavour substances through the mixed culture of lactic acid bacteria, yeast and acetic acid bacteria, which affect the amino acid catabolism. Lactic acid bacteria decompose the biological macromolecules into small product molecules and add a certain special functional flavour to the final. Lactic acid bacteria

TABLE 5 Determination of volatile flavor compounds of L_1 and kefir by GC–MS.

Classification	CAS	Formula	Comparative content(μg/mL)	
			L_1	Kefir
Esters				
Ethyl caproate	C123660	$C_8H_{16}O_2$	25.24 ± 0.41^b	33.31 ± 1.31^a
Diethyl succinate	C123251	$C_8H_{14}O_4$	19.94 ± 0.55^a	9.14 ± 0.19^b
Phenylacetic acid ethyl ester	C101973	$C_{10}H_{12}O_2$	3.57 ± 0.16^a	0 ± 0.00 ^{b}
Phenethyl acetate	C103457	$C_{10}H_{12}O_2$	7.64 ± 0.20^a	8.15 ± 0.29^a
Butyldecalactone	C705862	$C_{10}H_{18}O_2$	12.77 ± 0.24^b	13.95 ± 0.58^a
Ethyl palmitate	C628977	$C_{18}H_{36}O_2$	133.63 ± 3.20^b	194.84 ± 6.36^a
Delta-Dodecalactone	C713951	$C_{12}H_{22}O_2$	5.76 ± 0.20^a	6.02 ± 0.09^a
9-Octadecenoic acid, ethylest	C6114187	$C_{20}H_{38}O_2$	10.99 ± 0.47^b	15.19 ± 0.78^a
Isoamyl acetate	C123922	$C_7H_{14}O_2$	0 ± 0.00^b	22.74 ± 1.23^a
Lactic acid ethyl ester	C687478	$C_5H_{10}O_3$	0 ± 0.00^b	3.87 ± 0.18^a
Ethyl ocanoate	C106321	$C_{10}H_{20}O_2$	0 ± 0.00^b	15.83 ± 0.66^a
Ethyl salicylate	C118605	$C_{15}H_{22}O_3$	0 ± 0.00^b	3.09 ± 0.14^a
Acids				
Acetic acid	C64197	$C_2H_4O_2$	72.78 ± 3.32^b	193.59 ± 20.15^a
Butyric acid	C107926	$C_4H_8O_2$	16.22 ± 0.60^a	15.92 ± 0.64^a
Isovaleric acid	C503742	$C_5H_{10}O_2$	0 ± 0.00^b	17.16 ± 0.62^a
Octanoic acid	C124072	$C_8H_{16}O_2$	218.53 ± 2.81^b	353.56 ± 18.82^a
Decanoic acid	C334485	$C_{10}H_{20}O_2$	105.10 ± 2.29^b	132.29 ± 1.77^a
Lauric acid	C143077	$C_{12}H_{24}O_2$	12.15 ± 0.37^b	14.62 ± 0.52^a
Palmitic acid	C57103	$C_{16}H_{32}O_2$	4.66 ± 0.21^a	5.07 ± 0.22^a
Hexanoic acid	C142621	$C_6H_{12}O_2$	138.29 ± 5.31^b	155.51 ± 6.46^a
Benzoic acid	C65850	$C_7H_6O_2$	0 ± 0.00^b	3.06 ± 0.09^a
Alcohols				
2-Octanol	C5978701	$C_8H_{18}O$	54.38 ± 1.43^a	52.03 ± 2.46^a
1-Undecanol	C112425	$C_{11}H_{24}O$	10 ± 0.00^a	9.23 ± 0.31^b
Benzyl alcohol	C100516	C_7H_8O	14.33 ± 0.58^a	11 ± 0.00^b
Phenylethyl alcohol	C60128	$C_8H_{10}O$	7.64 ± 0.30^b	115.74 ± 5.62^a
Isobutyl alcohol	C763326	$C_4H_{10}O$	0 ± 0.00^b	15.00 ± 0.63^a
3-Methyl-1-butanol	C123513	$C_5H_{12}O$	0 ± 0.00^b	237.98 ± 10.46^a
Aldoketones				
Hexanal	C66251	$C_6H_{12}O$	3.78 ± 0.16^b	4.71 ± 0.25^a
2-Heptanone	C110430	$C_7H_{14}O$	46.20 ± 0.34^a	28.32 ± 0.66^b
Acetoin	C513860	$C_4H_8O_2$	6.52 ± 0.26^b	53.39 ± 1.14^a
2-Nonanone	C821556	$C_9H_{18}O$	15.22 ± 0.52^a	10.83 ± 0.54^b
1-Nonanal	C124196	$C_9H_{18}O$	13.50 ± 0.11^b	14.28 ± 0.41^a
Decylaldehyde	C112312	$C_{10}H_{20}O$	6.64 ± 0.28^a	6.78 ± 0.36^a

The data are the means of three independent experiments ± standard deviations ($n = 3$). ^{a,b}Values in the same row with different superscript letters differ significantly ($p < 0.05$).

decompose lactose into monosaccharides, produce lactic acid and provide carbon sources for the growth of yeast and acetic acid bacteria, promoting alcohol fermentation to produce special flavour substances, such as ethanol, CO_2, organic acids and aldehydes (De Vuyst and Leroy, 2020). The flavor profile and content of L_1 and kefir are shown in Figure 7. Kefir mainly detected octyl salicylate, isobutanol, ethyl lactate, isoamyl acetate, isovaleric acid, benzoic acid and ethyl caprylate, whilst the L_1 group did not

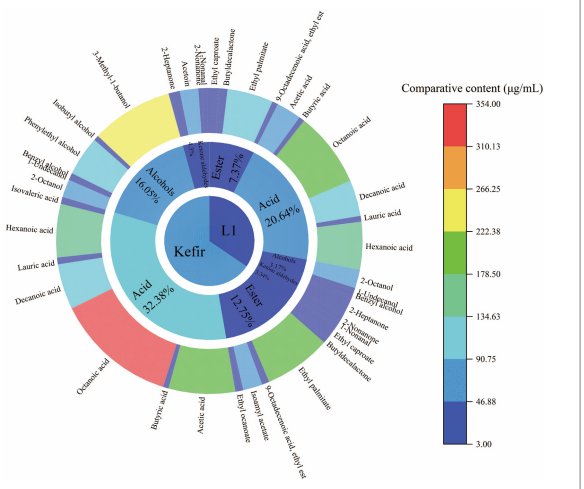

FIGURE 7
Sunburst diagram of flavor substances of L_1 and kefir.

produce special substances. Ethyl caprylate and isovaleric acid are the unique flavours produced by kefir to increase the fruity flavour of yoghurt. Lauric and palmitic acids are saturated higher fatty acids to protect the liver. Saturated fatty acids can not only protect the liver from alcohol damage and give energy to the body (fatty acid synthesis is necessary to supplement the body's energy consumption) but also increase the activity of some enzymes in the body. Ethyl lactate is a new product-ethyl lactate from lactic acid and ethanol. Acetaldehyde is converted into acetic acid and ethanol to produce malt aroma substance-isobutanol with the help of yeast, giving kefir unique soft mellow aroma. Furthermore, the higher content of two higher alcohols, phenylethyl alcohol and isoamyl alcohol in kefir, gave the typical rose aroma and fruit aroma in kefir fermented dairy products, respectively. Isobutanol, phenylethyl alcohol and isoamyl alcohol were rarely detected in ordinary yoghurt. The contents of 2-nonanone, 2-heptanone, nonanal, caprylic acid and acetoin significantly increased, which increased the cream flavour, proving that kefir was more palatable and had a special flavour that traditional kefir fermented yoghurt did not have. Therefore, the kefir treatment group can produce isobutanol, phenylethanol and isoamyl alcohol, which is of great significance to improve the flavour quality of kefir.

4. Conclusion and future research direction

This study found that L_1 and kefir fermented milk were pseudoplastic fluids, but their rheological properties and microstructure were affected to varying degrees after the addition of yeast and acetic acid bacteria. Meanwhile, the acidity increased following the addition of *A. tropicalis* A_3 and *S. cerevisiae* TN_1. Consequently, the protein structure denatured, and the isoelectric point decreased. During the high-temperature fermentation, kefir histone cross-linking becomes stronger, and the forming part of cheese, fat and protein binding is non-uniform. The apparent viscosity and viscoelasticity are significantly reduced with the increase in shear force, and the structure is not sufficiently stable. The fermented milk beverage is prepared by evenly stirring, which is conducive to removing the non-smooth feeling of cheese particles, resulting in a taste close to champagne and a smooth entrance. L_1 is more suitable for the preparation of set yoghurt. The gap between the L_1 protein clusters is smaller, the distribution is more uniform, and the gel water holding capacity is better. The results of the amino acid analysis showed no significant difference between the kefir and the L_1 groups, and the nutritional value was not affected. The decrease of some amino acid content was related to the flavour substances produced later. Compared to the L_1 group, the kefir group was supplemented with isobutanol, phenylethyl alcohol and isoamyl alcohol, consistent with the special flavors detected in traditionally made kefir milk (giving rose, fruit and malt flavors, mellow and champagne flavors).

The change of microstructure has a great influence on the texture of kefir yoghurt, but it is not enough to analyse the microstructure to determine the quality of kefir yoghurt. We will study the metabolites, use metabolomics to summarise and analyse the characteristic metabolites and find the law of the difference between the two. Furthermore, we explore whether the characteristic metabolites have a certain influence on macromolecules, such as proteins and polysaccharides. Kefir's industrial production, quality control and transportation storage has a certain degree of influence for the market to produce a real champagne yoghurt.

Data availability statement

The original contributions presented in the study are included in the article/supplementary material, further inquiries can be directed to the corresponding author.

Author contributions

RX: data curation, conceptualization, writing – review and editing, formal analysis, and supervision. ML: writing – review and editing, visualization, and supervision. XS, QT, and XH: conceptualization, and writing – review and editing. MH: writing – review and editing, funding acquisition, project administration, and supervision. All authors contributed to the article and approved the submitted version.

Funding

This work was financially supported by the research and application of microflora of yujiu, a sub-project of major science and

technology projects of Henan province, China (181100211400–8) and Henan University of Technology (No. 31401184).

Conflict of interest

The authors declare that the research was conducted in the absence of any commercial or financial relationships that could be construed as a potential conflict of interest.

Publisher's note

References

Ahmed, A., and Bajwa, U. (2019). Composition, texture and microstructure appraisal of paneer coagulated with sour fruit juices. *J. Food Sci. Technol.* 56, 253–261. doi: 10.1007/s13197-018-3484-4

Alinovi, M., Cordioli, M., Francolino, S., Locci, F., Ghiglietti, R., Monti, L., et al. (2018). Effect of fermentation-produced camel chymosin on quality of Crescenza cheese. *Int. Dairy J.* 84, 72–78. doi: 10.1016/j.idairyj.2018.04.001

Baniasadi, M., Azizkhani, M., Saris, P. E. J., and Tooryan, F. (2022). Comparative antioxidant potential of kefir and yogurt of bovine and non-bovine origins. *J. Food Sci. Technol.* 59, 1307–1316. doi: 10.1007/s13197-021-05139-9

Bensmira, M., and Jiang, B. (2012). Effect of some operating variables on the microstructure and physical properties of a novel kefir formulation. *J. Food Eng.* 108, 579–584. doi: 10.1016/j.jfoodeng.2011.07.025

Cautela, D., De Sio, F., Balestrieri, M. L., Casale, R., Laratta, B., Castaldo, D., et al. (2021). Amino acids, betaines and related ammonium compounds in Neapolitan limmo, a Mediterranean sweet lime, also known as lemoncetta Locrese. *J. Sci. Food Agric.* 101, 981–988. doi: 10.1002/jsfa.10706

Celik, O. F., Con, A. H., Saygin, H., Şahin, N., and Temiz, H. (2021). Isolation and identification of lactobacilli from traditional yogurts as potential starter cultures. *LWT* 148:111774. doi: 10.1016/j.lwt.2021.111774

Chen, Y.-H., Chen, H.-L., Fan, H.-C., Tung, Y.-T., Kuo, C.-W., Tu, M.-Y., et al. (2020). Anti-inflammatory, antioxidant, and antifibrotic effects of kefir peptides on salt-induced renal vascular damage and dysfunction in aged stroke-prone spontaneously hypertensive rats. *Antioxidants* 9:790. doi: 10.3390/antiox9090790

Chouchouli, V., Kalogeropoulos, N., Konteles, S. J., Karvela, E., Makris, D. P., and Karathanos, V. T. (2013). Fortification of yoghurts with grape (Vitis vinifera) seed extracts. *LWT-Food Science and Technology* 53, 522–529. doi: 10.1016/j.lwt.2013.03.008

Day, L., Cakebread, J. A., and Loveday, S. M. (2021). Food proteins from animals and plants: differences in the nutritional and functional properties. *Trends Food Sci. Technol.* 119, 428–442. doi: 10.1016/j.tifs.2021.12.020

De Vuyst, L., and Leroy, F. (2020). Functional role of yeasts, lactic acid bacteria and acetic acid bacteria in cocoa fermentation processes. *FEMS Microbiol. Rev.* 44, 432–453. doi: 10.1093/femsre/fuaa014

Ding, X., Wu, C., Huang, J., and Zhou, R. (2015). Changes in volatile compounds of Chinese Luzhou-flavor liquor during the fermentation and distillation process. *J. Food Sci.* 80, C2373–C2381. doi: 10.1111/1750-3841.13072

Dong, J., Liu, B., Jiang, T., Liu, Y., and Chen, L. (2018). The biofilm hypothesis: the formation mechanism of Tibetan kefir grains. *Int. J. Dairy Technol.* 71, 44–50. doi: 10.1111/1471-0307.12473

Duboc, P., and Mollet, B. (2001). Applications of exopolysaccharides in the dairy industry. *Int. Dairy J.* 11, 759–768. doi: 10.1016/S0958-6946(01)00119-4

Duran, F. E., Özdemir, N., Güneşer, O., and Kök-Taş, T. (2022). Prominent strains of kefir grains in the formation of volatile compound profile in milk medium; the role of lactobacillus kefiranofaciens subsp. kefiranofaciens, Lentilactobacillus kefiri and Lentilactobacillus parakefiri. *Eur. Food Res. Technol.* 248, 975–989. doi: 10.1007/s00217-021-03936-2

Farag, M. A., Jomaa, S. A., Abd El-Wahed, A., and El-Seedi, R. (2020). The many faces of kefir fermented dairy products: quality characteristics, flavour chemistry, nutritional value, health benefits, and safety. *Nutrients* 12:346. doi: 10.3390/nu12020346

Fontán, M. C. G., Martínez, S., Franco, I., and Carballo, J. (2006). Microbiological and chemical changes during the manufacture of kefir made from cows' milk, using a commercial starter culture. *Int. Dairy J.* 16, 762–767. doi: 10.1016/j.idairyj.2005.07.004

Gezginç, Y., Karabekmez-Erdem, T., Tatar, H. D., Ayman, S., Ganiyusufoğlu, E., and Dayisoylu, K. S. (2022). Health promoting benefits of postbiotics produced by lactic acid bacteria: exopolysaccharide. *Biotech Studies* 31, 62–63. doi: 10.38042/biotechstudies.1159166

Hamida, R. S., Shami, A., Ali, M. A., Almohawes, Z. N., Mohammed, A. E., and Bin-Meferij, M. M. (2021). Kefir: a protective dietary supplementation against viral infection. *Biomed. Pharmacother.* 133:110974. doi: 10.1016/j.biopha.2020.110974

Haque, A., Richardson, R., and Morris, E. (2001). Effect of fermentation temperature on the rheology of set and stirred yogurt. *Food Hydrocoll.* 15, 593–602. doi: 10.1016/S0268-005X(01)00090-X

Jiang, W., Zhu, H., Liu, C., Hu, B., Guo, Y., Cheng, Y., et al. (2022). In-depth investigation of the mechanisms of Echinacea purpurea polysaccharide mitigating alcoholic liver injury in mice via gut microbiota informatics and liver metabolomics. *Int. J. Biol. Macromol.* 209, 1327–1338. doi: 10.1016/j.ijbiomac.2022.04.131

Jung, M. K., Okekunle, A. P., Lee, J. E., Sung, M. K., and Lim, Y. J. (2021). Role of branched-chain amino acid metabolism in tumor development and progression. *J. Cancer Prevention* 26, 237–243. doi: 10.15430/JCP.2021.26.4.237

Karim, A., and Aider, M. (2022). Comprehensive utilisation of electro-activated whey-based media in cell growth, metabolite production and aroma compounds synthesis using a starter culture originated from kefir grains. *Int. Dairy J.* 126:105276. doi: 10.1016/j.idairyj.2021.105276

Khan, S. U., Pal, M. A., Wani, S. A., and Salahuddin, M. (2014). Effect of different coagulants at varying strengths on the quality of paneer made from reconstituted milk. *J. Food Sci. Technol.* 51, 565–570. doi: 10.1007/s13197-011-0525-7

Krzeminski, A., Großhable, K., and Hinrichs, J. (2011). Structural properties of stirred yoghurt as influenced by whey proteins. *LWT-Food Science and Technology* 44, 2134–2140. doi: 10.1016/j.lwt.2011.05.018

Laiho, S., Williams, R. P., Poelman, A., Appelqvist, I., and Logan, A. (2017). Effect of whey protein phase volume on the tribology, rheology and sensory properties of fat-free stirred yoghurts. *Food Hydrocoll.* 67, 166–177. doi: 10.1016/j.foodhyd.2017.01.017

Lim, J., Kale, M., Kim, D.-H., Kim, H.-S., Chon, J.-W., Seo, K.-H., et al. (2017). Antiobesity effect of exopolysaccharides isolated from kefir grains. *J. Agric. Food Chem.* 65, 10011–10019. doi: 10.1021/acs.jafc.7b03764

Liu, Y., Sun, B., Zhang, S., Li, J., Qi, J., Bai, C., et al. (2021). Glycine alleviates fluoride-induced oxidative stress, apoptosis and senescence in a porcine testicular Sertoli cell line. *Reprod. Domest. Anim.* 56, 884–896. doi: 10.1111/rda.13930

Liu, Z., Zhang, M., Bhandari, B., and Yang, C. (2018). Impact of rheological properties of mashed potatoes on 3D printing. *J. Food Eng.* 220, 76–82. doi: 10.1016/j.jfoodeng.2017.04.017

Lynch, K. M., Wilkinson, S., Daenen, L., and Arendt, E. K. (2021). An update on water kefir: microbiology, composition and production. *Int. J. Food Microbiol.* 345:109128. doi: 10.1016/j.ijfoodmicro.2021.109128

Lynch, K. M., Zannini, E., Wilkinson, S., Daenen, L., and Arendt, E. K. (2019). Physiology of acetic acid bacteria and their role in vinegar and fermented beverages. *Compr. Rev. Food Sci. Food Saf.* 18, 587–625. doi: 10.1016/j.copbio.2017.08.007

McAuliffe, O., Kilcawley, K., and Stefanovic, E. (2019). Symposium review: genomic investigations of flavor formation by dairy microbiota. *J. Dairy Sci.* 102, 909–922. doi: 10.3168/jds.2018-15385

Nguyen, P. T., Kravchuk, O., Bhandari, B., and Prakash, S. (2017). Effect of different hydrocolloids on texture, rheology, tribology and sensory perception of texture and mouthfeel of low-fat pot-set yoghurt. *Food Hydrocoll.* 72, 90–104. doi: 10.1016/j.foodhyd.2017.05.035

Nielsen, B., Gürakan, G. C., and Ünlü, G. (2014). Kefir: a multifaceted fermented dairy product. *Probiotics and antimicrobial proteins* 6, 123–135. doi: 10.3390/fermentation8010009

Ozcan-Yilsay, T., Lee, W.-J., Horne, D., and Lucey, J. (2007). Effect of trisodium citrate on rheological and physical properties and microstructure of yogurt. *J. Dairy Sci.* 90, 1644–1652. doi: 10.3168/jds.2006-538

Pan, L.-H., Liu, F., Luo, S.-Z., and Luo, J. P. (2019). Pomegranate juice powder as sugar replacer enhanced quality and function of set yogurts: structure, rheological property, antioxidant activity and in vitro bioaccessibility. *LWT* 115:108479. doi: 10.1016/j.lwt.2019.108479

Patil, A. P., Patil, T. M., Shinde, A. R., Vakhariya, R. R., Mohite, S., and Magdum, C. (2021). Nutrition, Lifestyle & Immunity: Maintaining Optimal Immune Function & Boost our Immunity. *Asian J. Pharmaceutical Res. Develop.* 9, 129–136. doi: 10.22270/ajprd.v9i3.970

Petrova, P., Ivanov, I., Tsigoriyna, L., Valcheva, N., Vasileva, E., Parvanova-Mancheva, T., et al. (2021). Traditional Bulgarian dairy products: ethnic foods with health benefits. *Microorganisms* 9:480. doi: 10.3390/microorganisms9030480

Qiu, L., Zhang, M., Mujumdar, A. S., and Chang, L. (2021). Effect of edible rose (Rosa rugosa cv. Plena) flower extract addition on the physicochemical, rheological, functional and sensory properties of set-type yogurt. Food. *Bioscience* 43:101249. doi: 10.1016/j.fbio.2021.101249

Rom, O., Liu, Y., Finney, A. C., Ghrayeb, A., Zhao, Y., Shukha, Y., et al. (2022). Induction of glutathione biosynthesis by glycine-based treatment mitigates atherosclerosis. *Redox Biol.* 52:102313. doi: 10.1016/j.redox.2022.102313

Ruocco, C., Segala, A., Valerio, A., and Nisoli, E. (2021). Essential amino acid formulations to prevent mitochondrial dysfunction and oxidative stress. *Current Opinion in Clinical Nutrition & Metabolic Care* 24, 88–95. doi: 10.1097/MCO.000000000000704

Sadiye, A. (2020). Impact of storage time on the content of kefir. *Eurasian J. Food Science and Technology* 4, 82–90.

Şahingil, D. (2019). Microbiological, chemical compositions and antioxidant capacity of tarhana chips fermented with kefir. *Eskişehir Technical University J. Science and Technol. A-Applied Sciences and Engineering* 20, 495–502. doi: 10.18038/estubtda.533168

Salari, A., Ghodrat, S., Gheflati, A., Jarahi, L., Hashemi, M., and Afshari, A. (2021). Effect of kefir beverage consumption on glycemic control: a systematic review and meta-analysis of randomized controlled clinical trials. *Complement. Ther. Clin. Pract.* 44:101443. doi: 10.1016/j.ctcp.2021.101443

Sharifi, M., Moridnia, A., Mortazavi, D., Salehi, M., Bagheri, M., and Sheikhi, A. (2017). Kefir: a powerful probiotics with anticancer properties. *Med. Oncol.* 34, 183–187. doi: 10.1007/s12032-017-1044-9

Sharma, H., Ozogul, F., Bartkiene, E., and Rocha, J. M. (2021). Impact of lactic acid bacteria and their metabolites on the techno-functional properties and health benefits of fermented dairy products. *Crit. Rev. Food Sci. Nutr.* 1–23. Advance online publication. doi: 10.1080/10408398.2021.2007844

Shi, X., Wang, X., Hou, X., Tian, Q., and Hui, M. (2022). Gene Mining and flavour metabolism analyses of Wickerhamomyces anomalus Y-1 isolated from a Chinese liquor fermentation starter. *Front. Microbiol.* 13:387. doi: 10.3389/fmicb.2022.891387

Silva-Cutini, M. A., Almeida, S. A., Nascimento, A. M., Abreu, G. R., Bissoli, N. S., Lenz, D., et al. (2019). Long-term treatment with kefir probiotics ameliorates cardiac function in spontaneously hypertensive rats. *J. Nutr. Biochem.* 66, 79–85. doi: 10.1016/j.jnutbio.2019.01.006

Souza, J. V., and Dias, F. S. (2017). Protective, technological, and functional properties of select autochthonous lactic acid bacteria from goat dairy products. *Curr. Opin. Food Sci.* 13, 1–9. doi: 10.1016/j.cofs.2017.01.003

Tao, J., Huang, X., Ling, F., Yu, B., Zhou, X., Shen, Q., et al. (2022). Immobilization of lactic acid bacteria for production of extracellular polysaccharides. *Food Science and Technology* 42:9021. doi: 10.1590/fst.99021

Vasbinder, A. J., van de Velde, F., and de Kruif, C. G. (2004). Gelation of casein-whey protein mixtures. *J. Dairy Sci.* 87, 1167–1176. doi: 10.3168/jds.S0022-0302(04)73265-8

Wang, X., Kristo, E., and LaPointe, G. (2019). The effect of apple pomace on the texture, rheology and microstructure of set type yogurt. *Food Hydrocoll.* 91, 83–91. doi: 10.1016/j.foodhyd.2019.01.004

Wang, F., Song, Y., Vidyarthi, S. K., and Zhang, R. (2022). Physicochemical properties, and volatile compounds of blackened jujube vinegar as prepared by optimized fermentation process. *Int. J. Food Prop.* 25, 288–304. doi: 10.1080/10942912.2022.2032735

Wang, L., Zhang, M., Bhandari, B., and Yang, C. (2018). Investigation on fish surimi gel as promising food material for 3D printing. *J. Food Eng.* 220, 101–108. doi: 10.1016/j.jfoodeng.2017.02.029

Wang, L., Zhong, H., Liu, K., Guo, A., Qi, X., and Cai, M. (2016). The evaluation of kefir pure culture starter: liquid-core capsule entrapping microorganisms isolated from kefir grains. *Food Sci. Technol. Int.* 22, 598–608. doi: 10.1177/1082013216628311

Xing, Z., Tang, W., Geng, W., Zheng, Y., and Wang, Y. (2017). In vitro and in vivo evaluation of the probiotic attributes of lactobacillus kefiranofaciens XL10 isolated from Tibetan kefir grain. *Appl. Microbiol. Biotechnol.* 101, 2467–2477. doi: 10.1007/s00253-016-7956-z

Xu, X., Cui, H., Yuan, Z., Xu, J., Li, J., Liu, J., et al. (2022). Effects of different combinations of probiotics on rheology, microstructure, and moisture distribution of soy materials-based yogurt. *J. Food Sci.* 87, 2820–2830. doi: 10.1111/1750-3841.16204

Xu, K., Guo, M., Du, J., and Zhang, Z. (2019). Okra polysaccharide: effect on the texture and microstructure of set yoghurt as a new natural stabilizer. *Int. J. Biol. Macromol.* 133, 117–126. doi: 10.1016/j.ijbiomac.2019.04.035

Yang, S., Yan, D., Zou, Y., Mu, D., Li, X., Shi, H., et al. (2021). Fermentation temperature affects yogurt quality: a metabolomics study. *Food Biosci.* 42:101104. doi: 10.1016/j.fbio.2021.101104

frontiers | Frontiers in Microbiology

TYPE Original Research
PUBLISHED 01 February 2023
DOI 10.3389/fmicb.2022.1073057

OPEN ACCESS

EDITED BY
Ana Lopez Contreras,
Wageningen University and Research,
Netherlands

REVIEWED BY
David Robert Greig,
UK Health Security Agency (UKHSA),
United Kingdom
Dai Kuang,
Shanghai Jiao Tong University, China

*CORRESPONDENCE
Silin Tang
✉ silin.tang@effem.com

SPECIALTY SECTION
This article was submitted to
Food Microbiology,
a section of the journal
Frontiers in Microbiology

RECEIVED 18 October 2022
ACCEPTED 22 December 2022
PUBLISHED 01 February 2023

CITATION
Wu X, Luo H, Ge C, Xu F, Deng X, Wiedmann M, Baker RC, Stevenson AE, Zhang G and Tang S (2023) Evaluation of multiplex nanopore sequencing for *Salmonella* serotype prediction and antimicrobial resistance gene and virulence gene detection.
Front. Microbiol. 13:1073057.
doi: 10.3389/fmicb.2022.1073057

Evaluation of multiplex nanopore sequencing for *Salmonella* serotype prediction and antimicrobial resistance gene and virulence gene detection

Xingwen Wu[1], Hao Luo[1], Chongtao Ge[1], Feng Xu[1], Xiangyu Deng[2], Martin Wiedmann[3], Robert C. Baker[1], Abigail E. Stevenson[1], Guangtao Zhang[1] and Silin Tang[1]*

[1]Mars Global Food Safety Center, Beijing, China, [2]Center for Food Safety, University of Georgia, Griffin, GA, United States, [3]Department of Food Science, Cornell University, Ithaca, NY, United States

In a previous study, Multiplex-nanopore-sequencing based whole genome sequencing (WGS) allowed for accurate *in silico* serotype prediction of *Salmonella* within one day for five multiplexed isolates, using both SISTR and SeqSero2. Since only ten serotypes were tested in our previous study, the conclusions above were yet to be evaluated in a larger scale test. In the current study we evaluated this workflow with 69 *Salmonella* serotypes and also explored the feasibility of using multiplex-nanopore-sequencing based WGS for antimicrobial resistance gene (AMR) and virulence gene detection. We found that accurate *in silico* serotype prediction with nanopore-WGS data was achieved within about five hours of sequencing at a minimum of 30× *Salmonella* genome coverage, with SeqSero2 as the serotype prediction tool. For each tested isolate, small variations were observed between the AMR/virulence gene profiles from the Illumina and Nanopore sequencing platforms. Taking results generated using Illumina data as the benchmark, the average precision value per isolate was 0.99 for both AMR and virulence gene detection. We found that the resistance gene identifier – RGI identified AMR genes with nanopore data at a much lower accuracy compared to Abricate, possibly due to RGI's less stringent minimum similarity and coverage by default for database matching. This study is an evaluation of multiplex-nanopore-sequencing based WGS as a cost-efficient and rapid *Salmonella* classification method, and a starting point for future validation and verification of using it as a AMR/virulence gene profiling tool for the food industry. This study paves the way for the application of nanopore sequencing in surveillance, tracking, and risk assessment of *Salmonella* across the food supply chain.

KEYWORDS

whole genome sequencing, Oxford Nanopore Technologies, *Salmonella*, serotype prediction, foodborne pathogens, food safety, antimicrobial resistance genes, virulence genes

1. Introduction

Using the historical data from 1998 to 2019, the recent published report from U.S. CDC has revealed that non-typhoidal *Salmonella* spp. caused most foodborne disease outbreaks and illnesses in the U.S. among four major pathogens including *Listeria monocytogenes*, *E. coli O157*, and *Campylobacter* (Batz et al., 2021; CDC, 2021). Similarly in the report from EFSA, *Salmonella* is the most detected agent and the second-most important cause of foodborne disease cases in the E.U. (EFSA and ECDC, 2021). In addition to the public health risk associated with *Salmonella*, it also imposes significant economic burden on governments and the food industry. To mitigate the risk of *Salmonella* contamination in the supply chain and food production, it is important to have an efficient surveillance and source attribution system. Although more than 2,600 serotypes of *Salmonella* have been identified (Grimont and Weill, 2007), only a small proportion of these serotypes is responsible for the majority of human salmonellosis (CDC, 2013; Jackson et al., 2013; Yin et al., 2020). To overcome the disadvantages of traditional serotyping, such as the substantial time and labor requirements and the need for large number of specific antisera (Wattiau et al., 2011; Shi et al., 2015), the application of whole-genome sequencing (WGS) for *Salmonella* serotype identification and source tracking is attractive and has been shown to provide accurate results (Allard et al., 2016; Ashton et al., 2016). Two WGS platforms have been used in most previous genomic studies of *Salmonella*, including (1) Illumina (URL: https://www.illumina.com/systems/sequencing-platforms.html), which has been widely used for *Salmonella* identification, source tracking, and surveillance (Allard et al., 2016; Ashton et al., 2016); (2) Oxford Nanopore Technologies (ONT), which provides a solution to sequence long-read nucleic acid fragments in a rapid, real-time manner (URL: https://nanoporetech.com/products). Illumina sequencing generally has a higher data quality than ONT (Fox et al., 2014; Rang et al., 2018), although several studies have demonstrated that ONT sequencing can provide for reliable serotype prediction (Diep et al., 2019; Banerji et al., 2020; Cooper et al., 2020; Xu et al., 2020; Wu et al., 2021). There are reports of completing several *Salmonella* closed genomes using ONT data (González-Escalona et al., 2018; Gao et al., 2020; Haendiges et al., 2021) as well as differentiation of highly similar variants (Xu et al., 2021). These studies used one or two well recognized bioinformatic tools, SISTR (Yoshida et al., 2016) and SeqSero2 (Zhang et al., 2019), for *Salmonella* serotype prediction. Regardless of the data quality, both tools could successfully identify the target *Salmonella* serotype.

WGS data can also be used for the identification of virulence and antimicrobial resistance (AMR) genes. These genes can play critical roles in predicting appropriate treatments and strategies for outbreak control. Initiatives and plans have been formed for proactive monitoring and containment of AMR (USDA, 2014; Smith et al., 2016; WHO, 2016), and these actions would consequently impact food related industries. WGS is currently being used as an effective tool for prediction, surveillance, and further analysis of AMR in different microorganisms (Köser et al., 2014; Oniciuc et al., 2018), such as *Campylobacter jejuni* (Hodges et al., 2021) and *E.coli* (Päivärinta et al., 2020). Compared with a phenotypic antimicrobial susceptibility test, which by definition cannot provide genetic information on the AMR determinants (Kahlmeter et al., 2003), WGS identifies genetic AMR determinants, which has a number of advantages, including more detailed information on AMR emergence. Multiple studies used WGS for genomic analysis and discovered that, as one of the most common food-borne disease-causing bacteria, *Salmonella* isolates from different origins have acquired a large number of AMR and disinfectant resistance genes, with a number of isolates and strains having developed multi-drug resistance (Davidson et al., 2018; Jajere, 2019; Marchello et al., 2020; Zhao et al., 2020; Chen et al., 2020a). As for data acquisition, Chen et al. (2020a) reported that ONT sequencing can provide data for the analysis of AMR genes as well as virulence factors, while a hybrid of ONT and Illumina sequencing data was believed to be a better solution for higher accuracy (Wick et al., 2017; Chen et al., 2020a,b; Neal-McKinney et al., 2021), since it leverages both the high sequencing quality of Illumina data, and the continuity of long-read ONT data. The hybrid method for assembling high quality genomes was introduced as the R9 flow cells have been showing generally lower raw read accuracy compared to Illumina sequencing (Liu et al., 2019). However, with the continuous development of the nanopore sequencing technology, the latest version of the R10 flow cells appears to have improved performance in obtaining high quality raw reads, therefore making it possible to generate near-finished bacterial genomes without Illumina sequencing data for a hybrid assembly (Sereika et al., 2022).

In our previous study, ONT sequencing with multiplexing of five *Salmonella* isolates was evaluated and both SISTR and SeqSero2 results indicated that accurate serotype prediction can be achieved when each multiplexed isolate reached a minimum of 50× genome coverage (Wu et al., 2021). Cross-contamination of barcodes was observed in both our study as well as by Xu et al. (2018), and we suspected the root cause of such cross-contamination was the remaining free adaptors during library preparation and pooling. Removal of the dissociative adaptors would solve the problem. Since only 10 isolates were selected in our previous study, the conclusions above are yet to be evaluated in a larger scale test. Moreover, our previous study only focused on the identification of serotype antigenic formula, neither AMR gene nor virulence gene identification was examined. Consequently, in this study, we aimed to: (1) further evaluate the feasibility and reliability of the five isolate multiplex strategy we proposed before (Wu et al., 2021) using a larger number of isolates; and (2) compare the ability of the ONT and Illumina platforms to identify AMR as well as virulence genes within the genomic data generated.

2. Materials and methods

2.1. Bacterial strains

Sixty-nine *Salmonella* isolates each representing a different serotype were assessed in the current study (Supplementary

Table 1). Thirty-nine of these isolates represented the most common serotypes, which were selected from (i) the most common serotypes reported by the U.S. national *Salmonella* surveillance system in 2016 from all sources (CDC, 2016), (ii) the 20 most frequent serotypes in 2019 in the European Union/European Economic Area (EFSA and ECDC, 2021), and (iii) the most frequently serotyped human *Salmonella* isolates from American, Asian, European, North American, or Oceania countries, based on data extracted from the World Health Organization Global Foodborne Infections Network Country Data Bank (Hendriksen et al., 2011). Five isolates represented rare serotypes found in the food industry (information obtained by personal communication) including serotypes Minnesota, Johannesburg, Cubana, Havana, and Liverpool. Eight isolates represented difficult-to-identify or differentiate serotypes with molecular-level serotyping methods, as described in our previous study (Xu et al., 2020) including serotype Typhimurium, its O5-variant, and serotype 4,[5],12:i:-, Paratyphi B var. Java, Choleraesuis, Virchow, Orion var. 15+, 34+ and Give. Two isolates represented serotypes with issues associated with detection from the food supply chain (information obtained by personal communication), including serotype Poona and 66:z41:- (*S. bongori* subspecies V). The other serotypes not within the above-mentioned categories were randomly selected from the Cornell Food Safety Lab *Salmonella* isolate storage to represent serotypes with relatively moderate prevalence from various sources. Detailed isolate information can be found at www.foodmicrobetracker.com under the isolate ID (e.g., FSL R8-1295).

2.2. Genomic DNA extraction

Salmonella genomic DNA of all isolates was extracted as previously described (Wu et al., 2021). Briefly, QIAamp DNA mini kit (Qiagen, Hilden, Germany) was applied to extract genomic DNA from single colonies on Trypticase Soy Agar, which were cultured at 37°C for 20 ~ 22 h. Quality of the genomic DNA was assessed with the NanoDrop 2000 (Thermo Fisher Scientific, Delaware, United States) for absorbance value (A value), and the double stranded DNA quantity was assessed with the Qubit 3.0 fluorimeter (Life Technologies, Paisley, United Kingdom). The genomic DNA samples that met the criteria from ONT's guidance for qualification requirements for successful sequencing were used for library construction: (i) A 260/280 between 1.8 and 1.9; (ii) A 260/230 between 2.0 and 2.2. for each flow cell (FC). For each of the FCs, all multiplexed DNA samples were normalized to the same concentration before input, ranging from 400 to 600 ng. FCs with 1,000–1,500 active pores were used for sequencing.

2.3. Oxford nanopore library preparation and sequencing

The 69 isolates were divided into 14 groups; each group included five different isolates (isolate *Salmonella* Typhi FSL R6-0540 was used in two groups; see Table 1). We multiplexed five DNA libraries from each group into one DNA sample with the rapid Barcoding Sequencing kit (SQK-RBK004) according to the manufacturer's instructions and sequenced it with qualified FLO-MIN106D FCs (R9.4.1, active pore number ≥ 800) for 24 h on a GridION (Oxford Nanopore Technologies, Oxford, UK; Figure 1). Five barcodes (Barcode 01 ~ 05) were assigned to five isolates in each group and on each FC (Table 1). To assess the capability of this method for differentiating closely related *Salmonella* serotypes, we arranged the serotypes with similar antigenic formulae in the same group. For instance, Group No.1 includes *Salmonella* serotype Typhi (9,12[Vi]:d:-), Barranquilla (16:d:e,n,x), Minnesota (21:b:e,n,x), Gaminara (16:d:1,7), and Johannesburg (1,40:b:e,n,x); two of them hold the same O antigen – "16," three of them hold the same H1 antigen – "d," two hold the same H1 antigen – "b," and three of them hold the same H2 antigen – "e, n, x." Serotype Typhi does not have an H2 antigen, we thus added it to this group in order to investigate if multiplexed ONT sequencing would lead to a false positive H2 antigen of the serotype Typhi due to possible *in vitro* or *in silico* cross-contamination. We performed basecalling with Guppy's basecalling model (v5.1.13) integrated in the MinKNOW software v21.11.17 installed on GridION. This model was modified for 6 mA dam/5mC dcm and CpG.

2.4. Genomic and serotype prediction analysis

Raw data (demultiplexed, unfiltered and untrimmed reads) obtained after basecalling were processed through essentially the same demultiplexing (qcat v1.1.0, https://github.com/nanoporetech/qcat) and genome assembling workflow described by Wu et al. (2021); Figure 1. We used NanoPlot (version 1.18.1) to analyze the quality of ONT raw sequencing data.

Original serotype information for isolates was received by the source that provided isolates; our understanding is that all serotype data for the isolates used here was based on classical, antibody-based, serotyping (and not based on serotype prediction based on molecular data, e.g., WGS data). A large proportion of the isolates was obtained from animals and humans; these isolates had typically been characterized by traditional serotyping performed by agglutination (as described by Edwards and Ewing, 1986) at either the New York State Department of Health (for human isolates) or the National Veterinary Services Laboratories (NVSL), a division of the United State Department of Agriculture (USDA) Animal and Plant Health Inspection Service (APHIS, Ames, Iowa; for animal isolates; Alcaine et al., 2006; Rodriguez-Rivera et al., 2014). Both SeqSero2 v1.1.2[1] and SISTR_cmd (The *Salmonella in silico* Typing Resource Command-line Tool) v1.1.0 (Yoshida et al., 2016) were used for serotype prediction with the sequence data generated in this study. As previously described (Wu et al.,

1 https://github.com/denglab/SeqSero2

TABLE 1 *Salmonella* isolates tested.

Group ID	Barcode ID	Serotype[1]	Isolate ID (Cornell Food Safety Lab ID)	Antigenic Formula[2]
1	No. 01	Typhi	FSL R6-0540	9,12[Vi]:d:-
1	No. 02	Barranquilla	FSL R8-1295	16:d:e,n,x
1	No. 03	Minnesota	FSL R8-2410	21:b:e,n,x
1	No. 04	Gaminara	FSL R8-5569	16:d:1,7
1	No. 05	Johannesburg	FSL S5-0703	1,40:b:e,n,x
2	No. 01	Mississippi	FSL A4-0633	1,13,23:b:1,5
2	No. 02	Poona	FSL R8-0115	1,13,22:z:1,6
2	No. 03	Cubana	FSL R8-3581	1,13,23:z29:-
2	No. 04	Roodepoort	FSL R8-7983	1,13,22:z10:1,5
2	No. 05	Worthington	FSL S5-0490	1,13,23:z:l,w
3	No. 01	Derby	FSL R8-2630	1,4,[5],12:f,g:[1,2]
3	No. 02	Typhimurium o5-	FSL R8-3714	1,4,[5],12:i:1,2
3	No. 03	Agona	FSL S5-0517	1,4,[5],12:f,g,s:[1,2]
3	No. 04	Typhimurium	FSL S5-0536	1,4,[5],12:i:1,2
3	No. 05	4,[5],12:i:-	FSL S5-0580	4,[5],12:i:-
4	No. 01	Sandiego	FSL R8-4447	1,4,[5],12:e,h:e,n,z15
4	No. 02	Enteritidis	FSL S5-0415	1,9,12:g,m:-
4	No. 03	Paratyphi B var. Java	FSL S5-0447	1,4,[5],12:b:1,2
4	No. 04	Heidelberg	FSL S5-0448	1,4,[5],12:r:1,2
4	No. 05	Saintpaul	FSL S5-0649	1,4,[5],12:e,h:1,2
5	No. 01	Bredeney	FSL R8-2629	1,4,12,27:l,v:1,7
5	No. 02	Kiambu	FSL R8-9562	1,4,12:z:1,5
5	No. 03	Wien	FSL R9-0007	1,4,12,[27]:b:l,w
5	No. 04	*S. enterica* subspecies IIIa -:z4,z23:-	FSL R9-0515	-:z4,z23:-
5	No. 05	Schwarzengrund	FSL S5-0458	1,4,12,27:d:1,7
6	No. 01	Give	FSL S5-0487	3,{10}{15}{15,34}:l,v:1,7
6	No. 02	Orion var. 15+, 34+	FSL R8-3858	3,{10}{15}{15,34}:y:1,5
6	No. 03	Alachua	FSL R8-2924	35:z4,z23:-
6	No. 04	Anatum	FSL R8-7981	3,{10}{15}{15,34}:e,h:1,6
6	No. 05	Muenster	FSL S5-0432	3,{10}{15}{15,34}:e,h:1,5
7	No. 01	*S. bongori* subspecies V 66:z41:-	FSL R9-0518	66:z41:-
7	No. 02	Meleagridis	FSL R8-6670	3,{10}{15}{15,34}:e,h:l,w
7	No. 03	Stockholm	FSL R8-4727	3,{10}{15}:y:z6
7	No. 04	Uganda	FSL R8-3404	3,{10}{15}:l,z13:1,5
7	No. 05	Weltevreden	FSL S5-0438	3,{10}{15}:r:z6
8	No. 01	Choleraesuis	FSL R9-0095	6,7:c:1,5
8	No. 02	Bareilly	FSL R8-7922	6,7,14:y:1,5
8	No. 03	Infantis	FSL S5-0734	6,7,14:r:1,5
8	No. 04	Rissen	FSL R9-0152	6,7,14:f,g:-
8	No. 05	Thompson	FSL S5-0523	6,7,14:k:1,5
9	No. 01	Braenderup	FSL R8-7984	6,7,14:e,h:e,n,z15
9	No. 02	*S. enterica* subspecies IV 45:g,z51:-	FSL R9-0517	45:g,z51:-

(Continued)

TABLE 1 (Continued)

Group ID	Barcode ID	Serotype[1]	Isolate ID (Cornell Food Safety Lab ID)	Antigenic Formula[2]
9	No. 03	Norwich	FSL R8-6279	6,7:e,h:1,6
9	No. 04	Mbandaka	FSL S5-0451	6,7,14:z10:e,n,z15
9	No. 05	Newport	FSL R8-7979	6,8,20:e,h:1,2
10	No. 01	Havana	FSL S5-0549	1,13,23:f,g,[s]:-
10	No. 02	Livingstone	FSL R8-5215	6,7,14:d:l,w
10	No. 03	Ohio	FSL R8-4333	6,7,14:b:l,w
10	No. 04	Putten	FSL A4-0590	13,23:d:l,w
10	No. 05	Virchow	FSL S5-0961	6,7,14:r:1,2
11	No. 01	Panama	FSL R8-2996	1,9,12:l,v:1,5
11	No. 02	Dublin	FSL S5-0439	1,9,12[Vi]:g,p:-
11	No. 03	Ibadan	FSL R8-4726	13,22:b:1,5
11	No. 04	Javiana	FSL S5-0395	1,9,12:l,z28:1,5
11	No. 05	Pomona	FSL R8-0451	28:y:1,7
12	No. 01	*S. enterica* subspecies VI [1],6,14,[25]:a:e,n,x	FSL R9-8566	[1],6,14,[25]:a:e,n,x
12	No. 02	Cerro	FSL R8-0370	6,14,18:z4,z23:[1,5]
12	No. 03	Senftenberg	FSL R8-5370	1,3,19:g,[s],t:-
12	No. 04	Hartford	FSL R8-5223	6,7:y:e,n,x
12	No. 05	*S. enterica* subspecies IIIb 6,7:l,v:z53	FSL R9-0516	6,7:l,v:z53
13	No. 01	Kentucky	FSL S5-0273	8,20:i:z6
13	No. 02	Typhi[3]	FSL R6-0540	9,12[Vi]:d:-
13	No. 03	Blockley	FSL S5-0648	6,8:k:1,5
13	No. 04	Muenchen	FSL R8-7982	6,8:d:1,2
13	No. 05	Apapa	FSL R8-5222	45:m,t:-
14	No. 01	Liverpool	FSL R9-1184	1,3,19:d:e,n,z15
14	No. 02	Oranienburg	FSL R8-7977	6,7,14:m,t:[z57]
14	No. 03	Ealing	FSL R8-2454	35:g,m,s:-
14	No. 04	Montevideo	FSL S5-0630	6,7,14,[54]:g,m,[p],s:[1,2,7]
14	No. 05	Tennessee	FSL R8-5221	6,7,14:z29:[1,2,7]

[1]Serotype information of each isolate was based on data from www.foodmicrobetracker.com under the isolate ID.
[2]Antigenic formula was extracted from Grimont and Weill (2007). Antigenic formulae of the *Salmonella serovars*, (9th ed.) Paris: WHO Collaborating Centre for Reference and Research on *Salmonella*, according to the serotype names.
[3]Isolate FSL R6-0540 (Serotype Typhi) was used in two groups - Group 1 and Group 13.

2021), both ONT raw reads and assembled contigs were used as input data for SeqSero2, while only assembled contigs were used as input data for SISTR. Default parameters were used according to the developer's manual. We collected different sizes of sequencing data from ONT to assess the influence of sequencing depth and sequencing time on the accuracy of serotype prediction. We defined the lowest depth of genome coverage that one multiplexed isolate could achieve among all the multiplexed isolates on one FC at a given sequencing time as $Depth_{min}$ of this FC. A one-way analysis of variance (ANOVA) followed by a Tukey HSD test was carried out to compare the difference of data yield between combined isolates in each FC.

2.5. AMR and virulence gene identification and precision-recall analysis

Assembled contigs generated from our serotype prediction workflow were used for AMR and virulence gene identification. RGI (resistant gene identifier) 5.1.1 (Alcock et al., 2020) and Abricate 1.0.1[2] were both loaded with the CARD database (ver. 2020-Apr-19; Alcock et al., 2020) and then launched for the identification of AMR

2 https://github.com/tseemann/abricate

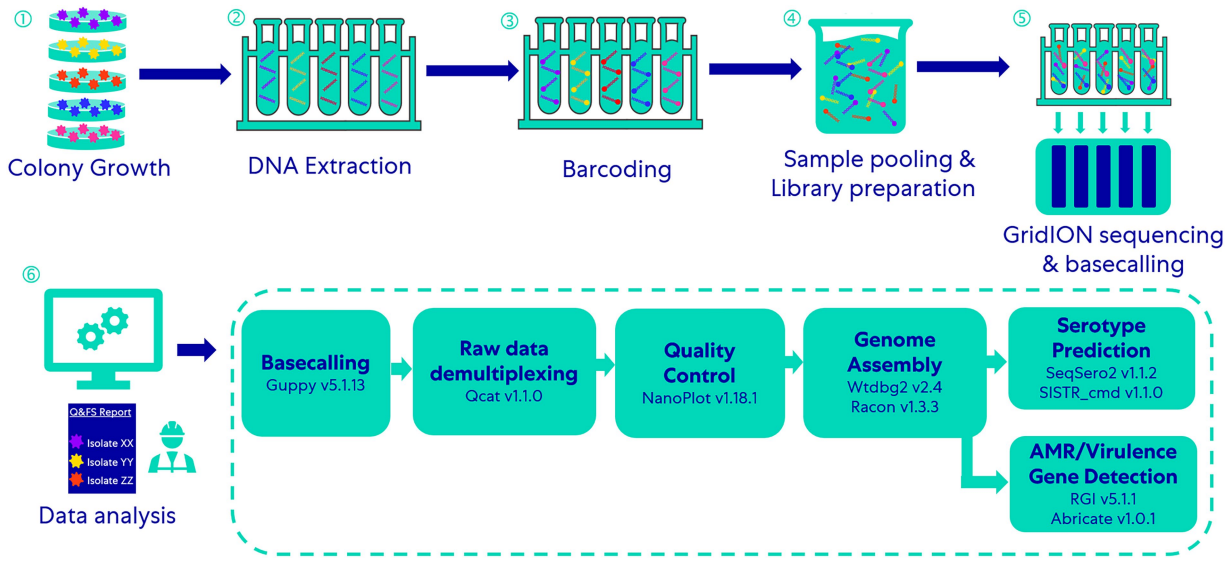

FIGURE 1
Workflow of the multiplex-ONT-sequencing-based WGS method for *Salmonella* serotype prediction and AMR/virulence gene detection.

genes under default arguments. For virulence gene identification, only Abricate was used to search against the VFDB database (ver. 2020-Apr-19; Liu et al., 2019), and arguments were defined as default.

A precision-recall analysis was performed to evaluate the differences between Illumina and ONT data regarding the AMR and virulence genes identified. AMR and virulence genes identified from Illumina data were assumed to be the benchmark. Therefore, for each isolate, genes identified in both Illumina and ONT data were true positive (TP) results, genes identified only in ONT data were false positive (FP) results, and genes identified only in Illumina data were false negative (FN) results. The following equations were used to obtain the values of "Precision," "Recall," "Accuracy," and "False-negative probability": False-positive probability was not calculated as we did not pursue the true negative number of AMR or virulence genes detected in this study.

$$\text{Precision} = \sum \text{TP} / \sum (\text{TP} + \text{FP})$$

$$\text{Recall} = \sum \text{TP} / \sum (\text{TP} + \text{FN})$$

$$\text{Accuracy} = \sum (\text{TP} + \text{TN}) / \sum (\text{TP} + \text{TN} + \text{FP} + \text{FN})$$

$$\text{False} - \text{negative probability} = \frac{\sum \text{False negative}}{\sum (\text{False negative} + \text{True Positive})} /$$

To investigate the impact of depth of genome coverage on Precision and Recall, different depths (15×, 30×, 50×, and 75×) of genome coverage data for the serotype Typhimurium isolate were extracted to perform genome assembling, the obtained contigs were analyzed through AMR and virulence gene identification by RGI and Precision-Recall analysis.

2.6. Identification of possible cross-assigned reads and influence of cross-assigned reads on the accuracy of serotype prediction

We detected possible cross-assigned reads from each FC as described previously (Wu et al., 2021). Cross-assigned reads were identified from serotype prediction errors caused by single ONT reads. We used 50× depth of genome coverage demultiplexed raw sequencing reads as input of SeqSero2 to identify this type of prediction error and the corresponding error-causing antigen determinant loci. ONT raw reads that could match these error-causing antigen determinant loci, by using BLAST[3] with identity ≥90% and coverage = 100%, would be classified as possible cross-assigned reads.

3. Results and discussion

3.1. Overview of multiplexed and demultiplexed nanopore sequencing data and assembly of *Salmonella* genomes

An average of 6.58 Gbp of raw ONT sequencing data per FC ($N = 14$ FCs) was obtained after 24 h of ONT sequencing. Data outputs of FCs ranged from 4.51 to 8.34 Gbp with a mean read

3 https://blast.ncbi.nlm.nih.gov/Blast.cgi

length of 9,248 bp and a mean N50 read length of 17,273 bp on average across all FCs (Table 2). Sequencing quality was shown to be highly consistent among FCs, with mean quality scores for a given FC ranging from 11.50 to 12.10. The average quality score across all FCs was 11.79.

Qcat failed to assign an average of 7.20% ± 0.52% (mean ± standard deviation, $N = 14$ FCs) reads per FC to any barcode; these reads were defined as Non-assigned reads. Qcat assigned an average of 0.03% reads per FC to barcodes that were not included in the FC, which was consistent with our previous study (Wu et al., 2021). These reads were defined as mis-assigned reads (Figure 2; Supplementary Table 2). The original demultiplexed ONT sequencing data were submitted to NCBI - SRA (Accession number: PRJNA694442).

Tukey HSD test indicated that Barcode 03 (BC03) showed significantly lower ($p < 0.05$, $N = 14$ FCs, overall ANOVA p-value = 0.0019, $\alpha = 0.05$) sequence data yields compared to two of the other four barcodes used, which implied that the data-yield performance varied among the barcodes provided by the same ONT rapid barcoding kit product (Figure 3). This may lead to uneven distribution of sequence data among multiplexed isolates on the same FC, impacting the minimum total ONT sequencing time, because the final total sequencing time needs to be long enough to allow the barcoded isolate that obtained the least sequence data to receive sufficient data (e.g., 50× depth of genome coverage) for downstream analysis. Our previous study also identified that, when multiplexing more than four isolates, some of the barcodes showed significantly lower data yield than the others (Wu et al., 2021).

3.2. Influence of sequencing time and depth on accuracy of *Salmonella* serotype prediction using ONT assembled genomes

With five isolates multiplexed on each FC, we assessed three levels of $Depth_{min}$ (15×, 30×, 50×) for the accuracy of *Salmonella* serotype prediction. Using assembled genomes as input to SeqSero2 and SISTR, when $Depth_{min}$ was 30× and 50×, SeqSero2 correctly predicted all 69 serotypes across 14 FCs, while the prediction accuracy of SISTR was 98.6% (68/69) at $Depth_{min}$ 30× and 50× of the FC (Table 3). The error result generated by SISTR showed that the O antigen of serotype -:z4,z23:- (subspecies IIIa, FSL R9-0515) was miss-called as "41" across all the depths tested (Table 4). The O antigen of the other four isolates multiplexed with FSL R9-0515 are all "4" rather than "41," and correctly predicted, indicating that this prediction error was not caused by cross-assigned reads. Cross-assigned reads analysis by BLAST did not identify any cross-assigned read that could cause the miss-calling of O antigen as "41."

With respect to the prediction errors at $Depth_{min}$ 15× of SeqSero2 and SISTR, BLAST analysis showed that the low depth of genome coverage (15×) with the relatively low sequencing quality of ONT data (average Qscore = 12.24 at $Depth_{min}$ of 15×, $N = 14$) led to failure in matching antigen determinant alleles of O antigen 1, 3, 6, 16, 19, 21, or 45, for five serotypes. For all the prediction errors of SeqSero2 at $Depth_{min}$ of 15× (Table 4), the low depth of coverage did not allow SeqSero2 to determine any O antigen for four of the tested serotypes.

TABLE 2 Statistics of ONT multiplex sequencing data for each group of isolates tested from 24h of sequencing.

Group No[1].	Total clean data yield in 24h (Gbp)	Mean read length (bp)	Mean quality score	Number of reads	Mean read length N50
1	6.70	8,527	11.50	786,309	17,240
2	6.17	8,842	11.70	697,460	16,854
3	7.19	8,240	12.10	872,570	15,974
4	6.68	8,747	11.20	873,088	17,622
5	7.19	8,772	11.50	819,834	16,281
6	5.31	9,253	12.10	573,709	17,183
7	5.90	9,205	11.80	640,597	16,709
8	7.64	9,629	11.90	693,913	17,290
9	5.78	8,431	12.00	685,709	15,234
10	7.20	10,475	12.00	687,001	19,509
11	8.34	8,486	11.90	982,440	15,686
12	5.68	11,081	11.90	512,726	19,932
13	7.79	10,304	11.70	756,070	18,957
14	4.51	9,475	11.70	476,383	17,348
Average	**6.58**	**9,248**	**11.79**	**718,415**	**17,273**

[1]Each group contains five isolates, each group of isolates were multiplexed and sequenced on one ONT flow cell.

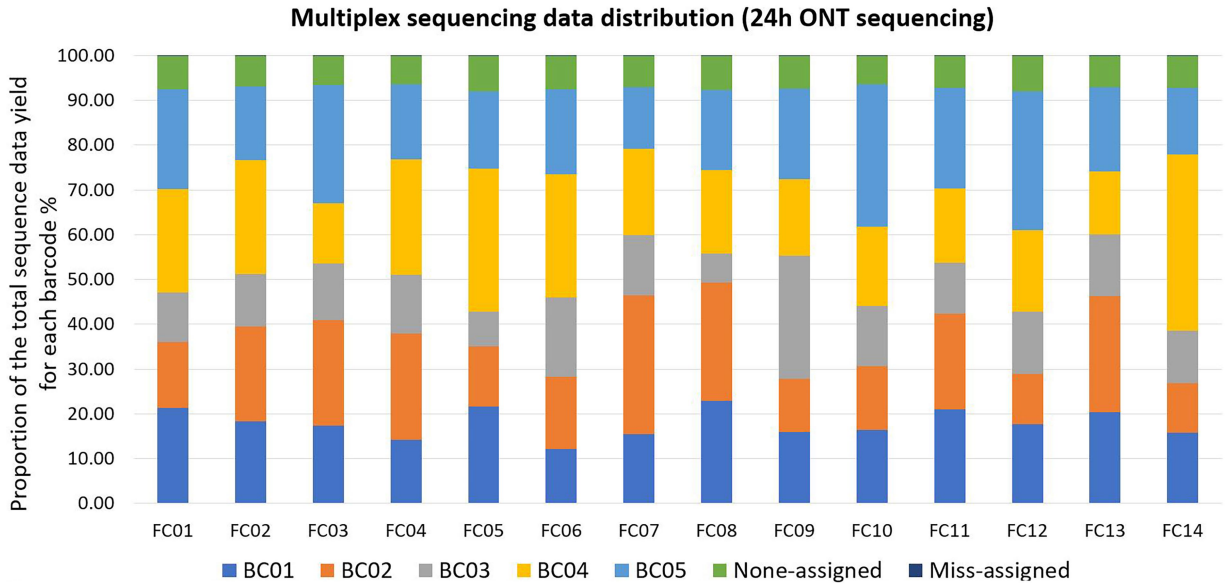

FIGURE 2
Multiplex sequencing data distribution within each flow cell (FC) for each barcode (BC) after 24h of ONT sequencing. Each color represents one BC or none-assigned/miss-assigned reads. Within each FC, ONT reads that were not assigned to any BC were defined as non-assigned reads, reads assigned to a BC that was not used in the FC were defined as miss-assigned reads. As the bars for miss-assigned reads were not easily visible, detailed proportions are listed here: the number of mis-assigned reads was 2% in FC02 and FC05, and 3% in all the other FCs.

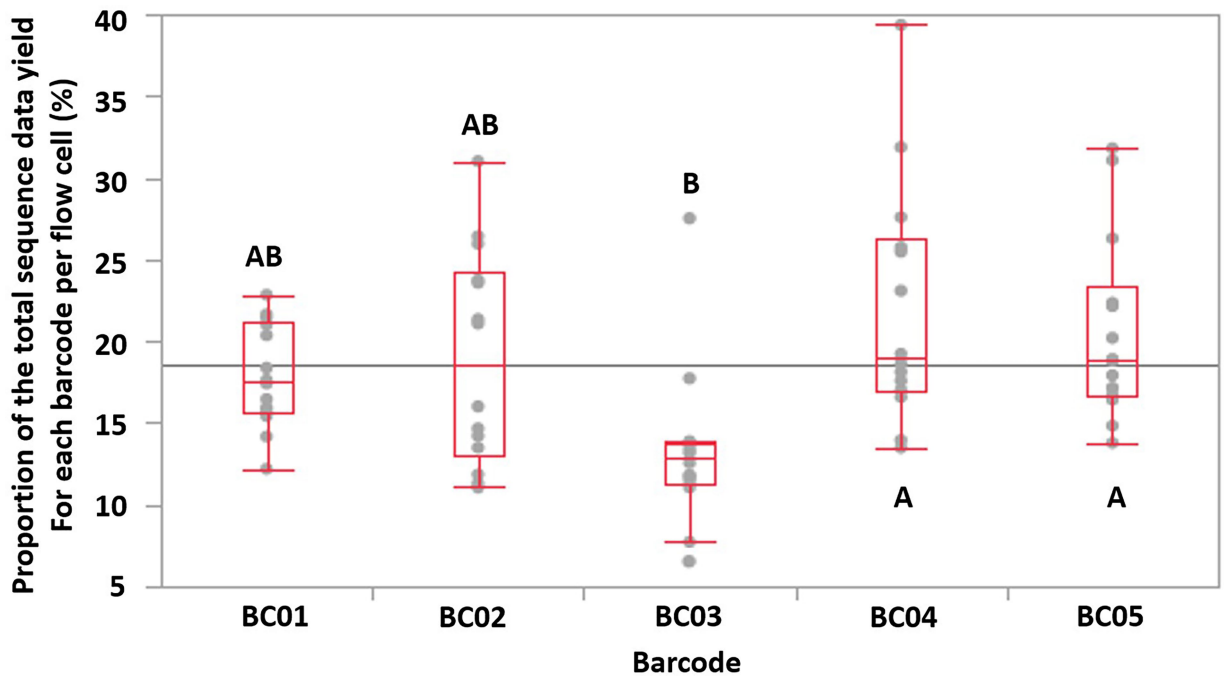

FIGURE 3
The proportion of the total sequence data yield for each barcode (labeled as BC01-BC05) per flow cell is shown as a single dot. The maximum/minimum (excluding outliers), 75, 50, and 25% quantile data yield of a barcode of each flow cell are labeled with red lines. Based on Tukey HSD test, barcodes that does not share the same letters were significantly different (p-value<0.05, overall ANOVA p-value=0.0019).

The ONT sequencing times for each $Depth_{min}$ level are shown below (Table 5). $Depth_{min}$ 15×, 30×, and 50× of one FC multiplexing five *Salmonella* isolates could be achieved within 2.36 ± 0.43 h, 4.32 ± 0.87 h, and 7.01 ± 1.57 h (mean ± standard deviation, N = 14), respectively.

In summary, accurate serotype prediction with ONT WGS data was achieved within about 5 h of ONT sequencing at a minimum depth of *Salmonella* genome coverage at 30× (assuming the genome size of a given *Salmonella* strain is 4.8 Mbp) with Guppy's basecalling model modified for 6 mA dam/5mC dcm and CpG, with SeqSero2 as the prediction tool. This minimum depth of ONT WGS data for serotype prediction is also consistent the minimum depth (for ≥10 kb reads) for bacterial assemblies recommended by ONT (URL: https://nanoporetech.com/sites/default/files/s3/literature/microbial-genome-assembly-workflow.pdf).

As we previously reported, multiplexing more than three isolates will inevitably cause uneven data allocation among multiplexed isolates. It is thus essential that the multiplexed isolate with the least data reaches a depth of 30× genome coverage for reliable serotype prediction, by extending overall sequencing duration to be longer than simply using the sequencing time required for a single isolate for a multiplexed run.

When using raw reads rather than assembled genomes as input for SeqSero2, one serotype prediction error was found for isolate FSL R9-0518 (*Salmonella Bongori*; Serotype 66:z41:-) with FC $Depth_{min}$ at 50×, where it was called as *Salmonella Bongori* Serotype 1,3,19:z41:l,w.. Cross-assigned reads analysis by BLAST indicated that the O and H2 antigen were mis-identified, possibly due to reads cross-assigned from the other isolates multiplexed in the same FC. These cross-assigned reads contained antigen determining alleles from the other isolates with O and H2 antigens different from serotype 66:z41:-. With a bead clean-up step added to the multiplexed library preparation process, we found an occurrence rate of read cross-assignment of 7% (1/14) in the current study, compared to 8% (2/24) reported in our previous study (Wu et al., 2021). The errors caused by cross-assigned reads were corrected by using an assembled genome, and this finding is consistent with our previous study (Wu et al., 2021).

TABLE 3 Accuracy of *Salmonella* serotype prediction using assembled genomes from ONT multiplex sequencing data.

$Depth_{min}$[1]	SeqSero2	SISTR
15 x	95.7% (66/69)	97.1% (67/69)
30 x	100% (69/69)	98.6% (68/69)
50 x	100% (69/69)	98.6% (68/69)

[1]We defined the lowest depth of genome coverage that one multiplexed isolate could achieve among all the multiplexed isolates on one flow cell at a given sequencing time as Depthmin of this flow cell.

3.3. AMR and virulence gene identification

At the single isolate level, some variations in AMR and virulence gene profile were observed between Illumina and ONT data (Supplementary Table 3). For an individual *Salmonella* isolate, Abricate generated similar AMR and virulence identification results using either Illumina or ONT data, while RGI showed substantial discrepancies between these two sequencing platforms. Taking results from Illumina data as ground truth, the average number of true positive AMR genes per isolate identified from ONT data by Abricate and RGI was 26.19 and 29.64, respectively (Table 6). With ONT data, Abricate and RGI (i) failed to identify an average of 0.36 and 11.81 AMR genes per isolate, respectively and (ii) identified an average of 0.19 and 5.91 false positive AMR genes per isolate, with false negative probabilities of 1.37 and 27.62%, respectively. When using Abricate with the VFDB library to scan ONT data for virulence genes per isolate, 99.64 true positive virulence genes on average were identified, with 1.25 false negative genes and 1.07 false positive genes identified. In general, if RGI was used for AMR gene identification, ONT data of the 69 isolates yielded an average precision of 0.84 and an average recall of 0.72 compared to Illumina data. Abricate on the other hand yielded both precision and recall of 0.99 for either AMR gene or virulence gene identification.

Through the results generated by Abricate, we calculated the total number of false negatives (FNs) and false positives (FPs) for each detected gene as well as for each isolate. A total of 26 isolates

TABLE 4 *Salmonella* serotype prediction errors.

Isolate ID	Serotype	Antigenic Formula	Predicted Antigenic Formula	Serotype prediction tool	Actual depth of genome coverage	$Depth_{min}$ of the flow cell
FSL R8-1295	Barranquilla	16:d:e,n,x	I -:d:e,n,x	SeqSero2	22×	15×
FSL R8-2410	Minnesota	21:b:e,n,x	I -:b:e,n,x	SeqSero2	16×	15×
FSL R9-0517	IV 45:g,z51:-	45:g,z51:-	IV -:g,z51:-	SeqSero2	17×	15×
FSL S5-0648	Blockley	6,8:k:1,5	I -:k:1,5	SeqSero2	17×	15×
FSL R8-5370	Senftenberg	1,3,19:g,[s],t:-	3,10:g,s,t:-	SeqSero2	20×	15×
FSL R9-0515	subspecies:IIIa -:z4,z23:-	-:z4,z23:-	IIIa 41:z4,z23:-	SISTR	60×; 122×; 206×	15×; 30×; 50×

were found as having FNs; these FNs were associated with a total of 13 AMR and 39 virulence genes (Figure 4), indicating these genes failed to be detected in at least some of the genome assemblies generated from ONT sequencing data. The raw reads containing these FNs might have been excluded due to low quality caused by ONT sequencing errors, while Illumina sequencing data seemed to provide a more complete profile of the AMR and virulence genes. On the other hand, FPs were associated with nine AMR genes and 31 virulence genes; these FNs were contributed by 23 isolates. The total number of FNs was higher than FPs, although many of the isolates had both FNs and FPs. Among all FPs, one virulence gene *shdA* has an exceptionally high number of FP hits from nine different isolates (Figure 4; Supplementary Table 3), with a mean coverage >97.95% and a mean identity >94.33%. *shdA* encodes an AIDA (Adhesin Involved in Diffuse Adherence)-like protein, with a total nucleotide length of 6,105 bp (Kingsley et al., 2000); such length can be fully covered by ONT long-reads while several Illumina reads are needed for assembly. The FP hits for *shdA* may represent true positives as the true composition of AMR genes and virulence genes of the tested isolates was unknown, because only the Illumina sequencing data were used as the benchmark. It is possible that some genes were not fully recovered during the Illumina-based genome assembly process, consequently causing low coverage or identification when detecting AMR and virulence genes using Abricate.

We compared the precision and recall of AMR/virulence gene identification between five different sequencing depths of one test isolate (FSL S5-0536) representing serotype Typhimurium to further explore the impact of sequencing depth on accuracy of AMR/virulence gene identification with multiplex-ONT WGS data. As all the isolates were tested with the same workflow, we speculated that the dynamics of the association between accuracy and sequencing depths for AMR/virulence gene identification with ONT data would be the same for these isolates. We therefore picked only serotype Typhimurium as the representative and assembled the genome of this isolate at sequencing depth 15×, 30×, 50×, 75×, and 100×. These assemblies then went through Abricate loaded with CARD and VFDB libraries and RGI loaded with CARD library. Recall and Precision statistics based on the identification results are shown below (Table 7). We found that with Abricate, sequencing depth of 30× or above was sufficient to obtain highest recall and precision for

TABLE 5 ONT multiplex sequencing time per flow cell.

Group ID	Sequencing Time in hours to achieve a minimum genome coverage for each isolate on a flow cell		
	15×	30×	50×
Group 1	2.80	4.96	7.67
Group 2	2.30	4.14	6.72
Group 3	1.94	3.49	5.52
Group 4	1.87	3.48	5.67
Group 5	2.66	5.12	8.60
Group 6	2.37	4.38	7.23
Group 7	1.98	3.51	5.65
Group 8	3.24	6.19	10.45
Group 9	2.38	4.32	6.98
Group 10	1.90	3.41	5.37
Group 11	2.17	3.76	5.82
Group 12	2.86	5.27	8.34
Group 13	1.97	3.47	5.41
Group 14	2.61	4.97	8.64
Average Sequencing Time ($N = 14$)	2.36	4.32	7.01

TABLE 6 Accuracy of AMR/virulence gene identification using ONT multiplex sequencing data.

	RGI (CARD)		Abricate (CARD)		Abricate (VFDB)	
	Average Value[2]	95% CI	Average Value	95% CI	Average Value	95% CI
True positive[1]	29.64	28.92, 30.36	26.19	25.64, 26.74	99.64	97.77, 101.51
False negative	11.81	10.49, 13.13	0.36	0.16, 0.56	1.25	0.56, 1.94
False positive	5.91	5.45, 6.37	0.19	0.06, 0.32	1.07	0.43, 1.71
Precision[3]	0.84	0.83, 0.85	0.99	0.99, 0.99	0.99	0.98, 1.00
Recall[4]	0.72	0.70, 0.74	0.99	0.98, 1.00	0.99	0.98, 1.00
False-negative probability[5]	27.62%	25.44, 29.80%	1.37%	0.61, 2.13%	1.18%	0.54, 1.82%

[1]The positive detections of AMR or virulence genes from Illumina sequence data were taken as true positives; any genes that were detected by Illumina sequence data, but not by ONT sequence data were taken as false negatives; any genes were detected by ONT sequence data, but not by Illumina sequence data were taken as false positives.
[2]N = 69 *Salmonella* isolates.
[3]Precision = ∑True positive/∑(True positive + False positive).
[4]Recall = ∑True positive/∑(True positive + False negative).
[5]False-negative probability = ∑False negative/ ∑(False negative + True Positive); False-positive probability was not calculated as we did not pursue the true negative number of AMR or virulence genes detected in this study.

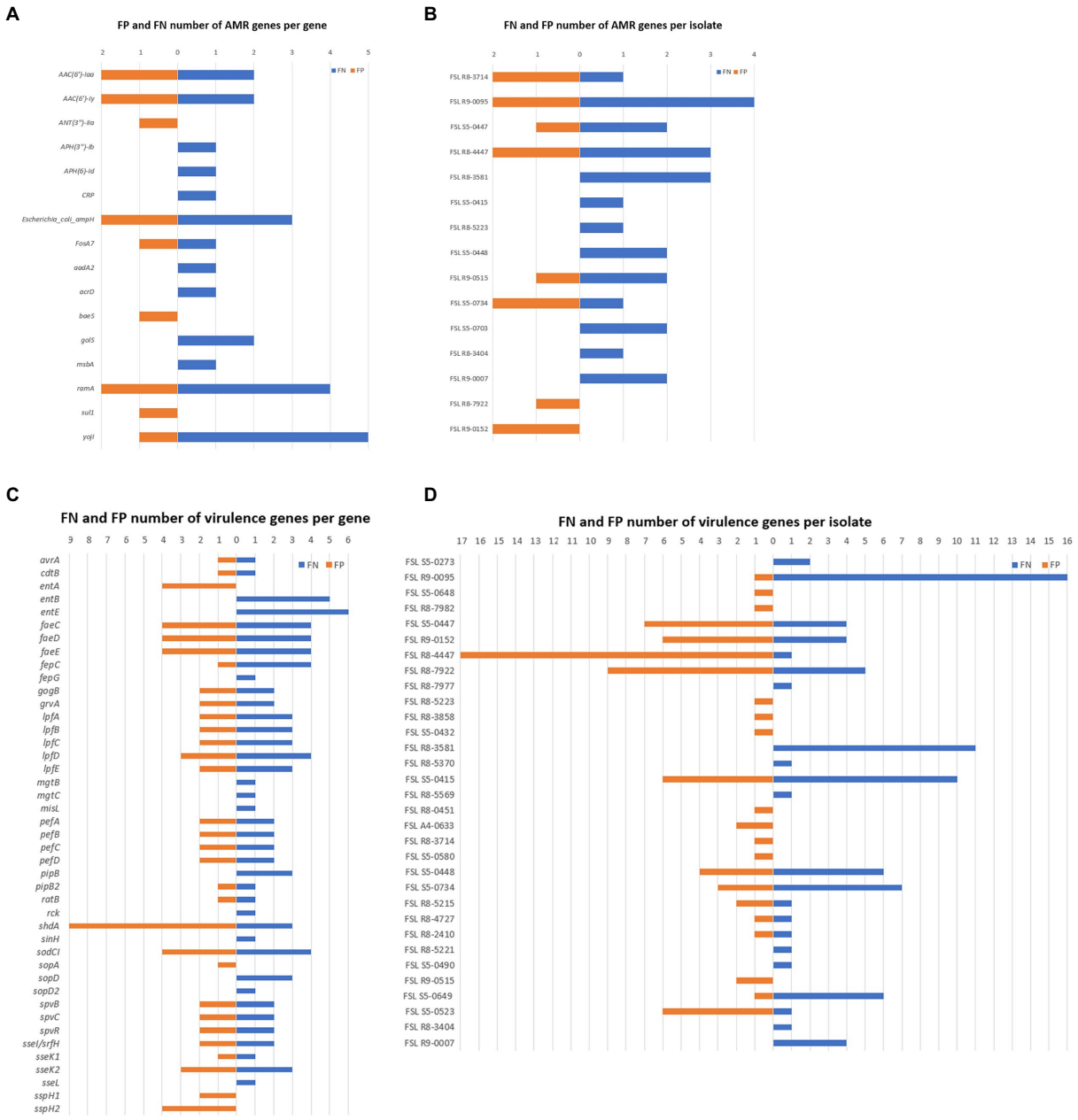

FIGURE 4
False Positive (FP) and False Negative (FN) numbers of AMR and virulence genes detected with ONT data, taking results from Illumina data as benchmark. **(A)** Number of AMR gene FN (in orange) and FP (in blue) results for different AMR genes; AMR genes not shown did not yield AMR gene FP or FN results; **(B)** Number of AMR gene FN and FP results for each given isolate; isolates not shown did not yield AMR gene FN or FP results; **(C)** Number of virulence gene FN and FP results for different virulence genes; virulence genes not shown did not yield virulence gene FP or FN results; **(D)** Number of virulence FN and FP results for each given isolate; isolates not shown did not yield virulence gene FN or FP results.

both AMR and virulence gene identification for isolate FSL S5-0536, while with RGI, precision and recall reached the highest value when sequencing depth was at 75×.

Previously, Gargis et al. (2019) also found that AMR markers could be correctly detected from the biothreat pathogens *Bacillus anthracis* and *Yersinia pestis* with 100,000 ONT raw sequencing reads per isolate. Noting that *Bacillus anthracis* and *Yersinia pestis* have similar genome sizes as *Salmonella* (assuming the genome size of a given *Salmonella* strain is 4.8 Mbp), our sequencing workflow could usually achieve an accurate AMR profile prediction with around 20,000 raw sequencing reads per isolate (at around 30 × coverage) using Abricate. The differences in precision and recall between RGI and Abricate were likely at least partially due to different default similarity cut-off values for sequence alignment through BLAST used with both softwares. In RGI (Alcock et al., 2020), sequence matching hits are classified into three types:

TABLE 7 Recall and precision of AMR/virulence gene identification for *Salmonella* serotype Typhimurium using assemblies from WGS data at different sequencing depths.

Parameters	Sequencing Depth (*Salmonella* genome size 4.8Mbp)				
	15×	30×	50×	75×	100×
Abricate + CARD (AMR gene identification)					
Recall	96%	100%	100%	100%	100%
Precision	100%	100%	100%	100%	100%
Abricate + VFDB (Virulence gene identification)					
Recall	100%	100%	100%	100%	100%
Precision	100%	100%	100%	100%	100%
RGI + CARD (AMR gene identification)					
Recall	68%	82%	81%	84%	84%
Precision	76%	86%	84%	84%	84%

Perfect, Strict, or Loose. Except for the 100% match as "Perfect," "Strict," or "Loose" hits will include hits with much lower identity or coverage. RGI generated results from all three types of sequence matching hits, this may have led to some inaccurate identification of AMR with "Strict" or "Loose" hits. In this study, more AMR genes were identified using RGI than Abricate, the least identity in RGI results was 51.35% with a gene coverage of 91.8%, whereas the Abricate results only included hits with minimum identity and coverage of 80 and 90%, respectively. Higher identity and coverage of sequence matching hits adopted by Abricate compared to RGI may increase the accuracy of AMR identification by Abricate when using ONT data. A more recent study (Tan et al., 2020) found that AMR profiles of *Streptococcus suis* could be identified for 100% of the 10 isolates tested using RGI (with CARD library) with ONT sequencing data generated by a MinION sequencer. "Loose" algorithm of RGI was also used for MinION assemblies in Tan et al.'s study, while our findings implied that some of the AMR genes identified by "Loose" algorithm of RGI from ONT sequencing data may not be accurate as compared to results generated by Illumina data for *Salmonella* when coverage is from 15× to 100×.

3.4. Recommendation for cost-effective multiplexing strategy for serotype prediction and AMR/virulence gene prediction

The current study shows that, when multiplexing five *Salmonella* genome DNA samples in one ONT FC, 50× or greater depth of genome coverage per isolate/sample allows for accurate serotype prediction and AMR/virulence gene profiling with accuracy comparable to Illumina data for *Salmonella*. The sequencing time for obtaining at least 50× per multiplexed isolate was 7.01 h on average (range: 5.37 to 10.45 h) based on data from sequencing of 14 FCs with five different serotypes multiplexed in each FC, and 69 different *Salmonella* serotypes tested in total. A cost estimation of ONT sequencing with five *Salmonella* isolates multiplexed in one FC has been made in our previous study (Wu et al., 2021). These recommendations are based on the ONT GridION sequencer, FC R9.4.1, sequencing kit SQK-RBK004, basecalling model modified for 6 mA dam/5mC dcm and CpG, as well as the corresponding bioinformatics pipeline developed for the current study. As various sequencing platforms, sequencing kits and bioinformatics tools are available for ONT sequencing, any deviation from or further improvement of the factors described above may change the prediction results and accuracy significantly. Although the sequencing kit (SQK-RBK004) used in this study has the capability of barcoding up to 12 different isolates in one FC, we focused on validating only five isolates multiplexed as we have demonstrated in our previous study that multiplexing five *Salmonella* genome DNA isolates could achieve the most efficient combination of sequencing time, data distribution stability, and cost reduction. Previously, we have demonstrated that the unevenness of data yield between each multiplexed isolate increases significantly as the multiplexing number of isolates increases; and multiplexing seven to 10 isolates resulted in only a small cost benefit, considering their much longer sequencing time (more than 19 h; Wu et al., 2021).

Abricate combined with the CARD/VFDB library is recommended for *Salmonella* AMR/virulence gene identification, as it showed relatively higher accuracy compared to RGI at 50× genome coverage for AMR identification. For AMR/virulence gene detection with ONT sequence data, the choice of appropriate algorithm and setting is particularly important to reduce the impact of relatively low sequencing accuracy of ONT data compared to Illumina data. And to maintain the advantage of the fast turnaround time of ONT sequencing. Meanwhile, a combination of SISTR and SeqSero2 results are recommended for predicting serotypes of *Salmonella*. Although SISTR had slightly lower accuracy compared to SeqSero2 in the current study, they each have advantages in different aspects as they use different algorithms and databases for serotype prediction (Yoshida et al., 2016; Zhang et al., 2019; Xu et al., 2020; Wu et al., 2021). Although it is unknown if certain strains of *Salmonella* would alter the accuracy of serotyping under the recommended settings, the 69 serotypes we covered in the current study represented the majority of common serotypes and major types of H and O antigens of *Salmonella*. Further validation and verification with more *Salmonella* serotypes can be carried out during practice, for example in the food industry or in public health.

4. Conclusion

In this study we evaluated the ONT-multiplex-sequencing-based WGS method for *Salmonella* serotype prediction and AMR/virulence gene detection, using Illumina sequencing data for bench marking. We demonstrated that for all the 69 *Salmonella* serotypes tested, accurate serotype prediction and AMR/virulence gene profiling can be obtained with an average of 7 h of ONT sequencing when multiplexing five *Salmonella* serotypes. The accuracy was comparable to results from Illumina data. Multiplexing five isolates results in a 23% reduction to the cost of ONT sequencing of a single

isolate per FC. Meanwhile, the workflow we developed also allows for *Salmonella* serotype prediction and AMR/virulence gene detection to be completed within one working day. This study is an evaluation of multiplex-nanopore-sequencing based WGS as a cost-effective and rapid *Salmonella* classification method. It is also a starting point for exploring the application of ONT-based WGS in AMR and virulence gene detection for the food safety area. Our findings pave the way for the application and standardization of ONT-based WGS in surveillance, tracking, and risk assessment of *Salmonella* across the food supply chain as a cost-effective and rapid *Salmonella* classification and AMR/virulence gene profiling tool.

Data availability statement

The original contributions presented in the study are publicly available. This data can be found here: NCBI, PRJNA694442.

Author contributions

ST, CG, XW, MW, RB, AS, and GZ contributed to conception and design of the study. XW and HL organized the database. ST performed the statistical analysis. XW, ST, and HL wrote the first draft of the manuscript. XD and FX contributed to sections of the manuscript. All authors contributed to the article and approved the submitted version.

Funding

This work was funded by Mars Global Food Safety Center, Mars, Incorporated. The funder was not involved in the study design, collection, analysis, interpretation of data, the writing of this article, or the decision to submit it for publication.

Acknowledgments

We thank Peter Markwell, Kristel Hauben, Jerome Combrisson, Aurelien Maillet, and Bala Ganesan for comments that greatly improved the manuscript. We thank Georgina Cuckston for her ideas for visualization of our findings. We also would like to thank Oxford Nanopore Technologies for supporting the establishment of ONT capability at the Mars Global Food Safety Center.

Conflict of interest

XW, HL, CG, FX, RB, AS, GZ, and ST were employed by Mars, Incorporated. MW received compensation to serve as consultant to Mars.

The remaining author declares that the research was conducted in the absence of any commercial or financial relationships that could be construed as a potential conflict of interest.

Publisher's note

All claims expressed in this article are solely those of the authors and do not necessarily represent those of their affiliated organizations, or those of the publisher, the editors and the reviewers. Any product that may be evaluated in this article, or claim that may be made by its manufacturer, is not guaranteed or endorsed by the publisher.

Supplementary material

The Supplementary material for this article can be found online at: https://www.frontiersin.org/articles/10.3389/fmicb.2022.1073057/full#supplementary-material

References

Alcaine, S. D., Soyer, Y., Warnick, L. D., Su, W. L., Sukhnanand, S., Richards, J., et al. (2006). Multilocus sequence typing supports the hypothesis that cow- and human-associated salmonella isolates represent distinct and overlapping populations. *Appl. Environ. Microbiol.* 72, 7575–7585. doi: 10.1128/AEM.01174-06

Alcock, B. P., Raphenya, A. R., Lau, T. T. Y., Tsang, K. K., Bouchard, M., Edalatmand, A., et al. (2020). CARD 2020: antibiotic resistome surveillance with the comprehensive antibiotic resistance database. *Nucleic Acids Res.* 48, D517–D525. doi: 10.1093/nar/gkz935

Allard, M. W., Strain, E., Melka, D., Bunning, K., Musser, S. M., Brown, E. W., et al. (2016). Practical value of food pathogen traceability through building a whole-genome sequencing network and database. *J. Clin. Microbiol.* 54, 1975–1983. doi: 10.1128/JCM.00081-16

Ashton, P. M., Nair, S., Peters, T. M., Bale, J. A., Powell, D. G., Painset, A., et al. (2016). A. and *Salmonella* whole genome sequencing implementation, G.: identification of *Salmonella* for public health surveillance using whole genome sequencing. *PeerJ* 4:e1752. doi: 10.7717/peerj.1752

Banerji, S., Simon, S., Tille, A., Fruth, A., and Flieger, A. (2020). Genome-based *Salmonella* serotyping as the new gold standard. *Sci. Rep.* 10:4333. doi: 10.1038/s41598-020-61254-1

Batz, M. B., Richardson, L. C., Bazaco, M. C., Parker, C. C., Chirtel, S. J., Cole, D., et al. (2021). Recency-weighted statistical modeling approach to attribute illnesses caused by 4 pathogens to food sources using outbreak data, United States. *Emerg. Infect. Dis.* 27, 214–222. doi: 10.3201/eid2701.203832

CDC (2013). *Salmonella atlas: An atlas of Salmonella in the United States, 1968–2011: Laboratory-based enteric disease surveillance.* Atlanta, Georgia: US Department of Health and Human Services.

CDC (2016). Salmonella serotypes isolated from animals and related sources. Available at: https://www.cdc.gov/nationalsurveillance/pdfs/salmonella-serotypes-isolated-animals-and-related-sources-508.pdf

CDC (2021). *Interagency food safety analytics collaboration (IFSAC): Foodborne illness source attribution estimates for salmonella, Escherichia coli O157, listeria monocytogenes, and Campylobacter using multi-year outbreak surveillance data*, United States, Atlanta, Georgia and Washington, District of Columbia: U.S. Department of Health and Human Services, CDC, FDA, USDA/FSIS.

Chen, Z., Erickson, D. L., and Meng, J. (2020a). Benchmarking hybrid assembly approaches for genomic analyses of bacterial pathogens using Illumina and Oxford Nanopore sequencing. *BMC Genomics* 21:631. doi: 10.1186/s12864-020-07041-8

Chen, Z., Kuang, D., Xu, X., Gonzalez-Escalona, N., Erickson, D. L., Brown, E., et al. (2020b). Genomic analyses of multidrug-resistant *Salmonella* Indiana, typhimurium, and Enteritidis isolates using MinION and MiSeq sequencing technologies. *PLoS One* 15:e0235641. doi: 10.1371/journal.pone.0235641

Cooper, A. L., Low, A. J., Koziol, A. G., Thomas, M. C., Leclair, D., Tamber, S., et al. (2020). Systematic evaluation of whole genome sequence-based predictions of

Salmonella serotype and antimicrobial resistance. *Front. Microbiol.* 11:549. doi: 10.3389/fmicb.2020.00549

Davidson, K. E., Byrne, B. A., Pires, A. F. A., Magdesian, K. G., and Pereira, R. V. (2018). Antimicrobial resistance trends in fecal *Salmonella* isolates from northern California dairy cattle admitted to a veterinary teaching hospital, 2002-2016. *PLoS One* 13:e0199928. doi: 10.1371/journal.pone.0199928

Diep, B., Barretto, C., Portmann, A. C., Fournier, C., Karczmarek, A., Voets, G., et al. (2019). *Salmonella* serotyping; comparison of the traditional method to a microarray-based method and an in silico platform using whole genome sequencing data. *Front. Microbiol.* 10:2554. doi: 10.3389/fmicb.2019.02554

Edwards, P. R., and Ewing, W. H. *Identification of Enterobacteriaceal. 4th Edition*, Burges Publishing Company, Minneapolis (1986).

EFSA and ECDC (2021). The European Union one health 2019 Zoonoses report. *EFSA J.* 19:e06406. doi: 10.2903/j.efsa.2021.6406

Fox, E. J., Reid-Bayliss, K. S., Emond, M. J., and Loeb, L. A. (2014). Accuracy of next generation sequencing platforms. *Next. Gener. Seq. Appl.* 1:1000106. doi: 10.4172/jngsa.1000106

Gao, R., Duceppe, M. O., Naushad, S., Chattaway, M. A., and Ogunremi, D. (2020). Complete genome assemblies of the rare *Salmonella enterica* Serovar Adjame using Nanopore and Illumina sequence reads. *Microbiol. Resour. Announc.* 9, e00280–e00220. doi: 10.1128/MRA.00280-20

Gargis, A. S., Cherney, B., Conley, A. B., McLaughlin, H. P., and Sue, D. (2019). Rapid detection of genetic engineering, structural variation, and antimicrobial resistance markers in bacterial biothreat pathogens by Nanopore sequencing. *Sci. Rep.* 9:13501. doi: 10.1038/s41598-019-49700-1

González-Escalona, N., Yao, K., and Hoffmann, M. (2018). Closed genome sequence of *Salmonella enterica* Serovar Richmond Strain CFSAN000191, obtained with Nanopore sequencing. *Microbiol. Resour. Announc.* 7:e01472-18. doi: 10.1128/mra.01472-18

Grimont, P., and Weill, F.: *Antigenic formulae of the Salmonella serovars*, (*9th ed.*) Paris: WHO Collaborating Centre for Reference and Research on Salmonella. (2007).

Haendiges, J., Davidson, G. R., Pettengill, J. B., Reed, E., Ramachandran, P., Blessington, T., et al. (2021). Genomic evidence of environmental and resident *Salmonella* Senftenberg and Montevideo contamination in the pistachio supply-chain. *PLoS One* 16:e0259471. doi: 10.1371/journal.pone.0259471

Hendriksen, R. S., Vieira, A. R., Karlsmose, S., Lo Fo Wong, D. M., Jensen, A. B., Wegener, H. C., et al. (2011). Global monitoring of *Salmonella* serovar distribution from the World Health Organization global foodborne infections network country data bank: results of quality assured laboratories from 2001 to 2007. *Foodborne Pathog. Dis.* 8, 887–900. doi: 10.1089/fpd.2010.0787

Hodges, L. M., Taboada, E. N., Koziol, A., Mutschall, S., Blais, B. W., Inglis, G. D., et al. (2021). Systematic evaluation of whole-genome sequencing based prediction of antimicrobial resistance in *Campylobacter jejuni* and *C. coli*. *Front. Microbiol.* 12:776967. doi: 10.3389/fmicb.2021.776967

Jackson, B. R., Griffin, P. M., Cole, D., Walsh, K. A., and Chai, S. J. (2013). Outbreak-associated *Salmonella enterica* serotypes and food commodities, United States, 1998-2008. *Emerg. Infect. Dis.* 19, 1239–1244. doi: 10.3201/eid1908.121511

Jajere, S. M. (2019). A review of *Salmonella enterica* with particular focus on the pathogenicity and virulence factors, host specificity and antimicrobial resistance including multidrug resistance. *Vet. World* 12, 504–521. doi: 10.14202/vetworld.2019.504-521

Kahlmeter, G., Brown, D. F., Goldstein, F. W., MacGowan, A. P., Mouton, J. W., Osterlund, A., et al. (2003). European harmonization of MIC breakpoints for antimicrobial susceptibility testing of bacteria. *J. Antimicrob. Chemother.* 52, 145–148. doi: 10.1093/jac/dkg312

Kingsley, R. A., van Amsterdam, K., Kramer, N., and Bäumler, A. J. (2000). The shdA gene is restricted to serotypes of salmonella enterica subspecies I and contributes to efficient and prolonged fecal shedding. *Infect. Immun.* 68, 2720–2727. doi: 10.1128/iai.68.5.2720-2727.2000

Köser, C. U., Ellington, M. J., and Peacock, S. J. (2014). Whole-genome sequencing to control antimicrobial resistance. *Trends Gen.* 30, 401–407. doi: 10.1016/j.tig.2014.07.003

Liu, L., Wang, Y., Yang, Y., Wang, D., Cheng, S. H., Zheng, C., et al. (2021). Charting the complexity of the activated sludge microbiome through a hybrid sequencing strategy. *Microbiome* 9, 205–215. doi: 10.1186/s40168-021-01155-1

Liu, B., Zheng, D., Jin, Q., Chen, L., and Yang, J. (2019). VFDB 2019: a comparative pathogenomic platform with an interactive web interface. *Nucleic Acids Res.* 47, D687–d692. doi: 10.1093/nar/gky1080

Marchello, C. S., Carr, S. D., and Crump, J. A. (2020). A systematic review on antimicrobial resistance among *Salmonella* Typhi worldwide. *Am. J. Trop. Med. Hyg.* 103, 2518–2527. doi: 10.4269/ajtmh.20-0258

Neal-McKinney, J. M., Liu, K. C., Lock, C. M., Wu, W.-H., and Hu, J. (2021). Comparison of MiSeq, MinION, and hybrid genome sequencing for analysis of *Campylobacter jejuni*. *Sci. Rep.* 11:5676. doi: 10.1038/s41598-021-84956-6

Oniciuc, E. A., Likotrafiti, E., Alvarez-Molina, A., Prieto, M., Santos, J. A., and Alvarez-Ordóñez, A. (2018). The present and future of whole genome sequencing (WGS) and whole metagenome sequencing (WMS) for surveillance of antimicrobial resistant microorganisms and antimicrobial resistance genes across the food chain. *Genes* 9:268. doi: 10.3390/genes9050268

Päivärinta, M., Latvio, S., Fredriksson-Ahomaa, M., and Heikinheimo, A. (2020). Whole genome sequence analysis of antimicrobial resistance genes, multilocus sequence types and plasmid sequences in ESBL/AmpC *Escherichia coli* isolated from broiler caecum and meat. *Int. J. Food Microbiol.* 315:108361. doi: 10.1016/j.ijfoodmicro.2019.108361

Rang, F. J., Kloosterman, W. P., and de Ridder, J. D. (2018). From squiggle to basepair: computational approaches for improving nanopore sequencing read accuracy. *Genome Biol.* 19:90. doi: 10.1186/s13059-018-1462-9

Rodriguez-Rivera, L. D., Wright, E. M., Siler, J. D., Elton, M., Cummings, K. J., Warnick, L. D., et al. (2014). Subtype analysis of *Salmonella* isolated from subclinically infected dairy cattle and dairy farm environments reveals the presence of both human- and bovine-associated subtypes. *Vet. Microbiol.* 170, 307–316. doi: 10.1016/j.vetmic.2014.02.013

Sereika, M., Kirkegaard, R. H., Karst, S. M., Michaelsen, T. Y., Sørensen, E. A., Wollenberg, R. D., et al. (2022). Oxford Nanopore R10.4 long-read sequencing enables the generation of near-finished bacterial genomes from pure cultures and metagenomes without short-read or reference polishing. *Nat. Methods* 19, 823–826. doi: 10.1038/s41592-022-01539-7

Shi, C., Singh, P., Ranieri, M. L., Wiedmann, M., and Moreno Switt, A. (2015). I.: molecular methods for serovar determination of *Salmonella*. *Crit. Rev. Microbiol.* 41, 309–325. doi: 10.3109/1040841X.2013.837862

Smith, E., Lichten, C. A., Taylor, J., Maclure, C., Lepetit, L., Harte, E., et al. (2016). Evaluation of the action plan against the rising threats from antimicrobial resistance: final report, European Commission, Directorate-General for Health and Food Safety, Publications Office, (2016).

Tan, S., Dvorak, C. M. T., Estrada, A. A., Gebhart, C., Marthaler, D. G., and Murtaugh, M. P. (2020). MinION sequencing of *Streptococcus suis* allows for functional characterization of bacteria by multilocus sequence typing and antimicrobial resistance profiling. *J. Microbiol. Methods* 169:105817. doi: 10.1016/j.mimet.2019.105817

USDA (2014). United states department of agriculture, USDA Antimicrobial Resistance (AMR) Action Plan. Available at: https://www.usda.gov/sites/default/files/documents/usda-antimicrobial-resistance-action-plan.pdf

Wattiau, P., Boland, C., and Bertrand, S. (2011). Methodologies for *Salmonella enterica* subsp. *enterica* subtyping: gold standards and alternatives. *Appl. Environ. Microbiol.* 77, 7877–7885. doi: 10.1128/AEM.05527-11

WHO (ed.) (2016) "Global action plan on antimicrobial resistance," in *WHO Library Cataloguing-in-Publication Data. World Health Organization, 2016.*

Wick, R. R., Judd, L. M., Gorrie, C. L., and Holt, K. E. (2017). Unicycler: resolving bacterial genome assemblies from short and long sequencing reads. *PLoS Comput. Biol.* 13:e1005595. doi: 10.1371/journal.pcbi.1005595

Wu, X., Luo, H., Xu, F., Ge, C., Li, S., Deng, X., et al. (2021). Evaluation of *Salmonella* serotype prediction with multiplex Nanopore sequencing. *Front. Microbiol.* 12:637771. doi: 10.3389/fmicb.2021.637771

Xu, F., Ge, C., Li, S., Tang, S., Wu, X., Luo, H., et al. (2021). Evaluation of nanopore sequencing technology to identify *Salmonella* enterica Choleraesuis var. Kunzendorf and Orion var. 15(+), 34(). *Int. J. Food Microbiol.* 346:109167. doi: 10.1016/j.ijfoodmicro.2021.109167

Xu, F., Ge, C., Luo, H., Li, S., Wiedmann, M., Deng, X., et al. (2020). Evaluation of real-time nanopore sequencing for *Salmonella* serotype prediction. *Food Microbiol.* 89:103452. doi: 10.1016/j.fm.2020.103452

Xu, Y., Lewandowski, K., Lumley, S., Pullan, S., Vipond, R., Carroll, M., et al. (2018). Detection of viral pathogens with multiplex Nanopore MinION sequencing: be careful with cross-talk. *Front. Microbiol.* 9:2225. doi: 10.3389/fmicb.2018.02225

Yin, Z., Liu, J., Du, B., Ruan, H. H., Huo, Y. X., Du, Y., et al. (2020). Whole-genome-based survey for polyphyletic Serovars of *Salmonella enterica* subsp. *enterica* provides new insights into public health surveillance. *Int. J. Mol. Sci.* 21:5226. doi: 10.3390/ijms21155226

Yoshida, C. E., Kruczkiewicz, P., Laing, C. R., Lingohr, E. J., Gannon, V. P., Nash, J. H., et al. (2016). The *Salmonella in silico* typing resource (SISTR): an open web-accessible tool for rapidly typing and subtyping draft *Salmonella* genome assemblies. *PLoS One* 11:e0147101. doi: 10.1371/journal.pone.0147101

Zhang, S., den Bakker, H. C., Li, S., Chen, J., Dinsmore, B. A., Lane, C., et al. (2019). SeqSero2: rapid and improved *Salmonella* serotype determination using whole-genome sequencing data. *Appl. Environ. Microbiol.* 85:AEM.01746-01719. doi: 10.1128/AEM.01746-19

Zhao, S., Li, C., Hsu, C. H., Tyson, G. H., Strain, E., Tate, H., et al. (2020). F.: comparative genomic analysis of 450 strains of *Salmonella enterica* isolated from diseased animals. *Genes (Basel)* 11:1025. doi: 10.3390/genes11091025

frontiers | Frontiers in Microbiology

TYPE Original Research
PUBLISHED 25 April 2023
DOI 10.3389/fmicb.2023.1112709

OPEN ACCESS

EDITED BY
Chun Cui,
South China University of Technology,
China

REVIEWED BY
Chengmin Wang,
Guangdong Academy of Sciences,
China
Hongliang Yao,
Institute of Zoology,
Guangdong Academy of Science (CAS),
China

*CORRESPONDENCE
Qiong Lin
✉ linqiong76@163.com
Jian-Huan Chen
✉ cjh_bio@hotmail.com

†These authors have contributed equally to this work

SPECIALTY SECTION
This article was submitted to
Food Microbiology,
a section of the journal
Frontiers in Microbiology

RECEIVED 30 November 2022
ACCEPTED 28 February 2023
PUBLISHED 25 April 2023

CITATION
Chen Y, Xia S-Y, Ru F-X, Feng J-J, Tao J, Wei Z-Y, Li X, Qian C, Lin Q and Chen J-H (2023) Gastric juice microbiota in pediatric chronic gastritis that clinically tested positive and negative for *Helicobacter pylori*. *Front. Microbiol.* 14:1112709. doi: 10.3389/fmicb.2023.1112709

Gastric juice microbiota in pediatric chronic gastritis that clinically tested positive and negative for *Helicobacter pylori*

Ying Chen[1†], Shou-Yue Xia[2†], Fu-Xia Ru[2†], Jun-Jie Feng[2†], Ji Tao[2], Zhi-Yuan Wei[2], Xiu Li[3], Chengjia Qian[4], Qiong Lin[1*] and Jian-Huan Chen[2*]

[1]Department of Gastroenterology, Affiliated Children's Hospital of Jiangnan University, Wuxi, China, [2]Laboratory of Genomic and Precision Medicine, Wuxi School of Medicine, Jiangnan University, Wuxi, Jiangsu, China, [3]Laboratory Animal Center, Jiangnan University, Wuxi, Jiangsu, China, [4]Department of General Surgery, Affiliated Hospital of Jiangnan University, Wuxi, China

Purpose: *Helicobacter pylori* (HP) infection is an identified risk factor for pediatric chronic gastritis (PCG), but its impact on gastric juice microbiota (GJM) remains to be further elucidated in PCG. This study aimed to analyze and compare the microbial communities and microbial interactive networks of GJM in PCG that clinically tested positive and negative for HP (HP+ and HP−, respectively).

Methods: A total of 45 PCG patients aged from 6 to 16 years were recruited, including 20 HP+ and 25 HP− patients tested by culture and rapid urease test. Gastric juice samples were collected from these PCG patients and subjected to high-throughput amplicon sequencing and subsequent analysis of 16S rRNA genes.

Results: While no significant change in alpha diversity, significant differences in beta diversity were observed between HP+ and HP− PCG. At the genus level, *Streptococcus, Helicobacter*, and *Granulicatella* were significantly enriched in HP+ PCG, whereas *Campylobacter* and *Absconditabacteriales (SR1)* were significantly enriched in *HP*− PCG. Network analysis showed that *Streptococcus* was the only genus positively correlated with *Helicobacter* (r=0.497) in the GJM network of overall PCG. Moreover, compared to HP− PCG, HP+ PCG showed a reduction in microbial network connectivity in GJM. Netshift analysis identified driver microbes including *Streptococcus* and other four genera, which substantially contributed to the GJM network transition from HP− PCG to HP+ PCG. Furthermore, Predicted GJM function analysis indicated up-regulated pathways related to the metabolism of nucleotides, carbohydrates, and L-Lysine, the urea cycle, as well as endotoxin peptidoglycan biosynthesis and maturation in HP+ PCG.

Conclusion: GJM in HP+ PCG exhibited dramatically altered beta diversity, taxonomic structure, and function, with reduced microbial network connectivity, which could be involved in the disease etiology.

KEYWORDS

gastric microbiota, *Helicobacter pylori*, pediatric chronic gastritis, network of microbial interaction, *Streptococcus*

Introduction

Chronic gastritis is a common health problem in children (Sipponen and Maaroos, 2015). *Helicobacter pylori* (HP) infection is an important cause of chronic gastritis, which occurs generally in childhood (Sabbagh et al., 2019), and is associated with peptic ulcer, gastric atrophy, intestinal metaplasia, and gastric cancer. It is important to study the impact of HP for the understanding of the etiology of pediatric chronic gastritis (PCG).

HP plays a pivotal role in the gastric microbiota. The stomach is a special area in the digestive tract, with gastric acid secretion constituting its unique ecological environment and characteristic microbial community (Caguazango, 2020). HP could promote inflammation in the gastric mucosa, and leads to changes in the gastric mucosa microbiota (GMM) in PCG (Zheng et al., 2021). In addition, the gastric juice microbiota (GJM) is typically affected by various factors such as diet (Martinsen et al., 2019), which could result in greater variation compared to GMM. The diversity of GJM has been reported to be higher than that of GMM. Sung et al. found that the relative abundance of *Actinobacteria*, *Bacteroidetes*, and *Firmicutes* was relatively higher in GJM than in GMM (Sung et al., 2016). Besides, FLéJOU et al. found that non-HP bacteria could have explicit effects on gastritis (Fléjou et al., 1990), and *Streptococcus* showed a higher relative abundance in HP− cancer patients. (Sohn et al., 2017). It is also noteworthy that the collection of gastric juice is less invasive compared with gastric mucosal biopsy.

In the current study, we recruited a cohort of PCG and analyzed the impact of HP abundance on the microbial communities and co-occurrence networks of GJM.

Materials and methods

Study design and participants

This study was approved by the Medical Ethics Committee of Jiangnan University and conducted in accordance with the Declaration of Helsinki. A total of 45 PCG were recruited in the current study, including 27 boys and 18 girls, with an average age of 9.03 ± 0.93 years old. Informed consent was obtained from all of the participants after explanation of the nature of the study. Gastritis diagnosis was made based on endoscopic observation and pathological features of gastric atrophy. Exclusion criteria included treatment with antibiotics or proton pump inhibitors (PPIs) within 6 months; serious mental or organ damage; or poor patient compliance. HP infection status of these PCG patients was tested using gastric mucosal biopsy and rapid urease tests, and confirmed with HP culture on brain heart infusion agar plate supplemented with blood, inoculated with gastric mucosal biopsy tissue homogenate in a microaerophilic environment (85% N_2, 10% CO_2, 5% O_2) at 37°C for 3 days.

Sample collection and 16S rRNA gene sequencing

Gastric juice samples were collected from all participants with sterilized 1.5-mL tubes containing ethanol on ice, and stored at −80°C until analysis. The V4 hypervariable region of the 16S rRNA gene was amplified from the gastric fluid samples with V4-specific primers 515F (5′-GTGCCAGCMGCCGCGGTAA-3′) and 806R (5′-GGACTACHVGGGTWTCTAAT-3′). Amplicons were checked using the 2% agarose gel, and purified using GeneJET Gel Extraction Kit (Thermo Fisher Scientific, Waltham). Constructed libraries were sequenced on an Ion S5XL sequencer (Thermo Fisher Scientific, Waltham) with a single-end 400-bp read length configuration following standard protocols provided by the manufacturer.

16S rRNA gene sequence analysis

The 16S rRNA gene sequencing reads were analyzed using the QIIME2 (version 2020.11.0) analysis pipeline as previously described (Bolyen et al., 2019; Wei et al., 2022). In brief, low-quality and chimeric sequences were filtered using DADA2. Amplicon sequence variant (ASV) tables at 100% sequence similarity were generated. Taxonomy classification was assigned to ASVs using q2-feature-classifier and the SILVA database (release r132) at a 99% similarity cutoff (Glockner et al., 2017). Microbiota diversity was analyzed using QIIME2: alpha diversity metrics including Pielou's evenness, the Chao1, Shannon and Simpson's indices, and beta diversity including weighted/unweighted UniFrac distances, and Bray-Curtis distances followed by non-metric multidimensional scaling (NMDS) analysis and Principal Coordinate Analysis (PCoA). The linear discriminant analysis (LDA) effect size (LEfSe) algorithm was used to identify group-enriched taxa (Segata et al., 2011). Phylogenetic cladograms were drawn using GraPhlAn (version 1.1.3). PICRUSt2 was used to predict microbiota function based on the 16S rRNA sequencing data (Douglas et al., 2020).

Microbial interactive network analysis

ASVs with average relative abundance >0.1% of the microbiome were subjected to correlation analysis of their occurrence patterns (Barberan et al., 2012; Cardinale et al., 2015). The SparCC algorithm was used to estimate the correlations among gut microbes(Friedman and Alm, 2012). 1,000 bootstrap replicates were applied to calculate the pseudo *p*-values, and correlations with |correlation coefficient $|(r)| > 0.2$ and $p < 0.01$ were considered significant. For each genus with significant SparCC correlations, its degree was calculated as an indicator of its weight in the network by summing up its edges. The SparCC network was further constructed using Cytoscape 3.9.1 (Shannon et al., 2003). In addition, NetShift [1] was used to evaluate potential driver microbes as described (Kuntal et al., 2019), and to calculate Neighbor shift (NESH) scores to quantify increased interactions in the network shift.

1 https://web.rniapps.net/netshift/

TABLE 1 Demographic and clinical characteristics of HP– and HP+ PCG in the current study.

Item	HP– (*n*, %)	HP+ (*n*, %)	*p**
Age	9.92 ± 2.33	10.25 ± 2.61	0.317
Gender			1
Male	15 (60.00)	12 (60.00)	
Female	10 (40.00)	8 (40.00)	
Endoscopic finding			0.040**
Normal	2 (8.00)	0 (0.00)	–
Superficial gastritis and duodenitis	2 (8.00)	2 (10.00)	–
Superficial gastritis and bile reflux	0 (0.00)	3 (15.00)	–
Superficial gastritis and duodenal ulcer	0 (0.00)	2 (10.00)	–
Superficial gastritis and gastric ulcer	1 (4.00)	2 (10.00)	–
Superficial gastritis without other findings listed above	20 (80.00)	11 (55.00)	–
clinical symptoms			
Abdominal pain			0.465
No	6 (24.00)	5 (25.00)	–
Yes, 0–1 month	7 (28.00)	3 (15.00)	–
Yes, 1–3 months	2 (8.00)	4 (20.00)	–
Yes, 3–6 months	2 (8.00)	4 (20.00)	–
Yes, 6 months and above	8 (32.00)	4 (20.00)	–
Abdominal distension	3 (12.00)	1 (5.00)	0.617
Nausea	1 (4.00)	1 (5.00)	1.000
Belching	2 (8.00)	0 (0.00)	0.495
Ozostomia	2 (8.00)	3 (15.00)	0.642
Acid reflux	1 (4.00)	0 (0.00)	1.000

*p-values are calculated using Student's t -test for continuous data or Fisher's exact test for frequency data.
**The p-value is calculated by comparing the proportion of superficial gastritis with duodenitis, bile reflux, duodenal ulcer, or gastric ulcer in HP+ PCG and HP– PCG.

Results

Demographic and clinical characteristics of study subjects

The demographic and clinical characteristics of 45 PGC patients were summarized in Table 1. Endoscopic findings showed a significantly higher proportion of gastritis with additional clinical conditions (GAC) including duodenitis, bile reflux, duodenal ulcer, and gastric ulcer in HP+ PCG than in HP– PCG (OR = 4.97, 95% CI: 0.97–34.69, $p = 0.040$). No significant difference was found in age, gender, and other clinical features between HP+ and HP– PCG (all $p > 0.05$).

GJM diversity in HP+ and HP– PCG

The results of the rarefaction curve shown in Supplementary Figure S1 indicated that our current study's sequencing data could sufficiently capture the majority of the microbial taxa. In addition, alpha diversity results showed no significant difference (all $p > 0.05$) in the Shannon, Simpson, evenness, and Chao1 (Figures 1A–D) indices between the two groups. Nevertheless, PCoA and NMDS results based on Bray-Curtis distances suggested a significant difference in beta diversity between HP+ and HP– PCG (PERMANOVA $p = 0.007$ and 0.007 respectively), although the two groups might not be completely separated (Figures 1E,F).

GJM composition in HP+ and HP – PCG

GJM in both HP+ PCG and HP– PCG patients was dominated by 8 phyla, including Firmicutes, Bacteroidetes, Proteobacteria, Fusobacteriota, Actinobacteriota, Campilobacterota, Patescibacteria, and Spirochaetota (Figure 2A). *Prevotellaceae*, *Streptococcaceae*, *Neisseriaceae*, *Pasteurellaceae*, *Fusobacteriaceae*, *Carnobacteriaceae*, *Veillonellaceae*, *Micrococcaceae*, *Porphyromonadaceae*, and *Gemellaceae* were the top 10 families, and *Prevotella*, *Streptococcus*, *Alloprevotella*, *Neisseria*, *Fusobacterium*, *Haemophilus*, *Granulicatella*, *Rothia*, *Porphyromonas*, and *Veillonella* were the top 10 genera in PCG GJM (Figures 2B,C). LEfSe analysis was then applied to identify the most relevant taxa responsible for differences between the two groups. As shown in the cladogram in Figure 3A, at the phylum level, Firmicutes and Campilobacterota were enriched in *HP*+ PCG. At the family level, *Streptococcaceae*, *Helicobacteraceae*, and *Carnobacteriaceae* were enriched in *HP*+ PCG, whereas *Campylobacteraceae* and *Absconditabacteriales (SR1)* were enriched in *HP*– PCG (Figure 3B). At the genus level, *Streptococcus*, *Helicobacter*, and *Granulicatella* were enriched in HP+ PCG, whereas *Campylobacter* and *Absconditabacteriales (SR1)* were enriched in *HP*– PCG (Figure 3C and Supplementary Figure S2).

In addition, as GAC was dramatically increased in HP+ *PCG*, we further divided *the* HP+ PCG patients into a group of gastritis only (GO) and a group of GAC according to the endoscopic findings, and compared GJM between the two groups. Our results showed that the genus *Absconditabacteriales (SR1)* was enriched in GO, whereas genera including *Prevotella*, *Megashaera*, and *Actinomyces* were enriched in GAC (Figure 4).

GJM network in HP+ and HP– PCG

To explore the interaction among microbes in GJM, we conducted a correlation analysis using the SparCC algorithm and the genus abundance of genera with average relative abundance ≥ 0.1%, and constructed microbial co-occurrence networks with cutoff set as $|r| >= 0.2$ and $p < 0.01$ in overall PCG, HP– PCG, and HP+ PCG. In the GJM network of overall PCG, *Streptococcus*, the most enriched genus in HP+ PCG, was found to be the only genus positively correlated with *Helicobacter* ($r = 0.497$) (Figure 5A). It was also positively correlated with *Granulicatella*, *Gemella*, *Actinomyces*, *Rothia*, *Atopobium*, and *Megasphaera*, ($r = 0.746$, 0.598, 0.504, 0.497, 0.484, 0.483, and 0.465, respectively), and negatively correlated with *Absconditabacteriales*

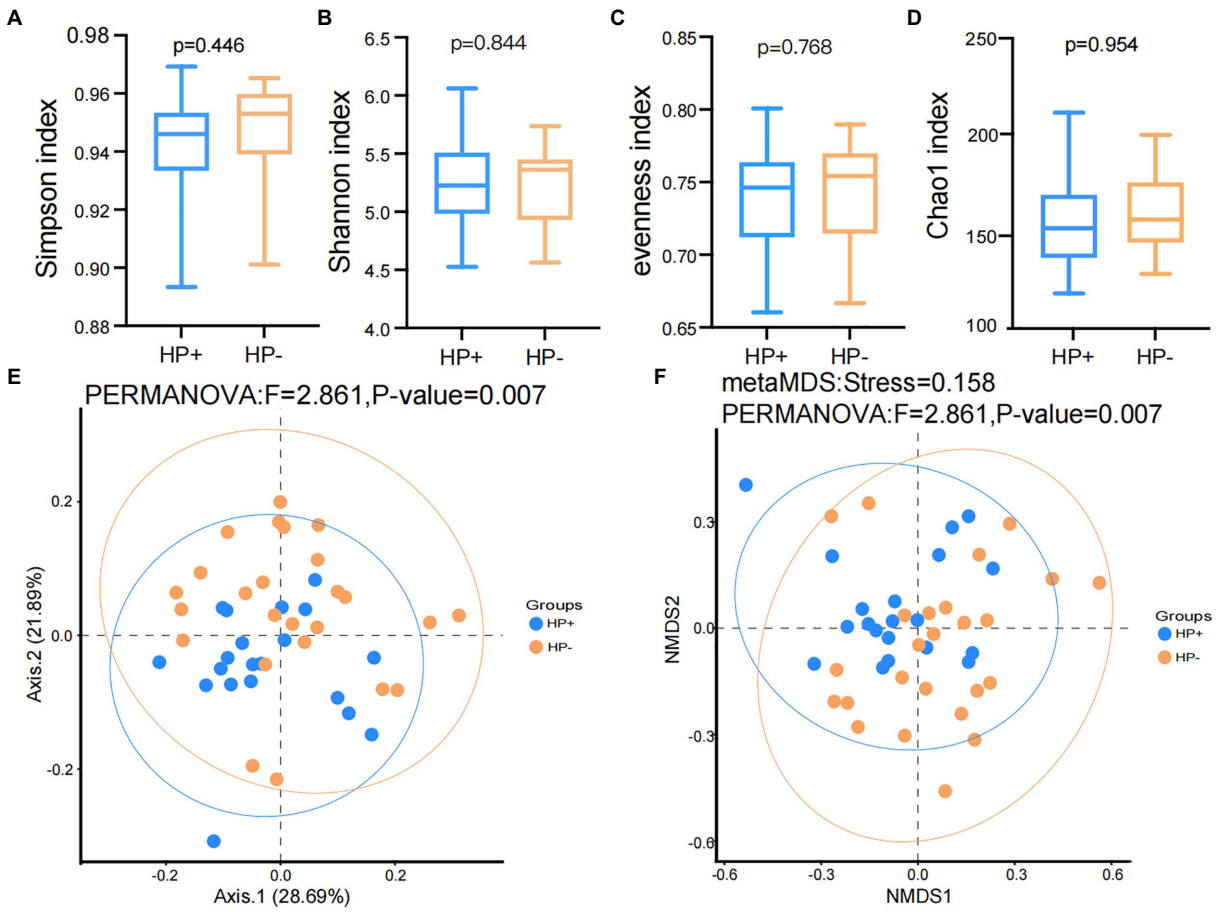

FIGURE 1
Comparison of Alpha and beta diversities between HP− and HP+ PCG. **(A)** Simpson index. **(B)** Shannon index. **(C)** Eveness index. **(D)** Chao1 index. **(E)** PCoA based on Bray-Curtis distances. **(F)** NMDS on Bray-Curtis distances.

(SR1), ($r = -0.402$). No significant correlation between other microbes and *Helicobacter* was found in GJM networks of either HP+ PCG or HP− PCG. Notably, lower network connectivity was found in HP+ PCG compared to that in HP− PCG or overall PCG (Figures 5B,C, and Supplementary Tables S1–3). Similarly, *Actinomyces* and *Prevotella 6* were the dominant members in overall PCG (Figure 5B). In *HP+* PCG, *Streptococcus* showed positive correlations with *Rothia* ($r = 0.716$), *Megasphaera* ($r = 0.708$), and *Gemella* ($r = 0.679$), (Figure 5C). In *HP−* PCG, *Streptococcus* showed positive correlations with *Granulicatella* ($r = 0.783$) and *Gemella* ($r = 0.621$). Furthermore, *Streptococcus* was identified as a driver microbe responsible for the microbial changes between *HP+* and *HP−* PCG in Netshift analysis (Table 2, Figure 5D). Additional driver microbes identified by Netshift analysis included *Capnocytophaga*, *Actinomyces*, *Neisseria*, and *Megasphaera*.

Predicted GJM function in HP+ and HP− PCG

PICRUSt2 predicted a dramatical difference in GJM function, with a total of 35 Kyoto Encyclopedia of Genes and Genomes (KEGG) pathways differentially abundant between HP+ and HP− PCG (Figure 6). The 30 pathways significantly upregulated in HP+ PCG were mainly related to the metabolism of nucleotides, carbohydrates, and L-Lysine, as well as endotoxin peptidoglycan biosynthesis and maturation. In addition, the urea cycle was also significantly upregulated in HP+ PCG. In contrast, pathways enriched in HP− PCG were related to the biosynthesis of thiamin diphosphate, CMP-3-deoxy-D-manno-octulosonat, flavin, and lipid IVA which was an intermediate in the biosynthetic pathway of lipid A and lipopolysaccharide (LPS).

Discussions

Since Warren and Marshall first cultivated *HP* from children's gastric mucosa, after two decades of in-depth research, *HP* has been identified as a pivotal pathogen of chronic gastritis and peptic ulcer (Kishikawa et al., 2020). More, the influence of HP on the gastric microbiota might contribute to the development of PCG. By analyzing GJM in HP+ and HP− PCG clinically tested by routine methods, our current study showed a substantial impact of HP abundance on GJM composition, microbial interactive network, and function.

By far, most existing studies have focused on the influence of HP on the gastrointestinal microbiota in adults (He et al., 2019; Tao et al., 2020), and there have been only limited studies in children, especially for GJM. Brawner et al. reported that HP infection significantly reduced the alpha diversity of GMM in PCG. Different from such results in GMM, our current study showed no significant difference in alpha diversity of GJM

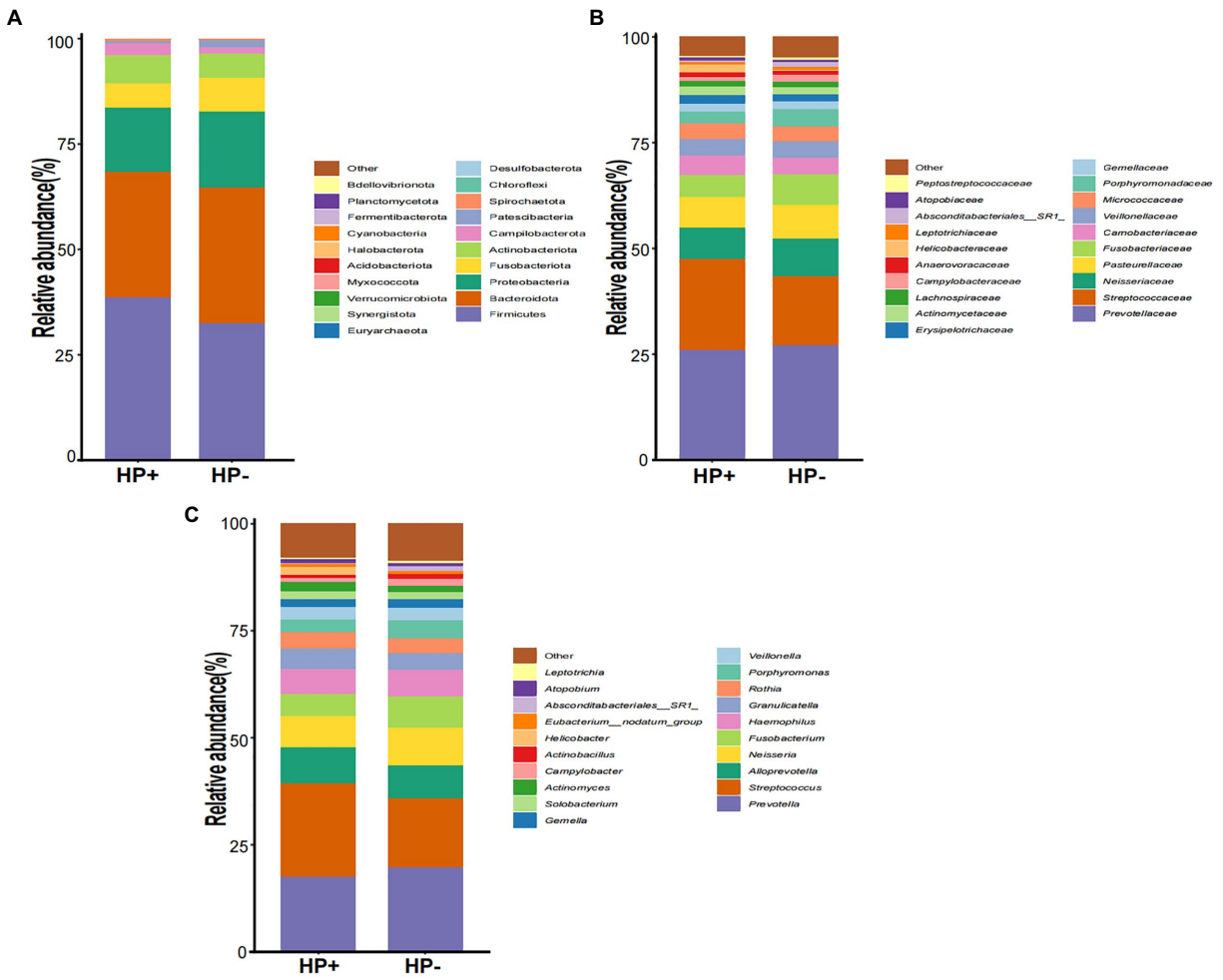

FIGURE 2
The microbial abundance of GJM in HP− and HP+ PCG. Microbial abundance is shown at the **(A)** phylum level, **(B)** family level, **(C)** and the genus level.

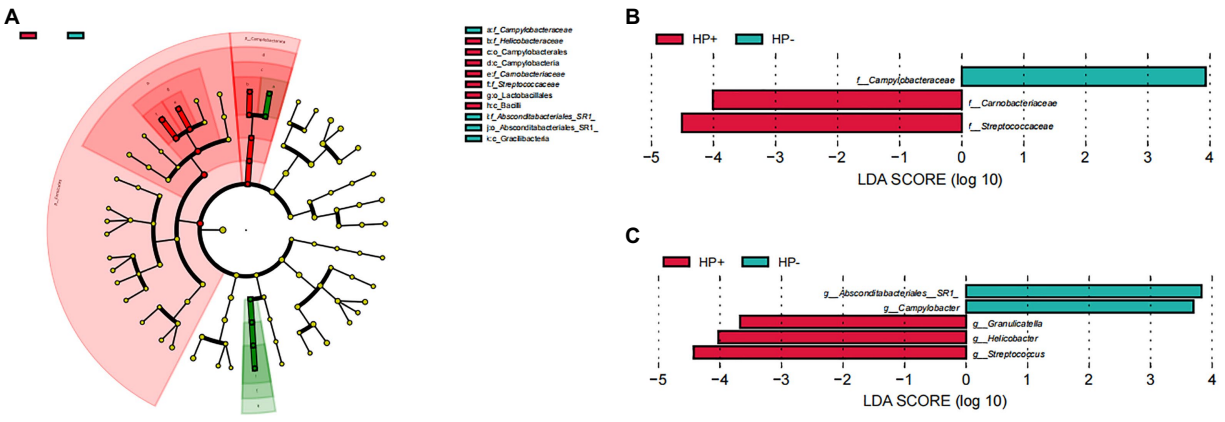

FIGURE 3
LEfSe analysis of GJM in HP− and HP+ PCG. Phylogenetic cladograms **(A)**, and barplots at **(B)** the family, and **(C)** Genus levels are shown.

between HP+ and HP− PCG, pointing to different effects of HP on GMM and GJM. Notably, *Helicobacter* could also be detected in HP−PCG clinically tested *via* routine methods, yet with an extremely low relative abundance than in HP+ PCG. 16S amplicon sequencing was recently reported with higher sensitivity in detecting HP in the gastric microbiota, by revealing HP existence in some cases that were tested negative for HP *via* routine methods (Gantuya et al., 2021). *Helicobacter* is commonly found in human children and non-human primate infants (Wei et al., 2022). Such findings suggested that an extremely low abundance of HP might still exist in samples that test negative by routine clinical methods.

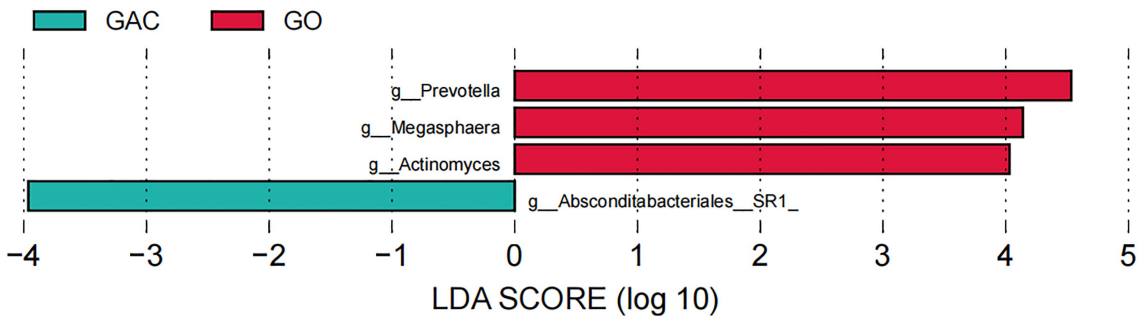

FIGURE 4
LEfSe analysis of GJM in GO and GAC subgroups of HP+ PCG.

Our results showed a significant difference in beta diversity with dramatic changes in taxonomic structure between HP+ and HP− PCG. The higher abundance of Firmicutes in HP+ PCG was similar to the gut microbiota of asymptomatic children with HP infection (Benavides-Ward et al., 2018). In addition, our study showed that a non-HP bacterium *Streptococcus*, with a significantly positive correlation with *Helicobacter* in all PCG, was the most enriched genus in *HP*+ PCG. *Streptococcus* is a gram-positive bacterium of spherical shape and has been reported to be involved in several diseases and health issues, such as gastritis (Minalyan et al., 2017). Moreover, our GJM networks revealed that *Streptococcus* acted as a driver that contributed to the shift of the GJM network from HP− PCG to HP+ PCG. Another non-HP bacterium *Granulicatella* is associated with atrophic gastritis or intestinal metaplasia in patients following successful HP eradication (Liu et al., 2022). In contrast, *Campylobacter* and *Absconditabacteriales (SR1)* were enriched in our *HP*− PCG patients. *Campylobacter* infection usually causes diarrhea, fever, and stomach cramps. *Absconditabacteriales* exhibited significantly lower abundance in the gastric microbiota in HP− Crohn's disease patients than in control subjects (Ostrowski et al., 2021). Such findings indicated non-HP pathogens could play a potential role in PCG.

The change of non-*HP* pathogens in the stomach may be due to the change in pH value in gastric juice. Rosen et al. reported that acid suppression resulted in the overgrowth of gastric bacteria such as *Staphylococcus* and *Streptococcus* (Rosen et al., 2014). In addition, *Streptococcus*, *Actinomyces*, *Megasphaera*, and *Granulicatella* were significantly increased in patients receiving proton pump inhibitor treatment (Jackson et al., 2016; Takagi et al., 2018).

Recent studies have demonstrated the importance of microbiota networks in understanding microbiota changes in diseases and aging. The reduced network connectivity observed in HP+ PCG suggested a dramatic change in microbial interaction in the group compared to that of HP− PCG, emphasizing the impact of HP on the microbial community. In addition, *Streptococcus* showed a significant positive correlation with *Helicobacter* in overall PCG, and contributed to the network shift from HP− to HP+ PCG by interconnecting with multiple hub or driver microbes. Such findings thus highlighted the importance of non-HP pathogens.

Although no significant difference in clinical symptoms such as abdominal pain and belching between the two groups, endoscopic findings showed a significantly higher proportion of PCG with duodenitis, bile reflux, duodenal ulcer, or gastric ulcer. Such findings were in line with previous reports that HP was a cause of duodenitis (Ohkusa et al., 2003), peptic ulcer, and possibly bile reflux (Ladas et al., 1996). Furthermore, our results also indicated GJM might also contribute to the development of duodenitis, bile reflux, and peptic ulcer.

Gastric acid secretion in the stomach constitutes a characteristic microbial community and its function in the gastric juice (Caguazango, 2020), which could be involved in HP infection and the development of PCG. Our PICRUSt2 results implicated a dramatic difference in the GJM function between HP+ and HP− PCG. In line with the positive findings in the clinical rapid urease test, the urea cycle pathway could be significantly upregulated in HP+ PCG compared to HP− PCG. In addition, our findings also indicated that biosynthesis and maturation of PGN were also enhanced in HP+ PCG compared to HP− PCG. PGN is a major cell wall component of Gram-positive bacteria. It is reported that HP cag + strains deliver components of PGN into epithelial cells *via* the cag secretion system, leading to decreased apoptosis, increased proliferation, and increased cell migration (Suarez et al., 2017). These changes indicated that PGN could play a potentially important role in modulating host inflammatory responses to HP, allowing the bacteria to persist and induce carcinogenic consequences in the gastric niche (Suarez et al., 2017). Interestingly, we also found that L-lysine biosynthesis increased significantly in HP+ PCG. L-lysine could significantly delay and inhibit gastric emptying (Uchida et al., 2017), which might be related to symptoms such as abdominal distension caused by HP.

Due to sample limitations, further studies will be necessary to confirm our findings in other cohorts with larger sample sizes. Nevertheless, the results of our current study demonstrate dramatic differences in GJM between HP+ and HP− PCG in terms of taxonomic structure, microbiota network, and function. GJM analysis could be a less invasive way to monitor and study the gastric microbiota dynamics in PCG.

Data availability statement

The raw sequence data presented in the study are deposited in the Genome Sequence Archive in the National Genomics Data Center, China National Center for Bioinformation/Beijing Institute of Genomics, Chinese Academy of Sciences (GSA-human), accession number PRJCA014620.

Ethics statement

This study was approved by the Ethics Committee of Jiangnan University, and was conducted in accordance with the Declaration

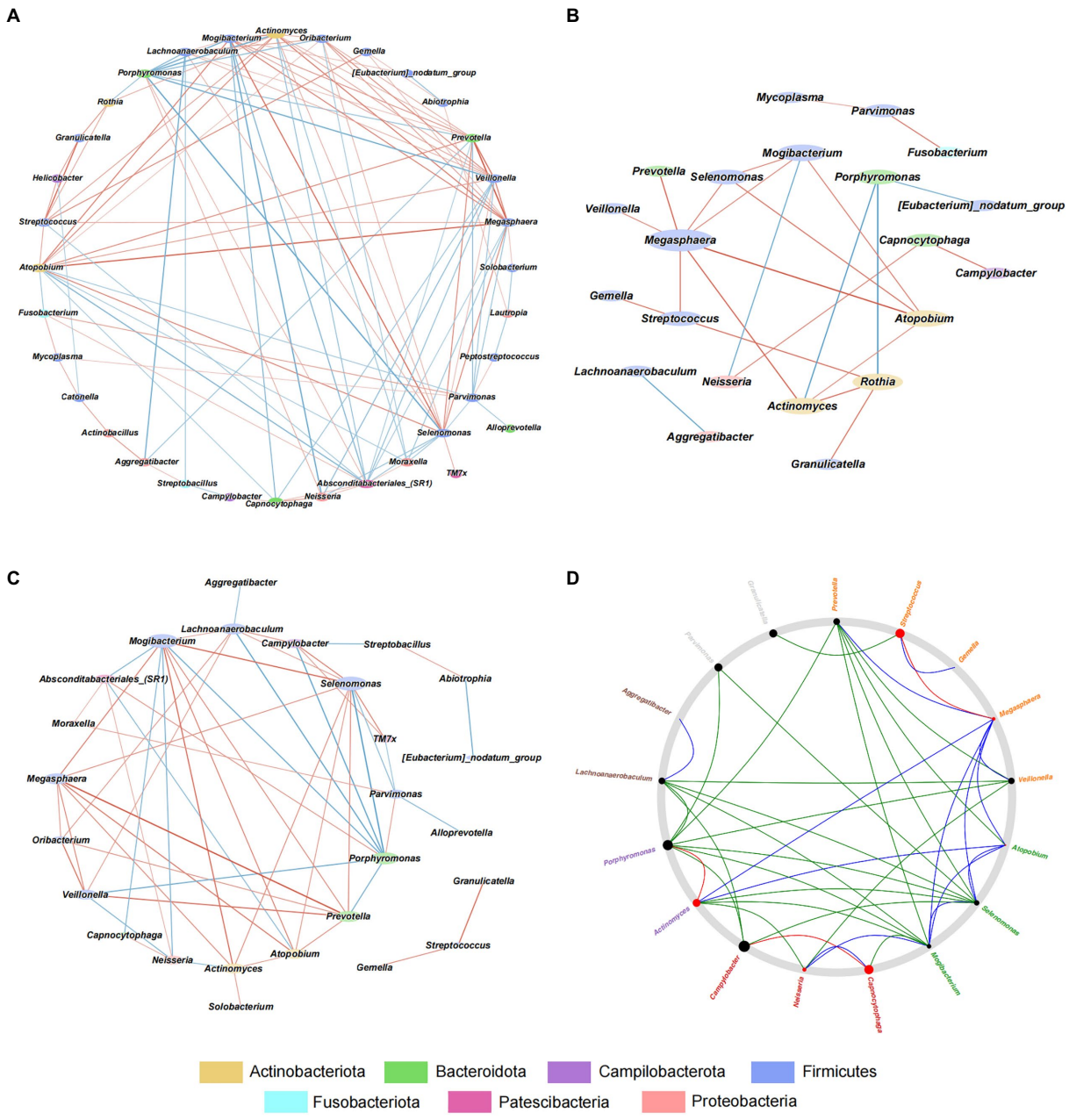

FIGURE 5
Interactive Network in HP–, HP+, and overall PCG at the genus level. **(A)** Interactive network analysis of HP– PCG. **(B)** Interactive network analysis of overall PCG. **(C)** Interactive Network analysis of HP+ PCG. **(D)** Netshift analysis of GJM between HP– and HP+ PCG.

TABLE 2 Genera with the top five NESH score in Netshift analysis.

Genus	n(HP–)	n(HP+)	core (HP+)	Intersect	NESH-score
Campylobacter	3	1	1	0	1.393
Porphyromonas	7	1	1	0	1.268
Streptococcus	2	2	1	1	1.143
Capnocytophaga	2	2	1	1	1.143
Actinomyces	5	3	2	2	0.976

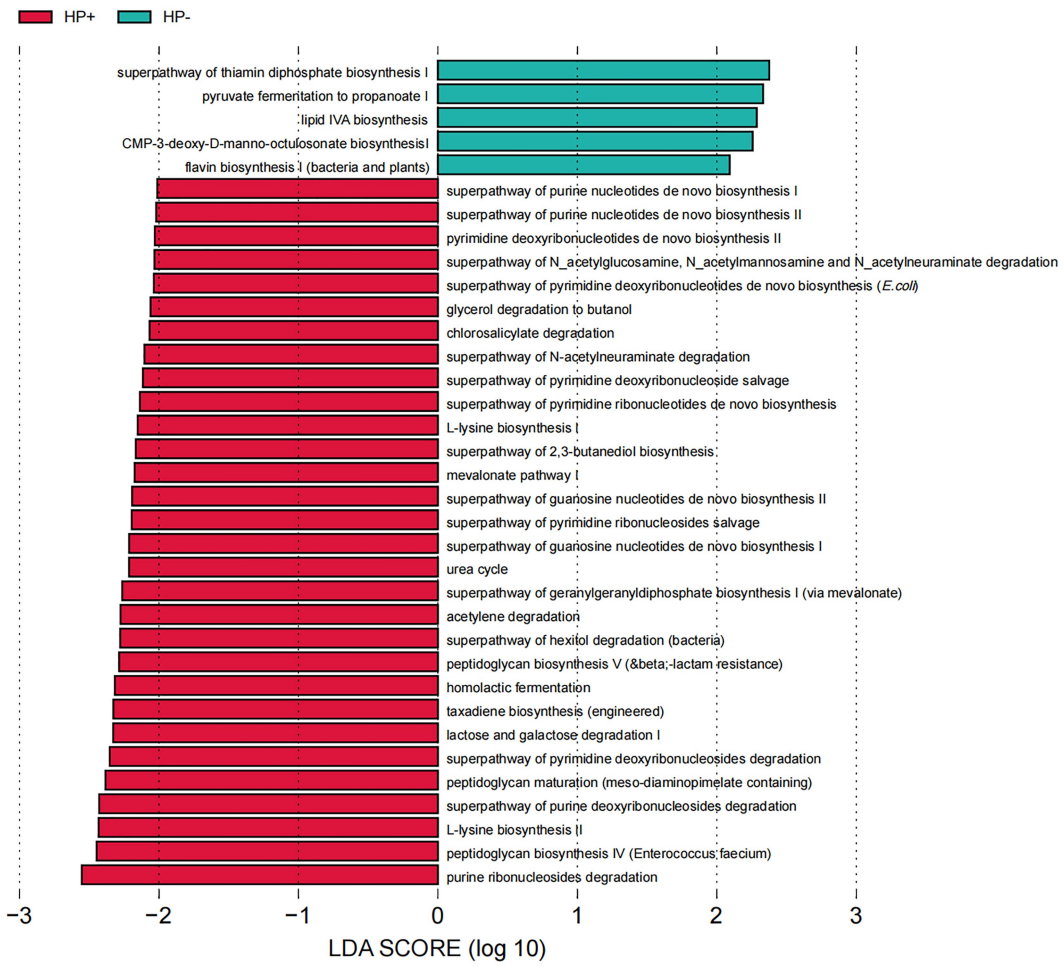

FIGURE 6
LEfSe analysis of GJM KEGG pathways differentially enriched in HP– and HP+ PCG.

of Helsinki. Written informed consent to participate in this study was provided by the participants' legal guardian/next of kin.

Author contributions

YC, S-YX, F-XR, and J-JF performed the data analysis and wrote the manuscript. YC collected the clinical data. JT and Z-YW conducted the experiments. XL and CQ contributed to the discussion. QL and J-HC conceived the project and planned the experiments. All authors contributed to the final manuscript.

Funding

This study was supported in part by grants from the Youth Research Program of Wuxi Health Commission (Q202011), Wuxi maternal and child health research project (FYKY202108), and Wuxi Medical Innovation Team (CXTD2021011).

Conflict of interest

The authors declare that the research was conducted in the absence of any commercial or financial relationships that could be construed as a potential conflict of interest.

Publisher's note

All claims expressed in this article are solely those of the authors and do not necessarily represent those of their affiliated organizations, or those of the publisher, the editors and the reviewers. Any product that may be evaluated in this article, or claim that may be made by its manufacturer, is not guaranteed or endorsed by the publisher.

Supplementary material

The Supplementary material for this article can be found online at: https://www.frontiersin.org/articles/10.3389/fmicb.2023.1112709/full#supplementary-material

References

Barberan, A., Bates, S. T., Casamayor, E. O., and Fierer, N. (2012). Using network analysis to explore co-occurrence patterns in soil microbial communities. *ISME J.* 6, 343–351. doi: 10.1038/ismej.2011.119

Benavides-Ward, A., Vasquez-Achaya, F., Silva-Caso, W., Aguilar-Luis, M. A., Mazulis, F., Urteaga, N., et al. (2018). *Helicobacter pylori* and its relationship with variations of gut microbiota in asymptomatic children between 6 and 12 years. *BMC. Res. Notes* 11:468. doi: 10.1186/s13104-018-3565-5

Bolyen, E., Rideout, J. R., Dillon, M. R., Bokulich, N. A., Abnet, C. C., Al-Ghalith, G. A., et al. (2019). Reproducible, interactive, scalable and extensible microbiome data science using QIIME 2. *Nat. Biotechnol.* 37, 852–857. doi: 10.1038/s41587-019-0209-9

Cardinale, M., Grube, M., Erlacher, A., Quehenberger, J., and Berg, G. (2015). Bacterial networks and co-occurrence relationships in the lettuce root microbiota. *Environ. Microbiol.* 17, 239–252. doi: 10.1111/1462-2920.12686

Caguazango, J. C. (2020). Ecological models of gastric microbiota dysbiosis: Helicobacter pylori and gastric carcinogenesis. *Med. Microecol.* 3:100010. doi: 10.1016/j.medmic.2020.100010

Douglas, G. M., Maffei, V. J., Zaneveld, J. R., Yurgel, S. N., Brown, J. R., Taylor, C. M., et al. (2020). PICRUSt2 for prediction of metagenome functions. *Nat. Biotechnol.* 38, 685–688. doi: 10.1038/s41587-020-0548-6

Fléjou, J. F., Diomandé, I., Molas, G., Goldfain, D., Rotenberg, A., Florent, M., et al. (1990). Human chronic gastritis associated with non-*Helicobacter pylori* spiral organisms (*Gastrospirillum hominis*). Four cases and review of the literature. *Gastroenterol. Clin. Biol.* 14, 806–810. PMID: 2276559

Friedman, J., and Alm, E. J. (2012). Inferring correlation networks from genomic survey data. *PLoS Comput. Biol.* 8:e1002687. doi: 10.1371/journal.pcbi.1002687

Gantuya, B., El Serag, H. B., Saruuljavkhlan, B., Azzaya, D., Matsumoto, T., Uchida, T., et al. (2021). Advantage of 16S rRNA amplicon sequencing in *Helicobacter pylori* diagnosis. *Helicobacter* 26:e12790. doi: 10.1111/hel.12790

Glockner, F. O., Yilmaz, P., Quast, C., Gerken, J., Beccati, A., Ciuprina, A., et al. (2017). 25 years of serving the community with ribosomal RNA gene reference databases and tools. *J. Biotechnol.* 261, 169–176. doi: 10.1016/j.jbiotec.2017.06.1198

He, C., Peng, C., Wang, H., Ouyang, Y., Zhu, Z., Shu, X., et al. (2019). The eradication of *Helicobacter pylori* restores rather than disturbs the gastrointestinal microbiota in asymptomatic young adults. *Helicobacter* 24:e12590. doi: 10.1111/hel.12590

Jackson, M. A., Goodrich, J. K., Maxan, M. E., Freedberg, D. E., Abrams, J. A., Poole, A. C., et al. (2016). Proton pump inhibitors alter the composition of the gut microbiota. *Gut* 65, 749–756. doi: 10.1136/gutjnl-2015-310861

Kishikawa, H., Ojiro, K., Nakamura, K., Katayama, T., Arahata, K., Takarabe, S., et al. (2020). Previous *Helicobacter pylori* infection-induced atrophic gastritis: a distinct disease entity in an understudied population without a history of eradication. *Helicobacter* 25:e12669. doi: 10.1111/hel.12669

Kuntal, B. K., Chandrakar, P., Sadhu, S., and Mande, S. S. (2019). 'NetShift': a methodology for understanding 'driver microbes' from healthy and disease microbiome datasets. *ISME J.* 13, 442–454. doi: 10.1038/s41396-018-0291-x

Ladas, S. D., Katsogridakis, J., Malamou, H., Giannopoulou, H., Kesse-Elia, M., and Raptis, S. A. (1996). *Helicobacter pylori* may induce bile reflux: link between *H. pylori* and bile induced injury to gastric epithelium. *Gut* 38, 15–18. doi: 10.1136/gut.38.1.15

Liu, D., Zhang, R., Chen, S., Sun, B., and Zhang, K. (2022). Analysis of gastric microbiome reveals three distinctive microbial communities associated with the occurrence of gastric cancer. *BMC Microbiol.* 22:184. doi: 10.1186/s12866-022-02594-y

Martinsen, T. C., Fossmark, R., and Waldum, H. L. (2019). The phylogeny and biological function of gastric juice-microbiological consequences of removing gastric acid. *Int. J. Mol. Sci.* 20:6031. doi: 10.3390/ijms20236031

Minalyan, A., Gabrielyan, L., Scott, D., Jacobs, J., and Pisegna, J. R. (2017). The gastric and intestinal microbiome: role of proton pump inhibitors. *Curr. Gastroenterol. Rep.* 19:42. doi: 10.1007/s11894-017-0577-6

Ohkusa, T., Okayasu, I., Miwa, H., Ohtaka, K., Endo, S., and Sato, N. (2003). *Helicobacter pylori* infection induces duodenitis and superficial duodenal ulcer in Mongolian gerbils. *Gut* 52, 797–803. doi: 10.1136/gut.52.6.797

Ostrowski, J., Kulecka, M., Zawada, I., Zeber-Lubecka, N., Paziewska, A., Graca-Pakulska, K., et al. (2021). The gastric microbiota in patients with Crohn's disease; a preliminary study. *Sci. Rep.* 11:17866. doi: 10.1038/s41598-021-97261-z

Rosen, R., Amirault, J., Liu, H., Mitchell, P., Hu, L., Khatwa, U., et al. (2014). Changes in Gastric and Lung Microflora With Acid Suppression. *JAMA Pediatr.* 168, 932–937. doi: 10.1001/jamapediatrics.2014.696

Sabbagh, P., Javanian, M., Koppolu, V., Vasigala, V. R., and Ebrahimpour, S. (2019). *Helicobacter pylori* infection in children: an overview of diagnostic methods. *Eur. J. Clin. Microbiol. Infect. Dis.* 38, 1035–1045. doi: 10.1007/s10096-019-03502-5

Segata, N., Izard, J., Waldron, L., Gevers, D., Miropolsky, L., Garrett, W. S., et al. (2011). Metagenomic biomarker discovery and explanation. *Genome Biol.* 12:R60. doi: 10.1186/gb-2011-12-6-r60

Shannon, P., Markiel, A., Ozier, O., Baliga, N. S., Wang, J. T., Ramage, D., et al. (2003). Cytoscape: a software environment for integrated models of biomolecular interaction networks. *Genome Res.* 13, 2498–2504. doi: 10.1101/gr.1239303

Sipponen, P., and Maaroos, H. I. (2015). Chronic gastritis. *Scand. J. Gastroenterol.* 50, 657–667. doi: 10.3109/00365521.2015.1019918

Sohn, S. H., Kim, N., Jo, H. J., Kim, J., Park, J. H., Nam, R. H., et al. (2017). Analysis of gastric body microbiota by pyrosequencing: possible role of bacteria other than *Helicobacter pylori* in the gastric carcinogenesis. *J. Cancer Prev.* 22, 115–125. doi: 10.15430/JCP.2017.22.2.115

Suarez, G., Romero-Gallo, J., Sierra, J. C., Piazuelo, M. B., Krishna, U. S., Gomez, M. A., et al. (2017). Genetic manipulation of Helicobacter pylori Virulence Function by Host Carcinogenic Phenotypes. *Cancer Res.* 77, 2401–2412. doi: 10.1158/0008-5472.CAN-16-2922

Sung, J., Kim, N., Kim, J., Jo, H. J., Park, J. H., Nam, R. H., et al. (2016). Comparison of gastric microbiota between gastric juice and mucosa by next generation sequencing method. *J. Cancer Prev.* 21, 60–65. doi: 10.15430/JCP.2016.21.1.60

Takagi, T., Naito, Y., Inoue, R., Kashiwagi, S., Uchiyama, K., Mizushima, K., et al. (2018). The influence of long-term use of proton pump inhibitors on the gut microbiota: an age-sex-matched case-control study. *J. Clin. Biochem. Nutr.* 62, 100–105. doi: 10.3164/jcbn.17-78

Tao, Z. H., Han, J. X., and Fang, J. Y. (2020). *Helicobacter pylori* infection and eradication: exploring their impacts on the gastrointestinal microbiota. *Helicobacter* 25:e12754. doi: 10.1111/hel.12754

Uchida, M., Kobayashi, O., and Saito, C. (2017). Correlation Between Gastric Emptying and Gastric Adaptive Relaxation Influenced by Amino Acids. *J. Neurogastroenterol Motil.* 23, 400–408. doi: 10.5056/jnm16153

Wei, Z. Y., Rao, J. H., Tang, M. T., Zhao, G. A., Li, Q. C., Wu, L. M., et al. (2022). Characterization of changes and driver microbes in gut microbiota during healthy aging using a captive monkey model. *Genomics Proteomics Bioinformatics* 20, 350–365. doi: 10.1016/j.gpb.2021.09.009

Zheng, W., Miao, J., Luo, L., Long, G., Chen, B., Shu, X., et al. (2021). The effects of *Helicobacter pylori* infection on microbiota associated with gastric mucosa and immune factors in children. *Front. Immunol.* 12:625586. doi: 10.3389/fimmu.2021.625586

Frontiers in Microbiology

Explores the habitable world and the potential of microbial life

The largest and most cited microbiology journal which advances our understanding of the role microbes play in addressing global challenges such as healthcare, food security, and climate change.

Discover the latest Research Topics

See more →

Frontiers

Avenue du Tribunal-Fédéral 34
1005 Lausanne, Switzerland
frontiersin.org

Contact us

+41 (0)21 510 17 00
frontiersin.org/about/contact